

University of South Wales



2053135

THE ENGINEERING GEOLOGY AND STABILITY OF
THE RAPIDLY ALTERNATING LIMESTONE AND MUDROCK
SEA CLIFFS OF GLAMORGAN

by

John N. Grimes B.Sc., M.Sc., C. Eng., M.I.C.E., F.G.S.

VOL I

Thesis presented in partial fulfilment of the requirement for the Degree of
Doctor of Philosophy, Council for National Academic Awards, London.

Sponsoring Establishment

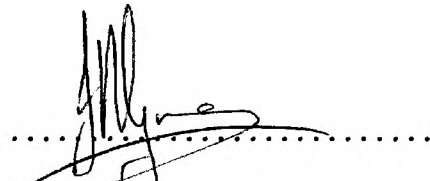
Department of Civil Engineering and Building, The Polytechnic of Wales
United Kingdom

Collaborating Establishment
The Glamorgan Heritage Coast Project


April 1986

Certification of Research

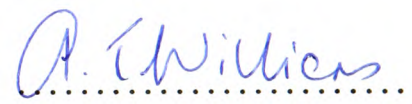
This is to certify that, except when specific reference to other investigations is made, the work described in this thesis is the result of the investigation of the candidate.


.....
J.N. Grimes
(Candidate)

24th April 86
.....
(Date)


.....
Mr. G.O. Rowlands
(Director of Studies)

24th April 86
.....
(Date)


.....
Dr. A.T. Williams
(Supervisor)

24.4.86
.....
(Date)

Declaration

This is to certify that neither this thesis nor any part of it has been presented or currently submitted in candidature for any degree at any other University or Polytechnic.



.....

J.N.Grimes
(Candidate)

DEDICATION

To my wife Patricia
and sons

Daniel and Benjamin.

ACKNOWLEDGEMENTS

The writer is greatly indebted to his Director of Studies Mr. G. O. Rowlands for his encouragement, interest and advice.. His critical reading of the manuscript not only provoked highly valued and interesting discussion, but also undoubtedly added much to the quality of this thesis.

Dr. A.T. Williams, provided the necessary impetus to initiate, and obtain funding for this research. Also acting as supervisor his encouragement, interest and advice throughout the course of this work is gratefully acknowledged.

The research involved laboratory work in several departments of the Polytechnic, including Civil Engineering, Science, Chemical Engineering, Mining and Mechanical Engineering. The writer would like to thank the Heads of Department for extending to me the use of their laboratory facilities, and members of academic and technician staff for their help and advice. Of the academic staff, the help and advice of Dr. K. Burton and Mr. G.I. Jones is gratefully acknowledged. Of the technician staff the assistance and advice of Messrs. B. Lloyd and L. Whiteman, technicians in the Geotechnics Laboratory where the majority of the laboratory work was undertaken, proved invaluable. The writer is particularly indebted to Mr. L. Whiteman for whom the word 'Lias' took on a fresh meaning after preparing the many cores and specimens tested during the course of this work !

Valuable discussion with post-graduate colleagues is gratefully acknowledged as was their willingness in providing assistance with laboratory work at times when an 'extra pair of hands' was desperately needed. In particular the writer wishes to acknowledge Miss B. Morris, Mrs. E. Southern, Dr. N. Caldwell, Dr. J. Lewis and Mr. S. Wersching. Of these special mention should be made of Miss B. Morris for her guidance and advice on analytical chemistry techniques which was undoubtedly most beneficial to the quality of results reported in Chapters 6 and 7.

The large field data base acquired was only made possible by readily available field assistance and this was enthusiastically provided by the Coastal Research Unit which was staffed by trainees of a Youth Opportunities Scheme. Mr. K. Abbot, a supervisor of this scheme, helped coordinate and supervise the field work and did much of the topographical surveying.

Mr. J. McBride of the Computer Centre was not only most helpful in advising on problems relating to the computing undertaken in the project, he also wrote several of the programs and routines used; these are gratefully acknowledged in the text.

The plates for this thesis were printed by Mr. V. Cole and Mr. M. Coundley of the Polytechnic's Media Resources Unit, and by Stuart Photo Services Ltd. of Plymouth. The writer wishes to acknowledge the excellent service received from all concerned, and would also like to thank the former for advice, help and photographic services throughout the course of the research.

The thesis was quickly and efficiently typed by Mrs. P. Hammett who rarely complained about those 'final' inevitable alterations. Her daughter Michelle helped by collating and photocopying.

The completion of this work would have been impossible but for the help, encouragement, understanding and tolerance of my wife Patricia. Not only did she have the task of persuading our two small children Daniel and Benjamin that they were probably too young to positively contribute to this thesis, but she did much to facilitate its production, and must be acknowledged for proof reading, all aspects of collating, draughting several of the figures and tables, and on occasions as a highly accurate alternative to the Oxford Dictionary.

The work was done in collaboration with the Glamorgan Heritage Coast Project, and the writer wishes to acknowledge valuable discussions with Dr. J. Howden, the Project Director, and several of his wardens.

During the initial stages of this research the writer was employed by the Polytechnic as a Supervisor on a Manpower Services Commission Youth Opportunities Scheme. Direct funding for the project was subsequently made available by the Welsh Office and the writer received financial support from that source between July 1981 and September 1984.

ABSTRACT

John N. Grimes - The Engineering Geology and Stability of the Rapidly Alternating Limestone and Mudrock Sea Cliffs of Glamorgan.

Processes, mechanisms and parameters significant to instability have been identified from an investigation which has included :

- 1) Geomorphological mapping and appraisal.
- 2) Field Monitoring.
- 3) Quantitative assesement of rock mass geometry, mineralogy, engineering properties and physical/physico-chemical behaviour.

The north coast of the Bristol Channel is exposed to severe marine attack. Weak lithologies are exploited and the cliffs undermined. Principal failure modes recognised were toppling and vertical translation.

Thermal gravimetry indicated allotropy of sulphide minerals. The least stable forms were identified in the more calcareous mudrocks, and a laboratory leaching experiment demonstrated that weatherability was greatest in such mudrocks. Pyrite oxidation was shown not only to enhance carbonate leaching, but to degrade the clay minerals and induce rehydration of the double layer.

Uniaxial compressive strengths of representative mudrocks were determined for a range of moisture contents. Mean values varied between 5 and 64 MPa. An investigation into deformation anisotropy of a clay shale is also recorded. Meso and micro scale carbonate filled discontinuities are apparent in the limestones. Hoek & Brown's criterion was used to characterise results of a programme of strength testing. Average uniaxial compressive strength of the intact limestone was 234 MPa.

In the field, many major discontinuities were identified as tensile in origin. Results from shear tests along limestone tension fractures could not be adequately represented by Barton's equation. A power relationship between shear strength and normal stress gave good correlation.

Leaching, moisture and temperature movements, freeze-thaw and pressure release all act to impair stability. Extreme weather was shown to trigger failure.

Limiting equilibrium analyses of toppling showed that torsional shear strength mobilized along the failure surface in the plane of toppling contributed significantly to forces resisting toppling.

Both local masonry protection and pre-split blasting are recommended as viable expedients in protection and stabilization works.

CONTENTS - VOLUME I

	Page No.
Certification of Research	i
Declaration	ii
Dedication	iii
Acknowledgements	iv
Abstract	vi
Contents - Vol. I	vii
Contents - Vol. II	xiv
CHAPTER 1 INTRODUCTION	
1.1 <u>General Introduction</u>	1
1.2 <u>Setting</u>	2
1.3 <u>Terminology</u>	4
1.4 <u>Previous and contemporary studies related to the area under investigation</u>	5
1.5 <u>Scope of present investigation</u>	8
1.6 <u>Summary</u>	11
CHAPTER 2 GEOLOGICAL SETTING	
2.1 <u>Introduction</u>	13
2.2 <u>Depositional and post-depositional history</u>	13
2.2.1 Permian to Tertiary	14
2.2.2 Quaternary	16
2.3 <u>Stratigraphy</u>	18
2.4 <u>Sedimentary geology and the origin of the rapidly alternating limestone/mudrock sequence</u>	19
2.5 <u>Tectonic structure</u>	21
2.6 <u>Summary</u>	24
CHAPTER 3 MORPHOGENIC ENVIRONMENT	
3.1 <u>Introduction</u>	26
3.2 <u>Rainfall and temperature</u>	26
3.3 <u>Chemical Analysis of Sampled Waters</u>	27
3.4 <u>The Coastal Zone</u>	28
3.4.1 Introduction	28
3.4.2 Wind	29

	Page No.	
3.4.3	Waves	29
3.4.4	Wave forces	33
3.4.5	Tides and exposure to marine attack	36
3.4.6	Longshore Drift	38
3.5	<u>The storm of 13th and 14th December 1981</u>	39
3.6	<u>Summary</u>	41
CHAPTER 4 GEOMORPHOLOGY		
4.1	<u>Introduction</u>	43
4.2	<u>Procedures and generalisations</u>	44
4.2.1	Surveys for location, level and foreshore profiles	44
4.2.2	Photography and Photogrammetry	44
4.2.3	Discontinuity orientation	46
4.2.4	Discontinuity persistence frequency Width and geometry	48
4.2.5	Accurate measurement of strata dips	49
4.2.6	Stratigraphic columns and Mudrock/(Mudrock + Limestone) Ratios	50
4.2.7	Mudrock Schmidt hammer rebound values	50
4.2.8	Marine Notches	51
4.2.9	Geomorphological maps	51
4.2.10	Geomorphological map, Toppling Fall SS 930 676	52
4.3	<u>Geomorphological appraisal</u>	52
4.3.1	Cwm Bach	53
4.3.2	Whitmore Stairs	54
4.3.3	Monknash	56
4.3.4	Nash	58
4.3.5	Nash - St. Donats	61
4.3.6	St. Donats Point	63
4.3.7	Tresilian	66
4.3.8	Dimhole	70
4.3.9	Col-Huw	72
4.3.10	Summerhouse	74
4.4	<u>Cliff Stability</u>	76
4.4.1	Lithological Control	77
4.4.2	Discontinuity Control	78
4.4.3	Rock Falls	78
4.5	<u>Summary</u>	80
CHAPTER 5 MUDROCKS		
5.1	<u>Introduction</u>	82
5.2	<u>Sample Description</u>	82
5.2.1	Rock type	84
5.2.2	Colour	85
5.2.3	Grain size	85

5.2.4	Texture and fabric	86
5.2.5	Cementation	86
5.2.6	Weathered State	87
5.2.7	Alteration	92
5.2.8	Strength	93
5.3	<u>Thermal gravimetry</u>	93
5.3.1	Apparatus	93
5.3.2	Procedure	94
5.3.3	DTG trace interpretation and diagnostic procedures	94
5.3.3.1	90°C Peak - largely non-structural water	95
5.3.3.2	140°C Peak - gypsum dehydration	95
5.3.3.3	Clay Minerals and gypsum dehydration	96
5.3.3.4	Dehydration/Dehydroxylation of limonite	96
5.3.3.5	300°C - 800°C weight losses	96
5.3.3.6	Low stability sulphides	98
5.3.3.7	Calcium Carbonate	100
5.3.3.8	Organic carbon determinations.	101
5.4	<u>Engineering Index Tests</u>	101
5.4.1	Dry density	101
5.4.2	Atterberg limits	102
5.4.3	Linear shrinkage	102
5.4.4	Hamrol (1961) Absorption test	102
5.4.5	Equilibrium moisture content	103
5.4.6	Slake durability index	103
5.4.7	NCB Indentor determined uniaxial strengths	104
5.5	<u>Discussion</u>	105
5.5.1	Mudrocks and influence on Engineering Geology	105
5.5.2	Mudrock classification	108
5.6	<u>Summary</u>	113
CHAPTER 6 THE MINERALOGY, PHYSICAL AND PHYSICO-CHEMICAL BEHAVIOUR OF SELECTED MUDROCKS		
6.1	<u>Introduction</u>	115
6.2	<u>Illite and mixed layer clay</u>	117
6.3	<u>Mineralogical investigations</u>	118
6.3.1	General procedure	118
6.3.1.1	Cleaning glassware	118
6.3.1.2	Sample washing procedure	118
6.3.1.3	Flocculation and handling dispersed samples	119
6.3.1.4	Centrifugal separation of small quantities	119
6.3.2	Trituration	119
6.3.3	Pretreatments	119
6.3.3.1	Carbonate destruction and removal	119
6.3.3.2	Oxidation of organic carbon and sulphides	120
6.3.3.3	Removal of free iron oxides	120
6.3.3.4	Dispersion and Flocculation	120

	Page No.	
6.3.4	Particle size analysis	121
6.3.4.1	Sample preparation	121
6.3.4.2	Specific gravity	121
6.3.4.3	Particle size analysis	121
6.3.5	Fractionation	122
6.3.6	X-ray diffraction - fraction coarser than 2 micron	122
6.3.7	Thermal gravimetry - fraction coarser than 2 micron	123
6.3.8	Cation exchange capacity of the clay sized fraction	125
6.3.9	Thermal gravimetry - fraction finer than 2 micron	126
6.3.10	X-ray diffraction of randomly orientated clay sized samples	127
6.3.11	Semi-quantitative x-ray diffraction analysis - clay sized fraction	128
6.3.12	Crystallinity	131
6.3.13	Cation analysis - free salts and HCl/H ₂ O ₂ extractions	131
6.3.13.1	Anions present in free salts	131
6.3.13.2	Extraction of free salts and cation analysis	132
6.3.13.3	HCl/H ₂ O ₂ extraction and cation analysis	132
6.3.14	Synthesis - (compilation of table 6-2)	135
6.4	<u>Carbonate Identification</u>	136
6.5	<u>Texture and Fabric</u>	137
6.6	<u>The clay phase and its influence on mudrock behaviour</u>	141
6.6.1	Introduction	141
6.6.2	Consolidation/swelling tests	141
6.6.3	Discussion	142
6.6.4	Summary	145
6.7	<u>Shrinkage</u>	145
6.8	<u>Mudrocks and limestones - temperature and environmental controlled movements</u>	147
6.9	<u>Compression strength testing (Sample S17)</u>	149
6.9.1	Strength criteria	149
6.9.2	Deformation characteristics	151
6.10	<u>Summary</u>	152
 CHAPTER 7 LEACHING		
7.1	<u>Introduction</u>	156
7.2	<u>Chemical weathering reaction</u>	159

	Page No.	
7.2.1	Hydrolysis	159
7.2.2	Solution weathering of Carbonates	159
7.2.3	Iron Sulphide Oxidation	160
7.2.4	Ion exchange	161
7.3	<u>Previous work</u>	161
7.4	<u>Experimental details and procedures</u>	162
7.4.1	Introduction	162
7.4.2	Specimens	163
7.4.3	Leaching water - Introduction and Collection systems	163
7.4.4	Monitoring for change in specimen circumference	166
7.4.5	Apparatus stress/deformation characteristics	167
7.4.6	Temperature effects	167
7.4.7	Contamination	168
7.4.8	Analytical water chemistry procedures	169
7.4.8.1	Specific conductance	169
7.4.8.2	pH	170
7.4.8.3	Eh	170
7.4.8.4	Alkalinity	172
7.4.8.5	Anions of strong acid	172
7.4.8.6	Sulphates	173
7.4.8.7	Chlorides	173
7.4.8.8	Silicates	174
7.4.8.9	Ferrous iron	175
7.4.8.10	Cation analyses by flame photometer and atomic absorption	175
7.4.9	General procedure for chemical analysis of leachate and other waters	176
7.5	<u>Rain water collection, analyses and storage</u>	178
7.6	<u>Monitoring and specimen response</u>	179
7.7	<u>Summary</u>	186
CHAPTER 8 LIMESTONES		
8.1	<u>Introduction</u>	187
8.2	<u>Sample description</u>	188
8.2.1	Introduction	188
8.2.2	Colour and Meso Scale Lithological Characteristics	189
8.2.3	Grain size, Composition and Texture	191
8.2.4	Carbonate Type	193
8.2.5	Meso and Micro Tectonic Structure	193
8.2.6	Weathered State	194
8.3	<u>Index Properties</u>	194
8.4	<u>Thermal Gravimetry</u>	194

8.5	<u>Strength and deformation</u>	196
8.5.1	Introduction	196
8.5.2	Specimen size and length to diameter ratio	197
8.5.2.1	Uniaxial and triaxial test specimens	197
8.5.2.2	Brazilian test specimens	198
8.5.3	Specimen Manufacture	199
8.5.3.1	Uniaxial and Triaxial test specimens	199
8.5.3.2	Brazilian test specimens	200
8.5.4	Test Procedures	200
8.5.4.1	General	200
8.5.4.2	Uniaxial and Triaxial Compression Tests	201
8.5.4.3	Brazilian Tests	201
8.5.5	Fracture	202
8.5.6	Failure Criterion	204
8.5.7	Deformation of specimens tested in Uniaxial compression	208
8.6	<u>Summary</u>	210

CHAPTER 9 ROCK MASS SHEAR STRENGTH

9.1	<u>Introduction</u>	212
9.2	<u>Limestone discontinuity shear strength</u>	212
9.2.1	Literature review	212
9.2.2	Rationale	217
9.2.3	Surface Texture	220
9.2.4	Field Assessment	224
9.2.4.1	Schmidt Hammer Tests	224
9.2.4.2	Discontinuity Profiles	225
9.2.5	Laboratory based investigation	226
9.2.5.1	Ancillary Procedures	226
9.2.5.2	Basic Angle of Friction Tests	227
9.2.5.3	Laboratory Shear testing of rough joints	228
9.2.6	Suggested Shear Strength Criterion	230
9.3	<u>Shear strength of filled Discontinuities</u>	231
9.4	<u>Mudrocks</u>	232
9.5	<u>Summary</u>	234

CHAPTER 10 FIELD MONITORING AND THE EFFECT OF
CONTEMPORARY SUBAERIAL WEATHERING PROCESSES ON
CLIFF STABILITY

10.1	<u>Introduction</u>	236
10.2	<u>Subaerial Weathering</u>	236
10.2.1	Chemical	237
10.2.2	Pressure Release	238
10.2.3	Climatic Effects	243
10.2.4	Salt Crystallization	245
10.2.5	Biological Disintegration	245

CONTENTS - VOLUME II.

LIST OF FIGURES

	Page No.
CHAPTER 1	
1.1 A simplified geological map of the Vale of Glamorgan after Wobber (1963)	1
1.2 Map adopted from 1:50000 Geological Survey, Roberts (1974) & Driscoll (1958)	2
1.3 Map adopted from 1:50000 Geological Survey, Roberts (1974 & Driscoll (1958)	3
CHAPTER 2	
2.1 Reconstruction of "St. Davids archipelago" showing the probable extent of the islands of carboniferous limestone (hatched) as they were in early Jurassic times	5
2.2 Post glacial climate reconstruction from the distribution of snails in recent deposits at Cwm Nash after Evans & French (in Perkins Gayer Baker & Williams (1979)	5
2.3 Diagrammatic representation of the relationship between 'normal' and marginal facies of the Mesozoic rocks of the Vale of Glamorgan after Cope (1971)	6
2.4 Maximum ice advances after Culver (1976)	7
2.5 The sequence in the <u>bucklandi</u> zone of the Lower Lias, Nash Point, after Trueman (1930)	8
2.6 Graphical representation of Lias Limestone - shale ratios for different offshore facies after Hallam (1960)	9
2.7 Joint systems in the Lower Lias of South Glamorgan after Roberts (1974)	10
CHAPTER 3	
3.1 Correlation between weathering and rainfall/temperature after Peltier (1950)	12
3.2 Monthly rainfall - Rhose (ST 063 679) - 1980-1983	13

	Page No.	
3.3	Wind roses for days on which rainwater for use in leaching experiment was collected.	14
3.4	Weekly maximum and minimum temperatures Rhoose (ST 063 679) 1980-1983 (2 sheets)	15
3.5	Weekly total no. of sunshine hours Rhoose (ST 063 679) 1980-1983	17
3.6	Location of Hydraulic Research Station wave study buoys A,B & C	18
3.7	Wind rose explanation	19
3.8	Average hourly wind speeds Rhoose (ST 063 679) 1.9.77 to 31.12.80 and 1.1.81 to 30.4.83	20
3.9	Yearly occurrence of wind speed \gg 25 and 30 knots.	21
3.10	Fetch distances	22
3.11	Tidal Hydrographs measured at Dimhole (SS 95200 67630) on 25.8.81 and 24.5.82 + associated data	23
3.12	Prediction of exposure to marine attack	24
3.13	Wind rose for the storm of 13th & 14th December 1981	25
 CHAPTER 4		
4.1	Significance of geomorphological appraisal in context of this investigation	33
4.2	Directional discontinuity data - lower hemisphere equal area stereonet (6 sheets)	34
4.3	Outline flow chart for stereonet program	40
4.4	Sequence and mudrock/(mudrock + limestone) ratios. Note: sheets 2&3 include mudrock Schmidt hammer rebound numbers (6 sheets)	41
4.5	Lateral variation in stratigraphy	47
4.6	Examples of <u>bucklandi</u> zone lower cliff profiles showing typical marine notches	48
4.7	Geomorphological mapping symbols (7 sheets)	49
4.8	Geomorphological maps (10 sheets)	56

	Page No.
4.9	Platform profiles (4 sheets) 66
4.10	Toppling fall SS 930 676 70
4.11	Sketch of systematic truncated discontinuities SS 92850 67540 71
4.12	Sketch showing buttress type support of upper strata where there is no interlock across major discontinuities striking parallel with the cliff 72
4.13	Schematic sketch showing toppling, and translating graben 73
4.14	Toppling failure 74
4.15	Shear and dilation mechanisms in vertical translation 75
4.16	Mechanisms involved in toppling 76
 CHAPTER 5	
5.1	Sampling (S14 & S15) Summerhouse (SS 99580 66424) 101
5.2	Selected mudrock thermal gravimetry curves 102
5.3	Typical mudrock differential thermal gravimetry trace - showing measured weight losses 103
5.4	Thermal gravimetry standards 104
5.5	Thermal and differential thermal gravimetry graphs for various iron sulphide polymorphs 105
5.6	The effect of grinding on thermal and differential thermal gravimetry of chalcopyrite (CuFeS_2) 106
5.7	Slake durability of representative mudrocks 107
5.8	Graphs of uniaxial compressive strength measured perpendicular to bedding, against moisture content for various mudrocks (using NCB cone indenter) (3 sheets) 108
5.9	Slake durability against plasticity with Gamble's (1971) durability classification superimposed 111
5.10	Graph slake/durability index against uniaxial compressive strength at equilibrium moisture content 112

	Page No.	
5.11	Cementitious material against uniaxial compressive strength	113
5.12	Graph of equilibrium moisture content against plastic index	114
5.13	Graph - uniaxial compressive strength against plastic index	115
5.14	Graph linear shrinkage against plastic index	116
5.15	Mudrock classification for characterisation of performance in a marine environment	117
 CHAPTER 6		
6.1	Procedure for mineralogical investigation of 3 mudrocks	131
6.2	Geochronological distribution of clay minerals, after Dunoyer De Segonzac (1970) (in Tucker 1981)	132
6.3	Thermal gravimetry - 3 pretreated mudrocks	133
6.4	Particle size analyses - 3 pretreated mudrocks	134
6.5	X-ray diffraction analysis of the Mg ⁺⁺ saturated clay fraction - 3 Lower Lias mudrocks	135
6.6	Compression ratios against applied pressure consolidation tests on 3 remoulded mudrocks	136
6.7	Graph a) Ratio of plastic index/% Phyllosilicates against primary compression ratio and b) % Phyllosilicates against primary swelling ratio	137
6.8	Shrinkage limit T.R.R.L. (1952) - 3 remoulded mudrocks	138
6.9	Shrinkage characteristics intact specimens from samples S14 and S15	139
6.10	Change in length against temperature for various mudrock and limestone specimens	140
6.11	Graph coefficient of linear expansion/contraction against carbonate content (initial heating)	141
6.12	Shear strength envelope for sample S17	142

	Page No.	
6.13	Mudrock deformation characteristics when loaded perpendicular to laminae (Sample S17)	142
6.14	Mudrock anisotropic deformation characteristics (1) when loaded parallel to laminae (Sample S17)	143
6.15	Mudrock anisotropic deformation characteristics (2) when loaded parallel to laminae (Sample S17)	144
6.16	Strain anisotropy shale (Sample S17) when loaded parallel to laminae	145
 CHAPTER 7		
7.1	Schematic arrangement of apparatus	166
7.2	Discharge against hydrostatic pressure for leaching experiment filter drainage, at various confining pressures	167
7.3	Calibration of circumferential measuring system	168
7.4	Deformation characteristics of triaxial apparatus with perspex pedestal and platen arrangement - used in leaching experiment	169
7.5	Leaching experiments - stress paths	170
7.6	Leaching experiment 1 - physical monitoring	171
7.7	Leaching experiment 2 - physical monitoring	172
7.8	Experiment 1 - Leachate analyses (1)	173
7.9	Experiment 1 - Leachate analyses (2)	174
7.10	Experiment 2 - Leachate analyses (1)	175
7.11	Experiment 2 - Leachate analyses (2)	176
7.12	Stress/strain curve for specimen L2 loaded to failure	177
7.13	Qualitative elemental analyses by SEM micro analyser - experiment leached mudrock specimens	178
7.14	Uniaxial compressive strength (determined using the NCB cone indenter) against moisture content, for two mudrocks, specimens from which were used in laboratory leaching tests	179

CHAPTER 8		Page No.
8.0	Selected limestone thermal gravimetry curves	189
8.1	Limestone strength representation and specimen data (11 sheets)	190
8.2	Limestone deformation under uniaxial compression (4 sheets)	201
CHAPTER 9		
9.1	Summary of rock discontinuity shear strength investigation	231
9.2	Definitions a) Bearing ratio b) High spot count and peak frequency	232
9.3	Typical discontinuity roughness profile with JRC characterisation after Barton & Choubey (1977)	233
9.4	Bearing ratio and peak frequency curves for typical joint profiles characteristic of JRC values (fig. 9.3 & Barton & Choubey (1977))	234
9.5	Tentative relationship between Bartons JRC, bearing ratio and peak height	235
9.6	Field record sheet - Schmidt hammer results	236
9.7	Examples of discontinuity profiles measured in the field	237
9.8	An example of chart recorder trace for dilation and horizontal movement recorded during laboratory shear box tests	238
9.9	Typical shear strength/normal stress plot for basic angle of friction tests	239
9.10	Morphology and wear - laboratory formed indirect tensile fractures tested in shear (5 sheets)	240
9.11	Graphs of shear strength against normal stress for rough joints with no correction for slope or roughness	245
9.12	Drained shear box test deformation graphs - remoulded WV mudrock (S21)	246
9.13	Drained shear strength of remoulded completely weathered mudrock material (sample S21)	247

	Page No.
9.14 Shear strength of mudrocks sheared along a predetermined plane orthogonal to the laminae	248
9.15 Shear strength of mudrocks sheared along a predetermined plane parallel to the laminae	249
 CHAPTER 10	
10.1 Arrangement of Demec points rock face monitoring. Dimhole (SS 95210 67619)	255
10.2 Change in discontinuity width and bed thickness against time measured at Dimhole (SS 95210 67619) between February 1980 and December 1981.	256
10.3 Change in discontinuity width, bed thickness and temperature against time - measured at Dimhole (SS 95210 67619) on 25/8/81.	257
10.4 Details of initial survey - March 27th 1981 - tension crack east of Nash Lighthouse.	258
10.5 Tension crack monitoring, east of Nash Lighthouse (SS 92990 67648).	259
10.6 Tension crack east of Nash Point (SS 92990 67648) - Geomorphological surveys.	260
 CHAPTER 11	
11.1 The development of instability, and proposed post-blasting profile where mudrock dominant lithology is exposed in the lower part of the cliff.	268
11.2 Stability Analysis SS 927 677	269
11.3 Stability Analysis - Tresilian (SS 94560 67740)	270
11.4 Stability Analysis - Unstable block - SS 92990 67648	271
11.5 Sketches relevant to torsion.	272

LIST OF TABLES

		Page No.
CHAPTER 2		
2.1	Synthesis of depositional and post-depositional history	4
2.2	Zonal succession in the Lower Jurassic of Glamorgan after Hallam (1960)	9
CHAPTER 3		
3.1	Analyses of rainwater collected at Nash (SS 917 682)	26
3.2	Analyses of various waters sampled from the field area November 22nd 1982	27
CHAPTER 4		
4.1	Compass/dumpy level survey closing errors	77
4.2	Dimensions of third counting net used in stereonet program	78
4.3	Discontinuity spacing after the Geological Society Engineering Group Working Party Report (1977)	79
4.4	Block size after the Working Party Report (1977)	79
4.5	Aperture of discontinuity surfaces after the Working Party Report (1977)	79
CHAPTER 5		
5.1	Mudrock terminology after Stow (1981)	118
5.2	Rock colour after the Engineering Group Working Party Report (1977)	118
5.3	Cementation classification for laminated calcareous mudrocks	119
5.4	Weathering/alteration grades (Working Party Report 1977)	119
5.5	Simple summary of weathering processes after Krumbein & Sloss (1958 in Fookes Dearman & Franklin - 1971)	120

	Page No.
5.6	Sample descriptions (mudrocks)(3 sheets) 121
5.7	Thermal gravimetry - mudrocks (3 sheets) 124
5.8	Pyrite stability numbers and potential mudrock weatherability 127
5.9	Engineering Index properties - mudrocks 128
 CHAPTER 6	
6.1	X-ray diffraction data for the size fraction coarser than 2 μm - 3 pretreated mudrocks 146
6.2	Approximate mineralogical composition of 3 mudrocks 147
6.3	Mineralogy of the clay sized fraction 3 mudrocks 148
6.4	Diagnostic x-ray diffraction data for Mg^{2+} - saturated clay minerals after Bullock & Loveland (1974) 149
6.5	Potassium & Aluminium oxides extracted by $\text{HCl}/\text{H}_2\text{O}_2$ digestion, expressed as a percentage of the total estimated phyllosilicates. 149
6.6	Cation analysis of free salts (neutral Ammonium acetate extraction) - for 3 mudrocks 150
6.7	Cation analysis of $\text{HCl}/\text{H}_2\text{O}_2$ extraction for 3 mudrocks 150
6.8	Procedure for diagnostic staining of carbonates after Dickson (1965) 151
6.9	One dimensional consolidation tests - 3 remoulded mudrocks 152
6.10	Conditions - laboratory controlled environment tests 153
6.11	Mudrock compression tests 154
 CHAPTER 7	
7.1	Details of specimens used in leaching experiments 180
7.2	Analyses of leaching experiment blanks and leachate 2L11 181

	Page No.
7.3 Thermal gravimetry - Laboratory leached specimens	182
CHAPTER 8	
8.1 A morphological limestone classification	205
8.2 Limestone classification based on composition - Folk (1959 & 1962) in Tucker (1981)	206
8.3 Limestone classification based on depositional texture - after Dunham (1962) with modifications of Embry and Kolvan (1972) in Tucker (1981)	206
8.4 Sample descriptions : limestones (3 sheets)	207
8.5 Limestone Index properties	210
8.6 Thermal Gravimetry limestones (2 sheets)	211
8.7 Comparison of carbonate content determinations (CO ₂ loss) by Schrotters apparatus and thermal gravimetry	213
8.8 Strength testing specimen schedule	214
8.9 Summary of Brazilian (indirect tensile strength) test results	215
8.10 Strength test specimen tolerances	216
8.11 Typical specimen record sheets	217
8.12 Various observed failure modes of cored specimens tested in uniaxial and triaxial compression	218
8.13 Rock deformation under uniaxial compression - specimen data and synthesis of results	219
CHAPTER 9	
9.1 Limestone discontinuity laboratory shear tests - synthesis of results (2 sheets)	250
9.2 Data relevant to drained shear box tests - remoulded completely weathered mudrock: sample S21	252
CHAPTER 10	
10.1 Tension crack morphology photographs.	261

LIST OF PLATES

CHAPTER 2		Page No.
2.1	Shear lens in mudrock (horizon 24a) - the result of horizontal shearing during flexing Nash Point (SS 915 682)	11
2.2	Chevrons on 350° striking discontinuity surface at Dimhole (SS 952 676)	11
CHAPTER 3		
3.1	Water sampling - seepage from horizon 28a Gwter Fawr (SS 91680 68094)	28
3.2	Water sampling - seepage from horizon 49a east of Nash Lighthouse (SS 92700 67700)	28
3.3	Oblique aerial photograph - in the vicinity of Whitmore Stairs (SS 898 713)	29
3.4	Oblique aerial photograph - showing wave refraction looking west along the Bristol Channel from Summerhouse	30
3.5	Plunging wave during abating storm, taken west of Nash (SS 916 679)	31
3.6	Small fall at Summerhouse (SS 99580 66425), first noticed after the storm of 13th & 14th December 1981	32
3.7	Flooding and storm damage; Col-Huw (SS 997 664) - 14th December 1981	32
CHAPTER 4		
4.1	Cwm Bach (SS 896330 71850)	80
4.2	Cwm Bach (SS 89730 71640)	81
4.3	Whitmore Stairs (SS 89885 71335)	82
4.4	Platform and cliff south east of Gwter Fawr (SS 90520 69900)	83
4.5	Variation in discontinuity frequency - Gwter Fawr (SS 90520 69900)	84

	Page No.	
4.6	Notch in the lower part of horizon 47a at SS 91615 68140 (80m North of Gwter Fawr)	85
4.7	Fall debris and fault east of Gwter Fawr (SS 91720 68080)	86
4.8	Caves under Nash Lighthouse (SS 91840 68040)	87
4.9	Cobble wedged notch - Horizon 28a east of Nash Lighthouse (SS 92320 67860)	88
4.10	Variation of discontinuity frequency and curvature in the horizontal plane and within the same strata - east of Nash Lighthouse (SS 92520 67760)	89
4.11	Site of large toppling fall - PRE-EVENT (SS 92700 67715)	90
4.12	Aerial photograph, site of large toppling fall - PRE-EVENT (SS 92700 67650)	91
4.13	Aerial photograph, site of large toppling fall - POST-EVENT (SS 92700 67650)	92
4.14	Toppling fall west of St. Donats Point (SS 930 676)	93
4.15	Well ordered toppling fall debris west of St. Donats Point (SS 930 676)	94
4.16	Toppling fall west of Tresilian - PRE-EVENT (SS 94550 67740)	95
4.17	Toppling fall west of Tresilian - POST-EVENT (SS 94550 67740)	95
4.18	Cliffs east of Maidens Folly (SS 95100 67620)	96
4.19	Buckling of strata west of Col-Huw (SS 95470 67525)	97
4.20	Large intact block part of a translation fall east of Col-Huw (SS 96095 67345)	98
4.21	Wedge failure - strata above horizon 21. west of Summerhouse (SS 98965 66570)	99
4.22	The cliff west of Summerhouse (SS 99290 66460)	100
CHAPTER 5		
5.1	Sampling (S14 & S15) Summerhouse (SS 99580 66424)	101
5.2	Micrograph of fractured surface, specimen S14 - perpendicular to laminae	129

5.3	Micrograph - fabric sample S19 - perpendicular to laminae	129
5.4	Sampling site (S18) Col-Huw (SS 95460 67523)	130
CHAPTER 6		
6.1	Inter-laminae sulphates - specimen S11 after prolonged storage	155
6.2	Micrograph of a fragment, sample S11: fractured parallel to bedding, stained with alizarin - red - S/potassium ferricyanide solution	155
6.3	Micrograph of a fragment sample S11 fractured perpendicular to bedding	155
6.4	Scanning electron micrograph of a low angled (near parallel to bedding) discontinuity - Sample S11	156
6.5	Scanning electron micrograph of a plane perpendicular to the bedding - sample S11	156
6.6	Triturated sample from S21 stained with alizarin - red - S/potassium ferricyanide	157
6.7	Triturated sample from S21 stained with alizarin - red - S/30% sodium hydroxide solution	157
6.8	Scanning electron micrograph of a plane perpendicular to laminae - sample S21	158
6.9	Scanning electron micrograph - sample S21	158
6.10	Scanning electron micrograph fragment-Sample S21	159
6.11	Micrograph of a fragment sample S24 fractured perpendicular to the bedding, and stained with alizarin - red - S/potassium ferricyanide solution.	159
6.12	Micrograph of thin section, - sample S24. (Orientation parallel to bedding.)	160
6.13	Micrograph of thin section, - sample S24. (Orientation perpendicular to bedding.)	160
6.14	Micrograph of thin section - Sample S24. (Orientation perpendicular to bedding.)	161
6.15	Scanning electron micrograph of a plane perpendicular to bedding - sample S24. Following etching with 20% hydrochloric acid (X200)	162

	Page No.	
6.16	Scanning electron micrograph of a plane perpendicular to bedding - sample S24, following etching with 20% hydrochloric acid (X2000)	162
6.17	Scanning electron micrograph of a near horizontal tectonic fracture surface, Sample S24	163
6.18	Sample S11. - Exfoliation on immersion in water after oven drying at 80°C	164
6.19	Triaxial compression failure modes, specimens from sample S17	165
6.20	Uniaxial compression failure modes specimens from sample S17	165
 CHAPTER 7		
7.1	False colour near infrared-Summerhouse (SS 99580 66424) - the seepage horizon coincides with horizon 28a	183
7.2	General arrangement of apparatus - leaching experiment	184
7.3	Cored specimens from samples S24 & S11 - prepared as specimens for leaching, but air dried (not used in leaching experiments)	184
7.4	Filter drain used in leaching experiment 1	185
7.5	Monitoring for circumferential movement	185
7.6	Specimen L2 after loading to failure	186
7.7	Leached surface specimen L1 (Sample S24)	187
7.8	Leached surface specimen L2 (Sample S11)	188
 CHAPTER 8		
8.1	Limestone L2 parallel to the bedding	220
8.2	Limestone L2 perpendicular to the bedding	220
8.3	Limestone L3 perpendicular to bedding	221

	Page No.
8.4	Limestone L3 parallel to bedding 221
8.5	Limestone L4 222
8.6	Limestone L4 parallel to the bedding 222
8.7	Limestone L4 parallel to the bedding 223
8.8	Limestone L6 223
8.9	Limestone L6 perpendicular to bedding 224
8.10	Limestone L8 224
8.11	Limestone L8 perpendicular to bedding 225
8.12	<u>Angulata</u> limestone L9 perpendicular to bedding 225
8.13	Limestone L10 226
8.14	Limestone L11 perpendicular to bedding 226
8.15	Limestone L12 parallel to bedding 227
8.16	Limestone L14 parallel to bedding 227
8.17	Scanning eElectron micrograph showing coring effects 228
8.18	Post uniaxial compression test specimens L2a 228
8.19	Post triaxial compression test specimens L13a 229
8.20	Fracture surfaces, Brazilian test specimens L6b 229
8.21	Brazilian test specimens L6b 230
8.22	Well developed fracture plane chevron structures - uniaxial compression test specimen L3a7 230
CHAPTER 9	
9.1	Closely spaced planar discontinuities associated with intense tectonic shearing at Col-Huw (SS 95705 67418) 253
9.2	Apparatus used for shot blasting samples prior to determining basic angles of friction 254
CHAPTER 10	
10.1	Site of rock face monitoring - Dimhole (SS 95220 67615) 262

	Page No.
10.2 Layout of rock face monitoring - Dimhole (SS 95220 67615)	263
10.3 Tension crack monitoring (SS 92990 67648) Chainage 9.0 - 12.3m March 1981	264
10.4 Tension crack monitoring (SS 92990 67648) Chainage 13.0 - 16.0m March 1981	264
10.5 Tension crack monitoring (SS 92990 67648) Chainage 0 - 12.3m March 1982	265
10.6 Tension crack monitoring (SS 92990 67648) Chainage 7.5 - 8.8m March 1982	265
10.7 Tension crack monitoring (SS 92990 67648) Chainage 7.5 - 8.8m March 1983	266
10.8 Features associated with secondary lines of weakness, site of tension crack monitoring (SS 92990 67648) March 1983	267
10.9 Features associated with secondary lines of weakness, site of tension crack monitoring (SS 92990 67648) March 1983	267
 APPENDICES	
Appendix 1	273

CHAPTER 1
INTRODUCTION

1.1 General Introduction

Magnitude of natural forces, and inherent topographical/geomorphological complexity of coastal areas mean that defence works are expensive, and all too often less than 100% successful.

"Retreat of cliffs implies a complementary broadening of the wave cut platform in front. This in turn reduces the energy of the waves that reach the cliffs until it becomes negligible" writes Holmes (p. 835 1965).

In reality, a constantly fluctuating sea level, and relatively small losses in wave energy due to sea bed friction, results in this being far from true.

Therefore, waves, and in particular storm waves, often attack shore lines with great ferocity. Effects of resulting erosion are more concentrated at, or near, mean high and mean low water levels where processes operate for longer. (Carr and Graff 1981.) Consequently marine erosion is effective in impairing cliff stability by toe erosion.

Spectacular slides are a characteristic feature of cliffs in weak argillaceous rocks of Southern and South-East England. These have attracted many workers, see for example Hutchinson (1965a, 1965b and 1965c) and Bromhead (1978 and 1978). Although modes of failure and mechanisms for rock slopes are well documented; e.g. Hoek and Bray (1972), little work has been done in relation to cliffs in lithified rocks. A notable exception is the work by Hutchinson (1970) on near vertical chalk cliffs at Joss Bay on the Isle of Thanet.

Research, quite rightly, is demand generated. Local Authorities have the responsibility under a 1949 Act of Parliament to maintain and

defend the coastal area. High vertical sea cliffs in well lithified rock are usually fairly remote from centres of population, buildings are only infrequently located in close proximity to the cliff edge, and beaches, if they do exist, are often only poorly developed and inaccessible. Consequently, such areas are designated 'low amenity value'; - with apparently small annual rate of cliff recession, little concern and only academic interest is generated.

The study area has recently been designated of 'high amenity value', in so much that it has been given Heritage Coast status. Although there are few buildings or structures of any importance, Local Authorities are only too aware of their responsibilities to the rapidly increasing number of users. In response, the Welsh Office sponsored this project to :-

- 1) Investigate mechanisms of instability
- 2) Make recommendations for possible low cost remedial measures.

1.2 Setting

A Pliocene shore platform (North 1929) and with a height above sea level of less than 100m A.O.D. (Above Ordnance Datum), the flat topography of the Vale of Glamorgan (for location see inset to fig. 1.1) contrasts with the more rugged upland scenery of the South Wales Coalfield, which is characterised by its steep sided U shaped valleys. Small agriculturally based communities of the Vale also contrast sharply with the highly industrialised ribbon development in the coal mining valleys, and large industrial centres such as Cardiff and Swansea.

Rocks of this coastal plateau largely comprise rapidly alternating limestones and shales of the normal offshore Blue Lias facies. A simplified map (fig. 1.1) shows the geology of the area in terms of major stratigraphical units. The study area is confined to the Heritage Coast and to cliffs comprising offshore facies only.

Sea cliffs along some 16km of coastline between Trwyn-y-Witch (SS 890 726) and Summerhouse Point (SS 995 663) largely expose Lower Lias lithologies of the bucklandi and angulata zones. Relevant Lower Lias stratigraphical zones are noted in table 2.2. Relative thickness of shales and limestones vary considerably throughout the succession both locally and between more widely spaced horizons. Such variations in lithologies are obviously highly significant in the context of stability. In the laqueus subzone mudrocks dominate, limestone bands are thin, widely spaced, highly discontinuous and frequently take the form of discrete nodules; stability is controlled largely by the engineering properties of the shale. Within the limestone dominant bucklandi zone, rock mass geometry and the degree of interlock are **important**, but so is the durability of intercalated shales. Where, for example, toward the top of conybeari subzone shale content locally increases, a marked line of weakness is found.

A number of workers, North (1929), Goskar and Trueman (1934), and Driscoll (1958) found evidence of different neogene marine planation levels in the Vale of Glamorgan.

The conjectured position of the 60m (210ft) Pliocene shore line defined by Driscoll (1958) is shown on figs. 1.2 and 1.3. Cliff top elevations to the north east of Nash Point frequently rise to over 60m A.O.D. Between Nash and Col-Huw, levels rarely exceed 35m A.O.D. while the cliff from Col-Huw to Summerhouse Point approaches datums of 50m A.O.D. Cliff top topography follows the line of the gently flexed Blue Lias strata, Upper bucklandi limestones form a competent "cap rock" resistant to erosion. Consequently where anticlines expose large thicknesses of angulata strata, cliff heights approach a maximum. At Whitmore Stairs, the highest location along this stretch of coastline 72m A.O.D., an anticline exposes some 40m of offshore facies angulata zone strata in the lower cliff and the more massive limestones of the littoral facies (Southern Down beds) in a shore platform elevated several metres above adjacent beaches.

Although erosion has been effective in removing strata above the bucklandi zone at most locations, considerable thicknesses of the more argillaceous semicostatum strata still exist at Gwter Fawr (SS 915 683), St. Donats (SS 935 677) and Lewis Thomas Stairs (SS 939 677).

Marine erosion is the most active instigator of instability. Formation of caves along major discontinuities and selective erosion at certain stratigraphical horizons, indicate both discontinuity and lithological controlled marine erosion. However, subaerial processes are also actively involved; degrading rock fabric, and opening discontinuities with a consequent loss in rock mass strength.

Rock falls and slides vary considerably in magnitude and mode from in excess of 30,000 tonnes to a single block or a small amount of debris from the cliff top. Failure modes considered include toppling, and translation along near vertical discontinuities. Rotational failure has been recognised by Williams (1980) in highly degraded material at Trwyn-y-Witch.

Although remarkably uniform in appearance, engineering and physical properties are far from such. Both marine erosion and subaerial weathering are active in the development of instability. The morphogenic environment is probably amongst the most aggressive in temperate zones; the tidal range in the Bristol Channel being one of the largest in the world.

This case study sets out to examine mechanisms contributing to the development of instability, develop a rationale for identifying impending instability, and suggest viable engineering solutions. Mineralogy, engineering and physical properties and physico-chemical behaviour of representative rock types have been investigated, coupled with an extensive programme of field work in an attempt to achieve this.

1.3 Terminology

Where necessary, explanation is given in the text, but in the main,

terminology in common use is given no such explanation. Terminology used in rock mass description and mapping is primarily that used in the Geology Society Engineering Working Party Reports (1972 and 1977).

1.4 Previous and Contemporary Studies related to the area under investigation

The writer is aware of only two papers which are directly concerned with aspects related to the engineering geology. Nevertheless, studies related to the area and which have a bearing on cliff instability are reviewed. Previous work related directly to the geology is considered in Chapter 2.

A contemporary study by Williams (1980) is the only work to the Authors knowledge directly concerned with engineering geology aspects of cliff instability. From an investigation in the area of Dunraven Bay/Trwyn-y-Witch (SS 886 727 - SS 890 7250), involving three lithologies :-

- i) Carboniferous limestone
- ii) Marginal Lias
- iii) Blue Lias

he concluded that instability was largely controlled by lithology and the presence or absence of discontinuities in the rock mass.

Recognising that undercutting was highly significant in the development of instability in the Blue Lias, he also demonstrated how both toppling and translation could occur.

In 1969 an unsuccessful attempt was made to stabilize, by blasting, a short trial section of cliff immediately east of Col-Huw Point (SS 958 673). Whilst removing dangerous overhangs and scarping the face to a safer angle it was intended that the blast debris would provide a protective apron against marine erosion. Williams and Davies

(1980) investigated the reason for the unsatisfactory performance of this apron. By 1978 marine action had removed half of the apron, and three further falls had occurred. They ascertained, by pebble tracer experiments, that material lying in close proximity to the cliff was moved along shore in an easterly direction more rapidly than material in a more seaward position; this is attributed to platform topography. Williams and Davies (op. cit.) also note that rock mass weakening has occurred. In the close proximity of the valley the limestones exhibit a vertical planar cleavage in two directions, 350° and 260°. The cliff adjacent to the valley is poorly restrained and blasting has clearly caused a number of these cleavage planes to open.

The rate of cliff recession is a subject which has attracted a number of workers, North (1929), Keatch (1965) and Trenhaile (1969). North suggested that remnants of iron age earthworks provided a method of estimating cliff recession. Several such earthworks are to be found along the coast. North considered topography and the strategy of the defensive earthworks at Nash (SS 914 684), and suggested that this encampment extended to its contemporary cliff line. He was thus able to conjecture that sea levels had been stable since construction i.e. 2000 years.

By tentative reconstruction of these forts and assuming a construction date of 2,000 years B.P. (Before Present), Trenhaile (1970) arrived at the following estimates for annual recessions :

- i) Cwm Bach (SS 897 717) 183mm/p.a.
- ii) Whitmore Stairs (SS 898 712) 584mm/p.a.
- iii) Col-Huw (SS 967 673) 610mm/p.a.
- iv) Summerhouse (SS 994 664) 407mm/p.a.

Wave energy is reduced by friction as it travels through shallow water. Drury (1976) indicates that these losses are small. However, if platform recession is greater than cliff recession, wave energy at the base of the cliff will increase. Trenhaile found no evidence of

a submarine cliff at the low tide mark. However, by comparing mean low tide marks on the 1875 and 1914 6" O.S. map he noted considerable advances up the foreshore, which he tentatively attributed to marine erosion. These were :-

- i) Cwm Bach (SS 987 711) - 54.9m
- ii) Nash Point (SS 914 683) - 27.5m
- iii) St. Donats Point (SS 934 676) - 24.2m-54.9m
- iv) Tresilian (SS 946 676) - 22.9m
- v) Col-Huw (SS 962 673) - 61.0m
- vi) Stout Point (SS 973 668) - 10.6m
- vii) Stout Bay (SS 978 671) - 91.5m

Keatch (op. cit.), assuming that the coastline of 2,000 B.P. approximated to the 5 fathom submarine contour, postulated the following annual cliff recession rates :

- i) Trwyn-y-Witch (SS 884 726) - 335.5mm/p.a.
- ii) Nash Point (SS 914 683) - 94.5mm/p.a.
- iii) Col-Huw (SS 955 674) - Lavernock Point (ST 188 681) - 549mm-640mm/p.a.

Trenhaile (1969) was primarily concerned with shore platform and high water ledge development. He recognised that certain shales were more readily quarried by marine erosion, and demonstrated that cliff ledges in the Vale of Glamorgan are dependent on lithology rather than former sea levels.

A small pebble beach is common at the head of rock platforms. Under tranquil conditions constructive waves develop a typical steep 'swell' profile. A protective apron is formed and even if the tide reaches the cliff, much of the wave energy is dissipated. However, when storm conditions prevail the swell profile is destroyed, material is spread over the platform, protection is greatly reduced and beach material provides ready 'ammunition' for wave attack at the foot of the cliff.

Contemporary sedimentology has been studied by Keatch (op. cit.) and Caldwell (1983). Keatch concentrated his work in Porthkerry Bay (ST 090 667). In observations on beach stability he noted that pebbles were concentrated on the most exposed part of the bay, and that the morphology fluctuated in the fortnightly cycle, with seaward extension during spring tides. Caldwell (op. cit.) chose two study areas :

- i) A high energy beach, immediately north-west of Nash Point (SS 915 683)
- ii) A low energy beach, Gileston beach (ST 015 663)

Classifying pebbles according to shape, he found that of an initial pebble tracer population deposited at Gileston, those subsequently located showed dissimilarity between :-

- i) Returned tracer populations and original tracer populations.
- ii) Individual tracers on the beach surface and neighbouring material.

From his results he was able to modify a model for selective sedimentary river deposition to explain beach sedimentation.

On both the high energy beach of Nash and the low energy beach of Gileston, he noted changes along the beach in sediment size and shape distribution. This was most pronounced at Nash with a marked increase in sediment size to the north-west.

Caldwell (op. cit.) also carried out experiments in the swash zone to measure swash force, breaking wave height, period and swash velocity, and pertinent results are reviewed and discussed in section 3.4.3.

1.5 Scope of present investigation

Chapter 2 The unconformity between Lower Lias and Carboniferous

limestone of the Glamorgan coast has, not surprisingly, attracted considerable attention, but until fairly recently relatively little work had been carried out on the Blue Lias facies. In this chapter, Geology, including depositional and post-depositional history, stratigraphy, sedimentary geology and tectonic structure, is reviewed and discussed in respect of available literature, and context of this work.

Chapter 3 The Bristol Channel can be classified as a macro-tidal storm wave environment (Trenhaile (1971)). Data relating to the morphogenic environment from available literature, contemporary weather data and tidal hydrographs, is presented.

Chapter 4 Includes a description of techniques used to facilitate field surveys and the acquisition of field data. Ten maps with associated descriptions (section 4.3) detail the engineering geology and geomorphology, focusing primarily on that relevant to cliff stability. Cliff stability is discussed in section 4.4 and mechanisms involved in translation and toppling falls presented.

Chapter 5 Variation in mineralogical composition, fabric and weathered state means that mudrocks exhibit a range of durabilities and strength. In a programme of testing, 27 mudrocks were examined. Fabric descriptions, major mineralogical phase chemistry and engineering index properties are reported. A mudrock classification for durability in a marine environment derived from the results is presented.

Chapter 6 Details and discusses the implication of an investigation into the mineralogy chemistry and physico-chemical behaviour of three of the mudrock samples tested as part of the programme described in Chapter 5. These samples were essentially end members i.e. the most competent fresh unweathered, incompetent fresh unweathered and incompetent completely weathered.

Chapter 7 Trenhaile (1971) and Keatch (1965) both refer to vadose

water leaching shales and effecting a reduction in strength. This chapter describes a laboratory experiment to investigate the effectiveness of leaching as such an agent.

Chapter 8 Morphologically, limestones range from discrete nodules to flaggy beds, often with thicknesses in excess of 500mm. Representative limestone samples are classified and described. Stained thin sections are described and micrographs presented. Thermal gravimetry was used in an attempt to quantify major limestone mineralogical phases and although not a great deal of confidence is placed in the results they are reported and discussed. A programme of strength testing to determine uniaxial, brazilian and triaxial strengths vertically and in two orthogonal directions are presented using the empirical criterion of Hoek & Brown (1980). Deformation under uniaxial compression was determined for several samples in up to three directions. Stress/strain curves and elastic constants are reported.

Chapter 9 It had originally been intended to adopt the discontinuity shear strength criterion of Barton (1971 and 1973). Back analysis of tests along rough limestone discontinuities, a programme of field work and computer analyses of surface roughness led the writer to suggest that an empirical relationship between normal stress and shear strength was more applicable to discontinuity shear strength in the Lower Lias of South Wales.

Colluvium derived from weathered mudrocks frequently gravitates into open discontinuities. If the discontinuity is sufficiently opened so that interlock of the rough limestone surfaces is lost, the shear strength reduces to that of a soil (Barton 1974). Drained shear box tests in remoulded completely weathered mudrock are reported. Shear strength of laminated mudrock parallel and perpendicular to laminae are also presented.

Chapter 10 Relevant subaerial weathering processes and their significance are considered in section 10.2.

At Dimhole, monitoring was installed, across a shale and several discontinuities, on a rock face freshly exposed by a recent fall. A graph of movement against time showed poor correlation but overall trends appeared extensional. Monitoring temperature against movement over a twelve hour period demonstrated why. Implications of these results are considered in the light of a higher than usual number of rock falls in the Summer of 1983.

Rock falls where the cliff is solely within the bucklandi zone are sudden and usually without warning. Consequently, recognisable tension cracks are unusual. One such crack did develop and was monitored during the course of this investigation. Results are presented and discussed.

Chapter 11 Analyses of two toppling falls and a site of potential instability is presented. In these analyses it was necessary to consider the influence of torsional restraint along discontinuities striking orthogonally/near orthogonally to the cliffs. Limiting ultimate torsional shear strength along critical orthogonal planes is reported.

In section 11.3 a strategy for cliff stabilization/protection works is considered.

Chapter 12 In the concluding chapter the major findings are summarised and possible future work is suggested.

1.6 Summary

In section 1.1 it is indicated that although many workers have been attracted to the cliff stability problems posed by the argillaceous sea cliffs often found in South East and Southern England, comparatively little work has been carried out on sea cliffs cut in well lithified rocks. This is attributed to their often geographically remote position, consequent lack of cliff top structures of great importance and designation as a low amenity

value. The Lower Lias cliffs of Glamorgan are afforded high amenity status by virtue of their designation as a Heritage Coast, and this provided the impetus for this Welsh Office sponsored study.

In section 1.2 the geographical variation between the Lower Lias of Glamorgan and the carboniferous Coal Measures to the north are contrasted. Major variations in Lower Lias stratigraphy and lithology are also referred to, as is the development of instability in the aggressive marine environment, in a brief scenario of the problem that instigated this work.

Terminology is that in common use and where necessary appropriate explanation is given in the text (section 1.3).

Literature relevant to the engineering geology and geomorphology of the sea cliffs is reviewed in section 1.4. Papers by Williams (1980) addressing cliff instability, and Williams and Davis (1980) discussing an attempt to stabilize the cliff at Col-Huw by blasting, are the only papers directly concerned with the engineering geology.

CHAPTER 2

GEOLOGICAL SETTING

2.1 Introduction

Ager (1974) in an introduction to the South Glamorgan Lias, commented that

"...the magnificent liassic cliffs of Glamorgan are probably the most neglected of all the much studied Jurassic cliffs of Britain....."

Even so, treatise on Geological aspects far outnumber those on other subjects related to this thesis. In this chapter, rather than attempting to review in sufficient detail to give due credit to such valuable work as that, for example, of Strahan and Cantrill (1904), Trueman (1920a, 1922 and 1930), Hallam (1960) and Wobber (1963), the writer's review concentrates on aspects which have particular relevance to this work.

The interested Engineer, with perhaps a limited knowledge of geology, is recommended in particular to read the Heritage Coast Guide to the Geology by Perkins, Gayer, Baker and Williams (1979).

To set the scene : Rocks of the off shore facies (i.e. laid down in deep water) which comprise rapidly alternating limestones and mudrocks, grade laterally westward into the more massive limestones of the near shore facies (i.e. laid down in shallow water) and these lie unconformably on Carboniferous limestone. This unconformity between Lias and Carboniferous rocks can be examined between Ogmore (SS 860 750) and Trywn-y-witch (SS 886 725).

2.2 Depositional and Post Depositional History

Rock mass behaviour is often significantly influenced by its depositional and post-depositional history. Major events are reviewed in this section and summarised in table 2.1.

2.2.1 Permian to Tertiary

Rapid erosion of Carboniferous strata that had been uplifted, folded and faulted during the Variscan Orogeny occurred in the hot and arid desert environment of Permian and Triassic epoch. Perkins, Gayer, Baker and Williams (1979) estimate that some 4600m of Upper Carboniferous rocks were removed from the Vale of Glamorgan, exposing Lower Carboniferous limestones. At the start of the Hettangian stage, a slowly retreating shoreline had resulted in submergence of much of the Vale of Glamorgan. Fig. 2.1 shows the probable extent of Carboniferous islands.

The unconformity and transition over a distance less than 1km of littoral Lias to the normal rapidly alternating limestones and mudrocks was recognised by De La Beche (1846). Tawney (1866) divided this transitional Lias into two lithological units.

i) Sutton Stone - ranging from massive to thinly bedded. When fresh it is bluish-grey in colour, but weathers to a creamy white colour. The basal 1.5m is conglomeritic, containing abundant pebbles and occasional boulders. Above a distinctive horizon 10m above the base, the limestone becomes more thinly bedded and is described by Hallam (1960) as only slightly conglomeritic with clast size generally not exceeding 25mm in diameter. Calcirudites are largely confined to horizons immediately overlying irregular partings.

ii) Southern Down beds - overlying the Sutton Stone are thin bluish-grey brown weathering calcilutites and subsidiary shelly calcarenites up to 0.6m in thickness, separated by marly partings with a maximum thickness of 0.6m (Hallam op.cit.).

There appears to be little doubt that the sediments for these rocks were derived locally from respective islands - Arkell (1933) and Wobber (1963). Not truly littoral in character, Hallam (op. cit.) considered these rocks to be more correctly described as near shore facies, while the rapidly alternating limestones and mudrocks laid

down in deeper water he termed the offshore facies. Lateral gradation from near to offshore facies is schematically represented in fig. 2.3 which also serves to emphasise that the near shore facies is diachronous throughout at least the planorbis angulata and bucklandi zones. No stratigraphical horizon above the semicostatum zone has been recognised. However, Ager (1974), reviewing the Jurassic, cites evidence to suggest that Wales was largely submerged beneath the sea, early in and throughout much of the Jurassic. i.e. at Mochras (approximately 3 miles South West of Harlech) some 1300 metres of Jurassic strata was measured; at Prees, in Cheshire, 123 metres of Lower Lias capped by 30 metres of incomplete Middle Lias; and an estimated 1600 metres of Jurassic strata in the Bristol Channel (Donovan, Lloyd and Stride 1971).

By the end of the Kimmeridgian period the Jurassic sea had receded from all except Southern England. North (1929) suggested that the magnitude of uplift was slight, and that under such conditions erosion was unlikely to have been rapid. Resubmergence took place in the Gault and Upper Green sand times. Wooldridge and Linton (1938) map the Vale as submerged but close to the palaeo-shoreline. No evidence of chalk has been found but it has long been conjectured that a considerable thickness was deposited over most of Wales (Ramsey 1878 in George 1974):

Earth movements, forerunners of the Alpine Orogeny, uplifted the area at the end of the Cretaceous period (North op. cit.). During Tertiary times erosion removed the majority of Mesozoic strata. Evidence of this erosion is still apparent in the Vale. Indicated in figs. 1.2 and 1.3, is the 63 metre Pliocene shore line, which is one of several well defined ancient shore lines of the Neogene (Driscoll 1958).

It is generally accepted that the stepped plateaux of South Wales are remnants of Neogene wave cut platforms (George 1974).

Tectonic structures in the Lower Lias of the Vale of Glamorgan have

long been attributed to the Alpine Orogeny. George (op. cit.) contends that many predate this, and that considerable orogenic activity occurred from mid-Mesozoic times, although he does concede that there was intensification of orogenic activity in mid-Tertiary times.

2.2.2 Quaternary

Although the lack of drift deposits indicate that the Vale was beyond the extent of the maximum Devensian ice advance, there is evidence of earlier glaciation. Strahan and Cantrill (1904) describe fills and erratics found to the north of St. Mary Church (ST 002 716) and Merthyr Mawr (SS 883 764). They inferred from the shell debris in the Pencoed drift that it did not form part of the South Wales ice sheet. Pre-Devensian Irish Sea ice invaded the Vale of Glamorgan, this was proved by both Griffiths (1940) and Crampton (1966) who traced distinguishing heavy minerals as far west as Cardiff. Fig. 2.4 shows the maximum advances of Wolstonian and Devensian Glaciation as plotted by Culver (1976).

Beyond the maximum advance of Devensian ice, the Vale of Glamorgan experienced a prolonged peri-glacial environment. Frozen ground meant that melt waters were largely conveyed in swollen surface streams - today the relatively high permeability of the bucklandi zone, and the much reduced volume of water, means that many valleys are dry, or at best convey 'misfit streams'. Upper limestone strata are often frost shattered and covered with a veneer of head deposits.

In two valleys, e.g. Cwm Macroes and Cwm Nash, angular fragmented limestone forms solifluction deposits, these are overlain by weakly cemented sands which include several vegetable soil horizons. By examining snail species within the deposits, Evans and French (in Perkins et. al. 1979) have been able to reconstruct post-Devensian climatic conditions (fig. 2.2). The junction of pene-contemporaneous hill wash deposits and cemented sands occurs at a date horizon 300 B.C., it would appear that a minor change in sea level then resulted

in terrace formation. At Nash - terrace level in close proximity to the beach is approximately 14.00m A.O.D. (fig. 4.8.4).

Adjacent to discontinuities, limestones and shales are both stained yellow brown and weakened. Evidence suggests (Chapters 5 and 8) that they have been leached. A majority of these discontinuities do not now convey water and consequently this weathering must have occurred during wetter periods in geologic history; i.e. :

i) During the warmer periods of periglacial environments, when thawing permafrost would allow considerably swollen glacial meltwater ready egress through the rock mass.

ii) Climate fluctuated during glacial interstadials, and it seems likely that during wetter periods some leaching may have occurred.

iii) From fig. 2.2 it is possible to conjecture periods post dating the Devensian glaciation which were wetter than the present day, but it is unlikely that even with a rainfall in excess of 250mm per annum, weathering on the scale evident would have been effected.

An increase of more than 120metres from the sea level of the Wolstonian glaciation accompanied the Ipswichian Interglacial. The raised Ipswichian Interglacial Patella beach at Gower, which is approximately 15 metres above the present day sea level gives an indication of relative levels (Bowen 1974). The maximum extension of Devensian ice occurred 20,000 - 17,000 years B.P., and sea level dropped to 130metres below those of present (Bowen 1974).

By 8,900 years B.P. the sea had invaded Swansea Bay and reached the position of the present coastline (Culver 1976); eustatic rise continued until about 5,500 B.P. The Flandrian transgression was followed by a minor transgression, circa 3,400 years B.P. (Goodwin and Willis 1964). The so-called Scrobicularia clay, noticed by Strahan and Cantrill (1904) on the foreshore half a mile west of Limpert Bay (ST 012 662) is attributed to this transgression.

The sea level has been relatively stable for the last 2,000 years (North 1929). However, North, in his treatise on the evolution of the Bristol Channel, describes major events leading to erosion and loss of land; e.g. Tusker Rock, which is now 2 km off shore and covered by every tide was recorded by him to "have been within living memory a sheep pasture".

2.3 Stratigraphy

The stratigraphical succession for the Glamorgan Lias was largely established by Trueman (1920, 1922a and 1930) and is confirmed by Hallam (1960) as being essentially correct. Strata correlation based on the distribution of various ammonites and as modified by Hallam (op. cit.) is recorded in table 2.2. Along the 16km of cliff line between Trwyn-y-witch (SS 886 725) and Summerhouse Point (SS 995 663)(the extent of the study area), the only planorbis zone rocks exposed are of Southern down beds type lithology of the near shore facies (Wobber 1963). Although the existence of gmwendense subzone has been established at Gwter Fawr (SS 915 680), because of inaccessibility both Hallam (1960) and Wobber (1963) were unable to ascertain the sub-zone thickness or the presence of higher sub-zones.

At Lewis Thomas Stairs (SS 937 677), a trough fault, the increase in mudrock/limestone ratio suggests rocks of the semicostatum zone. More accessible than those at Gwter Fawr they offer an opportunity for a stratigrapher to examine in some detail the upper horizons of the remaining Glamorgan Lias succession.

Identifiable ammonites within these Lower Lias rocks are rare, and the problems presented by few, poorly preserved or fragmented ammonites, particularly in the more calcareous bucklandi zone, have been referred to in principal stratigraphical studies, i.e. Trueman (1922a), Hallam (1960) and Wobber (1963). The problem led Trueman (1922b) to propose the evolutionary trends of the commonly occurring oyster gryphaea as a correlation fossil. Although now shown by Hallam (1959) to be unsuitable, the work of Trueman (1920, 1922a and

1930) remains a most valuable source of information. In particular, Trueman (1930), in mapping the bucklandi zone at Nash Point (SS 915 683) indicated distinctive horizons which can be readily recognised along the whole 16km section. The bucklandi zone is essentially continuously exposed in this length of cliff and the great value of Truemans section (fig. 2.5) which provided the basis of strata correlation in this work, will become obvious to the reader in Chapter 4.

Horizon identification is not so readily achieved within the angulata zone. However, unlike the bucklandi zone, where there is considerable rapid variation in vertical lithology, and particular horizons significantly influence cliff stability, local variation in lithology is less pronounced and far less significant in terms of stability.

In the Glamorgan succession, lithology does vary with stratigraphy and Hallam (1960) has graphically represented limestone/mudrock ratios of the offshore facies rocks for Glamorgan, Dorset, Tolcis (near Axminster) and North Somerset (fig. 2.6). The very low limestone/mudrock ratio of the laqueus sub zone is readily recognised where exposed, e.g. east of Trwyn-y-witch and at Whitmore Stairs. Although more calcareous than the laqueus, the limestones in the angulata sub-zone are more consistently flaggy or semi-hummocky (table 8.1) varying in thickness between 100 and 300mm, and it is the consistency of lithology that distinguishes it from the bucklandi zone rocks. The buckland/angulata contact as defined by Trueman (1930) is readily determined by the location of bed 5 (fig. 2.5) which provides a fairly prominent marker band.

2.4 Sedimentary Geology and the origin of the rapidly alternating limestone/mudrock sequence

Not surprisingly, considerable attention has been focussed on the rapidly alternating rhythmic nature of the succession. Dilemma as to whether the sequence is of primary (i.e. sedimentary in origin) or

secondary (i.e. result of sediment remixing) has long been contended. Even evidence presented in this thesis, although far from intending to address this dilemma, may be considered conflicting. In section 3.2, the concretionary appearance of many of the limestones is alluded to, suggesting secondary remixing of sediments, while in Chapter 6, dealing specifically with the mineralogy and physico-chemical properties of mudrock, variation in particle size and mineralogy in the different mudrocks suggest quite different sedimentary environments, lending credence to a primary mode of formation. Hallam (1960) reviews the arguments and postulated mechanisms. Hallam (1964) proposed a model, confirmed by Wobber (1963) and involving both primary and secondary processes. He suggested that limited rhythmic remixing took place soon after deposition, and involved solution migration and reprecipitation of part of the carbonate fraction leading to the formation of the banded sequence now apparent, and explaining the concretionary appearance of many of the limestones.

* While under prep.

Wobber (1968) presented convincing micro-sedimentary evidence to suggest cyclic changes in sea levels. Variation in sea level would have resulted in variation in aerobic state of bottom water and recently deposited sediments. The more anaerobic, and the higher the pH of the bottom environment, the more conducive to the formation of stable authigenic pyrite. In Chapters 5, 7 and 8, weatherability and the apparent variation in pyrite stability is attributed to such varying bottom conditions.

Wobber (1965) identified four morphological types of limestone. In table 8.1, nine morphological types are detailed, including two composites. However, with the exception of a limestone nodule sample L2 (table 8.5), all showed similar 'intact' mechanical properties. Mineralogy and petrography is dealt with subsequently - Chapters 5 and 6, Mudrocks; and Chapter 8, Limestones.

Post depositional structures increase towards the near shore facies (Wobber 1967). Not all undulations in the limestone can be

attributed to secondary migration. Load casts, the result of unequal loading of soft calcareous mud by overlying calcilutites are an example of early post depositional structures commonly seen and are described by Wobber (op. cit.). Late post depositional structures described by Wobber (op. cit.) include inter stratal sliding and boudinage.

2.5 Tectonic Structure

Along the 16km section of cliff a series of gentle folds with wave length varying between 1 and 2 km, are exposed. Principal Axes are indicated on figs. 1.2 and 1.3, and these plunge gently in a west south-west direction.

Horizontal and low angled discontinuities are common in the laminated mudrocks and are attributed to flexure induced horizontal shearing of strata. Plate 2.1 shows a shear lens in horizon 24a at Nash Point (SS 915 683). These horizontal discontinuities are highly significant to the processes which are active in the degradation of the cliffs.

The most apparent discontinuities run vertically/near vertically through the cliff, bisecting both limestones and mudrocks, but frequency is generally greater in the former. Master and major discontinuities often persist throughout the full height of the cliffs. Discontinuity stereonets at thirty-two locations along the field area are reproduced in fig. 4.2. Roberts (1974) has carried out a survey of tectonic structures along the foreshore between Ogmere (SS 860 750) and Lavernock Point (ST 188 680). Between Col Huw (SS 964 675) and Trwyn-y-witch (SS 885 727) he notes that a 350° - 330° striking double discontinuity set dominates, with a 185° - 190° trend becoming increasingly apparent at higher stratigraphical levels and east of Llantwit Major. Discontinuity surveys in this work concur, although because primarily concerned with stability, surveys have not been limited to measuring master and major discontinuities only. Discontinuity systems commonly observed in the platform and plotted by Roberts (op. cit.) are reproduced in fig. 2.7.

Numerous small movement faults, displacement less than 1m., are common, persisting laterally for several hundred metres and vertically for the full height of the cliff. Fault zones are narrow, and invariably less than 2 metres.

Major fault strikes are marked on figs. 1.2 and 1.3. Roberts (op. cit.) notes that there are four major sets, each exhibiting strike and slip dip:-

Set 1 - 350° to 330° strike - the dominant set, and exhibiting right-hand strike slip.

Set 2 - 215° to 190° strike - a strong trend similar to Set 1 only with left-hand shearing.

Set 3 - 295° to 280° strike - subordinate to sets 1 and 2, usually right-hand shearing.

Set 4 - 260° to 250° strike - the subordinate fault trend.

Thrust faults are apparent at two sites along the 16 km field area section, at Trwyn-y-witch (SS 887 726) and Pigeon Point (SS 970 671), and at both of these sites they are associated with drag folds.

A considerable amount of mineralisation is associated with these tectonic structures; infilling minerals are usually calcitic or dolomitic and euhedral calite crystals are frequently to be found in major discontinuities.

Roberts (op. cit.) considers that the Lias fractured as a single structural unit and that existence of N.N.W. and W.N.E. conjugate shears are indicative of a major sub-horizontal principal compressive stress, acting in a north-south direction.

The small dihedral angle, Roberts (op. cit.) suggests is either

indicative of extensional fracture or interference patterns produced by azimuth variation of a single, but divergent joint set.

The propensity for chevron marked discontinuity surfaces (e.g. plate 2.2) were noted by Roberts (op. cit.) who expressed the opinion, proved in this work (section 8.5.5), that they are the result of tensile stress induced fracturing or the propagation of existing fractures in a tensile type mode.

Roberts (op. cit.) stated that chevron markings are indicative of high strain energy. It occurs to the writer that, on the basis of work described in section 8.5, they also suggest that strain energy is largely dissipated as crack surface energy, as postulated by Griffiths (1921) for flow induced brittle fracture.

The small dihedral angle observed in the horizontal plane (i.e. less than 30°) between many discontinuities in major sets is frequently evident in both vertical and horizontal planes. Conjugates of major sets are often not differentiated between by stereonet plots (fig. 4.2.3) but implied only by the elongate shape of population contours and polar plots.

The small dihedral angle between discontinuity pairs suggests an intermediate sub-vertical principal stress and a minor east-west principal stress. Surface fracture markings are conducive with markings on extensional fracture surfaces, and therefore it seems likely that stress levels in the east-west direction must, at the time of fracturing, have been orders of magnitude lower than the other principal compressive stresses.

Frequency of vertical/sub-vertical fractures typically varies between 200mm and 2m (e.g. plate 4.5 - classification wide to very wide - table 4.3), and component rock blocks are tabular. Although many master and major discontinuities persist both horizontally and vertically over several tens of metres, fracture frequency generally decreases as thickness and competence of limestone increases and in mudrock as ductility increases; which is conducive with a tensile fracturing mode.

Roberts (op. cit.) also noted micro jointing described in section 8.2.5. His study was sufficiently detailed to identify two well defined sets, which were not associated with major discontinuities, and assign global strike trends of 280°-285° and 190°-195°. Roberts (op. cit.) indicated that as far as he was aware, similar micro jointing had only previously been described in crystalline basement structures and therefore such jointing appears to be somewhat unique.

2.6 Summary

Fabric, rock mass stress state, weathered state and weatherability to some extent depend on the sedimentary environment and subsequent events. A study of relevant literature has been reviewed in section 2.2. Major events affecting the Lower Lias rock mass are summarised in table 2.1.

Trueman (1930) studied the stratigraphy of the bucklandi zone at Nash Point. He indicated several horizons within the sequence which could be readily recognized and used as marker bands (section 2.3). Consequently Truemans system of numbering (fig. 2.5) has been adopted in this work.

Only rocks of the angulata, bucklandi and semi costatum zones are represented in the offshore facies.

Although the exact delineation between ammonite sub-zones by fossil evidence is complex, limestone/mudrock ratios (fig. 2.6), and other lithological characteristics vary giving sub-zones quite different distinctive appearances.

The limestone, particularly those of the bucklandi zone, frequently appear to be concretionary. Other evidence suggests that no large scale remixing of sediment took place. Hallam (1964) postulated that the limestone/mudrock rhythm is largely primary in origin, with some solution, migration and reprecipitation of the carbonate phase.

Described in section 2.4 this mechanism explains the apparently conflicting evidence in Chapter 6 where mineralogy and particle size suggest a primary mode of formation, and Chapter 8, which suggests that the majority of bucklandi limestones are concretionary.

Tectonic structure is described in section 2.5. The most important discontinuity set in terms of instability is the double set striking at 330° - 350° and it is conjectured that at the time of fracturing the minor principal stresses in the east/west direction were orders of magnitudes lower than the north/south major and vertical intermediate values.

Horizontal discontinuities within mudrocks, the result of folding induced intra-strata shearing, are also described. Where exposed to wave action these lines of weakness are readily exploited by erosion processes.

It was not the writers intention to provide a broad review of geology in this chapter, but rather to hone in on aspects of particular relevance to this study. The interested reader is recommended to the several texts referenced, and perhaps as an introduction the Heritage Coast Guide by Perkins, Gayer, Baker and Williams (1979).

CHAPTER 3

MORPHOGENIC ENVIRONMENT

3.1 Introduction

In a high energy marine environment such as the Bristol Channel, it might appear that other morphogenic factors are insignificant. However, although marine erosion is irrefutably the major instability instigator, it gradually became apparent that other factors were significant; i.e.:

- i) Temperature (incidence of failure increased during extreme climatic conditions - both hot and cold)
- and
- ii) Rainfall (wetting and drying influences, rock strengths, moisture controlled movements and durability).

Temperature, sunshine hours, rainfall, wind and tide data are presented in this chapter together with discussion and data appertaining to the marine environment.

3.2 Rainfall and Temperature

On the basis of temperature and rainfall, Petlier (1950) classified morphogenic environments (fig. 3.1a); fig. 3.1b shows the relative importance of various weathering modes, within these classified environments. Therefore, on the basis of rainfall and temperature only, and according to Petlier (op.cit), rocks of the field area are likely to experience moderate chemical weathering with frost action.

Groundwater level is below the intersection of the platform and sea cliff. Less competent shales and the more argillaceous Angulata zone effectively form impermeable horizons to vadose water. Therefore although small in extent, restricted by intersecting major discontinuities, perched water tables develop. Seepage from sea cliffs is intermittent. In wet periods there is a rapid response to

increased rainfall, while during extensive dry periods seepage is relatively non-existent, and very low discharges are confined to a few locations, usually gouge filled faults. Therefore, vadose water and perched ground water appear to be largely derived from local rainfall. Although significant hydrostatic disturbing forces are unlikely to develop in the rock mass, resisting forces are modified. Consequently, local rainfall is highly pertinent. Monthly rainfall measured at Rhoose (ST 063 679) for the years 1980 - 1983 inclusive is recorded in fig. 3.2.

Rainwater collected on the cliff top at Nash (SS 917 682) was used in leaching experiments described in Chapter 7. Chemical analysis of rainfall collected at various times of the year and during different weather conditions are recorded in table 3.1. (Collection method and details of analytical procedures are described in Chapter 7). Fig. 3.3 shows relevant wind roses. Following prolonged dry periods, pH values indicated an increase in acidity. The high ionic strength of rainwater sample RW6 collected under storm conditions, is indicative of contamination from sea spray. Similar conductivity for rainwater collected at Marcross (SS 925 692), also under storm conditions, suggests that rain over a large area is so contaminated, and consequently water introduced into the vadose zone can vary considerably in quality.

The risk of cliff falls is greater during extremes of temperature (chapter 10); ice action is not the only mechanism, relatively small temperature and moisture controlled movements in rock material can modify resisting forces sufficiently to instigate instability. Weekly maximum and minimum air temperatures for Rhoose (ST 063 679) for the years 1980 - 1983 inclusive are recorded in fig. 3.4, and the weekly total of sunshine hours for the same period in fig. 3.5.

3.3 Chemical Analysis of Sampled Waters

Locally derived rainwater percolating into the vadose zone has a high oxygen content, and may be acidic or contaminated by sea spray (table

but only on one occasion exceeded 3.5m, and at sites B and C seldom rose above 2m. Although the H.R.S. found that relationships between wind speed and wave conditions were influenced by a number of different factors; e.g. storm duration, variability of wind speed, wind direction, effective fetch distance and the state of tide, they demonstrated that, in the absence of wave data, wind data could be used to identify storm generating conditions.

In section 3.4.2, wind data for the period 1.9.77 to 30.4.83 is presented and considered in the context of earlier data. Aspects of coastal zone hydraulics with relevance to cliff stability is considered and discussed in sections 3.4.3, 3.4.4, 3.4.5 and 3.4.6. Conditions and effects of a severe storm on the 13th and 14th December 1981 are also described (section 3.5).

3.4.2 Wind

The computer program of Caldwell (1983) was used to analyse and present wind data from Rhoose (ST 063 679) in rose diagram form. The rose provides a measure of each Beaufort scale wind frequency, as well as cumulative direction frequency - an explanation is given in fig. 3.7. Wind roses of average hourly wind speeds for the periods 1.9.77 to 31.12.80, and 1.1.82 to 30.4.83 are given in fig. 3.8. Dominant wind direction is westerly. The number of occurrences where average hourly wind speed exceeded force 7 are noted in brackets at the top of each frequency block. The wind rose for the first period shows 8 such events, while for the shorter second period 43 events were recorded. Reference to fig. 3.9 suggests that these observations fit in with an increasing trend, and that gale frequency may be cyclic.

3.4.3 Waves

The interested reader could be referred to a number of texts for exposition on wave theory and coastal hydraulics, e.g. Muir Wood (1968). Caldwell (1983) deals with aspects of coastal hydraulics appertaining to sedimentological processes in the field area.

Deep water waves entering shallow or shoaling water (depth less than $L_0/2$, where L_0 is the wave length - Minkin 1963), are dramatically modified. Wave crests become higher and sharper, the troughs longer and flatter. Orbital velocity of water particles increases in the shoaling zone, and a wave breaks when crest velocity exceeds or equals that of the main body of water. Two types of breaking wave are common.

i) Plunging : occurring when crest velocity exceeds wave celerity.

ii) Spilling : when crest velocity remains approximately equal to wave celerity but gradually loses energy and height as water shoals.

The wave spectrum comprises both locally generated 'trains' and these originating from well outside of the area of interest. Direction range of the larger fetch distances (i.e. 5,000km) is restricted by estuary boundaries (fig. 3.10). Nevertheless the North Coast of the Bristol Channel is noted for its exposure to severe wave conditions.

Heathershaw, Carr and King (1980) explain:

".....Wind transfers energy to the sea over a wide range of angles up to 45° on either side of the direction in which it is blowing. Thus open ocean fetches are a measure of the wave energy arriving at a point from a similar range of angles"

From 1951 data Keatch (1965) identified that, on most days, more than one swell train entered the Bristol Channel.

In defining the wave spectrum affecting Swansea Bay (Worms head to Nash Point), Ferentinos (1978) notes that :

"....southwesterly winds can create seas and swell from storm centres as near as the Bristol Channel approaches, or as far as the outer Celtic sea. Oceanic swell enters the Bristol Channel from areas of generation far out into the Atlantic and, in these circumstances, the effective fetch can be from westwards as far as the Caribbean. The wave-climate of the area under investigation is, therefore,

characterised by locally generated wind-waves (most effectively south through to south east) superimposed upon a more fully developed (but partly refracted) sea from the south-west approaches, both regimes being superimposed upon refracted Atlantic swell of much longer period and wave length....."

Dominant wave approach is 240° W.C.B. (Whole Circle Bearing); (Ferentinos - op. cit.) this coincides with prevailing and strongest winds. East of Nash Point (SS 915 683), east-west striking cliffs are relatively well protected from the full ferocity of south-west approach or Atlantic originating storm waves. North-west of Nash Point (SS 915 683), cliffs striking at 330° (W.C.B.) are orientated at right angles to the dominant 240° (W.C.B.) wave direction and exposed to their full ferocity.

Considering the geometry of the Bristol Channel, the writer was surprised to find the 330° (W.C.B.) noted as a significant wave direction (Ferentinos - op. cit.), although, ironically, the only aerial photograph readily available, and adequately showing wave hydrology in that area, depicts such waves (plate 3.3). Plate 3.4 shows the 280° (W.C.B.) striking cliffs from Summerhouse (SS 995 664 - foreground). Dominant westerly waves are advancing up the Channel.

In shoaling water, waves are refracted parallel to bottom contours and in both plates 3.3 and 3.4 refraction is occurring in close proximity to the shore. Distance between lines orthogonally intersecting wave crests can be used to estimate energy loss. Multiplied by a factor for other losses, the ratio of distance measured between adjacent orthogonals at different locations is defined by the U.S.Army Coastal Engineering Research Centre (1973) as the Energy factor. Aerial photographs (plates 3.3 and 3.4) indicate that the spacing of orthogonals at the surf zone would be very much wider than in mid channel, suggesting that only a relatively small amount of wave energy is expended on the shore under the apparent wave regimes.

Coarse sediment entrainment is greatest in the turbulent surf zone. The waves, armed with fragments, attack the base of the cliffs. Impact of high energy waves as they hurl their armoury, and abrasion

as swash, backwash and currents drag fragments across the platform and ledges, are collectively defined as corrasion (Holmes 1965).

Caldwell (1983) measured surf zone parameters on a beach directly exposed to dominant westerly waves, - north-west of Nash Point (SS 915 683). A robust device for measuring wave height was unable to sustain storm conditions, during such an event it remained in service long enough to measure a 4m high breaker. Swash velocity measured across a pebble beach, gradient typically 1 in 4 to 1 in 5, was in the range 2 to 6.5 m/sec. Recorded T_b (breaker period) values varied between 11.0 and 4.0 seconds. Longer periods characterised, but were by no means confined to, south-west/westerly swells. Corresponding deep water wave periods (T_o) ranged between 5.9 and 2.3 seconds. For completed experiments, measured breaker heights ranged between 1220mm and 300mm with corresponding \bar{H}_3 (significant deep water ave heights measured at H.R.S. buoy B) values ranging between 850mm and 150mm. The ratio of T_b to swash period (t), the time taken for a breaking wave to complete its run up the beach face, is defined by Kemp (1958, 1960 and 1963) as the 'phase difference' - he showed that this simple parameter could be used to predict beach erosion; i.e. :

Constructive - low phase difference $T_b/t \leq 0.6$

Transitional - medium phase difference $0.6 \leq T_b/t \leq 1.0$

Erosive - high phase difference $T_b/t > 1.0$

Caldwell (op. cit.) recorded a maximum phase difference of 1.32 when a strong south-westerly swell prevailed ($H_b = 1220\text{mm}$ $T_b = 8.2$ seconds). Although there was little change in profile, attributed to an already well developed storm beach, considerable beach material sorting was reported.

The maximum dynamic pressure recorded (2.5 kN/m^2) was in the surf zone of an irregular wave field (i.e. both spilling and plunging waves, $H_b = 1220\text{mm}$ $T_b = 7.6$ seconds).

As a rough approximation, the simple Bernouli relationship (3.1)

$$\frac{v^2}{2g} = \frac{p}{\rho_w g} \quad (3.1)$$

where v = velocity
 p = pressure
 g = gravitational acceleration
 ρ_w = density of water

suggests that this pressure would be generated by a swash velocity of 2.2 m/sec; i.e. less than that which is likely to have occurred.

3.4.4 Wave forces

Forces generated by breaking waves impinging on vertical barriers are frequently orders of magnitude higher than those measured, by Caldwell (op. cit.), in the swash zone. These slamming forces, or shock pressure impulses have been studied most notably by Bagnold (1939) who has deduced that a wave breaking close, and approximately parallel to a wall, will confine and compress air. Apparently, when the volume of air is large, generated pressures are not significantly larger than those developed by non-breaking waves, but a sufficiently small volume of confined air can produce an extremely high pressure impulse. From model analyses, Bagnold (op. cit.) determined the following relationship :

$$p_m \approx \frac{2.7 \rho_w U_o^2 K}{gD} \quad (3.2)$$

where p_m = pressure impulse
 ρ_w = water density
 U_o = horizontal component of orbital deep water wave velocity.
 $K = H_b/H_o$ breaking wave height/deepwater wave height.
 D = a measurement of uncompressed air volume.

Full scale measurements showed that K approximated to $H_b/5$ giving :

$$p_m = \frac{0.54 \rho_w U_o^2}{gD} \quad (3.3)$$

p_m was shown to be highly localised, occurring between still water level and breaking wave crest height.

Denny (1951) extended Bagnolds (op. cit.) work, and included an extensive survey of statistical data. He showed that, in reality, average shock pressures are approximately:

$$28 \rho_w g H_o \quad (3.4)$$

while extreme shock pressures may reach

$$110 \rho_w g H_o \quad (3.5)$$

Muir-Wood (op. cit.) also notes :

...."In practice, it is apparent that there are many factors, including dynamic response of the wall, to modify such laboratory results....."

but suggested that maximum slamming force per unit length of wave crest, could be approximated from :

$$\frac{1}{2} \rho_w g^{1/2} H_b^{5/2} \quad (3.6)$$

Dean (1966), writing on the interaction of structure and waves, considered that, in practice, only relatively few waves arrived at a structure in favourable positions to induce large shock forces, and that resulting short duration impulses from such events were not of great consequence to design. Nevertheless, a large catalogue of dramatic failures exist. The writer is aware of a storm in early 1975, at the seaside resort of Weston-Super-Mare, on the south side of the Bristol Channel, when a 5 tonne block of masonry was quarried from the upper part of Knightstone sea wall, lifted at least 8.0m, to fall through a swimming bath roof, coming to rest some 15m from its original site.

Discussion of slamming force has been largely confined to sea walls, little valid work having been done to assess such forces generated in sea cliffs. In reality, the relatively smooth face of a sea wall is much different from the discontinuous rock exposed in highly irregular cliffs. The removal of rocks by such action has been recognised and is defined by King (1972) as 'quarrying'.

Where cavities, notches or discontinuities exist in cliffs, air is likely to be trapped by breaking waves. Systems of discontinuities may be sufficiently open, permitting venting, avoiding air compression and consequent shock pressure impulses. The discontinuity system will frequently only partially vent a cavity, and reduced shock pressures will be introduced to the rock mass. However, magnitude and rate of attenuation is only partly dependent on venting system efficiency, it is also dependent on air pocket size, geometry and the degree of air compression the wave is able to induce.

The magnitude of shock pressures along the cliff, generated by a favourable wave, is likely to be varied. An upper limit is set by the hypothetical value of Bagnold (op. cit.) and a lower limit the dynamic velocity pressure head such as that measured in the swash zone by Caldwell (op. cit.).

Minkin (1963) notes that breaking waves are unlikely where water height is greater than 1.25 times the wave height. A plume of water, or clapotis, results from the collision of incident and reflected waves. Wave pressure generated by shallow water clapotis are discussed by Minkin (op. cit.), who considers that, as a reasonable approximation, maximum pressure occurs at still water level and is equal to hydrostatic pressure head of the open sea wave. Pressure at the base is equal to that at still water level, and above still water level, decreases linearly to zero at 1.66 times deep sea wave height.

At high tide there are a number of locations where the development of clapotis are likely, and such phenomenon have been noted as "a common occurrence" by Trenhaile (1967).

3.4.5 Tides and Exposure to Marine Attack

Tide predictions, assuming standard meteorological conditions, are published annually by the British Transport Docks Board.

Statistics are published in two categories :

i.e.

i) **Standard Ports** - where tides have been continually monitored for a period of at least one year (Accuracy \pm 60mm and \pm 3 mins.)

ii) **Secondary Ports** - data is determined from Standard Port predictions to an accuracy of \pm 300mm and \pm 20 mins.

Trenhaile (1967) was able to use measurements he made at Nash and Lavernock to validate linear interpolation of published tidal measurements and predictions. He noted that relatively small deviation in meteorological conditions could result in substantial difference between predicted and recorded tide heights. Exact time or height is not critical to this investigation, therefore predicted tide heights for the Secondary Port of Barry are considered sufficiently accurate, and are generally used in this thesis.

Trenhaile (op. cit.) recognised features of marine erosion above normal high tide levels. At datums of about 10.00m A.O.D. the writer has noted evidence of active marine erosion.

Under normal meteorological conditions interpolated from tide tables, heights of high tide might be expected to range between 5.8m A.O.D. (spring) and 1.6m A.O.D. (neap). Eleven tidal surges in the Bristol Channel between 1920 and 1955 raised the sea level, at Avonmouth, by between 1.8m and 3.5m (Lennon 1963). Surge associated with the storm of 13th-14th December 1981 (described in Section 3.5) raised the sea level at Cardiff by 1.50m.

Exposure to wave attack is an important parameter in assessing instability potential. In fig. 3.11 tidal data to facilitate such an assessment is presented. Neap and spring tidal hydrographs (swash/land contact plotted against time) were determined by levelling along the indicated profile line. Swash run-up is above still water level and below wave crest level. Although the major criteria for choosing the point of maximum swash advance is convenience, it can be used to estimate the total duration of cliff exposure to marine attack. Period of wave contact and wave energy are amongst major marine erosion criteria. The line of action of wave slamming forces is above still water level. Caldwell (op. cit.) reports a 4.0m high storm wave. Plate 3.5 shows a 3m high plunging wave; photograph taken to the east of Nash Point during an abating storm.

Pertinent wind roses indicate fresh westerly breezes on the 24th May 1982, and conducive to long wave period westerly swell. Plotted daily and monthly, predicted tide data (Barry) shows the hydrograph in relation to fortnightly and annual cycles.

The Hydrograph is, of course, cyclic. Amplitude about Ordnance datum is \pm 3m for the neap and \pm 6m for the spring tides. However, curves deviated from the sinusoidal. The spring high tide peak is

considerably sharper than the low tide trough, at the $\pm 4.0\text{m}$ horizons the ratio of trough to peak width is 1.67. A conjectured continuation of the neap curve suggests the same is also true.

In fig. 3.12a, high tide parts of the hydrographs (fig. 3.11) have been reproduced, and equations to estimate time of exposure to marine attack fitted; general form:

$$x = 2 \sqrt{C(A-y)^D} \quad (3.7)$$

x = duration of marine attack (Hours)

A = maximum tide height (metres A.O.D.)

y = horizon of interest (metres A.O.D.)

C and D = constants, a function of tide height A .

In developing this rationale it was necessary to conjecture a 9.0m hydrograph shown as a broken line in fig. 3.11a. Constants C and D are plotted against A in fig. 3.11b.

Unfortunately, equation 3.7 can not be related directly to intensity of cliff marine attack. Force magnitude changes through the period of contact; initially relatively low swash zone forces apply, followed by wave attack, and as water deepens, reflection and clapotis.

Extensive topographical surveying along the field area (fig. 4.8.1 to 10) can be used in conjunction with formula 3.7 as part of a marine erosion significance assessment.

3.4.6 Longshore Drift

Defined by U.S.Army Coastal Research Centre shore protection manual (1973) as

"...The littoral current in the breaker zone moving essentially parallel to the shore, usually generated by waves breaking at an angle to the shoreline....".

Muir Wood (op. cit.) notes that it is frequently of larger magnitude where tidal ranges are high.

Acting from west to east, long shore current magnitude was demonstrated by rapid removal of blast debris from the base of the cliff at Col-Huw - it was thought that this material would provide a protective apron against marine erosion. Within 10 years the blast debris has been reduced from 21,450m³ to 6,350³ (Williams and Davies : 1980).

3.5 The Storm of 13th and 14th December 1981

Immediately preceeding what was probably the most severe storm during the period of this research, was the spell of coldest weather. 40mm of lying snow was measured at Rhoose on the 12th, and maximum and minimum recorded temperatures, the lowest for December were -1.7°C and -8.2°C respectively. The storm coincided with spring tides; predicted maximum height for Barry 5.9m A.O.D. Fig. 3.10 shows that this predicted height is some 600mm below the high spring tides of 1979. A wind rose for the period 0400 hours on the 13th to 0400 hours on the 15th is plotted in Fig. 3.12.

Early on the 13th, a light north easterly breeze was blowing, this veered to a south easterly and by 1600 hours a force 8/9 gale with gusts up to 62 knots was blowing. By 2000 hours the gale had veered to a westerly, and increased to force 9, with gusting up to 65 knots.

At high tide, the predicted 2034 hours at Cardiff, a storm surge of 1.5m was recorded. During the day (0900-2100 hours) rainfall was 11.4mm (Rhoose ST063 679) and Rhoose weather station observations indicate that both snow/sleet and hail fell.

During the night of 13th/14th, wind dropped and by 0600 hours on the 14th only a moderate westerly breeze was blowing. Coinciding with high tide, wind increased to a fresh breeze, and subsequently dropped before increasing to force 8 (gusting up to 66 knots) in the early

evening. No appreciable surge was recorded for either morning or evening tide at Cardiff (i.e. 0.2m and 0.4m respectively).

The gale caused considerable damage, numerous trees were uprooted and property damaged, e.g. at Rhoose Airport the wind caused severe damage to a hangar roof.

On 14th December between Summerhouse (SS 997 664) and Monkash (SS 904 700), a 'walk over survey' was carried out. No evidence to suggest that any large falls had resulted was found. However, much fall debris would have been removed by swollen seas and the writer cannot confidently claim to have recognised all new low magnitude fall scars. Configuration of beach material was modified extensively.

At Summerhouse (SS 997 664), cliffs rapidly lose height and end. A large volume of pebbles were steeply banked up against the low cliff. Some 300mm of 3.4 metre high cliff at the extremity had been eroded. Plate 3.6 shows a small fall of possibly 50 tonnes which occurred in a deeply undercut section of 10m high cliff. Just to the west of the fall (SS 99580 66420) a block of some 150 tonne which had previously rotated approximately 5° in an overturning mode was also removed.

At Col-Huw (SS 957 674) immediately to the rear of the beach and immediately behind the car park, the Afon valley was flooded (plate 3.7). Large boulders stacked at the rear of the beach to protect the car park, were spread across it, along with a considerable quantity of beach material. Some 600mm of cliff was eroded from the westerly facing cliff end (background : plate 3.7).

At Nash, the beaches to the west and east of the Point both had a 'dragged out' storm profile, and much beach material had been eroded. Fresh fall material (approximately 10 tonnes) was noted on the 6.6m A.O.D. ledge north of Nash Point (SS 91475 68530).

Considering storm ferocity, there appeared to be surprisingly little effect.

What erosion did occur was in low cliffs where shales were comparatively more highly weathered; at Summerhouse, in the vicinity of a fault zone, and at Col-Huw a narrow spaced vertical fracture cleavage in limestone (plate 9.1) opened by blasting (Williams and Davies : op. cit.), was readily exploited.

3.6 Summary

Although perhaps the large amount of discussion dedicated to marine action is indicative of its relative significance, climatic conditions, as demonstrated subsequently (Chapter 10), are of some importance.

In fig. 3.2, presented rainfall records for the years 1980-1983, show that approximately 1000mm of rain falls annually. Chemical analysis of rainwater varied according to pre-collection climate and winds which existed at the sampling time. Under strong winds blowing off the sea, spray contaminated the rainfall for a distance of at least 1 mile inland, while after a drought and under a southerly breeze, rainfall was acidic (fig. 3.3 and table 3.1). Air temperature and hours of sunshine for Rhose are recorded for the same period in figs. 3.4 and 3.5. In July of 1983, air temperature reached a maximum for the four year period, of over 30°C.

Chemical analysis of perched ground, sea and stream water is presented in table 3.2, with discussion in section 3.3. Although chemical equilibrium with the dominant carbonate phase is suggested, the presence of sulphates in perched groundwater is indicative of the oxidation of sulphides - present in mudrocks and some limestones.

Average hourly wind speed for the periods 1st September 1977 and 30th April 1983 are presented in two similar wind roses (fig. 3.8). It is noticeable that the number of times force 7 was exceeded for the second period far exceeds the first. This fits in with a trend recognised by the H.R.S. (Hydraulic Research Station - fig. 3.9).

Significant deep water wave height measured in the Bristol Channel rarely exceeds 3.5m. Ferentinos (1978) notes that dominant wave approach is 240° (W.C.B.) and 330° (W.C.B.). Cliffs striking east from Nash Point are not exposed to a ferocity of wave attack experienced by the coast striking north west of Nash Point.

Maximum attack is achieved by waves breaking at the cliff face. Entrained sediments are the tools of corrosion and wave generated air compression, causing high shock pressures, excavate large blocks in a process known as "quarrying".

Tidal range is one of the worlds highest, and contemporary marine erosion recognised at Ordnance datums of 10.0m indicates the large extent of the marine attack zone. Equation 3.7 has been derived from measured tidal hyrographs to facilitate computation of marine attack duration.

The strength of west to east longshore drift is emphasised by Williams and Davies (1980) by their erosion measurements of a protective rock apron.

During the storm of 13th and 14th December 1981, a 1.5m surge, and winds gusting up to 66 knots (section 3.5) were recorded. Although lowland flooding was widespread and considerable damage recorded, the writer was surprised to note the little effect on cliff stability.

CHAPTER 4
GEOMORPHOLOGY

4.1 Introduction

A brief, but accurate scenario for the geomorphological processes responsible for cliff instability would be 'Marine Erosion'.

However, it was not until considerable geomorphological investigation had been carried out that the writer appreciated the complexity and the large number of aspects implied by that simple and readily defined scenario.

The collection of geomorphological and morphogenic data, although in itself very valuable and an essential starting point to any geotechnical investigation of this kind, provides no quantitative data in respect of rock material behaviour, properties and response to the environment.

Fig. 4.1 shows the significance and the importance of geomorphological appraisal to this investigation and its use, not only to define a qualitative and quantitative geomorphological data base, but in decisions relating to the subsequent investigatory programme.

In a study of this kind the collection of field data is usually limited by resources. However, this research is unusual in so much as it benefitted from the support of the Polytechnic Coastal Research Unit. This unit was set up by Dr. A.T. Williams under the auspices of the Youth Opportunities Training Scheme and provided valuable field assistance to this and several other contemporary coastal projects.

The geomorphology of the coast, and in particular the extensive broad Lower Lias shore platform has been documented by others; most notably by Keatch (1965), Trenhaile (1969) and Caldwell (1983). A

useful introduction is provided in the Heritage Coast Guide by Williams, Caldwell and Davies (1981).

In this thesis the writer has concentrated on aspects particularly relevant to cliff instability, and the interested reader is referred to the other works previously mentioned for a more general appraisal.

4.2 Procedures and Generalisations

4.2.1 Surveys for location, level and foreshore profiles

Cliff heights, inadequate landmarks and only a few locations from where the foreshore could be accessed precluded survey methods such as resection. An approximate survey method, (by engineering standards) necessitated by restricted theodolite availability, using prismatic compass and dumpy level with horizontal circle and stadia tacheometry facility, was adopted for several closed traverse surveys. Although relatively approximate, the survey method to establish level and location of sites of interest, and spot levels along the cliff base and top was considered satisfactory for the purpose of ^(cliff's location) geomorphological mapping. (Survey closing errors are recorded in table 4-1.)

Temporary bench marks were established principally at sites photographed as part of the photogrammetric survey, and sites profiled for foreshore cross sections. Topographical data, together with cross section positions are recorded on geomorphological maps (fig. 4.8). Cross sections (fig. 4.9) across the foreshore, and approximately at right angles to the cliff line, were measured using a dumpy level for both level and distance, and the latter by stadia tacheometry.

4.2.2 Photography and Photogrammetry

Measurements from near vertical cliffs, often highly unstable and from which small falls were a frequent occurrence, necessitated the

use of a photogrammetric method. Collins, Madge and Evans (1985) describe a photogrammetric method which they name 'tangential radiation'; a photo theodolite is used to take a single photograph, scales are introduced into the photograph in planes where measurement is required. Collins, Madge and Evans (op. cit.) indicate a high degree of accuracy and quote a precision of 1:500. As early as 1939 Matheson attempted such a method in an aerial survey of the River Dee estuary. Although there were clear advantages, primarily because of lens quality, accuracy was seriously impaired. Since that time lenses have been improved considerably and recently Anders and Leatherman (1982) have successfully used a similar technique for mapping records of the Nauset Spit, Massachusetts.

In this particular study, the relatively planar nature of cliff platform and coastal plateau facilitated the use of such a method. Grimes (1980) describes an investigation to appraise an application of this technique using a 35mm camera. Transparencies of a 'curtain wall' type facade with frequent and regular spaced mullion and transome members were taken using a tripod mounted Pentax K1000 camera and at angles with up to 15° deviation from the facade orthogonal. Transparencies were projected on to a purpose made tilting screen and correction for facade/camera orientation was made by movement of screen/projector to a similar orientation. Correct orientation was best achieved by scale measurement of in-plane scale controls incorporated in the photograph. In this instance a high degree of control was afforded by the regular mullion and transome members. Maximum recorded error in any of the measurements made was 3%.

The method was adopted for measurement from both terrestrial photographs of cliff and platform (the latter photographed from the cliff top) and aerial photographs. Terrestrial and aerial photographs were taken using a number of different film types, including :-

- 1) Kodachrome 64 A.S.A. film (transparencies)
- 2) Agfa dia Direct 32 A.S.A. black and white film (transparencies)

- 3) Kodak Ektachrome near Infrared film (false colour transparencies)
- 4) Kodak Infrared film (plates)
- 5) Pan f 50 A.S.A. (plates)
- 6) Ektachrome 200 A.S.A. (transparencies)

Of these films the best definition was obtained with Kodachrome 64 A.S.A. film. There was no obvious benefit gained from near infrared and infrared film.

At sites of interest, temporary bench marks were established and the cliff photographed to facilitate vertical plane measurement. Scale controls incorporated were a plumbed levelling staff clamped to a tripod, several vertical ranging rods and lines fitted with tags at 1.0m centres suspended from the cliff top.

Tagged lines were on occasions only just discernable and in recent work the writer has successfully used 2m ranging rods suspended from cliff tops.

The platform has been photographed using a telephoto lens (e.g. plate 4.5) and incorporated scales facilitated discontinuity frequency assessment.

Orientation adjusted oblique aerial photographs projected on to a 1:2500 scale Ordnance Survey maps provided valuable geomorphological detail and facilitated the plotting detail on geomorphological maps (fig. 4.8).

4.2.3 Discontinuity orientation

The representation of discontinuity orientation data using equal area stereonets together with application to rock slope stability is described in detail by Hoek and Bray (1977).

In fig. 4.2 (1-6) some 33 contoured stereonets, recording discontinuity orientation along the field area have been reproduced. The number of measurements made is indicated in brackets. Five

figure O.S. (Ordnance Survey) grid references are given and the position of each stereonet is indicated on the relevant geomorphological map, fig. 4.8 (1-10).

The horizontal/sub-horizontal population represent bedding planes. Measurement of mudrock low angled discontinuity orientation would have necessitated impracticable excavation in often notched mudrock horizons. Although orientation data would undoubtedly be of great interest to any tectonic study their role in cliff instability is one of facilitating erosion and mudrock weathering (Chapter 5 & 7); consequently their orientation is not greatly significant to rock mass shear strength.

A suite of three computer programs to run on the Polytechnics DEC 20 system were developed to plot poles and facilitate contouring of the stereonets. The first of these is listed in Appendix 1 and an outline flow chart is presented in fig. 4.3. The program generates the cartesian coordinates necessary to plot a southern hemisphere projection of poles. Using first the two counting nets proposed by Denness (1972) and secondly the net generated by the dimensions in table 4.2, population of hemisphere surface area percentile cells together with locating coordinates are determined. Sensitivity is enhanced where adjacent cell values vary. Cells are rotated by an amount equal to half the included angle formed by the two radial sides and the population again determined.

McBride (1980) wrote the two plotting routines which complete the suite of programs. 150mm diameter plots were used in this work, and reduced examples of both pole plots and polar population plots are presented in Appendix 1. Contoured plots were readily and quickly prepared from the polar population plots.

Many of the master discontinuity sets have conjugates, the dihedral angle between these conjugates is often small; i.e. less than 30° in both vertical and horizontal planes (section 2.5). The apparent 202° striking set at SS94550 67750, St. Donats - Tresilian (stereonet u -

fig. 4.2(2), and computer plots appendix 1) is an example of the contoured plots insensitivity to such discontinuity pairs. The sets are in fact a pair with one less frequent set striking at 210° and the other at 192° (pole plot Appendix 1). Although these low angled conjugates are not readily apparent from the contoured stereonet, they are to an extent implied by the elongate shape of the contour.

4.2.4 Discontinuity Persistence frequency width and geometry

Classifications adopted for the spacing and aperture width of discontinuities are those suggested by the Geological Society Engineering Group Working Party Report (1977) and are reproduced in tables 4.3 and 4.5. The Working Party (op. cit.) suggestions for classifying block size are also used and reproduced in table 4.4.

The more major and master discontinuities are often persistent throughout the full height of the cliff. However, discontinuities apparently following the same strike and thereby characterised as belonging to the same set are frequently not persistent throughout the cliff height. Variation in horizontal persistence of such discontinuities is usually not as marked, and is often in the order of several 10's of metres. The variation in stratum discontinuity frequency is demonstrated in plate 4.5, and is attributed to fracturing mode and bed competence (section 2.5).

However, with a few notable exceptions, which are referred to in section 4.3, discontinuity spacing falls within the classification 'wide to very wide' (table 4.3) and changes with such great frequency that any attempt to differentiate would be abortive.

Likewise, discontinuity aperture width, with the exception of several master discontinuities, falls within the classification 'very narrow to extremely narrow' (table 4.5).

Master discontinuities along which there has been some movement are often no more than 20mm wide and filled with a clayey gouge material.

Carbonate infilling of discontinuities is frequently observed. Along several master discontinuities the formation of euhedral calcite has been recorded. Micro and meso scale discontinuities in both limestones and mudrocks are invariably carbonate filled. The infilling carbonate is usually calcium dominant, but both magnesium and iron are frequently present (sections 6.4 and 8.2.4 and 5).

Where the ratio of length to radius of a discontinuity trace is less than $\pi/8$ the discontinuity is planar. (Fookes and Denness 1969.) There are only a few locations where this ratio is greater. e.g. East of Nash Lighthouse SS 925 677 and extending to the location of plate 4.9 but not fully apparent in that plate because of photographic scale. At this site the length/radius ratio does not exceed $\pi/4$ and under the scheme of Fookes and Denness (op. cit.), is classified semi-curved. Such large scale curvatures little affect stability; however, meso scale waviness and roughness do, and these are considered in Chapter 9.

A record of platform discontinuity traces was made photogrammetrically at each site established (indicated by T.B.M.'s on fig. 4.8 (1 to 10)) by photographing from the cliff top using a camera with a 135mm focal length lens. A triangle or rectangle of known geometry was set out on the platform and included in each photograph for scale. Although the angle between the camera axis and perpendicular to the platform was considerably greater than 15° , a reasonable accuracy was achieved because of the high degree of scale control. Plates 4.5 and 4.10 are examples of these records while fig. 4.11 shows an approximate scale reproduction from one of these photographs.

4.2.5 Accurate measurement of Strata Dips

Where indicated on geomorphological maps (fig. 4) strata dips have been determined from levelling. A dumpy level was used to determine difference in level between three points of a continuous stratum on

the platform. Distance between the three points (typically 10-15m) was measured with a linen tape and the dip, and direction of dip, computed. These values have also been used as stereonet data but statistically given a weighting of 5 because of their high degree of accuracy.

4.2.6 Stratigraphic Columns and Mudrock/(Mudrock + Limestone) ratios

Stratigraphical sections for Monknash, Nash, Tresilian, Col-Huw and Summerhouse (fig. 4.4 (1-6)) have been plotted using the photogrammetric technique described in section 4.2.2. The horizons indicated on the sections (fig. 4.4) have been found to be the most useful marker horizons in this work, remaining consistently identifiable along the length of the field area, and are indicated on several of the plates prefixed 4.

Although the sequence is highly consistent laterally, there is some gradational variation (fig. 4.5) which is reflected in the geomorphology, e.g. the low mudrock/(mudrock + limestone) ratios and greater continuity of limestones at Tresilian (map 4.7) partly contribute to the high degree of stability exhibited by the cliffs along that section.

4.2.7 Mudrock Schmidt Hammer rebound values

Between Nash Point (SS 914 683) and Gwter Fawr (SS 916 681) all bucklandi zone strata are readily accessible. Schmidt hammer hardness values, the average of the five highest from ten readings in close proximity and orientated parallel to bedding, have been determined and are reported in fig. 4.4 (2 and 3). In fig. 5.8 considerable variation of uniaxial compressive strength with moisture content is demonstrated, and, as mudrock moisture contents at the time of measurement were unknown, no attempt at strength correlation has been made. Nevertheless, because all readings were taken during dry weather in August 1981, they provide a relative measure of mudrock strength and competence.

4.8, 1 to 10) are reproduced in fig. 4.7. Many of the symbols adopted are those suggested by the Geological Society Engineering Group Working Party Report (1972).

Geomorphological maps represent a collation of data prepared from :

- 1) Walk over surveys.
- 2) 1:5000 aerial survey by Fairey Surveys in 1971.
- 3) Oblique aerial photographs taken during the course of the project.
- 4) Photography and photogrammetry.
- 5) Topographical surveys.
- 6) Discontinuity measurement.
- 7) Accurate measurement of strata dips.

Methodologies adopted are briefly described in the previous subsections of section 4.2.

4.2.10 Geomorphological Map, Toppling Fall SS 930 676

A detailed geomorphological survey has been carried out at the site of a large toppling fall and a highly unstable block, where tension cracking in the cliff top was monitored (described in section 10-4). A geomorphological map of the fall and relevant cliff detail is reproduced in fig. 4.10, and detail of platform discontinuity patterns plotted using the techniques described in section 4.2.2, in fig. 4.11.

4.3 GEOMORPHOLOGICAL APPRAISAL

Ten 1:2500 scale geomorphological maps showing sections representative of the coastline between Witches Point (SS 887 726) and Summerhouse Point (SS 996 664) are reproduced in fig. 4.8 (1-10).

Section 4.6 is split into ten subsections, each a descriptive element complementary to, and forming with the relevant map, an integral part of a geomorphological appraisal.

4.3.1 Cwm Bach

Map - fig. 4-8(1)

Section - fig. 4-9(1)

Stereonets - fig. 4-2(1)a

Section (1) (position indicated on fig. 4.9 (1)) shows a well developed 'swell' beach profile (i.e. formed during tranquil conditions). The beach crest elevated at approximately 7.00m A.O.D. (Above Ordnance Datum) suggests that during tranquil conditions the swash zone never reaches the foot of the cliff (fig. 3.11). However, during a storm the swell beach would be destroyed and the flatter storm profile, rather than protecting the beach, supplies the breaking wave with the implements of corrosion.

No well developed notches are apparent although a very shallow, rounded notch is evident for a length of some 20m just south east of the stream (SS 71850 71840) and although not readily defined, its site is shown in plate 4.1.

Cwm Bach is cut along a line of major structural weakness, structural synthesis is difficult, but it is apparent that considerable faulting has taken place. Stereonet fig. 4-2 (1)a shows directional discontinuity data measured from the cliff face and valley at Cwm Bach. Discontinuities through both angulata and bucklandi zones were frequently persistent over several tens of metres, and spacing although wide (200 - 600mm; table 4.3) is relatively close for macro scale fractures in angulata zone strata.

Cliffs along the Cwm Bach section are high, approximately 60m, and with the exception of Cwm Bach which is dipping seawards at approximately 75°, they are vertical. Although, towards the south east margin of the section, mudrock dominant laqueus sub-zone strata are exposed basally (plate 4.2) and slope seaward at approximately 65° - 75°.

The fall at SS 89590 71950 occurs at a site in close proximity to an anticlinal axis, and where tectonic fracturing is intense. A slide of highly fragmented more argillaceous mudrock material has resulted in vertical translation of limestone dominant material.

A failure of similar mode has occurred on the south side of Cwm Bach (SS 89685 71810) where translation of bucklandi strata 'en bloc' has left displaced rock 'pillars' (plate 4.1). In plate 4.2, two well defined discontinuity sets above horizon 39 (Trueman 1930), i.e. striking at 230°-260° and 148°-160° are apparent. Surfaces of these discontinuities are planar, and the shearing resistance which can be mobilised relatively small; consequently failure is readily instigated by the loss of basal support. Both sets are apparent in lower strata (stereonet fig. 4.2(1)a), but as is readily discernable in plate 4.2 the 230°-260° set generally lacks the persistence of the 148°-160° set which runs parallel to the cliff strike.

Falls not associated with major tectonic disturbances in general are of high frequency and low magnitude.

Location means that this section is exposed to the full fury of waves entering the Bristol Channel from the Atlantic, or generated in the South West approaches. The relative lack of marine notching in this environment and in low durability mudrock dominant basal strata would tend to imply high frequency, low magnitude falls.

Vadose water seeps from the cliffs at horizons where the lithology becomes more argillaceous, generally seepage is intermittent and only major lines are indicated. With the exception of the seepage line to the south of Cwm Mawr (SS 89450 72130) where the water finds egress close to the top of the cliff the seepage horizon is close to cliff mid height and approximates to the angulata/bucklandi zone junction.

4.3.2 Whitmore Stairs

Map - fig. 4.8(2)

Sections - fig. 4.9(2 and 3)

Stereonets fig. 4.2(1)b & c

Bucklandi strata form an erosion resistant capping to the cliffs. At Whitmore Stairs an anticline raises these strata to their highest elevation, attaining a level of 72m above ordnance datum. Durable strata of the near shore facies are also sufficiently elevated to be exposed in the base of the cliff, and form an erosion resistant rock platform. This platform, elevated above adjacent sand covered platforms cut in angulata zone type lithology, is characterised by higher scarps, several of which exceed 1.0m in height, and steeper platform gradients than those measured on the adjacent angulata platforms.

Platform elevation has meant that fall debris has not been readily removed by the action of the sea. Consequently an appreciable debris cone has developed and to some extent forms a protective apron.

Failure modes described for the Cwm Bach section (4.6.1) are also applicable. Although no major fault planes are apparent, discontinuity frequency, aperture of surface and persistence have been increased by tectonic fracturing associated with the close proximity of the fold axis.

The influence of the major discontinuity sets striking at 85°, 110° and 140° can be seen in the platform scarp (plate 3.3). Although it may be implied from the sharp lines of the scarp that it is receding rapidly, the upper surface has remained intact sufficiently long for solution pitting to have developed to a fairly advanced state.

To the south east of Whitmore Stairs some 250m of cliff is afforded partial protection from marine attack by the elevated platform. The more argillaceous angulata lithology below the upper vertical limestone dominant bucklandi zone strata dips at 75° to the platform and beach below.

A large amount of fall debris exists at another zone of high intensity fracturing (SS 90100 71100), similar failure modes to Cwm Bach and Whitmore Stairs are again apparent.

High level ledges exist at SS 89790 71450, and Whitmore Stairs (SS 89885 71335). The latter, shown in plate 4.3, is associated with a horizon of marked weakness (strata 21a and 28a). Immediately above, highly discontinuous limestone and weak mudrock (up to horizon 39) have been removed, and the upper cliff undermined. Intermittent seepage lines, marked on fig. 4.8(2), occur at the break in cliff slope, associated with lithology change from calcareous bucklandi strata to more argillaceous angulata strata. Ponds marked on fig. 4.2, although seen water filled on several occasions, are seen as dry hollows on aerial photograph taken during an anticyclone in January 1981 (plate 3.3). Rainfall for the month was average (fig. 3.2) suggesting that the ponds drain fairly rapidly.

4.3.3 Monknash

Map - fig. 4.8(3)

Section - fig. 4.9(4)

Stereonets - fig. 4.2(1)d

A syncline brings bucklandi strata down to a level where they are exposed to marine erosion.

Marine action exploits the least durable strata and deep notches confined to weak horizons are common. Thick shales (fissile mudrock) assessed from Truemans (1930) section (fig. 2.5) as 21a and the angulata/buckland junction bed (0a), are both notched deeply. Where strata 0a is exposed to marine attack, the cliffs above are vertical and 21a not notched. However, where horizon 0a is below platform level 21a has been eroded at datums up to 11.5m A.O.D. (Above Ordnance Datum. Horizon 28a, the least durable of mudrock strata is some 4m above horizon 21a and along this section is never deeply notched.

Datums of platforms cut in erosion resistant bucklandi zone strata between horizon 1 and 21 are several metres higher and gradients are steeper than those that are cut in angulata strata. The vertical rise of the cliff at the rear of the platform is broken by ledges. At Monknash these are within the zone of marine erosion, and undoubtedly the most prominent of these is formed by horizon 21.

Large blocks derived from cliff falls and platform destruction are strewn across the platform south east of Gwter Fawr (SS 90520 69917 - plate 4.4). These blocks, often as large as 4m x 4m x 1m are transported west to east by the action of longshore drift.

Rock mass geometry and discontinuity frequency is such that where bucklandi rocks are basal in the cliffs, small magnitude translatory falls between horizons 21 and 39 are common following the erosion of basal support.

Both the 225° and 180° joint sets are persistent vertically and horizontally over lengths in excess of 30m, and joint profiles are planar.

Frequency is more difficult to describe with considerable variation depending on the competence of the particular limestone and adjacent units. Frequency measurement showed variation from 1m to 200m (i.e. very wide to wide, table 4.3) spacing. Plate 4.5 indicates such variation within successive angulata limestone units south east of Cwm Nash (SS 90525 69900).

Abundant rock fall debris is to be seen along the ledge which has developed at horizon 21 and along a line running due north from SS 90500 69900. Much of this debris has come from fallen rock originating from below horizon 39/40; which is a thick composite limestone type VIII (table 8.1). Limestone 39/40 forms the 'lintol' strata to the caves developed along a north east striking master discontinuity (SS 90510 69950) and also acts as the major corbel

strata along the cliff to the south east of the tear fault - SS 90568 69920 (plate 4.4). Major falls where angulata strata are basally exposed in the cliff are similar to those described at Cwm Bach and Whitmore Stairs.

A vertical section together with a representation of mudrock limestone ratio has been plotted for bucklandi zone rocks of Monknash and is reproduced in fig. 4.4 (1).

Generally, vadose seepage occurs from above horizon 61, and to the north west of Cwm Nash much of the cliff face is covered by a thin tufa deposit.

The stream from Cwm Nash is a permanently flowing small stream. Solifluction deposits are overlain by weakly cemented glacial sand outwash material. Grassed valley slopes are frequently characterised by a stepped type profile, or terracettes, which are imposed on the landscape by the Lower Lias type lithology.

4.3.4 Nash

Map - fig. 4.8(4)

Sections - fig. 4.9(5, 6 & 7)

Stereonets - fig. 4.2(1&2) e,f,g,h&i

As at Monknash a syncline brings bucklandi strata to a level where they are exposed to marine erosion, which is selective, exploiting horizons of lithological and structural weakness. At some locations notch depths exceeding 5.0m have been recorded. Support to the rock column over is often enhanced by corradng cobbles becoming wedged in notches.

Fig. 4.6 shows typical lower cliff profiles measured at a number of different sites. Three of these examples are taken from this section, two north of Nash Point and the other at Gwter Fawr (SS 91615 68080). Some 80m north of Gwter Fawr a notch in the lower part of the relatively competent mudrock 47a (Schmidt hammer rebound value 38) exceeds depths of 1.0m. Marine erosion has exploited the bottom part of this stratum which is more highly fractured and shows a greater degree of weathering (i.e. WII) than that of the upper part of the stratum (plate 4.6).

At Castell y Dryw (SS 91570 68223), marine erosion has exploited lines of major structural weaknesses, and an arch and two caves have formed along master discontinuities.

A persistent discontinuity set striking at 170° is the only major discontinuity set north of Nash Point. The effect on platform morphology is clearly seen from the air and is recorded on the map. To the south, discontinuity sets striking at 146° and 131° also become significant, while west of the Gwter Fawr fault (SS 91670 61800), sets striking at 170° and 265° form major lines of weakness.

Strata dips indicated on the map are relatively steep and the large number of faults mean that, within the relatively short length of this section, the majority of the bucklandi zone strata are brought down to a level where they are exposed to marine action.

At Gwter Fawr, a scarp of 3 to 4m raises the platform to the top of horizon 55, the high durability of this strata is demonstrated by severe solution pitting; long term exposure is obviously necessary for such to have developed.

At Gwter Fawr, strata above horizon 55 are terraced facilitating examination up to horizon indicated X on fig. 4.4 (3). Below horizon 61 a number of the thin mudrocks are notched, and these contain major horizontal discontinuities with adjacent material weakened by weathering.

Above horizon 61 the texture of the mudrocks varies considerably, by becoming more silty, containing abundant bioclastic debris and with the degree of cementation often varying rapidly within stratum from strong to weak (table 5.3). e.g. sample S27 (table 5.6 (3)).

North of Nash Point and Gwter Fawr frequent, persistent planar discontinuities striking parallel to the cliff result in frequent small vertical translation type failures, as basal support is lost. Abundant debris is to be seen on the ledge (horizon 21) north of Nash

Point. Surface profiles of a minor discontinuity set striking approximately at right angles to the cliff are such as to afford some degree of interlock. A tenuous equilibrium of upper cliff strata, spanning as much as 15 to 20m in a direction parallel to the cliff, is maintained by buttressing action of basally supported end members. These end members themselves appear to be in an unstable state of equilibrium (fig. 4.12).

To the east of Gwter Fawr fault (SS 91670 68100) it is possible to surmise from the remainder of poorly orientated fall debris that toppling had occurred, probably following the removal of basal support and after translation of the rock column to the platform. Weathered, highly discontinuous upper strata translated vertically downwards and formed a graben (fig. 4.13). Plate 4.7 shows the remains of fall debris at the east end of the fall. No ledge at horizon 28 is apparent west of the low throw fault indicating quarrying of 21a which is basal. However, east of the fault which down throws strata by approximately 1.0m, a pronounced notch is to be seen in horizon 28a (elevation 7.5m A.O.D.).

Fig. 4.4 (2) indicates a relatively high proportion of mudrock in strata between horizon 28 and 39 and that limestones immediately above 28 are highly discontinuous. Consequently the durability of this zone is relatively poor. Plate 4.8 shows caves in the cliffs under the Nash Lighthouse; the basal stratum is 28 and lintol Strata 39/40 is a highly competent composite bed (type VIII - table 8.1). In the year 1860, buttressing and underpinning on behalf of Trinity House was carried out to the cliff foot for the length of the lighthouse site by a Mr. Walker. This was subsequently augmented by slight underpinning executed principally by Sir James Douglas. Trinity House have no records of any other work (Vennings 1980).

The masonry buttress, maximum height 6m, is located between SS 91790 68050 and SS 91840 68020. Underpinning is in the form of a single masonry course at the front of the notched mudrock 28a, and highly localised areas of masonry infill, most of these are to be found in the intermediate pillars between caves.

The masonry appears to have very effectively acted as a revetment. There is little sign of recent or impending large scale instability. At some locations masonry has been removed from the notches and notch depths in the range 3 - 5m were apparent. Seepage response to weather change is rapid and thin tufa deposits have formed on the cliff face.

Within the lighthouse grounds cracks have opened, several of these run along the 350° discontinuity direction, the recorded width of one such crack midway between the flagstaff and West Lighthouse is 125mm.

These are attributed to soil migration which has occurred because of carbonate dissolution, and is a feature unique to the lighthouse site, where stability has been maintained by underpinning and basal protection from marine erosion.

With the exception of the lighthouse site, the mudrock within the upper 0.75-1.5m of the cliff are highly to completely weathered, and limestones are highly discontinuous with little interlock. This upper zone slopes towards the beach with a dip often no greater than 45°. Isolated falls, and frequently just single blocks, are common from this weathered zone at the top of the cliff.

The upper cliff slope at the lighthouse site is more pronounced and stable sloping at 1 in 1 towards the platform over a height of 2 to 5m. Levels indicate a general fall towards a north/south striking valley (SS 92200 67960 - fig. 4.8(5)) suggesting that the cliff is along the line of an east/west tributary valley. Marcross Brook, is the permanently flowing small misfit stream of Cwm Macroes, a valley of similar geomorphology to Cwm Nash (fig. 4.8(3)).

4.3.5 Nash - St. Donats

Map - fig. 4.8(5)

Section - fig. 4.9(8,9 and 10)

Stereonets - fig. 4.2(2&3) j,k,l,m & n

Along this section, incompetent mudrock 28a is elevated at between 5.5m and 7.5m A.O.D. At, or close to, the cliff base it is within the zone of marine erosion and is often deeply notched.

Plate 4.9 shows how erosion is confined to the relatively incompetent lithology of this horizon. Cobbles wedged into the notch are apparent in plate 4.9. These cobbles frequently effectively underpin the rock mass over. At several locations the writer has observed fractured 'support cobbles', suggesting a high stress transfer from the overlying rock. At SS 92205 67932 notch depth exceeds 5m, the cliff face and rock mass for some 2 metres behind are effectively supported by cobbles, while the strata above, but below horizon 39, and towards the rear of the notch, have translated vertically down to the platform across the width of the notch.

Stereonets j, k, l, m and n (fig. 4.2(2&3)) show two strong discontinuity orientation trends; i.e. striking at 255° and 145°. However, infrequent but of considerable significance to stability are persistent planar discontinuities striking at 200°. Plate 4.10, taken from the cliff top shows that although remote from major structural disturbances, rapid variation in discontinuity frequency orientation and in this case curvature (i.e. from planar to semi-curved, classification after Fookes and Denness 1969) can occur within the same stratum.

Both horizons 39 and 49 are competent limestones, the former composite type VIII and the latter flaggy type I (table 8.1), and form corbel strata. At SS 92355 67883, an opening discontinuity striking parallel to the cliff and below horizon 39, indicates impending toppling, while a small toppling failure of strata below 49, and estimated at some 200 tonnes has occurred at SS 92570 67800.

Fairly large toppling failures have occurred at SS 92630 67750 and SS 92700 67715, the latter during the course of this research.

On the afternoon of July 2nd 1983, during a spell of very hot weather (fig. 3.4) and soon after a neap high tide, which would not have reached the foot of the cliff, the writer came across this fall, probably within hours of occurrence. Small rock debris, soil and vegetation were spread across the platform beyond the main cone of rock debris, and vegetation floating in the sea all suggested that the fall had been very recent and occurred in tranquil conditions. Plate 4.11 shows the cliff prior to the fall; debris from low magnitude toppling of strata below 49, and the resulting undermining of the cliff prior to the main fall are both apparent. Aerial photographs 4.12 and 4.13 show the site before and after the major fall, which is estimated to be of the order of 20,000 tonnes.

The sloping upper cliff section of the lighthouse site (described in section 4.3.4) is truncated by what would appear to be the head of a small north/south striking valley at SS 92210 67940. A small permanently running stream in the valley cascades some 20m to the platform below. As well as an established stream, the valley slopes are frequently marshy, suggesting the presence of springs.

Wet weather seepage is common from the cliff, usually from the upper strata above horizon 49 and thin tufa deposits, together with moss and lichen growth are not uncommon. At SS 92270 67910, within the confines of a graben where seepage flows are greater and less intermittent than those from the adjacent cliff, fairly thick tufa deposits have developed on the cliff face.

4.3.6 St. Donats Point

Map - fig. 4.8(6)

Section - fig. 4.9(11)

Stereonets - fig. 4.2(3) o,p & q.

Along this section, low durability mudrock 28a is never elevated above the level of marine erosion and is only elevated towards the higher limit at St. Donats Point. West of the fault (SS 93420

67680), strata rising at 5° in a north easterly direction rapidly elevates horizon 21 above the platform, and a pronounced ledge at that horizon results. Both mudrocks 21a and 28a are notched.

Strata between horizons 21 and 28 are readily eroded and where horizon 21 is below the level of the platform or beach, ledges at the level of horizon 28 do not generally develop to the same extent. Horizon 28a is rarely elevated more than 3m above the platform and is frequently below the surface of a 'swell' profiled beach. Nevertheless, it still forms a marked line of weakness and is frequently notched to depths of 5m and more.

Stereonet o, p and q (fig. 4.2 (3)) all indicate a strong discontinuity set striking at 155° and another set at 245°. It can be inferred from stereonets p and q that there is an additional set striking at 260° (the reader is referred to discussion in respect of stereonet sensitivity and discontinuity sets with small dihedral angles - Section 4.2.3).

Toppling is the common mode of failure along this section of cliff, small falls of material from below competent strata such as 49 and 39 are common (e.g. SS 93340 67650 and SS 93390 67660), and corbelling, particularly at horizon 39 is a frequent feature.

At SS 92870 67640 geometry of the failure surface and the lack of orientation and proximity of fall debris all suggest a low magnitude translatory fall (approx. 120 tonnes). The 150° striking discontinuities are highly persistent throughout the cliff height, and typically spaced at less than 400mm. Subsidiary 245° striking discontinuities are frequently truncated by the major 150° striking set.

Between SS 92950 67640 and SS 93020 67630, a large toppling fall has occurred (plate 4.14), the eastern part of the cliff, i.e. east of a master discontinuity SS 92990 67640, remains in a highly unstable condition. A detailed survey of this fall is plotted in fig. 4.10.

A part plot of discontinuity traces relevant to the fall and apparent in the platform in fig. 4.11, and cliff top tension crack monitoring of the unstable block recorded in section 10.4 also supplement the information presented in the 1:2500 geomorphological map and this section. Notching of 28a is apparent east of the master discontinuity SS 92990 67640, implying that a notch also existed at the toppling fall site immediately to the west. However the bench about which toppling took place is several metres higher (fig. 4.10) suggesting that the rock mass was effectively underpinned by cobbles wedged into any notch. The rock mass above horizon 28 but below 39 is a relatively weak zone, and although the persistence of the 240° striking discontinuities is typically less than 10m both vertically and horizontally in the lower cliff, discontinuities tend to dip into the cliff and consequently quarrying undermining and toppling is facilitated. Plate 4.15 shows the fairly well ordered fall debris of the western part. Although fig. 4.11 indicates systematic/truncated discontinuities at platform level, the back face of fall debris suggests a relatively persistent 240° striking discontinuity. A change in the persistence of the 240° striking discontinuity set is clearly demonstrated above horizon 55, in plate 4.14, where surfaces appear highly planar and the cliff face takes on a high amplitude 'saw tooth' like profile. The unstable zone of the eastern part overhangs appreciably apart from basal erosion of horizon 28a, small magnitude toppling has taken place below horizon 42, exacerbating the situation with the lower part now dipping into the cliff along a discontinuity plane at 75°. Cliff top tension cracks were first observed in March 1981 and were subsequently monitored, results and relevant discussion are presented in section 10.4.

Well ordered toppled debris, the remnants of a full height cliff fall, is to be seen at SS 93340 67650.

East of St. Donats Point fault SS 93430 67730, strata of the semi costatum zone are brought down towards beach level, and the broad valley which bisects the pliocene platform and in which Atlantic College is situated has been readily eroded in these less durable mudrock dominant strata.

Intermittent seasonal seepage sites are frequently observed along this section with horizon 49a forming the most commonly occurring seepage line. Thin tufa deposits are common, and mosses and other plants are occasionally observed on the cliff face. West of the fault SS 93420 67670 such growth is a pronounced feature.

4.3.7 Tresilian

Map - fig. 4.8(7)

Sections - fig. 4.9(12-15)

Stereonets - fig. 4.2(3&4)r,s,t&u

Although not mapped, several interesting geomorphological features exist between SS 93600 67800 and SS 94200 67880, and are briefly described in the opening paragraph of this section.

East of St. Donats, evidence of complex faulting is to be seen in the platform. West of Lewis Thomas Stairs (SS 941 677) massive competent limestones (horizons circa 49) are exposed at the base of the cliffs, and caves with horizon 55 or 58 forming lintol strata have been eroded along major discontinuities. At Lewis Thomas Stairs, a cove has formed in less durable mudrock dominant strata down thrown in a graben. Difference in lithology is clearly emphasised by the cliff profile which slopes seaward at some 70° and although steep, steps, as indeed suggested by the name, allow access to the foreshore. Another pronounced feature of this graben is the high seepage flows from side walls and resultant thick tufa deposits.

At SS 94360 67883 a persistent major fault intersects the cliff line; horizon 21, which forms a pronounced ledge is elevated some 6.0m above the platform to the west, while to the east the ledge is down thrown approximately 7m. To the west of the fault, horizon 21a and 28a are both notched, 21a more deeply; however, to the east the reverse is true.

Between SS 94550 67760 and SS 94555 67728 a large toppling fall of some 17,000 tonnes has occurred. Plate 4.16 (taken in the summer of 1978) and plate 4.17 (December 1980) show the site before and after toppling. The fall was first noted in January 1980, since that time much of the fall debris has been removed by the action of the sea. Initial configuration, quantity and subsequent rapid removal of debris, suggest that the fall occurred during the winter of 1979/80. Mudrock 28a is basal in the cliff (plate 4.16), it is notched, and the overlying rock mass effectively underpinned by wedged cobbles. Figs. 4.4 (2 & 4) show that the amount of limestone between horizons 28 and 39 has increased, nevertheless undercutting is still apparent in plate 4.16. Toppling has taken place about horizon 32a; although, at the north end of the fall the toppling bench steps up to horizon 40. It can be inferred from stereonet s (fig. 4.2(4)) that single discontinuity sets strike at 306° , 266° and 201° . Of particular relevance to the toppling fall is the apparent 201° set, the polar plot distribution indicates the presence of two sets with low dihedral angle of 18° and 10° in the horizontal and vertical planes respectively. An intersecting discontinuity pair of this set is evident in the freshly exposed cliff face (plate 17). The $192^\circ/210^\circ$ striking discontinuity pair (plate 17) about which toppling has occurred dips back into the cliff and is highly planar. Interlock with the toppled rock mass is indicated by the freshly fractured rock surfaces, and this is restricted to the north limb of the fall (i.e. along the 266° discontinuity set) and at the intersection between the 192° and 210° striking discontinuity (SS 94561 67739).

Between eastings SS 94500 and 94700, platform elevations adjacent to the cliff are the lowest recorded along the parts of the coastline considered in this project. Horizon 28 forms the platform surface, and these lower than usual levels are attributed to the lithological weakness of horizon 28a.

A large cave, known locally by two names; i.e. Reynards or Cathedral Cave (SS 94670 67730), has been quarried along a 140° striking major discontinuity, the thick competent flaggy limestone horizon 49, some 700mm thick, forms the lintol strata.

The formation of a cove between Reynards Cave and the previously described fall is attributed to a more highly fractured rock mass. Deeply notched horizon 28a was seen exposed on the east side of the cove when a storm removed much of the beach material. The cliff is undermined below horizon 39 and is corbelled between that horizon and 49.

Horizon 28a is exposed in the cliff north of Reynards Cave, although it is deeply notched it is again effectively underpinned by wedged cobbles.

At Tresilian Bay a valley has been eroded along a major line of structural weakness, the approximate position of the master discontinuity is indicated (SS 94780 67650). Vertical displacement caused by the fault is small; the approximate datum of the base of horizon 49 measured at:

- 1) SS 94685 67726 on the west side of the bay is 12.5m A.O.D.
and
- 2) SS 94848 07660 on the east side is 8.3m A.O.D.

This displacement is sufficient to lower horizon 28a to a level where it is not exploited by high tide wave attack - amongst many authors Carr and Graft (1981) have shown that erosion potential is greatest at mean high and low water levels.

The platform is elevated to approximately 3.00m A.O.D. in the vicinity of the cliffs and it is bisected by persistent discontinuities striking at 150°-170°, along which well developed runnels (or gutter shaped depressions) have been formed by the action of water discharging on to the platform via. numerous small caves, each quarried along the line of these discontinuities. Although horizon 39/40 forms the platform surface at cave sites, quarrying has often effectively removed the platform strata in the vicinity of major discontinuities and pebbles and cobbles are retained in the resulting depressions, and provide a ready source material for corrosion.

Two sections of cliff appear relatively stable, there is little sign of any recent major instability, angular surfaces have been rounded by corrasion and the distinctive yellowish brown discolouration of freshly exposed limestone surfaces (i.e. imparted by iron oxide staining Section 2.2) has been leached.

- 1) East of Tresilian Bay to Maidens Folly (SS 94810 67710 to SS 96000 67624). The most durable rocks of the sequence are lowered to platform level, discontinuities and caves are favourably orientated and consequently not directly exposed to the storm waves travelling up the Bristol Channel.
- 2) The cliff west of Tresilian Bay, (SS 94640 67100 and SS 94670 67730). Although the weakest horizon (28a) is exposed at the base of the cliff, it is effectively underpinned by wedged cobbles, and the lithology immediately above is generally more limestone dominant (fig. 4.5). Platform level is quickly elevated by strata dip to the north of SS 94670 67730, and the cliff section does not appear as stable. Along the stable section and adjacent to the cliff, datum is typically less than -1.00m A.O.D. This is some 5.0m lower than mean high water level. Clapotis have been observed at high tide in the vicinity and this is indicative of less severe marine attack than that instigated by breaking waves (section 3.4.4). Therefore enhanced stability can at least partly be attributed to datum.

Although these two sections of cliff appear highly stable in terms of large scale falls, low magnitude falls (often less than 1 tonne) are a common occurrence from the cliff top. In the upper horizons, limestones are highly fractured, possibly by the action of frost during peri-glacial times (block size small-table 4.4).

Mudrocks within this upper zone which can extend to a depth of 2.5m range from highly weathered (WIV) to residual soils (WVI - table 5.4).

4.3.8 Dimhole

Map - fig. 4.8(8)

Section - fig. 4.9(16 & 17)

Stereonets - fig. 4.2(4)v & w

Highly durable strata, horizons 39 and 40 form a plateau like platform between Tresilian (SS 64850 67655) and Maidens Folly (SS 95010 67630). Strata above these horizons are also highly durable and erosive processes have tended to exploit discontinuities rather than any lithological weakness. In the vicinity of Maidens Folly, strata dip elevates horizon 39/40 to its maximum and the platform between there and Dimhole (SS 95200 67630) steps down, exposing the weaker lithology of strata between horizons 28 and 29. With this stepping, a transition from discontinuity to lithological controlled erosive processes takes place. Plate 4.18 shows the cliff at SS 95100 67620, the low platform scarp is through horizon 33, the lintol stratum 49, and the cliff top weathered mantle similar to that described at the end of the previous section is apparent above horizon 55.

Both stereonets at Tresilian (SS 94840 67650) and Dimhole (SS 95200 67630)(i.e. u & v) indicate a strong 350°/360° striking discontinuity set. Discontinuities are planar and often persistent throughout the full height of the cliff and horizontally for distances exceeding 50m. Discontinuity spacing reduces from 1.5m - 2m at Tresilian to 600mm at Dimhole. It is suggested by stereonet v that the 350° striking set is complimented by a second set with small dihedral angle. Plate 10.1 shows a small translatory fall at Dimhole which has resulted from the erosion of basal support. This fall occurred in the winter of 1979/1980, demec point monitoring was subsequently installed and the results are presented and discussed in section 10.5.

Strata below horizon 39, with less massive and more highly fractured

limestones and weaker mudrock lithology, are readily eroded. Corbel action has principally been observed from horizons 39, 41, 48 and 49, suggesting that failure often tends to be vertically progressive.

At Dimhole, two major discontinuities indicated on the map and readily discernable in plates 10.1 & 2 have zonal widths of approximately 1.0m. Within these zones discontinuity spacing is narrow (6-20mm, table 4). This highly fractured rock is bonded by meso scale width carbonate infilling (section 8.2.5). Boundaries of these discontinuity zones are characterised by the presence of well developed euhedral calcite.

From the east of Dimhole to Cwm Col-Huw (SS 95520 67510) the cliff follows the line of what appears to have been a valley, and tributary to the Afon Col-Huw. The low cliffs are overlain by a metre or so of head deposits. Mudrocks exposed in the cliff face are moderately to highly weathered and low magnitude falls of less than 20 tonnes are common. Toppling induced by the lateral pressures from the overlying head is the major mode of failure. The cliff is afforded some protection from marine erosion by the widening of the platform at Col-Huw point, and the development of a highly stable beach. (8-10m A.O.D. adjacent to the cliff.) Plate 4.19 shows a mechanism for the reduction in width of basal support prior to toppling. Horizon 39/40 is apparent in the top part of the photograph. Mudrocks weakened by weathering and partially eroded have permitted the rock facade to buckle under the action of vertical load. Local buckling failure of the lower cliff will effectively increase the eccentricity of the load and the instability of the mass originally buttressed by the 'facade'. East of SS 95485 67520, horizon 28a, is exposed and deeply notched.

Along section line 17, platform gradient is 1 in 60, the most seaward datum recorded, -1.293m A.O.D., was 280m from the cliff. The platform at Col-Huw is much flatter and more extensive, and more highly elevated at the seaward extremity, than is generally the case:

It is strewn with frequent sub-angular to sub-rounded boulders, the

maximum axial length of the smallest typically 600mm. Where the Afon Col-Huw flows across the foreshore the platform is covered with sand.

Valleys at Dimhole and Maidens Folly are both dry, however between these two sites appreciable quantities of water seep along major discontinuities and discharge on to the platform, frequently via caves.

4.3.9 Col-Huw

Map - fig. 4.8(9)

Sections - fig. 4.9(18)

Stereonet - fig. 4.2(4 & 5)(x,y,z and aa)

At Col-Huw Point, the Afon Col-Huw, a misfit stream but the largest within the field area, spreads across the broad platform.

Stereonets w and x (fig. 4.2(4)) indicate no major discontinuity striking parallel with the valley, but strata dips measured either side suggest an anticlinal axis. The anticline (SS 96200 67220) exposes angulata zone strata in the lower cliffs; Fig. 4.4(5) suggests that some 6.0m are exposed at SS 96045 67330.

To the east of Cwm Col-Huw the cliff rises steeply to reach a datum of 40m A.O.D. at SS 96000 67340. Spacing between planar major discontinuities, often persistent for 10's of metres both vertically and horizontally, drops to less than 600mm at many locations along this section. Along some 150m of cliff immediately to the east of Col-Huw valley, joint spacing is typically narrow (i.e. 6-20mm). These joints strike parallel to the major discontinuity trends, and often, but usually only just apparent on a meso scale inspection, they are calcite filled. As a result individual blocks cleave readily along vertical planes to give them tabular like and, to a lesser extent, rod like sections. The proximity of the Col-Huw valley has facilitated weathering penetration which has extended deep

into the rock mass. Immediately adjacent to the valley, mudrocks throughout the height of the cliff have been altered and weakened by weathering. To the east, such alteration has been effected to the level of relatively impermeable horizon 28a which is always elevated above the level of marine erosion.

Good access has long meant that Col-Huw beach has been recreationally important, and the poor stability of these cliffs gives much cause for concern. A paper by Williams and Davies (1980), reviewed in section 1.4, describes an attempt, in 1969, to enhance stability by using bulk blasting techniques to profile the upper cliff and protect the lower cliff with an apron of blast debris. The attempt proved less than successful, not only did the blasting succeed in opening the 'meso scale joints' previously described in this section, but the resulting debris cone which was to provide the protective apron had, by 1978, been substantially removed by marine action.

Exposed to marine attack since the late 1970's, shallow notches less than 1m deep have been cut in a number of the weathered mudrocks, but are most persistent and pronounced in the assumed angulata/bucklandi junction bed (i.e. the bed containing two horizons of thin discontinuous limestones (fig. 4.6 and fig. 4.4(5))).

East of the limit of blasting (SS 95920 67360) a broad marine notch across several beds exists, but where the thick mudrock shown at the base of the section (fig. 4.6(5)) is exposed, this is generally more deeply notched.

Williams and Davies (op. cit.) have recorded three small rock falls along the site of blasting in the period 1969-1978. Although sections of the blasted cliff look highly unstable, the writer is not aware of any sizeable fall occurring within this section during the period of this project. However, small amounts of debris (less than 1 tonne) falling from the cliff face, and talus covered sloping benches (produced by the blasting operations), are common.

At SS 96045 67330, the basal thick mudrock (fig. 4.4 (5)) is the upper horizon of argillaceous dominant strata. To the east of the anticline (SS 96200 67220) these strata are exposed increasingly to a 5m maximum, a further low amplitude anticlinal flex ensures their continual exposure for 0.75km to Pigeon Point (SS 96960 67080 - not mapped) where an impressive fault down throws erosion resistant bucklandi strata (horizons 39 to 49) to platform level. Debris from several vertical translation falls can be observed and, at the intersection of a vertical and one of several steeply inclined discontinuities, a wedge failure of some 50 tonnes was noted.

Plate 4.20 shows a large intact block which has translated vertically (SS 96095 67345) and is part of a larger fall affecting some 40 to 50m length of cliff. The weaker mudrock dominant lithology has been eroded, and the cliff undermined. Discontinuities of the north/south striking set (stereonet aa - fig. 4.2(5)) are often persistent over 10's of metres both vertically and laterally; however, the set trending east/west is less so and affords some degree of interlock. Block size appears generally to be medium (table 4.4). The writer is unable to date this fall but from Ordnance Survey maps and aerial photographs it would appear to have occurred after 1970. Immediately west, and in the foreground of plate 4.20 (SS 96090 67330) vertical translation of angulata zone rocks located immediately above a deep cut marine notch occurred early in 1980.

Horizon 28a forms a prominent horizon indicative of inherent weakness, and suggests that it is the weakest lithology within the cliff section. It forms not only a common seepage line, but also it is notched, even though it is above the level of marine attack.

4.3.10 Summerhouse

Map - fig. 4.8(10)

Sections - fig. 4.9(19 & 20)

Stereonets - fig. 4.2(5 & 6) ab, ac, ad, ae, af & ag

East of SS 98900 66578 and as far west as SS 99200 66510, the assumed angulata/bucklandi junction bed is close to the cliff base, exposed to marine erosion and notched (plate 4.21). Immediately west of the toppling fall SS 99170 66520, horizon 0a drops below a rising beach which has accreted as a result of the groyne action afforded by the fall debris nearby. Notching and ledge formation becomes increasingly apparent in horizons 21a and 28a to the east of SS 99260 66460 and SS 99360 66430, where the dip brings each of these horizons respectively to elevations of 12.0m A.O.D.

In plate 4.22 (SS 99290 66460) horizons 21, 28 and 39 are indicated; cobbles are apparent on the narrow ledge formed by 21 and although elevated at some 15.0m A.O.D., at this site horizon 28a appears notched.

Inset in the bottom right hand corner of the geomorphological map is a typical notch profile. The lower part of the profile, i.e. that immediately above beach level, varies according to the durability of basal strata.

A profile where basal strata are relatively durable is apparent in the background of plate 4.22.

Mudrock 28a, a shale, is the least competent lithology in the field area; from the cliffs at Summerhouse, vadose water consistently finds egress from the rock mass at this horizon. Results presented in table 5.9 for sampled mudrocks and described in table 5.6 suggest that at Summerhouse this shale is particularly weak.

Comparison of stratigraphical sections (figs. 4.4 (1 to 5) and 4.5) shows that at Summerhouse, between horizons 21 and 28 mudrock percentage approaches a maximum and that the limestones are relatively discontinuous. Plate 4.21 shows a failure where a wedge in the upper part of the cliff, bounded by vertical intersecting planar discontinuities, has fallen as a result of shearing in strata

between horizons 28 and 21 along a plane dipping at approximately 45°. There are a number of similar falls, at SS 99220 66510 an inclined bench suggests such a failure, possibly of some 2,000 tonnes, and at SS 99350 66430 displacement of a 200 tonne wedge implies instability.

Toppling has taken place at SS 99170 66520, about a major planar discontinuity with a dip/direction of 80°/30° (plate 7.1). Discontinuities are orientated to facilitate toppling and although horizon 0a is below beach level, site assessment suggests that it is above platform level. Notching of this strata to the west has been demonstrated (plate 21). Erosion and notching of this strata at this site would have impaired stability to its limiting value by enhancing eccentricity of vertical load.

Toppling at SS 99520 66430 is the result of extensive notching of horizon 28a. At SS 90575 60425 the small fall noted after the severe storm of 13th/14th December 1981 is typical of frequent low magnitude falls which occur towards the end of the cliff where mudrocks (WII) have been weakened by weathering and are readily eroded.

Between SS 99290 66470 and SS 99320 66440 caves have been quarried along major discontinuities. Horizon 5 provides a competent basal strata at beach level over the short length of cliff where caves are a feature. Such competent basal strata would appear to be common to all caves along the field area. At Summerhouse the most impressive of these is quarried along a discontinuity pair with a vertical plane dihedral angle of 30°. In all cases lintol strata are below horizon 21, the small lintol spans, i.e. less than 1.0m, are indicative of a relatively low degree of strata competence.

Although corbelling is a common feature in stratum 39 and higher, rapid and frequent variation is indicative that small translatory falls are common.

4.4 Cliff Stability

In the previous section the geomorphology primarily related to cliff

stability, but specific to selected mapped areas, has been described.

In this section major factors controlling instability are considered and the mechanisms involved in failure identified.

4.4.1 Lithological Control

Although an appraisal of the Stratigraphical sections (figs. 4.4 (1 to 5) and 4.5) suggest little variation in lithology these variations do influence stability. At Tresilian (SS 947 677) the strata between horizon 21 and 39 when compared with other rocks at that location appear incompetent; however, they are competent when compared laterally with strata between the same horizons and although the basal mudrock horizon 28a, is deeply notched the cliffs on the west side of Tresilian Bay are relatively stable.

A classification of mudrock durability in a marine environment is presented in fig. 5.15. Horizons 0a, 21a and in particular 28a, regardless of location form lines of weakness which are readily exploited by erosive processes.

These three mudrocks were included in the programme of testing reported in Chapter 5. Table 5.9 indicates slake durabilities of 80.3%, 91.2% and 11.9% to 0% for mudrocks 0a, 21a and 28a respectively. Slake durability data presented in Chapter 5 suggests that horizon 0a and particularly 21a should not be so prominent as a line of weakness. Both strata 0a and 21a contain horizons of discontinuous nodular limestone, which would facilitate quarrying. Horizon 21a is immediately above a thick competent limestone and a relatively strong durable strata zone. The development of a ledge at horizon 21 means that cobbles, pebbles and fall debris which collect on the ledge provide a ready source of material for corrosion at the horizon of attack. Horizon 28a, a weak shale, is much weaker than other mudrocks of the succession and forms a marked line of weakness regardless of elevation. e.g. Plates 4.3, 4.9, 4.21 and 4.22. In an investigation into the range of mineralogy and physico-chemical behaviour and properties (Chapter 6), the relative incompetence of

this mudrock is demonstrated. Marine erosion exploits these horizons, undermining, and thereby impairing stability. The very low strength and durability of horizon 28a is demonstrated by evidence of erosion at this horizon even when elevated above the level of marine attack, and subjected to the far less active subaerial processes only.

4.4.2 Discontinuity Control

Caves form along major and master discontinuities primarily at sites where lithology in the zone of marine erosion remains intact long enough for discontinuities to be exploited by wave attack. Cave formation is indicative of relatively stable cliffs. As erosive and weathering processes continue, flat arching at lintol level (the buttressing action which the adjacent rock mass affords) relaxes and over a long period of time the lintol strata progresses up from one suitably competent strata to the next.

At Summerhouse (SS 99160 66520) and Tresilian (SS 94560 67740) large inevitable toppling falls have taken place - major discontinuities striking parallel with the cliff dip back into the rock mass at some 75°.

Horizontal/sub horizontal discontinuities within mudrocks are frequently exploited by corrasion (section 3.4.3) and quarrying (section 3.4.4) within the marine zone. Mudrock material adjacent to these discontinuities is often weakened by weathering and substantial notches develop e.g. fig. 4.6 (Gwter Fawr) and plate 4.6.

4.4.3 Rock Falls

Both translation along near vertical discontinuities and toppling are commonly observed failure modes.

Translation is particularly common where angulata mudrock dominant strata are basal. Weathering and erosion processes remove and weaken

the mudrocks, and pressure release taking place in the mudrock dominant strata (section 10.2) opens discontinuities in the overlying limestone, reducing interlock and discontinuity shear strength. Discontinuity shear strength reduction is progressive, residual soil material from the weathered mantle gravitates into the opening discontinuity and effects further opening by the mechanisms indicated in fig. 4.15. Filled discontinuity shear strength is described in section 9.3. At limiting equilibrium, resisting forces are mobilised along a critical shear plane within the reduced basal support and by shear strength mobilised along the colluvium filled discontinuity. Translation of the unstable block is associated by shearing in the basally supported mudrock e.g. Cwm Bach (SS 89680 71810 plate 4.1) and Col-Huw (SS 96095 67335 plate 4.20).

Fig. 4.13 shows a common type of toppling failure; i.e. where limestone dominant strata are exposed basally in the cliff. Erosive processes, primarily corrasion, exploit low durability mudrock horizons eroding a notch within that horizon, quarrying of the discontinuous rock mass above follows, reducing the effective basal support of underpinning cobbles. The process increases the overturning moment, and toppling occurs when limiting equilibrium is reached.

Although a major discontinuity set often strikes approximately parallel to the cliff, frequently the set along which shear strength is a minimum strikes approximately at right angles to the cliff line.

Fig. 4.14 shows an idealised sketch of a toppling failure. As a generalisation, toppling progresses in a west to east direction; i.e. in the direction of maximum wave attack. Some resistance to toppling is proffered by interlock with the rock mass behind, but the greatest proportion of resisting forces are contributed by the torsional shear strength mobilised along the discontinuity striking at right angles to the cliff (section 11.2).

A prerequisite to toppling is the establishment of a competent fulcrum point, and where discontinuity dip direction is vertical/sub

vertical rather than dipping back into the rock mass, the development of this fulcrum is less certain. Fig. 4.15 demonstrates shear and dilation mechanisms inherent in translation. Failure takes place along minimum energy paths; i.e. paths where the work to overcome resistance proffered by interlocking blocks and discontinuity shear strength is a minimum. As disturbing forces increase, response of the low elasticity moduli mudrocks (section 6.9.2) is to induce small scale articulation in the rock mass over, facilitating dilation, which is associated with low normal stress discontinuity shearing. The elastic response in mudrock increases stress levels in any intact limestone block proffering high restraint by virtue of the amount of interlock. Shear fracturing of these blocks precede translation. Dilation is enhanced by lateral pressure of any infilling colluvium material.

If eccentricity of load exists and during translation the failing rock mass establishes a fulcrum, i.e. a protruding competent limestone which may be the basal platform or ledge, toppling will occur.

Small rock falls, often no more than 1 tonne in size and instigated by subaerial processes, are a frequent occurrence from the more highly weathered upper cliff.

At several sites at Summerhouse (SS 98960 66565 plate 4.21), rock falls from strata above horizon 21 have taken place, and are the result of shearing along an oblique plane though weak mudrock dominant lithology between horizons 21 and 28a.

4.5 Summary

In section 4.2 adopted geomorphological procedures are described. Perhaps, of these, the application of a mono-photogrammetric technique (described by Collins, Madge and Evans (1985)) to 35mm photography is of most interest.

Procedural shortcomings are also noted and discussed - e.g. many major discontinuity sets have conjugates; the dihedral angles formed between these conjugate pairs is small, often contoured stereonet (fig. 4.2) do not differentiate between two such sets, and conjugate pairs can frequently only be implied from the elongated contours of a population centre.

Where the frequency of similar observations would make their reporting highly repetitive, general observations are considered adequate and are made in the relevant sub-sections of section 4.2. The frequency of discontinuities is a typical example, varying both laterally and vertically. Vertically, frequency is in part dependant on the competence of the limestone stratum, and therefore often unique to each stratum. However, spacing is almost inevitably within the range 'wide to very wide' (table 4.3 and section 4.2.4) and unless there is a pertinent exception further differentiation is not made.

In section 4.3, ten 1:2500 geomorphological maps are presented for selected coastal sections (fig. 4.8). Split into ten sub-sections, the text is written as a commentary which is complementary to these maps, although other geomorphological features are indicated and referred to, this section is strongly orientated towards the cliffs and the mechanisms which are relevant to instability.

Toppling and vertical translation are identified as the two main failure modes. In section 4.4 these are considered and the mechanisms of failure, namely discontinuity shearing, shear fracturing and dilation, identified.

CHAPTER 5

MUDROCKS

5.1 Introduction

De Freitas (1981), in his introduction to the proceedings of the Geological Societies' Engineering Group meeting on 'Mudrocks in the United Kingdom', alluded to the highly contended debate on the adoption of a 'collective term' for the range of argillaceous materials. In the absence of a more suitable alternative 'Mudrock' was adopted, and it is as such an 'envelope term' that it has been used in this thesis.

Mudrocks of this rapidly alternating limestone/mudrock succession exhibited marked variation in properties. This chapter details a laboratory investigation, in which the range of these properties and variation in major mineralogical phases of some 27 samples is examined.

5.2 Sample description

In their report "the description of rock masses for engineering purposes", the Geological Society Engineering Group Working Party (1977) recommended the use of the following indices to describe rock material.

- Rock type
- Colour
- Grain size
- Texture and fabric
- Weathering
- Alteration
- Strength

Within the Lower Lias of Glamorgan, the degree of mudrock induration is

variable and although a relationship between organic carbon and carbonate cement contents and uniaxial compressive strength is conjectured (section 5.5.2) there are a number of anomalies. In the less well cemented mudrocks, the clay phase is able to dominate mudrock physical behaviour, this ability diminishes with increasing induration (section 6.6.). Consequently, cementation is an important descriptive engineering parameter, and is included with the indices listed above.

Although the adopted descriptive scheme is largely that recommended by the Working Party Report (1977), modifications, relevant to this particular suite of mudrocks and investigation, have been made. Whereas such amendments may be pertinent to mudrocks in general, without extensive use on a variety of lithologies they must at best be considered tentative. In the following sections 5.2.1 to 5.2.7 various indices are discussed and the adopted scheme for the description of 27 sampled mudrocks (table 5.6) stated.

Terminology used is that recommended by Stow (1981) who, in an attempt to improve communication between related earth science disciplines, proposed the scheme outlined in table 5.1.

In quoting limiting particle sizes for the clay and silt sized fractions, Stow (op.cit.) is quoting the Udden-Wentworth particle size classification. Engineers conventionally used the M.I.T. (Massachusetts Institution of Technology) System (i.e. silt sized 2 - 60 μm and clay sized $< 2 \mu\text{m}$). The M.I.T. system is used in this thesis, and consequently the arbitrary maximum size of the clay sized particles is assumed to be 2 μm .

Mudrock samples were obtained from the cliff face. Recorded in table 5.6 are horizons after Trueman (1930), approximate elevation above ordnance datum, location of sampling site, in situ moisture content, sampling date and description in accordance with the scheme described in sections 5.2.1 to 5.2.8. Location and elevation data were facilitated by closed traverses, levelling and photogrammetrical surveys, and were described in Chapter 4.

5.2.1 Rock Type

The Geological Society Engineering Group Working Party (1977) recommend the adoption of a slightly modified version of Dearmans' (1974a) petrographic description. Stow's (op.cit.) basic terms (table 5.1) largely concurs with the working party recommendation.

Angulata/bucklandi mudrocks are calcareous with carbonate content typically 20-50%. When the carbonate content exceeds 50%, according to Dearmans (op. cit.) modified scheme, calcareous mudrocks should be classified as limestone. Maximum measured carbonate content of a mudrock (i.e. intercalated between stronger limestones) was 54.1% (sample S.20). Because it usurps the position of a mudrock in the rapidly alternating limestone mudrock sequence, it is considered such. Petrographic examination (section 6.5) indicated laminated structure in all 'end member' mudrocks S.11, S.21 and S.24 least competent (fresh unweathered), incompetent (highly weathered) and most competent (fresh unweathered) (plates 6.3, 9 & 11). However, the more highly indurated was non-fissile, while fissility in the less competent was well developed. Ingram (1953) and Folk (1974) both note a decrease in fissility with increasing cementation. In thin section micrograph (plate 6.13-S.24) particle orientation is discernable, but as well as increased inter-laminae cementation, patchy spar (section 6.4) also acts to decrease fissility.

Ingram (1953) noted that :

- i) fissility is associated with parallel arrangement of clay particles and that the tendency for such is enhanced by the presence of organic carbon.
- ii) fissility is reflected by colour and that darkening from grey to black was marked by an increase in carbonaceous material and fissility.
- iii) given a certain critical, but small, amount of clay, fissility is independent of mudrock particle size.

Clayton, Simons and Matthews (1982) define shale as

"..... finely laminated and/or fissile".

The term 'shale' implies fissility (Working Party Report op. cit. - and Stow, op. cit.) and in this work is only used to describe such mudrocks.

Chemical and mineralogical analyses are described in Chapter 6. Compositional descriptors (table 5.1) are used where applicable as part of a prefix to the rock name. All mudrocks are calcareous. Table 6.2 suggests that the pyrite content of all mudrocks is sufficient to warrant the description pyritiferous. In section 6.2, ambiguity in the use of the terms illite and mica are discussed. In this thesis, micaceous particles of clay size are defined as illite. Nevertheless, the mica content (micaceous particles $> 2 \mu\text{m}$) in the three mudrock 'end members' (table 6.2) suggest the descriptive prefix 'micaceous' is warranted. Organic carbon content was determined by thermal gravimetry (section 5.3.3.8) and where the content is greater than 1% the compositional descriptor 'carbonaceous' is used.

5.2.2 Colour

The scheme suggested by the Working Party (op. cit.) (table 5.2) is adhered to. Fresh (unweathered), the mudrocks grade from grey to black. Iron hydroxides, products of pyrite oxidation, impart a brownish yellow (yellow ochre) colour to the rock material.

5.2.3 Grain Size

Various rocks are designated by the prefix silt, mud or clay, depending on the relative amounts of fine grained particles - silt ($2 - 60 \mu\text{m}$), and very fine grained particles - clay ($< 2 \mu\text{m}$) (table 5.1). Based on this, and fig. 6.4, sample S.11 is clay dominant,

while samples S.21 and S.24 are mud dominant. Particle size distributions have been determined for only the three samples just referred to. However, assessment has been facilitated by these gradings, thermal gravimetry (section 5.3), index testing (section 5.4) and feel (Clayton, Simons and Matthews 1982).

5.2.4 Texture and fabric

Texture and fabric are defined in section 6.5 in which a more detailed examination of the three mudrock end members is described. Examination of fragments and triturated specimen at low magnification under an ocular microscope facilitated description.

As well as highly continuous discontinuities sub-parallel to the mudrock bedding, meso/micro scale discontinuities are common and included as a fabric element. Horizontal shearing in many of the rocks has resulted in very narrowly spaced (i.e. table 4.3 $< 6\text{mm}$), sub-horizontal and low angled discontinuities. Weak bonding between adjacent discontinuity surfaces is frequently effected by a thin carbonate infill, which is often no thicker than 0.1mm. A fracture cleavage; e.g. as in sample S.24 where fractures are spaced 5mm and dip at 8° to the stratification) might readily be confused for fissility.

5.2.5 Cementation

On the basis of the classification by Clayton, Simons and Matthews (1982) unweathered mudrocks vary in induration from strongly to weakly cemented. The large difference in behaviour of strongly cemented and weakly cemented mudrocks is demonstrated in Chapter 6.

Fissility decreases with increasing induration (Ingram 1953). A classification characterising the cementation state by the degree of fissility (table 5.3) has been developed, and is used in the description of mudrocks (table 5.6).

5.2.6 Weathered State

The definition of weathering widely accepted by Engineering Geologists; e.g. Fookes, Dearman and Franklin (1971), Dearman (1974) and Working Party Report (op. cit.) is that of Saunders and Fookes (1970) based on Weinert (1965)

"....that process of alteration of rocks occurring under the direct influence of the hydrosphere and atmosphere".

Classification has been derived from the identification of gradational, but distinctive zones within the weathering mantle.

Historical development pertinent to British practice is reviewed by Dearman (1974 and 1984).

The classification recommended by the Working Party (1977) is reproduced in table 5.4. Cripps and Taylor (1981) deleted all references to core stones, and, perhaps inadvertently, strength and volume change in a modification applicable to mudrocks. Fookes, Dearman and Franklin (op. cit.) define the three main weathering types.

i) **Disintegration** - Physical breakdown of the rock material without significant change in constituent materials.

ii) **Decomposition** - Many of the constituent minerals are chemically altered.

iii) **Biological weathering** - disintegration and decomposition by bio-chemical and bio-physical action. The process is usually subordinate to those defined in i) and ii).

Weathering processes are summarised in table 5.5. Fookes, Dearman and Franklin (op. cit.) list three conditions on which weathering rate is dependant :-

- 1) **Environment** - i.e. parent material, time scale, climate, temperature, hydrology, biological conditions and topography.
- 2) **Rock material properties**, i.e. mineral composition, weathering grade, clay content, permeability and intergranular cohesion.
- 3) **Rock mass properties** - Discontinuity spacing and rock mass permeability.

Contemporary land surface in the Vale of Glamorgan is largely the result of late Tertiary marine planation. Differential weathering is apparent in near surface limestones and shales. Usually the upper limestone typically weathering grade III (WIII) is covered by a thin veneer of weathered material WIV to WVI, often no more than 450mm thick. Limestones quickly grade to WII but very few, even where there are large thicknesses of fresh (WI) shale dominant angulata Strata above, are unweathered.

Weathering in near surface mudrocks is frequently at an advanced state (i.e. WIV to V). With the exception of the rock immediately adjacent to persistent master and major vertical discontinuities which facilitates weathering, at depths of 20 to 30m, weathering has typically graded to WIB (table 5.4).

Although the amount of finely disseminated pyrite generally appears to increase as the carbonate content decreases, its stability is greater (section 5.3.13.6 and table 5.7). Consequently, weatherability, defined by Fookes, Dearman and Franklin (op. cit.) as the susceptibility to short term weathering, is often greatest in the more calcareous mudrocks and argillaceous limestones.

In describing the weathered state of mudrock samples (table 5.6), two classifications based on table 5.4 are given

- i) Material weathering applicable to sampled material tested.

ii) Material weathering applicable to sampled and adjacent material (i.e. at sample location).

For example, samples used in index tests may comprise decomposed material only, but may have been sampled from a WIII zone.

Fookes, Dearman and Franklin (op. cit.) from their examination of rock weathering in the Dartmoor area (South West of England) concluded that in early stages of weathering mechanical processes have greater significance, while in later stages chemical decomposition is dominant.

Pyrite oxidisation is a major weathering mechanism in the Lower Lias of South Glamorgan. The typical brownish yellow discolouration of iron hydroxide/hydrated iron oxide staining means that table 5.4 can be readily applied to these mudrocks. However, more clay dominant mudrocks weathered to an advanced state with no apparent decomposition of integral pyrite have been observed. In these cases, weathering is attributed to disintegration and carbonate solution. In the following discussion a comparison is made between similar mudrocks where pyrite oxidation has and has not contributed to weathering.

Sampled from the same horizon (28a - Trueman 1930) and only separated by a small distance, Samples S.14 and S.15 (excluding surface material) both came from zones graded WIV. Unweathered, this weakly cemented shale could be considered a soil (Simons, Clayton and Matthews - op. cit.). However, although the fabric is preserved, the majority of the ^material is considerably weaker than WI samples from the same horizon (table 5.6). Fig. 5.1 and plate 5.1 show details and relative location of samples. Mineralogy determined from Thermal Gravimetry and physical and index properties are presented in tables 5.7 and 5.9. Sample S.14 black in colour, indicating no oxidation of disseminated pyrite, is friable rather than cohesive. Plate 5.2, a micrograph of a fractured fragment from this sample suggests no rehydration of clay minerals. Low angle complimentary shear micro fractures also appear open.

Although not apparent in plate 5.2, intra-discontinuity and inter-laminae sulphates (ascertained by qualitative test-section - 6.3.13.1) were common; their precipitation undoubtedly contributing to physical disintegration. Gypsum is the least soluble of the common marine evaporite minerals and consequently is the most likely precipitate to be found in marine environment exposures, and particularly so within the splash zone above high tide level. However, generally the concentration of sulphates in this mudrock is greater than those of adjacent horizons. In leaching experiment 2 (Mudrock 28a - chapter 7), sulphate concentration was restricted to the first leachate sample. Stratum 28a forms a highly effective impermeable boundary and sulphates are largely attributed to precipitation from low magnitude, intermittent seepage (section 7.1). Carbonate contents lower than those measured for unweathered samples from the same horizon (table 5.7) suggest leaching. Although elevated above the highest predicted spring tide for the years 1979-1982 (fig. 3.11), the site is not elevated above the range of marine attack. It is conceivable that sulphates are at least partially precipitated from aggressing sea water. However, the exclusion of fine detritus, relatively lack of chlorides, and relatively high sulphate content (assessed by test described in 6.3.13.1) indicate intermittent seepage as the major precipitation mechanism.

Sample S.15 was taken from a discoloured zone at the base of a major water carrying discontinuity. The material is cohesive rather than friable, a comparison of plasticity index with sample S.14 (table 5.9) suggests some rehydration of clay minerals. Modifications in clay mineralogy, the result of acid weathering are discussed in section 6.6. As might be expected Pyrite stability is similar in both samples (table 5.7) undoubtedly the discoloured zone is exposed to greater seepage quantity and various catalytic mechanisms, such as described in section 7.2, may also have been instrumental in triggering oxidation.

Seepage is intermittent resulting shrinkage and swelling is an effective weathering mechanism as is freezing (section 10.2.3).

In sample S.15, both chemical decomposition and mechanical disintegration has been active, i.e. pyrite oxidation has enhanced carbonate dissolution, and modified clay minerals. Although in sample S14 there has been a certain amount of carbonate dissolution, primarily weathering has been and is by mechanical disintegration.

The example of samples S.14 and S.15 serve to demonstrate the influence of various weathering mechanisms. Dearman (1974b) suggested different classifications for solution, disintegration and chemical decomposition. The Working Party Report (1977) emphasised that the suggested scheme (table 5.4)

"..... is not applicable to all types of rock masses and ad hoc schemes may be necessary".

Another problem, the subject of considerable dilemma - defining when a rock such as a weakly cemented mudrock (weak enough to be classified as a soil) has been sufficiently weakened to warrant the description "disintegrated or decomposed to a soil" (table 5.4).

The thermogravimetry trace for sample S.21 WV (fig. 5.2) shows considerable quantities of low stability pyrite, indicating that decomposition and modification of clay minerals is potentially still considerable. Yet the properties and behaviour of what appears to have been a highly competent mudrock (chapter 6) have been modified to that of a soil.

In defining the degree of weathering the following rule has been adopted :

Where fresh material shows signs of having been modified by weathering, and where the weathering products behave as a soil, they are classified according to the relative amounts of fresh and modified material, i.e. as in table 5.4

Clay mineral rehydration/degradation is effected by dilute sulphuric acid attack resulting from pyrite oxidation (section 6.6). Plasticity indexes of the two samples S.14 and S.15, used as examples in foregone discussion on different weathering processes, add weight to this assertion. Consequently colour, along with index properties and thermal gravimetry (table 5.7), can be assumed to be an indication of clay mineral modification. Therefore weathering involving pyrite oxidation processes is relatively easily defined and classified according to table 5.4, but processes involving mechanical mechanisms especially wetting and drying are more difficult to define (see comment relating to samples 5.7 - 5.10 incl. - discussion, section 5.5.2.)

5.2.7 Alteration

Defined by the Working Party Report (op. cit.) as:

"...Those changes in the chemical or mineralogical composition of a rock produced by the action of hydrothermal fluids..."

The definition given for weathering in the previous section excludes any alteration unless by the direct influence of the atmosphere and hydrosphere.

A thin layer or laminae of calcite is often apparent in discontinuities, and is most probably the result of tectonic pressure solution. Immediately adjacent to discontinuities, material is often weaker. It seems likely that during tectonic activity carbonates from these zones migrated to discontinuities, forming a thin calcitic layer. A similar phenomenon, the formation of a calcitic cutan on cored surfaces, the result of cutting action, is recorded in section 8.5.3.

Discolouration with some weakening is common adjacent to horizontal discontinuities in the mudrocks, and a reduction in weatherability can be partly attributed to enhanced permeability, and the result of carbonate pressure solution and migration during tectonic shearing.

Alteration, although pertinent in terms of this discussion is not used as a descriptive element in table 5.6.

5.2.8 Strength

Field estimations of strength suggested by the Working Party Report (op. cit.) are not reported, as they only serve to confirm those assessed by using the N.C.B. cone indenter (Section 5.4.7)

5.3 Thermal Gravimetry

Temperature initiated chemical reactions involving weight loss can be used to both identify and quantify reactant minerals. Analyses of 27 mudrock and 12 limestone samples (section 8.4) showed such analysis to be a powerful tool for the identification and quantification of major mineralogical phases.

A Perkin-Elmer TGS 2 thermo-gravimetry system was used. Samples were heated from room temperature to above 900°C, at 20°C a minute, and, to avoid the complication of oxidation initiated weight gains, in an inert nitrogen atmosphere.

In an inert atmosphere, organic carbon weight losses are small (fig. 5.4) and impossible to quantify from the constant heating rate thermal gravimetry method employed. The method adopted for determining organic carbon is described in section 5.2.3.8.

5.3.1 Apparatus

The Perkin-Elmer T.G.S. 2 equipment comprises a balance accurate to 0.0001 mg, its weighing pan suspended in a furnace capable of heating the sample at a controlled rate to 1000°C. A gas cylinder, connected to the furnace, provided the required atmosphere, and a restrictor valve was used to control gas flow rate.

Weight losses were measured from chart recorder plots - two traces are drawn.

- 1) Thermal Gravimetry (TG) - Weight loss against time.
- 2) Differential Thermal Gravimetry (DTG) - Rate of weight loss against time.

5.3.2 Procedure

Methods of thermal analyses are described in detail by Todor (1976).

Approximately 25mg of sample was crushed, placed in a small aluminium alloy crucible and accurately weighed in the apparatus prior to test commencement.

A twin pen chart recorder was set so that full chart scale was equivalent to 30% of the sample weight for TG analysis and DTG chart, scales were varied between 0.2 and 4.0 mg/minute full chart scale depending on the rate of weight loss, so that maximum diagnostic potential was achieved (e.g. fig. 5.2).

5.3.3 DTG Trace interpretation and Diagnostic Procedures

Interpretation is based largely on the work of Todor (op. cit.), Jackson (1979), Grim (1968) and curves for mineralogic and reagent specimens determined during the course of this work. Below the DTG graph line, (fig. 5.3) assumed boundaries of each specified weight loss are marked by broken lines. These to an extent are idealised - e.g. the presence of small quantities of feldspar were detected by x-ray diffraction (table 6.2). Standard curves for two feldspars (fig. 5.4) show only small weight losses and consequently the error incurred by ignoring feldspar is negligible.

Grim (1968) defines dehydration as:

"...the loss of any water adsorbed, interlayer or lattice OH water..."

In these analyses dehydration is used to describe loss of adsorbed, interlayer or any other held water, and the loss of OH water is referred to as dehydroxylation.

The total area under the DTG curve and areas of each numbered weight loss (fig. 5.3) were determined by means of a planimeter. Area ratios, (i.e. individual to total areas) were multiplied by the total % weight loss (TG curve) in order to determine discrete weight losses. Results for the 27 mudrocks tested are recorded in table 5.7.

5.3.3.1 90°C Peak - Largely non-structural water

Weight loss is largely attributed to non-structural water. BS.1377 (1975) recommend that for organic soil moisture content determinations the drying temperature is kept to 60°C. In these mudrocks, organic material is fully converted to carbon, and therefore stable at such low temperatures. At a temperature of 100°C Grim (1968) shows, for illite, dehydration losses of 0.5% and 1% - at a similar temperature those for mica are zero. Rehydration, an effect of acid weathering, is demonstrated in section 6.6. Consequently, on the assumption that maximum clay mineral content is not likely to exceed 30% (table 6.2), dehydration weight loss of 0.3% might be expected.

5.3.3.2 140°C Peak - Gypsum dehydration

BS.1377 (1975) test 1A recommends a temperature of 80°C when determining the moisture content of gypsiferous soils. It is generally recognised that gypsum ($\text{Ca}_2\text{SO}_4 \cdot 2\text{H}_2\text{O}$) loses $1\frac{1}{2}$ molecules of water at approximately 120°C (Uvarov, Chapman and Isaacs - 1971). The employed heating rate of 20°C is fairly rapid and therefore it is unlikely that any dehydration occurred at a lower temperature. Analyses indicate that at this heating rate, partial dehydration occurs between 120°C and 200°C (area 2 - Fig. 5.3).

5.3.3.3 Clay minerals and gypsum dehydration (area 3 - Fig. 5.3)

The further gypsum half water molecule is lost in completing the conversion to anhydrite at approximately 180°C.

Typical illite thermal gravimetry curves show a sharp weight loss below 150°C, gradual between 150°C and 350°C, steep between 350°C and 650°C and gradual between 650°C and 900°C (Grim op. cit.); with most of the dehydroxylation occurring between 350°C and 600°C. Montmorillonite dehydration typically occurs below 300°C (Jackson 1969).

With small samples, thermal gravimetric reactions are more immediate, and consequently by taking the boundary of area 3 (fig. 5.3) as 300°C the error is negligible. If a higher temperature boundary had been adopted, errors resulting from area 5 losses would have been incurred.

5.3.3.4 Dehydration/Dehydroxylation of Limonite

Limonite, a weathering product of iron pyrite oxidation, is a hydrated ferric oxide/hydroxide, the amount of held water is variable. According to Todor (op. cit.) the dehydration and dehydroxylation of limonite occurs at temperatures between 350°C and 400°C while goethite dehydroxylation occurs in the temperature range 250° - 360°C. Although it was always in the temperature range 240° - 350° C, peak 4 (fig. 5.3) was found to exist only in samples stained brownish yellow, and consequently it is confidently attributed to limonite. Read (1947) gives the molecular formula for limonite as approximately $2\text{Fe}_2\text{O}_3 \cdot 3\text{H}_2\text{O}$ and this has been adopted in quantitative approximations.

5.3.3.5 300°C - 800°C weight losses

Several important reactions occur in this temperature range,

including the dehydroxylation of clay minerals and decomposition of organic carbon, pyrites and carbonates. It is possible to readily recognise unstable iron sulphides and calcium carbonates, (fig. 5.3) but difficult to distinguish between other groups.

Hydroxyl losses calculated from DTG analyses (fig. 6.3) of pretreated clay fraction samples S11, 21 and 24 were attributed to both smectites and illites, an assumption of a 5% hydroxyl loss from illite meant that smectite dehydroxylation ranged between 4.6 and 9.2% (section 6.3.9).

Fig. 5.4 shows a thermal gravimetry curve for coal. In an inert nitrogen atmosphere only 9% of the total weight is lost. Mudrock organic carbon content is typically less than 3% (table 5.7), such weight losses are relatively insignificant in terms of the total weight loss and not discernable from the DTG curves (e.g. Fig. 5.2). Ingram (1953) demonstrated that with higher organic carbon contents, parallel arrangement of clay particles increased as did mudrock toughness. Consequently, organic carbon content was considered a sufficiently important phase to warrant separate determination (section 5.3.3.8).

The structure of pyrites is described by Brownlow (1979). Each iron (Fe_2) atom is surrounded by six sulphur atoms forming an octohedron, and each of these is covalently bonded to another sulphur atom in adjacent octohedra. Varying amounts of metallic bonding also occur. Consequently, it is not surprising that iron sulphide minerals vary considerably in stability - the influence of pyrite on weatherability is discussed in section 7.1.

In fig. 5.5, TG and DTG traces are reproduced for three pyrite polymorphs; sulphur released from readily decomposed or low stability pyrite is indicated by sudden weight losses. Pyrite content in sample S11 was estimated at 3.4%, and in samples S21 and 24 - 1.7% (table 6.2). Highly reactive sulphur weight loss is readily recognised in samples S21 and 24 (fig. 5.2), and discussed further in

section 5.3.3.6 . However, no characteristic feature from the DTG curve (fig. 5.5) is apparent in the trace for sample S11, (reproduced in fig. 5.2).

Todor (op. cit.) shows an endothermic weight loss for both ferrous and magnesium carbonates in this temperature range, i.e. 450° - 600°C and 600° - 800°C respectively, while for dolomite ($\text{MgCa}(\text{CO}_3)_2$) and ankerite ($(\text{MgFe})\text{Ca}(\text{CO}_3)_2$) decomposition occurs in stages and at similar temperatures to constituent carbonates. Generally magnesium and iron carbonates were not recognisable from the DTG trace. The rather low temperature at which the carbonates were lost from the sample S11 (DTG trace fig. 5.2) was shown to be the result of a new furnace fitted towards the completion of the analytical work.

In reporting weight losses (table 5.7) inert atmosphere organic carbon weight loss has been estimated from muffle furnace determinations (section 5.3.3.8) and deducted from 300°C - 800°C weight loss. Reported weight losses are a measure of clay minerals, high stability pyrite, and magnesium and ferrous carbonates. Although a combination of several different phases, this calculated weight loss can be a useful quantitative indicator. In an indurated sample the clay and pyrite content is more likely to be low and consequently a large recorded weight loss indicates ferrous and magnesium carbonates, while in a poorly cemented specimen a large weight loss is likely to indicate both a high clay and pyrite content.

5.3.3.6 Low stability sulphides

Diagnostic thermal gravimetry characteristics of low stability iron sulphides were described in the preceding section (fig. 5.5). Two iron sulphide varieties exhibiting well defined crystalline structures (fig. 5.5) are characterised by DTG curves showing a relatively broad peak between 580° - 700°C. Marcasite (fig. 5.5) and Chalcopyrite (FeCuS_2 - fig. 5.6) were both poorly crystalline, and DTG traces show a series of sharp peaks with the majority of activity between 390° and 580°C.

In an oxidising atmosphere, Pyrite oxidation is characterised by an exothermic maximum in the temperature range 450° - 500°C (Todor op. cit.). Thermal gravimetry of chalcopyrite samples in an oxidising atmosphere showed a single sudden weight loss at 610°C followed immediately by a weight gain.

The sharp DTG peaks imply energy release (exothermic) and broad peaks energy absorbance (endothermic). Todor (op. cit.) notes that in an inert atmosphere pyrite gives one single marked endotherm effect situated between 600° and 800°C, but he makes no mention of crystallinity. However, figs. 5.5 and 5.6 show the exothermic nature of reactions induced in the lower crystalline forms. Exothermic reactions are undoubtedly catalytic, and also imply a lower stability. Consequently, when low stability forms are found in mudrocks, weatherability, as defined by Fookes, Dearman and Franklin (1971) is higher. Although inert atmosphere thermal gravimetry does not provide a reliable means of quantifying total iron sulphide content, it can be used to identify and estimate the amount of low stability pyrite.

Two potential problem areas were recognised :-

- i) Sample grinding
- ii) Distribution of pyrite in mudrocks.

i) Sample Grinding

During trituration pyrite emitted a sulphurous smell, and the effect of grinding on the DTG trace is indicated in fig. 5.6. Mudrock samples, although not sieved to avoid preselection of material, were typically ground to pass a 425 μ m sieve but not to pass a 75 μ m mesh.

ii) Distribution of pyrite in mudrocks

Sedimentary anoxic bottom conditions are not prerequisite for the formation of pyrite. In a reducing environment hydrogen sulphides

liberated at depth within the sediment may react with iron hydroxides/oxides to form sulphides (Shaw 1981).

The release of hydrogen sulphide from decaying organisms was almost certainly fairly uniform with the Lower Lias and consequently the distribution and size of the pyrite is dependant on that of the iron. Pyrite in mudrocks has generally been shown to be finely disseminated throughout (e.g. Taylor and Spears 1981).

Pyrite rarely exceeding 0.2mm diameter and often framboidal, was noted by Wobber (1965) from his examination of thin sections, as a frequent occurrence. He noted that pyrite accumulations were often found below shell concavities, associated with worm burrows, organic material and collophane. Duplicate wet chemical analyses of relatively small mudrock samples (table 6.7) showed good agreement for iron, suggesting that generally iron sulphides were fairly evenly distributed throughout the mudrocks.

Replicate thermal gravimetry analyses were performed on several of the tested mudrocks. Although the presence of unstable sulphide minerals were reliably detected, quantifiably, comparison was poor; e.g. low stability sulphide attributed weight losses for consecutive TG runs were 0.18% and 0.53% (sample 24). However, from the reaction temperature, number of peaks and their magnitude, stability numbers defined in table 5.8 were confidently assigned (table 5.7).

5.3.3.7 Calcium Carbonate

Todor (op. cit.) reports decomposition of calcite at 920°C. Many of the calcite decomposition peaks did occur at this temperature; although several were recorded at lower temperatures. Analytical reagent grade calcium carbonate decomposed at 750°C (fig. 5.4) suggesting that calcium carbonate can decompose over a range of temperatures between 750°C and 920°C. However, the issue cannot be confidently discussed as, towards completion of analyses and following the fitting of a new furnace, calcite was shown to

consistently decompose at a lower temperature than 920°C. The calcite peak, being relatively large, is easily recognised and it was readily verified by addition of water to the sample after cooling, reheating and measuring the 490°C calcium hydroxide peak.

5.3.3.8 Organic Carbon determinations

The necessity for a low temperature determination in an oxidising atmosphere is explained in section 5.3.3.5. Pre-weighed oven dried samples of Marcasite and Coal from Lady Windsor Colliery, South Wales, were heated at 370°C in a muffle furnace for 24 hours. Average percentage weight losses from duplicate samples showed only negligible pyrite weight losses/gains (i.e. $\pm 0.008\%$ max.) and for the coal an average weight loss of 78.3% (variation 2.85%). Weight loss increased to 96.85% after heating samples for an additional 2 hours at 800°C - resulting in a total weight loss of 96.85%. Average sulphur content for Lady Windsor coal is 0.8% (N.C.B. Pers. Com. 1984). Making due allowance for this, a correction factor of 1.236 was calculated and used to correct all 370°C measured values. Organic carbon contents reported in table 5.7 are generally means of duplicate values with variation less than 10%, (adjusted to the 800°C value, as previously described). Where variation was greater than 10%, a third test was carried out and if this suggested an error in one of the previous values, the average of the two closest values is reported, but if three results all showed variation wider than 10%, the mean value of all three results is reported in table 5.7, and marked with an asterisk.

5.4 Engineering Index Tests

A programme of index tests familiar and meaningful to the Engineer are described in this section, and results are tabulated in table 5.9.

5.4.1 Dry density

Roughly trimmed to a regular shape, samples at their natural moisture

content were first weighed and then sealed with paraffin wax. Contemporary moisture contents were determined, and the waxed sample weighed in air and a known weight of water. The specific gravity of wax previously determined as 0.914 was used in the calculation of dry density.

5.4.2 Atterberg limits

Triturated Sample passing the 425 μ m sieve and mixed with deionised water, was allowed to cure for 24 hours prior to Cone Penetrometer liquid limit and plastic limit determinations; carried out in accordance with BS.1377 (1975 - tests 2a and 3 respectively).

5.4.3 Linear shrinkage

Linear shrinkage was determined from material mixed to approximately the liquid limits using the method specified in BS.1377 (1975 - test 5).

5.4.4 Hamrol (1961) Absorption test

Hamrol (op. cit.) recognised two distinct weathering types.

Type I - Excluding cracking of any kind.

Type II - Consisting exclusively of cracking.

In reality both types occur contemporaneously. Hamrol suggested a quick absorption test for measuring the degree of Type I weathering, where the absorption index is the % moisture content measured after immersion, and this appeared viable for mudrocks. Prior to final moisture content determination, following a 1 hour immersion in deionised water, surfaces were dried with paper tissue. A number of fissile mudrocks slaked (see for e.g. S11, plate 6.18) and in others, water penetrating between laminae or along discontinuities gave a false value. Where non-absorbed water is likely to have grossly affected results, (i.e. slaked samples) values in table 5.9 are marked with an asterisk.

5.4.5 Equilibrium moisture content

Although with increased weathering a usual feature of mudrocks is increased hygroscopy, absorption coefficients as suggested by Hamrol (op. cit.), for the reasons discussed in 5.4.4, were unsatisfactory.

Samples protected from dust were left in the laboratory for a seven day period to allow the moisture content to come to equilibrium with the surrounding atmosphere. Hygrometer records showed that, for the duration of these tests, laboratory relative humidity fluctuated between 60 and 70%. Moisture contents are recorded as equilibrium moisture content values, they reflect the mudrock weathered state, and more particularly that of constituent clay minerals, e.g. samples S14 and S15 described in section 5.2.6 as both weathered (WV), S14 exhibiting features of mechanical and S15 features of chemical weathered, showed varied equilibrium moisture. The higher value recorded for sample S15 is another indicator of the greater clay mineral degradation implied in earlier discussion (section 5.2.6) and other test results reported in table 5.9.

In retrospect, diagnostic potential of these determinations would have been greater if sample moisture contents had been equilibrated in 100% relative humidity; such an atmosphere would exist in a concrete curing room.

5.4.6 Slake durability Index

The test described by Franklin and Chandra (1972) and recommended by the International Society for Rock Mechanics - ISRM (1979) was adopted.

Each sample was subjected to three slaking periods in sea water (chemical analysis table 3.3) i.e. two standard periods of 10 minutes, and a longer third period of 30 minutes.

Fig. 5.7 shows the weight loss recorded against slaking time for each period. General graph shape (concave up) suggests that salt precipitated inter laminae and in discontinuities during oven drying has only a minor role in mudrock breakdown. The slake durability index reported in table 5.9 is the ratio of the weight loss in the second 10 minute slaking period divided by the total sample weight expressed as a percentage, as recommended by ISRM (op. cit.).

5.4.7 NCB Indentor determined uniaxial strengths.

The method is described in manufacturers literature (Anon - 1977). Szlavín (1974) found good correlation between the NCB cone indentor values and uniaxial compressive strength, validating its use for rapid uniaxial compressive strength assessment.

Strength testing of a mudrock sample (S17) is described in section 6.9.1. At moisture contents of 3.29% and 2.23% average recorded uniaxial compressive strengths were 29.63 and 47.57 MPa respectively (table 6.11); corresponding results predicted from NCB index tests were 33 and 42 MPa (fig. 5.8). These are well within the 90% confidence limits suggested by NCB indentor test results.

The preparation of uniaxial compressive test mudrock, and in particular shale, specimens, as well as being time consuming, was highly problematic (section 6.9). However, fissility facilitated NCB test specimen preparation, and consequently it was possible to carry out a large programme of tests for a wide range of moisture contents (fig. 5.8). Specimens were allowed to dry gradually in the laboratory and at various time intervals NCB uniaxial strengths were determined; together with corresponding moisture contents from the tested specimens. For several high strength, low moisture content mudrocks, samples were soaked in deionised water prior to strength determinations. In fig. 5.8, the mean uniaxial compressive strength and the first and ninth decile values are plotted against moisture content. These values are based on a minimum of ten results. In stronger mudrocks first and ninth decile values, or the distribution

90% confidence levels, although frequently wide, are within the expected range. Standard deviation quoted by Anon (op. cit.) for corrected and Standard values, is 13.85 MPa, which is equivalent to a 90% confidence level of ± 22.85 MPa.

The uniaxial compressive strength at equilibrium moisture content (relative humidity 60%–70%) interpolated from fig. 5.8 is reported in table 5.9 and used as the characteristic uniaxial strength in figs. 5.10, 5.11, 5.13 and 5.15.

5.5 Discussion

In previous sections of this chapter descriptions, mineralogy and engineering index properties have been presented with little reference to the engineering geology of the South Glamorgan Lower Lias sea cliffs. In the first of a two part discussion, results presented in earlier sections are considered in respect of observed and assessed, behaviour and performance.

In Part 2 the result of this investigation and that of Chapter 6 are used to develop a classification.

5.5.1 Mudrocks and influence on Engineering Geology

Mudrocks included in the testing programme are representative of the full range found in the field area. As well as examining samples from various strata, horizons 28a, 34a and 38a were sampled at several different sites facilitating assessment of lateral variation.

With the exception of the upper part of the zone, which tends to be limestone dominant, mudrocks from the angulata zone are typically durable and strong mudstones (table 5.6(1)). Thick mudstones are intercalated with thin discontinuous limestones, and consequently stability is largely governed by mudrock behaviour and performance. Vertical cliffs are characterised by high frequency low magnitude falls. A small eccentricity, developed by undermining, is adequate

to instigate instability. In section 10.2 it is conjectured that pressure release in mudrock dominant successions has a deleterious effect on rock mass stability resulting in frequent low magnitude falls. Small rotational failures in weathered angulata slopes at Dunraven (SS 889 726)(Williams 1980) also suggest mudrock dominant behaviour. However, high magnitude falls, although not uncommon, are largely discontinuity controlled.

Sample S3 horizon 0a indicated a relatively high organic carbon content; on excavation the shale readily broke into flaggy fragments typically 50-75mm by 3.5mm thick (measured at right angles to bedding). Although competent at Nash Point (SS 915 683) and Monknash (SS 904 699) when compared with adjacent mudrocks this shale is extensively notched.

Unweathered overlying strata up to horizon 21a are strong and highly durable and typified by sample S4 (horizon 6a). The deleterious effect of weathering is demonstrated at Col-Huw (SS 957 674) - weathered mudrocks from this zone are so weakened that they offer little resistance to erosive forces. Unweathered, stratum 2a is a highly competent mudrock and typical of other mudrocks in this zone. The engineering index properties for sample S5 taken from this horizon (table 5.9) demonstrate the effect of weathering.

Slake durability index (in sea water) and the comparative uniaxial compressive strength suggest that sample S6 (horizon 21a) should be competent. However, immersion in deionised water for 1 hour affected sample breakdown. In the field strata 21a is frequently seen to be more deeply notched than incompetent strata above; although to some extent this must be attributed to the wide ledge formed by this competent limestone 21 facilitating corrosion. Intercalated with thin discontinuous limestone weaker shales between horizons 21a and 28a form the most pronounced zone of weakness in the succession. Descriptions, mineralogy and engineering index properties for representative samples S7 to S9 are recorded in tables 5.6, 5.7 and 5.9. Samples S11 and S15 are taken from the incompetent weakly

cemented shale (28a). Although variation between the amount of cementitious material present in the three fresh unweathered samples is not as great as might be expected (table 5.7) from the engineering index properties (table 5.9) the shale undoubtedly forms a very distinct line of weakness, which is readily traced along the cliff even when elevated above the level of marine attack. To an extent sampling was selective rather than random, probably favouring the stronger material, i.e. East of Gwter Fawr, the only place shale (28a) could be confidently sampled was in close proximity to a fault.

East of Nash Lighthouse the face of the notched shale (28a) formed a cusped type profile; cusps extending several metres into the cliffs while the horns were located within a metre of the face. Sample S13, the most durable of samples from shale (28a), was taken from one of these horns.

Stronger and more durable than mudrocks between 21a and 28a, but less competent than those above, are those from the zone between horizons 28a to 38a. However the samples S16 - S20 were all sufficiently weathered to be classified WII. Mudrock samples S17, S18 and S19 were all from horizon 34a. Table 5.6 records their exact location, the considerable variation in mineralogy and engineering index properties is recorded in tables 5.6, 5.7 and 5.9.

Three weathered mudrock samples from horizon 38a were taken in close proximity. Sample S20, although weathered, comprised intact pieces of mudrock from a WIV zone while samples S21 and S22 were both assessed as WV material from the same zone (table 5.6). Considering the close proximity of the three samples, they show marked variation in both mineralogy and engineering index properties (table 5.7 and 5.9). Similar degraded material is common close to the cliff top and consequently there is always considerable risk of small falls from the upper part of the cliff. Mudrocks above horizon 38a and up to 54a are, unless weathered, highly competent and resistant to erosion (tables 5.6 and 5.9). With increasing elevation above horizon 54a, mudrocks decrease in competence. Where exposed to marine attack e.g. Gwter Fawr (SS 915 680) they are frequently deeply notched. Silty in

texture they appear poorly cemented and compacted. The apparently high slake durability index recorded in table 5.9 for sample S27 is not truly representative; concretionary in character the material strength and competence is varied. Sample requirements for the slake durability tests precludes the use of all but shaped lumps of specified size. Material which crumbled on excavating was automatically excluded and it is estimated that some 30% of this sample behaved in this way.

Mudrocks of similar mineralogy and engineering index properties tend to occur in discrete zones of several metre thicknesses. Although mineralogy properties vary both vertically and laterally, overall zonal competence appears relatively unaffected. However, weathering clearly has had considerable effect on the competence of even the strongest and most durable of mudrocks, in fact in section 5.2.6 it was indicated that weatherability of the more calcareous mudrocks may well be greater.

An indication to the relative competence of mudrocks in adjacent zonal horizons is readily available. The distinctive shape of cliff profiles characterises zone competence. Highly competent mudrocks appear prominent in relation to less competent zones.

5.5.2 Mudrock Classification

It might be assumed from the scenario of the previous section that any mudrock classification is superfluous. The harsh energy environment exposing inherent weaknesses in the succession is rather like a breaking chain, only the weakest link failing and showing any sign of distress. Instability develops primarily because nature exploits the line of greatest weakness. Consequently, if protection to the 'weakest link' were to be provided other weaknesses may be critical (and not so readily recognised). Mudrock performance is consequently best characterised by a classification.

In developing this classification several of the determined

properties were investigated for interdependent relationships, and their pertinence as classification parameters. Investigations leading to the development of the classification presented in fig. 5.15 form the basis of the subsequent discussion.

The extent to which the clay phase is less than fully restrained by cementitious material is undoubtedly implied by an increase in measured plasticity index (section 6.6). Increased plasticity is likely to indicate a decrease in slake-durability; such a relationship is suggested in fig. 5.9. However, weathered state and the general effectiveness of the cementitious phase as a restraint are both reflected in deviation from the conjectured graph line. Gamble (1971) suggested that mudrocks could be characterised by these two properties, and his classification is superimposed. Equilibrium moisture contents reflect the ability of the particular mudrock to absorb water. Consequently uniaxial compressive strengths at these moisture contents reflect field value differentials. A relationship between uniaxial compressive strength and slake-durability index is implied by fig. 5.10. However, the scatter of results is only to be expected. Uniaxial compressive strength when determined by the NCB cone indenter is more accurately a measure of inter-particle cohesion. Slake-durability not only depends on this but also flaws in the mudrock fabric.

Determined slake-durability index values with the exception of highly indurated competent rocks were frequently greater than expected; e.g. 89.3% and 91.2% for samples S8 and S9 respectively (table 5.9) is higher than field performance and other index properties suggest. As indicated in the previous section the requirement for samples of specified size and shape can preclude all but the most competent mudrock in a weak variable stratum. In table 5.9 an asterisk is used to denote samples which showed signs of slaking during a 1 hour immersion in deionised water - Hamrols test. Nevertheless, slake-durability is highly pertinent in a classification of this kind. However, as well as exposure to attack from the sea, water seeping through the cliff, i.e. locally derived rain water of much

lower ionic strength (section 7.1), suggests that slaking characteristics in deionised water are also relevant. Slake-durability characterisation adopted for the classification (fig. 5.15) utilizes an inverse log scale, enhancing sensitivity at the top end of the scale where mudrocks differing markedly in degrees of competence, exhibit only relatively small differences in slake-durability index. Two scales are adopted; the larger reach one for mudrocks not slaking during deionised water immersion, and the short reach one for those that do.

In fig. 5.11 a plot of a function representing the amount of diagenetic cementitious material (excluding limonite) against uniaxial compressive strength is presented. Organic and carbonate contents were expressed as a ratio of maximum considered values (see fig. 5.11). Values other than from samples designated weathering grade WI or WII were ignored. However, all samples graded WII deviated to some extent from the conjectured 'best fit line'. The organic carbon content coefficient of 0.4, used to give the best straight line solution, was determined by trial and error. Plotted against the uniaxial compressive strength, the amount of cementitious material recorded in samples S25 and S26 appears erroneously low (fig. 5.11). Although sample S26 (horizon 54a) is apparently uniformly strong, it is concretionary in nature; - limestone nodules frequently occurring. It appears highly probable that the small thermal gravimetry sample was far from fully representative.

Amounts of cementitious material recorded for samples S7, S8, S9 and S10, from horizons 24a, 25a, 26a and 27a respectively (fig. 5.7), was greater than that which could be anticipated from fig. 5.11. All come from the west side of Nash Point (table 5.6). Using the criteria described in section 5.2.6 to assess weathered state, test material was all designated weathering grade WIA, while each sampling location was classified grade WIB. The site was subject to regular, intermittent seepage, and whereas no substantial carbonate leaching appears to have occurred, the shales are weakened, perhaps by frequent wetting and drying. Weathering by such a mechanical

mechanism is difficult to detect and possibly these mudrocks should have been designated WII. If the values alluded to are ignored, then scatter in fig. 5.11 is greatly reduced and the straight line graph for cementitious material content against cone indenter uniaxial compressive strength appears convincing.

Graphs of equilibrium moisture content against plasticity index (fig. 5.12) and uniaxial compressive strength at equilibrium moisture content against plasticity index (fig. 5.13), imply that moisture content and uniaxial compressive strength are at least both partly dependant on influence of the clay phase.

The characterisation value of uniaxial strength at equilibrium moisture content has been demonstrated, but again a log scale plot was necessary in the classification (fig. 5.15), this time to enhance sensitivity at the low end of the scale.

The reader is reminded that equilibrium moisture contents were determined in 60% - 70% relative humidity, and that a 100% relative humidity environment would have greater diagnostic potential.

Plasticity index was adopted as a parameter being sensitive to the mudrock texture; i.e. claystone, mudstone, or siltstone. Before its adoption, linear shrinkage, which is more rapidly determined and with less possibility of operator error, was considered (fig. 5.14). A graph of linear shrinkage against plasticity index shows good correlation, although the relationship determined by linear regression analysis is different to that indicated by Head (1980). Despite fairly good correlation, compared with plasticity index, linear shrinkage was found to be far less sensitive and unreliable.

In sample S3, organic carbon/calcium carbonate ratio is considerably greater than in other samples (table 5.7). Although uniaxial compressive strength and slake-durability index is relatively low, the sample is moderately strongly cemented (table 5.6). The degree of restraint exercised on the clay phase by the cementing agents is

relatively small, indicated by comparatively high plasticity index and linear shrinkage.

Marine origin carbonaceous mudrocks are likely to have been laid down in deep water and further off shore. Consequently they have a higher clay content. With increasing competence, fissility decreases, and shales with high organic carbon contents are likely to exhibit flaggy fissility (Ingram 1953). Thus, it has been possible to define a zone in the classification (fig. 5.15b) where the principal cementing agent is organic carbon.

In sections 6.6, 6.7 and 6.8, physical and physico-chemical aspects of mudrock behaviour have been assessed, enabling establishment of a zone defining mudrock whose behaviour is influenced by the clay phase (fig. 5.15b). Clay phase influence increases with decreasing induration and increasing clay content. The classification readily permits such characterisation.

The classification (fig. 5.15) also defines zones of competence and degrees of induration, these were established by cross referencing slake-durability and uniaxial compressive strength. Four such zones are marked on the classification chart 5.15b.

Plotting data on the triangular graph (5.15b) is explained in the figure and examples of interpretation are given below.

- 1) Sample S1 - A highly competent, strongly cemented, erosion resistant mudstone.
- 2) Sample S3 - A competent, carbonaceous clayshale, eroded when exposed to severe marine attack. Clay phase has a significant influence on mudrock behaviour.
- 3) Sample S20 - Incompetent moderately cemented readily eroded mud shale/stone.

The classification gives both a high degree of characterisation along with an indication of engineering performance and behaviour. This work adequately demonstrates the potential of the suggested scheme, but without further work it can only be tentatively regarded as suitable for mudrocks of different geologic horizons.

5.6 Summary

To investigate the variation in mineralogy, physical and physico-chemical behaviour, twenty-seven mudrocks from both angulata and bucklandi zones have been sampled from different horizons. To investigate the effect of lateral variation, samples from a number of horizons were duplicated, but taken from different sites. Descriptions largely adopting the scheme suggested in the Working Party Report (1977) are tabulated in table 5.6. Thermal gravimetry analysis was used to quantify major mineralogic phases, and recorded weight losses are reported in table 5.7. Engineering index properties are reported in table 5.9.

The descriptive 'element' for cementation state is based on the degree of fissility exhibited by the mudrock, developed classification is described in section 5.2.5 and the 'descriptor set' presented in table 5.3.

Sulphide oxidation appears to be a major weathering mechanism in these, as in many other, mudrock sequences. Curtis (1976) has shown pyrite to be thermo-dynamically unstable. Yet, paradoxically, in some mudrocks, although present, there is little indication of pyrite oxidation. Inert atmosphere thermal gravimetry offers a method of distinguishing between potentially stable and unstable pyrite; thereby facilitating assessment of mudrock weatherability; the method is described in 5.3.3.5 and 5.3.3.6.

Organic carbon contents were determined from the 24 hour 370°C weight loss; the method adopted is described in section 5.3.3.8.

Uniaxial compressive strength was determined using an NCB cone indenter, and graphs against moisture contents for each of the 27 samples are plotted in fig. 5.8.

The hygroscopic properties vary with induration, clay mineral content and weathered state. The greater the ability to absorb moisture the lower the durability. Mudrock moisture contents determined after the mudrocks had come to equilibrium with the surrounding atmosphere is termed the equilibrium moisture content. The uniaxial compressive strength at equilibrium moisture content was found to be particularly useful, and along with plasticity index and slake-durability index was adopted as parameters in a mudrock classification, for characterisation of performance in a marine environment (fig. 5.15).

The properties of mudrocks in relationship to the engineering geology of the Glamorgan sea cliffs is discussed in section 5.5.1. Adjacent mudrock strata do not frequently show marked difference in competence, - variation, usually zonal, leads to distinct cliff profiles depending on the level of competent strata. Horizon 28a (Trueman 1930) is the most significant line of weakness, and this inherent weakness is reflected in the measured index properties.

As well as providing a comprehensive survey of the mineralogy and engineering index properties of the Glamorgan Lower Lias, and the resulting classification, which is tentatively proposed as a general characterisation of mudrocks, the method used for identifying low stability pyrite is seen as of particular importance in the prediction of mudrock weatherability.

CHAPTER 6

THE MINERALOGY, PHYSICAL AND PHYSICO-CHEMICAL BEHAVIOUR OF SELECTED MUDROCKS

6.1 Introduction

Although, undoubtedly, index tests provide valuable and useful data, without a more detailed knowledge of mineralogy, physical and physico-chemical behaviour, reliable prediction of long term mudrock behaviour would not be possible. Weathering can frequently and dramatically change index properties.

E.g. Quigley (1962) notes that acid weathering removes considerable interlayer potassium from illites, producing a swelling clay, and also that the process is reversible.

Surface rocks are not in equilibrium with their surroundings and are consequently metastable. Index properties, and even mineralogy, are transient as the system adjusts from an old to a new equilibrium. In perhaps a majority of cases the transition is slow, and the degradation time scale precludes engineering consideration. However, there are many cases where the reverse is true, in these, or indeed where reasonable doubt exists, a detailed knowledge of the system and its surroundings is prerequisite.

The wide ranging properties and weathered slates of mudrocks in this sequence were demonstrated in Chapter 5. With decreasing induration, the clay phase increasingly influences engineering performance and behaviour.

End member mudrocks (i.e. the most competent, least competent and most highly weathered of those sampled) were selected for detailed mineralogic analysis and included :-

S24 Competent with high carbonate and silt content. (WIa)

S11. Incompetent low carbonate and high clay content. (W1b)

S21 Incompetent weathered with high carbonate and silt content. (Wv)

Sequence of procedures and analyses for the silt and clay fractions are shown in fig. 6.1, methodology is generally that recommended by Jackson (1969), and Bullock and Loveland (1974). Selected cation analysis of free salts and major mineralogical phases were facilitated by Ammonium acetate extracts and Hydrochloric acid/Hydrogen peroxide digestions. Texture and fabric were studied by means of an S.E.M. (scanning electron microscope), and ocular microscopy of thin sections and fragments.

Index tests (section 5.4) provide durability and strength assessments of representative mudrocks. Clay phase influence on mudrock physical and physico-chemical behaviour is implied from linear shrinkage and liquid and plastic limits, determined from triturated but otherwise untreated samples. One dimensional consolidation swelling tests and T.R.R.L. (1952) shrinkage limit tests described in this chapter provide a more quantitative assessment of clay phase influence. Rock face monitoring, (section 10.3) indicates significant seasonal and diurnal movements within the rock mass. Performance of intact shale specimens (S24, S11 and an intermediary S17 WII), and two limestone specimens (L6a and L7a) when subjected to various controlled temperature environments, are compared. Paradoxically, low magnitude but significant shrinkage was recorded in the less competent mudrocks at moisture contents much lower than the T.R.R.L.(1952) shrinkage limits.

Difficulty experienced in safely obtaining suitable mudrocks for coring, and problems in obtaining adequate cores for testing, limited compression testing to sample S17 only. A testing program included uniaxial and triaxial compression tests. Uniaxial compression test specimens orientated both perpendicular and parallel to bedding were strain gauged.

Compression strength testing and comprehensive index tests, together with major phase mineralogy compiled for representative mudrocks, provide a basis for conjecturing the mudrock stress strain behaviour.

6.2 Illite and Mixed Layer Clay

In the presence of elevated temperatures, pressure and potassium, both Smectites and Kaolinites can be converted to Illite and Mica (Tucker 1981). Crystallinity is dependant on stress and thermal history. Tucker (op. cit.) notes an increase in illite and chlorite with geological age (fig. 6.2). Illite, perhaps a somewhat contentious term, was introduced by Grim, Bray and Bradley (1937) for mica like clay minerals. Diagenesis and formation of illite via mixed layer complexes is predominantly from Smectities but also from Kaolinites. Grim (1968) notes some confusion in definition; i.e. a number of cases where expansive mixed layer clays had been wrongly defined as illite. Illites and micas are both phyllosilicates with non-expansive lattices, giving strong x-ray diffraction (001) peaks at 10\AA . These silicate - gibbsite or brucite 2-1 structures occur in stacks bonded together by inter-laminae potassium. In the dioctohedral end member, muscovite, approximately 25% of the silicons are replaced by aluminium, the charge deficiency balanced by interlaminae potassium. Octohedral gibbsite layers characterise muscovite, while in the trioctohedral end member, phlogopite, the octohedral layer is comprised entirely of brucite.

Mitchell (1976) defines illite as hydrous mica. Grim (p.334 op. cit.) noted that essential diagnostic differences are exhibited on heating.

1. Illite loses water below 110°C , mica does not.
2. Dehydroxylation is more abrupt in illite and usually between 300°C and 600°C .

Depending on size and crystallinity, cation exchange varies between 10 and 40 m.eq./100 grams. With decreasing size and crystallinity, inter-laminae cations become more readily replaceable (Grim - op. cit.).

Soil scientists prefer the generic name Mica (Jackson op. cit.), but size and crystallinity, and the degree of hydration are of considerable significance to engineering behaviour and properties. Consequently the term illite is preferred, and will be used to describe micaceous particles in the clay sized fraction. Hydrous micas in the silt, and coarser fractions often of greater crystallinity as well as size, will be described as mica.

Expansive components of mixed layer complexes are defined by the presence of a 17\AA peak on x-ray diffraction trace of a glycol solvated sample.

Interstratified and mixed layer are used synonymously to describe clays where the stratified platlet-like clay minerals are of varied mineralogical structure and composition. A fuller definition is given in Grim (1968).

6.3 Mineralogical Investigations

6.3.1 General Procedure

6.3.1.1 Cleaning Glassware

Where necessary, detergents and scouring powder were used to clean glassware prior to using cleaning procedures specified in section 7.4.7 (i.e. 10% Decon 90 solution and 10% nitric acid).

6.3.1.2 Sample Washing procedures

Polypropelene 250ml centrifuge bottles were used. Sample suspensions were facilitated by mechanical shakers and agitation with glass stirring rods. On completion of stirring, and after unavoidable sample transference, containers and glass rods were washed with a fine jet from a wash bottle, and washings collected and added to samples.

An M.S.E. 18000 centrifuge with angled rotor was employed for separation.

6.3.1.3 Flocculation and Handling dispersed samples

Attempts to flocculate dispersed clay suspensions were usually made by the addition of acetone. If unsuccessful a chloride salt addition, which had to be subsequently removed, was made. Removal was achieved by washing in a non-polar liquid such as ethanol. Checks for the removal of chlorides were made by the addition of silver nitrate to the decanted supernatant washing liquid. Dispersed samples were kept in methanol and stored in polypropylene centrifuge bottles.

6.3.1.4 Centrifugal separations of small quantities

In analytical work and pretreatment of small quantities such as for cation saturation, 50ml or 15ml centrifuge tubes were used; mixing was facilitated by vortex mixer, and separation by a M.S.E. centair bench centrifuge.

6.3.2 Trituration

Mortar and pestle were used to finely grind approximately 70 grams of sample. To avoid pre-selection, samples were not sieved.

6.3.3 Pretreatments

6.3.3.1 Carbonate destruction and removal

Strong mineral acids are known to attack certain clay minerals; e.g. a well documented test for chlorite is its destruction with 50% v/v HCl (Bullock and Loveland 1974). A solution of HOAc Anal R (glacial acetic acid) and 1 M NaOAc Anal R (sodium acetate) buffered at pH 4.0 was used to destroy carbonates. Although only containing a small percentage of magnesium, their destruction could not be efficiently

effected with the recommended pH 5.0 solution even with heating. Treatment and subsequent washings were otherwise carried out in accordance with Jackson (1969). Thermal gravimetry was used to verify carbonate destruction.

6.3.3.2 Oxidation of organic carbon and sulphides

30% w/v H_2O_2 G.P.R. (hydrogen peroxide) was primarily used to decompose organic carbon. Procedures followed were those recommended by Jackson (op. cit.). H_2O_2 also effects the oxidation of sulphides, products either being removed in subsequent washings or by dithionite treatment.

Ingram (1953) noted that in his experience H_2O_2 was frequently less than 100% effective in the removal of organic carbon. More than 2.5 litres of H_2O_2 was used in an extensive treatment, continued for 1 week, after which time decomposition was assumed complete. Sample S24 had the highest organic carbon content, and consumed the most hydrogen peroxide, and the writer was least confident of a complete H_2O_2 organic carbon reaction.

Thermal gravimetry of the fraction coarser than 2 micron indicated the presence of phyllosilicates (figs. 6.3 d, e and f), possibly clay sized, and cemented by non-decomposed organic carbon. (For further discussion see section 6.3.6).

6.3.3.3 Removal of free iron oxides

Limonite, the natural weathered product of iron sulphides, frequently cements clay crystallites, prohibiting complete dispersion. Removal was facilitated by the Sodium citrate - bicarbonate - dithionite method (Jackson op. cit.).

6.3.3.4 Dispersion and flocculation

Dispersion is indicated by Brownian Movement. Samples previously

flocculated in 1M NaCl and acetone were washed with ethanol. On completion of a washing cycle, the decanted supernatant ethanol was tested for the presence of chlorides, using a silver nitrate solution. Ethanol washing was continued until all chlorides were removed. Dispersion was checked by taking up the centrifugally separated sediment in a small quantity of deionised water. Separation of NA^+ saturated dispersed samples, following iron oxide removal, was achieved by the addition of approximately 80% acetone. Samples were allowed to stand for 24 hours and centrifuged for 30 minutes at 9000 r.p.m.

6.3.4 Particle Size Analysis

6.3.4.1 Sample preparation

Approximately 20 grams of sample were taken for specific gravity determinations and particle size analyses. After centrifuging, the samples were allowed to air dry in a fume cupboard, and then transferred to the oven and dried for 24 hours at 105°C.

6.3.4.2 Specific Gravity

Density bottle method (BS 1377:1975, test 6B) was employed using paraffin as density bottle fluid. The average of three values, with deviation less than 0.03 are reported for each sample in fig. 6.4.

6.3.4.3 Particle Size analysis

Samples used in the specific gravity tests were carefully transferred to 250ml centrifuge bottles, centrifuged, and the supernatant liquid decanted; followed by washing in acetone and air drying in a fume cupboard prior to oven drying for 24 hours at 105°C. Dried samples of approximately 15 grams were suspended in 100ml of deionised water and transferred to a 63 micron sieve. Washings, and the fractions passing, were transferred to 500ml sedimentation cylinders. No peptizer was necessary for dispersion. Procedure for particle size

analysis was carried out in accordance with BS 1377 1975 (test 7C). Wet sieving, using 425 micron, 350 micron and 212 micron sieves to fractionate the sample retained on the 63 micron sieve was used to grade the coarser fraction.

The fraction finer than 0.2 micron was separated centrifugally (using the M.S.E. centair bench centrifuge) in 50ml centrifuge tubes. The method adopted was that detailed by Jackson (op. cit.).

Sediment coarser than 0.2 micron collected in the centrifuge tube had segregated into three distinct layers, the bottom and coarsest buff in colour, the intermediate greyish white, and the finer top layer dark grey. Particle size graphs for the three pre-treated mudrocks are shown in fig. 6.4.

6.3.5 Fractionation

Although, arguably, it is desirable to investigate the mineralogy of several size fractions finer than 2 micron, in this work investigation was limited to the fractions coarser and finer than 2 micron. Fractionation was carried out in the M.S.E. centair centrifuge following a similar procedure adopted for the 0.2 micron separation carried out in particle size analysis.

6.3.6 X-ray diffraction fraction coarser than 2 micron

A Guinier Hagg XDE 700 focussing camera with chromium K α radiation was employed for this work. Silicon added to the randomly orientated samples provided an internal calibrating standard. Atomic spacings were calculated from Braggs law, derivation of which is well documented. e.g. Mitchell (op. cit.)

$$\frac{d}{n} = \frac{\lambda}{2 \sin \theta} \quad (6.1)$$

where d is the distance between atomic planes

n is an integer defining reflection order

θ is the angle made by the incident ray striking the atomic plane, and is equal to that of the reflected ray and atomic plane.

λ is the monochromatic x-ray wavelength.

λ for Cr K α radiation = 2.290 Å

Cu K α radiation = 1.542 Å

Radius of Guinier Hagg XDE 700 camera = 100mm.

X-ray diffraction data found in Griffin (1971), Grim (op. cit.), Mitchell (op. cit.) and Jackson (op. cit.), facilitated recognition. Interpretation of the x-ray films is presented in table 6-1.

6.3.7 Thermal Gravimetry fraction coarser than 2 micron

Major diagnostic differences between illite and mica, apparent on heating, are noted in Section 6.2. Reproduced TG and DTG (Thermal and Differential Thermal Gravimetry) traces, fig. 6.3 d, e and f are typically those of micas - illites (Todor 1976, Grim (op. cit.) and Jackson (op. cit.)). On heating, the three specimens showed weight loss below 110°C indicating hydrous mica.

In section 6.3.3.2 it was noted that Hydrogen peroxide pre-treatment may not have been entirely successful in removal of organic carbon, and that as a result the coarse fraction may contain organically cemented clay sized particles. However, diagenetic alteration of detrital clay minerals to illites (section 6.2) or end product mica, implies increases in both particle size and crystallinity.

Differential thermal gravimetry traces (figs. 6.4a-f) show maximum rate of weight loss occurred at higher temperatures in the coarse fractions. Grim (op. cit.) notes that the likely reason for micas being more reticent than illites in losing hydroxyl water, is particle size.

Traces for sample S24 (6.4f) warrant special consideration. Reference to table 6.1 shows the presence of a very weak 7.07 Å reflection; i.e. Kaolin or Chlorite. Grim (op. cit.) and Jackson (op. cit.) both show abrupt dehydroxylation losses for kaolin between 450°C and 520°C. Assuming the 470°C peak indicated kaolin dehydroxylation then the coarse sized fraction contains 1.8% kaolin. For kaolin, Jackson (op. cit.) quotes a weight loss of 12% of the 105°C oven dry weight occurring between 400°C and 530°C. Although Grim (op. cit.) refers to a possible maximum kaolin plate dimension of 4 micron, it seems likely that there is some cementing of kaolin by organic carbon.

The broad mica dehydroxylation peak is likely to be indicative of larger, more crystalline micas than are present in the other specimens.

Kaolinite content of sample S24 is clearly much greater in the coarse fraction than in the clay fraction, but, the slight flexion at 510°C in fig 6.3c suggests a higher kaolin content than is present in the clay phase of other samples.

As a comparison, part of the thermal and differential thermal gravimetry traces for sample S24 (fig. 6.3g), i.e. immediately following pre-treatment to remove carbonates, are reproduced. A broad peak at 530°C is partly attributed to the decomposition of organic carbon. However, total organic carbon weight loss in an inert nitrogen atmosphere would be less than 0.4% of the sample weight. The probable effect of the clay-organic complex is increased resistance to dehydroxylation. A relatively sudden weight loss at 600°C, superimposed on a broad illite/mica dehydroxylation peak, is likely to be pyrites.

It is probable that not all organic carbon was decomposed and particularly so in sample S24, but it is also highly likely that particles larger than 0.2 micron exist in the illite/mica phase. Illite hydroxyl water, lost between 300°C and 900°C is approximately 4% of the 300°C sample weight (Jackson op. cit.). For the purposes of approximating mineral composition (table 6.2), thermal gravimetry coarse fraction weight losses have been attributed to mica and kaolinite only. It is possible that a few irregularities on the traces are those of feldspar. Comparison of Fig. 6.3 d, e and f with the three feldspar standards (fig. 5.4) show that this cannot be asserted with any confidence. X-ray analyses show, very weakly, only the strongest feldspar reflections. Therefore, it seems likely that only a negligible error will have resulted from ignoring feldspars in approximating silt phase mineralogy.

6.3.8 Cation Exchange Capacity of the Clay sized fraction

The procedure followed was that recommended by Jackson (op. cit.). Following hydrogen peroxide treatment, to ensure that the clay was bacteria free, and flocculation with subsequent ethanol washing, samples for cation exchange capacity determinations were taken, washed in acetone, and air dried in a fume cupboard. To minimize moisture content they were placed, overnight, in a desiccator containing silica gel.

Approximately 100mg of dried clay was then placed in 15ml centrifuge tubes and sample weight recorded to 0.0001g accuracy. Samples were washed three times in 1 M CaCl₂ and five times in 0.02 M CaCl₂, and the supernatant solutions discarded after each washing. Centrifuge tubes, with samples and excess solution were weighed to the nearest 0.01g. Samples were then washed five times in 1 M MgCl₂, the supernatant solution transferred to a 100ml volumetric flask and made up to volume with 1 M MgCl₂ after the final washing. Calcium standards, including a blank, for flame photometer analysis, were made up from Anal R spectrosol atomic adsorption stock solutions, in 1 M MgCl₂ acidified to give a 10 M HCl concentration. LaCl₃ to

suppress interference, was also added to give a final concentration of $10 \text{ mgml}^{-1} \text{La}^{3+}$. 15 ml aliquots from the saved sample washings were added to a $\text{HCl/LaCl}_3/\text{MgCl}_2$ 'cocktail' solution (to concentrations as standards) and made up to volume in 25ml flasks. Analysis for calcium was carried out using a Corning 400 flame photometer.

The cation exchange capacity expressed in m eq/100 gram of dry soil is determined by calculating the total amount of calcium removed by 1 M MgCl_2 washings, less that in the excess solution after the final 0.02 M CaCl_2 washing. Duplicate analyses gave the results indicated in table 6.3.

Reference to table 6.3 indicates that the cation exchange capacity of sample S21 is higher than might be expected. Weathering processes have apparently resulted in isomorphic substitution in the clay crystallite lattice. Resulting larger negative surface charges are neutralised by double layers of greater ionic strength.

6.3.9 Thermal Gravimetry - fraction finer than 2 micron

Adsorbed water is removed more readily from potassium saturated clay, since the K^+ ion has little tendency to retain water (Jackson op. cit.) who recommended that potassium saturation should be a prerequisite of thermal gravimetry on two counts :

- 1) Abrupt weight losses are of greater diagnostic potential.
- 2) The standardisation of results.

Sodium saturated aliquots of approximately 1.5 grams were washed five times in 1 M KCl , once in deionised water, five times in methanol and finally in acetone. Following this, the supernatant liquid was tested for the presence of chlorides. Prior to thermal gravimetry, the separated clay sized fraction was air dried in a fume cupboard. Differential thermal and thermal gravimetry traces and weight losses attributed largely to dehydroxylation are presented in figs. 6.3 a, b and c.

Percentage illite and smectite calculated from x-ray diffraction analyses (section 6.3.11) is not in agreement with that calculated from thermal gravimetry using the criteria of Jackson (op. cit.); i.e. Percentage hydroxyl loss of the 300°C weight is 5% for smectites and 4% for illites. Dehydroxylation curves given by Grim (op. cit.) indicate weight losses of 5.5% for illite and between 4.2% and 8.5% for smectites. Assuming the results of semi-quantitative x-ray diffraction analyses are correct, and making an assumption that the hydroxyl weight loss from illite is 5% of 300°C weight, smectite dehydroxylation from S11, S21 and S24 respectively would be 7.1%, 9.2% and 4.6%. These values cannot be assumed in any sense to be quantitative, for instance, Jackson (op. cit.) notes that -

"Both micas and chlorites appear to be variable in octahedral cation content with corresponding variability of OH."

However, the values make interesting comparison with the clay sized fraction mineralogy (table 6.3). They indicate structural variations which are reflected in cation exchange capacities.

Only sample S11 exhibits a dehydration peak between 150°C-300°C, which is indicative of montmorillonite. A small flexion at just above 500°C in sample S24 verifies the slightly stronger presence of kaolin suggested by x-ray diffraction (section 6.3.10).

6.3.10 X-ray diffraction of randomly orientated clay sized samples

The (060) spacing is diagnostic between trioctohedral and dioctohedral 2:1 layered phyllosilicates. Dioctohedral illite is indicated by an approximate 1.50 Å spacing and a strong (002) reflection. Trioctohedral forms have spacings between 1.525 Å and 1.534 Å, and the (002) spacing is absent (Jackson op. cit.). The only opportunity to study these small (060) spacings was afforded by the Guinier Hagg XDE 700 focussing camera, using Cu K α radiation. Unfortunately, the camera broke down during this series of tests, and only the results obtained for sample S21 proved satisfactory.

Glycerol solvated Ca^{2+} saturated, randomly orientated powder samples were prepared using the procedures recommended by Jackson (op. cit.). To provide an internal calibrating standard, silicon was added, the sample was then packed into a glass capillary tube for x-ray diffraction. Sample S21 showed a weak quartz reflection at 1.54\AA , and a weak, but broad line at 1.505\AA was assumed to be the (060) spacing for dioctohedral illite. However, instead of a strong second order reflection, the film showed only a broad dark zone in the vicinity of 5.00\AA .

Basal reflections are of course stronger from orientated samples, and results from all such samples (section 6.3.11) show the 5.00\AA peak to be of similar strength to the first order reflection. Grim (1968) suggests that the octohedral layer is highly alluminous where 1st, 2nd and 3rd order reflections are similar in intensity. The peak at 3.33\AA , the 3rd order basal illite reflection, is a compound peak including a strong quartz reflection and consequently cannot be readily compared with 1st and 2nd order reflections. Nevertheless, evidence suggests that dioctohedral illite is dominant.

Grim (op. cit.) notes that the (060) spacing is also useful for differentiating between chlorites and kaolinite. The presence of a very weak 1.485\AA reflection on the film for S21 indicates kaolin.

6.3.11 Semi-quantitative x-ray diffraction Analysis - clay sized fraction

Lack of suitable equipment at the Polytechnic necessitated Mg^{2+} and k^+ saturated samples, prepared using methods recommended by Jackson (op. cit.), being x-rayed elsewhere. This was done by staff at the Department of Environmental Science, University of Lancaster, using a Phillips diffractometer (PW 1050 vertical goniometer), with proportional counter and pulse height selection, fitted with a curved graphite monochromating crystal, and using $\text{Cu K}\alpha$ radiation. Procedures adopted for recognition and semi-quantitative estimates of clay minerals were those recommended by Bullock and Loveland (1974).

Five slides were prepared for x-ray diffraction from the slurried Mg^{2+} saturated samples:-

- i) Air dried
- ii) Air dried, placed in desiccator with ethylene glycol and then heated at 80°C for 4 hours.
- iii) Slide heated in a furnace at 335°C for 4 hours.
- iv) Slide heated in a furnace at 550°C for 4 hours.
- v) An aliquot was digested in 50% HCl for 15 minutes at 100°C, followed by slide preparation and glycollation.

The various preparations (i) to (iv) provided diagnostic x-ray diffraction data (table 6.4). Chlorite solubility in HCl is high, while kaolinite is low, - Slide 5 provides a test to distinguish between these two groups.

A semi-quantitative method for determining relative amounts of illite and smectite is described by Bullock and Loveland (op. cit.); i.e. relative proportions of expansive and illite groups are obtained by comparing the 10 Å reflection of the glycollated samples, and that heated to 335°C half the proportional difference in peak area indicates the proportion of expansive clay.

Quartz was quantified by the method of known additions - Brindley (1980). Quartz additions, equal to 15% of sample weights, were added to K^+ saturated samples. Specimens were x-rayed under the same conditions as air dried Mg^{2+} saturated specimens and the difference in area of the two 4.26 Å peaks, used to estimate the amount of quartz present in each sample.

Diffraction patterns show the presence of quartz and clay minerals only, and pertinent diagnostic portions are reproduced for samples S11, S21 and

S24 (fig. 6.5). Atomic spacings (d/n) were calculated from formulae (6.1). In all cases glycollation is accompanied by enhancement of peak 2, (peaks referenced on fig. 6.5) the illite (001) reflection. The broad peak (1), interstratified clays, disappears and expansion of smectite perpendicular to the (001) plane gives a 17.7\AA reflection (peak 3). On heating to 335°C peak 3 disappears, smectite (001) spacing closes to 10\AA , and consequently peak 2 is enhanced. Peak 1, interstratified clay minerals are predominantly smectite/illite mixture.

The small peak marked 4, at 7.00\AA could represent the kaolinite (001) or chlorite (002) reflection. On heating to 550°C , the 7.00\AA peak disappeared and a possible small peak (5) at 14.0\AA - sample S24 (after heating to 335°C) is not present in the 550°C diffractogram. However, after treatment with HCl, the subsequently glycollated specimen showed no 7.00\AA peak. Consequently it is not possible from this analysis to differentiate between chlorite and kaolinite; however, differential thermal gravimetry (section 6.3.7 and 6.3.9) indicated typical kaolinite dehydroxylation. Grim (op. cit.) notes a solubility of 10% for kaolinite digested for 2 hours in 50% HCl at 85°C . He makes no mention of particle size or crystallinity. Susceptibility to acid attack is partly dependant on these, and it is conceivable that a small amount of poorly developed kaolinite might be destroyed by such 50% HCl digestion.

The clay size fraction is dominated by illite, interstratified illite/smectites and quartz. Assuming that the clay fraction contains these minerals only, and using the methods described earlier in this section, relative proportions have been approximated and are tabulated (table 6.3).

6.3.12 Crystallinity

Peak sharpness can be used as a measure of crystallinity. Kubler (1966) used peak width at mid-height, and Weaver (1960) the $10\text{\AA}/10.5\text{\AA}$ ordinate ratio of the (001) peak to measure the crystallinity of illite. Jackson (1969) notes that peak broadening occurs when particle size decreases below 0.02 micron. Many illite particles have diameters between 0.1 and 0.3 micron (Grim 1968). Consequently, only the smectite component of mixed layer clays is likely to be smaller than 0.02 micron and it would appear reasonable to assume that peak sharpness reflects illite crystallinity.

Crystallinity determined by both approximations are reported in fig. 6.5. Little variation in crystallinity is implied. Comparison with clay phase mineralogy and cation exchange capacities (table 6.3) indicates that Weavers (op. cit.) value is unlikely, and, although the measure suggested by Kubler (op. cit.) is rather more plausible, neither are particularly sensitive to variation in crystallinity suggested by table 6.3 and indicated by microscopy (section 6.5).

6.3.13 Cation Analysis - free salts and HCl/H₂O₂ extractions.

6.3.13.1 Anions present in free salts

Addition of barium chloride and silver nitrate to neutral solutions are well established tests for the presence of sulphates and chlorides (Vogel 1945). Surface and inter-laminae salts as shown in plate 6.1 were found to develop on most shales after prolonged storage. Quantitative tests on extracts made with approximately 0.01 M HNO₃ and 0.01 M HCl neutralized with sodium hydroxide to test for chlorides and sulphates, proved the latter to be the only significant anion.

Perhaps a better idea of proportion can be obtained from leachate analysis (chapter 7). Although prior to leaching test 2 no sulphates were visible on leaching surfaces, analysis of the 1st leachate sample indicated concentrations of $17 \mu\text{g ml}^{-1}$ chlorides and $673 \mu\text{gml}^{-1}$

sulphates, and total anions of strong acid showed that other species only existed in negligible proportions.

6.3.13.2 Extraction of free salts and cation analysis

Approximately 1 gram of finely ground but not sieved sample (known moisture content) was added to 15ml centrifuge tubes, and extracted by centrifuge washing three times in 1 M NH_4OAc (ammonium acetate) of pH7 (Jackson 1958) at 2000 rpm. Washings were collected, acidified with 1 ml of concentrated HCl, made up to volumes of 25ml and filtered through Whatmans No.1 filter paper.

Standards for cation analysis were prepared in 1 M NH_4OAc , and acidified with HCl to give the same concentration as in samples. Details of analytical technique employed for K^+ , Na^+ , Ca^{2+} , Mg^{2+} , Al^{3+} , Fe^{total} and Cu^{total} are to be found in section 7.4.8.10.

Results of duplicate analysis expressed in meq/100g of dry soil are tabulated in table 6.6. Although a sulphate complex involving Na^+ , K^+ , Mg^{2+} and Ca^{2+} is indicated, the free salt which will be hydrated is largely gypsiferous.

6.3.13.3 HCl/H₂O₂ extraction and Cation analysis

Rees and Hilton (1978) describe the successful extraction of heavy metals from sewerage sludges using a 2 hour digestion on a heated water bath. Church (1983) proved the method successful for extracting heavy metals from sediments in the River Taff. Clay minerals, in particular illites and muscovites, are not completely stable in such digestions, However, clay phase solubilities, indicated by determined aluminium concentrations, provide an additional measure of particle size, crystallinity and weathering degradation; they also make interesting comparison with cation exchange capacity (6.3.8) and thermal gravimetry dehydroxylation (6.3.9). Quantitative data pertinent to the sulphide and carbonate phases are also derived.

Residues from the NH_4OAc extraction were washed into wide necked conical flasks, 10ml of concentrated HCl and 15ml of 30% w/v H_2O_2 were added. Digestions were carried out on a hot plate at 70°C for two hours and allowed to cool before filtering through the Whatmans No.1 filter papers used in the NH_4OAc extractions. Samples were then evaporated at 70°C to dryness; and stored for cation analysis.

Samples were analysed for the same cation species as was the NaOAc and duplicate results are recorded in table 6.7. If errors were confined to Mg^{2+} and Ca^{2+} only, they would have been attributed to large aliquot dilutions. Although replicate variation occasionally exceeds 10%, results from a sample are not consistently lower or higher than their duplicate.

Summating the concentrations of non transition elements and expressing the difference between totals as a percentage, the difference appears much less, i.e. 0.62%, 2.52%, and 0.56% for S11, S21 and S24 respectively. Therefore variation is attributed to heterogeneity. Replicate total iron concentrations are more consistent suggesting a regular distribution. The majority of iron is in the form of sulphides with one major exception : approximately 20% limonite of sample S21 (calculated from Reads (1947) tentative limonite formulation, i.e. $\text{Fe}_2\text{O}_3 \cdot 3\text{H}_2\text{O}$ and dehydration measured by thermal gravimetry).

Sulphide minerals are apparently distributed evenly throughout the mudrocks. This seems conducive to the mechanism postulated by Hallam (1960), who noted that pyrite is largely interstitial, formation is related to the liberation of hydrogen sulphide and a fall of pH from 8 to 7.5 - the possible result of previous calcite precipitation. Groundwater maintains a high pH, following oxidation limonite is rapidly precipitated, or more likely, oxidised iron hydrate remains at its original site.

To some extent the heterogeneous nature of the rock contributes to

these variations but there are three factors which slightly impair the validity of comparison.

1. In calculating the carbonate content from thermal gravimetry, it was assumed that calcite only was present (section 6.3.14).
2. The measurement technique employed for quantitative analysis of the thermal gravimetry traces, results in a small over estimation (section 5.3.3).
3. In approximating carbonate content from cation analysis, a small ferrous content was ignored (section 6.4).

Although a decrease in error magnitude would result for samples S21 and S24, it would increase for sample S11. Consequently, variation can only be attributed to heterogeneity.

Thermal gravimetry (section 6.3.9) indicated a greater OH content in the clay sized fraction of the weathered sample S21, and cation exchange capacity was also much higher than that suggested by mineralogy (table 6.3). "Acid attack begins around the edge of the particles and works inward" - Grim (1968). Enhancement of clay mineral solubility is therefore likely where particle size is small, poorly crystalline or degraded by the action of weathering. K_2O (potassium oxide) and Al_2O_3 (aluminium oxide) contents for the total estimated phyllosilicates are presented in table 6.5, these are much lower than total contents suggested by Grim (op. cit.); e.g. approximately 25% Al_2O_3 and 6 to 8% K_2O for dioctohedral illites with little isomorphic substitution. As expected, sample S21 (WV) showed the greatest solubility. Particle size analysis (fig. 6.4) of sample S11 indicates that more than 60% of the pretreated residue was finer than 0.2 micron and the clay phase appears only slightly less soluble than the sample S21. Particle size and crystallinity is greatest in sample S24, and this is reflected by the recorded solubilities (table 6.5).

6.3.14 Synthesis (compilation of table 6.2)

Carbonates were calculated from CO_2 losses measured by thermal gravimetry, assuming them to comprise only CaCO_3 . Errors incurred by such an assumption, and the interpretation technique have been previously discussed (section 6.3.12.3).

Organic carbon was estimated by thermal gravimetry (section 5.3.3.8).

Total iron determined by wet chemical analysis was assigned to sulphides only, except in sample S21 where 20% was attributed to limonite. Copper and manganese are also likely to be present as sulphides, reference to table 6.7 suggests that the magnitude of error caused by ignoring them is very small. Conversely, staining with potassium ferricyanide and alizarin-Red-S solution indicated carbonates to be slightly ferroan - errors are to some extent compensatory.

Sulphates and iron hydroxides were calculated from thermal gravimetry (section 5.3.3.2 & 3). Sulphates were assumed gypsiferous, and the small error incurred is discussed in section 6.3.12.2).

Clay and silt sized fractions were determined from particle size analysis, and assigned proportionately to the residual, after deducting cementitious phases, sulphides and free salts. Thermal gravimetry was used to approximate mica and kaolin (section 6.3.7), which was deducted from the silt content to give the quantity of quartz. Feldspar appears to be present only in negligible amounts and has been ignored (sections 6.3.6 and 6.3.7).

Quartz content in the clay sized fraction was determined by Brindleys (1980) method of known additions. The remainder of the clay sized fraction has been attributed to illites and the smectite component of an illite/smectite mixed layer complex, and was apportioned to each phase as indicated in section 6.3.11.

6.4 Carbonate Identification

Thin sections and small fragments etched with 1.5% v/v HCl and stained with alizarin-red-S and potassium ferricyanide solution, facilitated carbonate identification. Details of staining solutions and diagnostic reactions are given in table 6.8.

Necessitated by the tendency of less competent mudrocks to slake, etching and staining were achieved by adding small quantities of solution to specimens by dropper pipette.

Sample S11 : wet chemical analysis (table 6.7) indicates an approximate $\text{Ca}^{2+}/\text{Mg}^{2+}$ ratio of 20:1. Although fragments were readily stained, because of the relatively low carbonate content some colour intensity is lost. In plate 6.2, small areas with a pale burgundy tone are typical, and suggest a low ferroan calcite. Allochems, presumably bioclastic, are unstained and turquoise. Both are dolomitic, the turquoise colour indicating a ferroan content.

A "whisker" shaped allochem similar to the turquoise stained one showed a deep blue colour suggesting a high ferrous dolomite, possibly ankerite.

Sample S21 : the approximate $\text{Ca}^{2+}/\text{Mg}^{2+}$ ratio from table 6.7 is 33:1. Disaggregated specimens when stained with alizarin-red-S and potassium ferricyanide showed no stain, - indicative of calcite. Plate 6.6 shows a small amount of turquoise staining only. Friedman (1970) indicated that magnesium-calcite and dolomite stain purple when immersed in a boebeling alizarin-red-S/30% sodium hydroxide solution for 5 minutes. Plate 6.7 indicates a magnesium content. Friedman (op. cit.) also notes that alizarin-red-S solution (as table 6.8) will stain magnesium-calcites red/pink, indicating this sample to be dolomitic, and this presents a dilemma when considering the relatively high $\text{Ca}^{2+}/\text{Mg}^{2+}$ ratio.

Sample 24 : Both thin sections (plates 6.12 to 6.14 inclusive) and fragments were stained. Generally alizarin-red-S/potassium ferricyanide stained sections (including limestone thin sections) appeared purple, magnified and in plane polarized light, both micrite and matrix maintained a brown hue typical of unstained calcillutite.

Apparent in both thin section and fractured fragments, was a propensity of randomly distributed poorly crystalline sparite. Also noted by Wobber p65 (1963) this was attributed to aggrading neomorphism. However, it is likely that some of this patchy sparite is the result of post deposition infill of small cavity structures, initially formed by the release of hydrogen sulphide gases from decomposing organic material - i.e. fenestral structures. Aggrading neomorphism is inhibited by the presence of magnesium, (Tucker 1981) and staining suggests that this spar is dolomitic. Although dolomitisation may have been a subsequent phase to neomorphism, contention as to its origin is not of any significance in terms of this thesis and such structures are subsequently described as Patchy Spar.

In plate 6.12 to 6.14 the reluctance of the patchy spar to accept stain is clear. However, along grain boundaries and adjacent to cleavages, both pink and turquoise hues can be seen.

A fractured fragment (plate 6.11) taken in a zone apparently free of the patchy spar shows a strong burgundy colour, and is indicative of low ferroan calcite. Lower $\text{Ca}^{2+}/\text{Mg}^{2+}$ ratios, approximately 13:1 (table 6.7), and reluctance to accept stain, suggest a high Mg^{2+} content in the patchy spar.

6.5 Texture and Fabric

The Geological Society Engineering Group Working Party Report (1977) define :-

a) Texture - as referring to individual grains, and in particular geometric aspects of, and mutual relationship amongst, component particles and crystals.

b) Sedimentary rock fabric - as the orientation (or lack of it), in space, of elements (discrete particles, crystals and cement) comprising the rock.

It is in these senses that the terms texture and fabric are used, although micro discontinuities are also included as a fabric element.

Texture and fabric studies have been facilitated using the S.E.M. (Scanning Electron Microscope), a low magnification ocular microscope - to examine fractured fragments, and in the case of sample S24, microscopic examination of thin sections.

Micrographs (plates 6.2 to 6.17), with the exception of plates 6.6 and 6.7, show the fabric of the three mudrocks (S11, S21 and S24). Descriptive notes accompany each micrograph.

i) Fissility and laminated structure.

In earlier discussion (section 5.2.1), the definition fissile mudstone was adopted to describe a shale. The three mudrocks all exhibit laminated structure, but sample S24 is not fissile. Observations of increased fissility with weathering are recorded by Ingram (1953). Reference to mineralogy suggests that, unweathered, sample S21 would be unlikely to exhibit fissility.

ii) Discontinuities

The action of tectonic horizontal shearing in these mudrocks has been discussed (section 2.5). Resulting low angled fractures are consistently found. Regularly spaced (approximately 5mm centres), low angled discontinuities are noted in the meso description of sample S24 (table 5.6.3).

A propensity of carbonate filled gashes, orientated parallel, and at low angles to the bedding, are apparent in thin sections (plates 6.13 and 6.14 - sample S24). These are attributed to tectonic and horizontal shearing, and with the low angled discontinuities contributed to strength anisotropy.

Petrological studies of the limestones (section 8.2.5) show that tectonic micro fractures are filled almost exclusively with a sparry ferroan/dolomite. Lineations of slightly higher relief than surroundings, in scanning electron micrographs (plates 6.8 and 6.15) of completely weathered sample S21, and an etched specimen from sample S24, suggest that micro discontinuities are again dolomite filled. However, carbonate development is frequently poor, and adjacent fractured surfaces are only weakly bonded.

On some of these fractured surfaces, veneer like carbonate has developed on both limbs (plates 6.8 and 6.9). Cone in cone type structures described by Richardson (1923) in the much thicker, so called 'beef' of the Dorset Liassic shales, were not found in any of several examined specimens. More major meso scale horizontal discontinuities are frequently 'open' and the adjacent rock fabric exhibits a degree of weathering. Fractured fragments (plates 6.3 and 6.11) show systems of micro scale low angled discontinuities, these look "open" but the poor micrograph quality precludes the positive identification of any infilling carbonate.

iii) Sulphates

Sulphate formation has been referred to in section 6.3.13.1. Seepage along horizontal discontinuities in low permeability shales is described in section 7.1. Frequently this seepage is intermittent, and drying out leads to crystallisation. Discontinuity located sulphate crystals are indicated on plate 6.3

iv) Patchy spar

In reviewing related research, Tucker (op. cit.) notes that

neomorphism is inhibited by the presence of Mg^{2+} . Therefore, formation of patchy spar in the mudrocks is somewhat paradoxical and may be the result of neomorphism and subsequent dolomitisation and/or the infilling of fenestral cavities (section 6.4). In sample S24 the amount and frequency of patchy spar and organic carbon is a maximum; while Ca^{2+}/Mg^{2+} a minimum. The influence of patchy spar on engineering properties and behaviour, is a reduction in strength anisotropy and fissility.

v) Peloids

Peloids are described in the notes to plate 6.12, largely faecal matter they are high in organic carbon content.

vi) Silt Sized Quartz

Micrograph (plate 6.10) shows abundant quartz, maximum size 20 microns and exhibiting a high degree of orientation. Neomorphic spar is recognised by its patchy and irregular morphology. On the other hand quartz particles will be subrounded/rounded. Such particles are also apparent in thin section (plates 6.12 and 6.14).

vii) Fine grained matrix material

Matrix material is typically brown in thin section, even though stained (plates 6.12 and 6.14), and largely comprises clay, fine quartz, finely disseminated pyrite and micrite. Partially masked by patchy spar, the crenulated structure indicated in plate 6.5 (sample S11) is similar to that indicated by Davis (1977) for a predominantly illitic mudrock. Plate 6.8 shows the fabric of sample S21. Location of discontinuities and adjacent particle arrangement, suggest tectonic modification. The structure is not crenulated, but the form suggests considerable crystallinity degradation. Apertures apparent in fractured surface may have been sites of allochems or authigenic minerals which formed soon after deposition. Matrix material forms "interweaving bunches" (see Collins and McGowan 1974) around these

apertures. Although after etching much of the matrix material in plate 6.16 is still masked by carbonates, a planar laminated structure is apparent. Particles appear more crystalline than those in both samples S21 and S24.

6.6 The Clay Phase and its influence on mudrock behaviour

6.6.1 Introduction

The physical and physico-chemical behaviour of various clay minerals have been the subject of much research, e.g. Osion and Mesri (1970). As crystallinity and particle size decrease, cation exchange capacities, plasticity, compressibility, swell and potential shrinkage increase.

When cementation completely encapsulates clay minerals, not only inhibiting the ability to absorb water but also prohibiting swelling, the clay phase has no influence on the physical/physico-chemical behaviour of the rock.

In section 5.2.5, Clayton, Simons and Matthews (1982) classification was used to define the degree of cementation. Sample S21 (WV) was unclassified; however, at low moisture contents on a meso scale it could be considered compact. Cementation of clay crystallites by both iron hydroxides and carbonates possibly impair full physical/physico-chemical response to a greater extent than that suggested by the degree of meso cementation.

6.6.2 Consolidation/Swelling Tests

Crushed samples (majority of material passing 425 micron mesh, but excluding none) were made up at their liquid limits and allowed to cure for 24 hours. To investigate the physical/physico-chemical reaction of cemented clay crystallites, and therefore assess the influence of the clay phase on the cemented mudrocks, one dimensional consolidation and swelling tests were carried out to BS 1377 (1975)

test 17. The 'Logarithm of time' fitting method was used to assess c_v (coefficient of consolidation). In sample S24, the majority of settlement was immediate elastic, and differentiation between this and primary settlement was not possible using the 'square root of time' fitting method. Consolidation test data has been summarised in table 6.9. Although c_v generally decreased with increasing overburden, results produced a far from smooth curve.

Compression ratios (r_o , r_p & r_s) defined in fig. 6.6 provide a relative measure of immediate elastic, primary and secondary consolidation. Both physical and physico-chemical mechanisms contribute to primary consolidation. Oslon and Mesri (op. cit.) described platelet buckling and relative displacements as physical or mechanical, and noted that osmosis, adsorbed water chemistry and Van der Waal forces are the major influence in physico-chemical mechanisms. Using different pore liquids to study physical and physico-chemical mechanisms of consolidation and swelling, they showed that illite is dominated by physico-chemical behaviour. However, they proved that after high compression, double layer swelling is inhibited.

6.6.3 Discussion

In section 7.1, pyrite oxidation is discussed and enhanced carbonate leaching attributed to resulting acidity. Grim (1968) notes that in strong mineral acid/clay reactions, sulphuric acid is the most aggressive. Therefore it seems likely that acid weathering is also responsible for the modification of clay minerals.

At low applied pressures zero slope of the compression r_p /applied pressure graphs (fig. 6.6) indicates physico-chemical dominated primary consolidation; while zero slope at high pressures suggests dominant physical mechanisms.

Activity is defined by Skempton (1953) as :

$$\frac{\text{Plastic index \%}}{\text{Clay sized fraction \% (by wt)}} \quad (6.2)$$

This includes minerals other than clays, e.g. fine quartz, it also excludes phyllosilicates coarser than 2 micron. Activity, strictly speaking, is a function of the amount of clay, and not the amount of clay sized material. In fig. 6.7a activity given by equation (6-2) and activity given by equation (6-3) below, has been plotted against r_p values for overburden pressures of 100 kN/m².

$$\frac{\text{Plastic index \%}}{\text{Phyllosilicates : (by wt)}} \quad (6.3)$$

Phyllosilicates were readily quantified from the work presented in section 6.3.11. Graphs (fig. 6.7a) both show linear relationships; however, a small variation in quartz finer than 2 microns could prove misleading when using equation (6.2). Comparison of fig. 6.7 and table 6.2 clearly demonstrate that clay activity and not content are more important in assessing clay influence on mudrock behaviour and performance.

Fig. 6.7b shows swelling r_p 's increase linearly with phyllosilicate content. This suggests that during consolidation, structural water had become almost equally compressed in all three samples. Consequently results concur with the suggestion of Osion and Mesri (op. cit.) that mechanical mechanisms are the major swell contributors.

Availability of divalent and trivalent cations, coupled with diagenetically highly compressed double layers minimize physico-chemical response of clay minerals.

Acid weathering is active only at sites immediately adjacent to those where pyrite oxidation has occurred. (Ground/Vadose water quickly re-establishes equilibrium with the carbonate phase (section 7.1)). Highly reactive pyrite (section 5.5.1) is more prevalent in the strongly cemented mudrocks and argillaceous limestones. Consequently, mudrocks with low clay content are more vulnerable to acid attack. As well as crystallinity degradation, the degree of hydration increases.

Jackson (1969) notes that adsorbed water is lost between 25°C and 350°C. In the differential thermal gravimetry trace for sample S21 (WV)(fig.6.3) no weight loss below 350°C other than that of soil water was recorded. It is quite likely that part of this was adsorbed water.

Hydroxyl water measured by thermal gravimetry (section 6.3.12), especially in sample S21, was higher than expected. Grim (1968) notes that interlayer potassium ions can be replaced by hydronium ions ($(H_3O)^+$). Enhanced T.G. (thermal gravimetry) illite - pyrite - organic carbon peak weight losses (section 5.5.1 and table 5.7) in other acid weathered mudrocks can only be attributed to illite dehydroxylation, suggesting that a similar reaction has occurred.

As with double layer water, the compressed interlayer hydronium ion is unlikely to freely swell following consolidation. Replacement of interlayer K^+ with $(H_3O)^+$ is conducive with observations made in consolidation tests, and it appears a reasonable assumption that more strongly held interlayer 'water' would enhance T.G. dehydroxylation.

Skempton (1953) classified clays with an activity less than 0.75 as inactive. The three mudrocks tested all have activities lower than this.

Sample S24 with an activity of 0.2 is strongly cemented and the clay phase has little influence on mudrock performance.

Sample 11 is weakly cemented and easily eroded, and its horizon forms a line of marked weakness regardless of elevation. Fairly high in clay content, it acts as an effective impermeable barrier and is subject to seasonal swelling and shrinkage. Although inactive it is conjectured that shrinkage/swelling is of a magnitude that could develop considerable traction generated stress in adjacent limestones (section 10.3). Thermal gravimetry indicates relatively high sulphide stability (table 5.7). Although unlikely without a catalyst, pyrite oxidation is occasionally indicated by the presence of yellow brown

staining. However, such acid weathered zones exhibit higher plasticity (e.g. Samples S14 and S15 - section 5.2.6) enhancing the influence of the clay phase on the mudrocks. Although clay mineral response is largely mechanical, the clay phase dominates mudrock behaviour.

Sample S21 Although low in clay content the sample contains readily oxidisable sulphides (table 5.7). Increased by acid weathering, activity is greater than in Sample S11 even though the phyllosilicate content in that sample is twice as high. The influence on consolidation is demonstrated in fig. 6.6 and 6.7. In spite of being highly calcareous, clay particles appear to be relatively unrestrained by cementitious material.

6.6.4 Summary

In strongly cemented mudrocks, phyllosilicates are cementitiously restrained to an extent where they exert little influence on mudrock behaviour. The reverse is true in weaker mudrocks. However, in the absence of acid weathering, response of the phyllosilicate clay phase is largely mechanical. Acid weathering is prone to attack more indurated mudrocks, in which the sulphide phase is highly reactive. As well as enhancing carbonate destruction and increasing fissility, it modifies phyllosilicate structural water. Increased activity results in physico-chemical mechanisms enhancing clay phase influence on mudrock behaviour.

6.7 Shrinkage

Moisture contents of freshly sampled mudrocks ranged from just under 1% to approximately 30% (table 5.6). Only mudrocks weathered to an advanced state, and from horizon 28a (Trueman 1930) had moisture contents above 20%.

Shrinkage limits of remoulded specimens (using triturated, but otherwise untreated material - majority passing 425 micron sieve, but

to the exclusion of none) from samples S11, S21 and S24 were determined using the T.R.R.L. (1952) method. Results of duplicated tests are presented in fig. 6.8. The low clay content and activity of sample S24 prevented specimens being remoulded at moisture contents above the shrinkage limit. Because activity is dependant on clay content and on the physico-chemical properties of the clay phase, it is conjectured that an inverse relationship between activity and shrinkage limit exists. Therefore, shrinkage limit of sample S24 is likely to be in the region of 20%, but this is only of passing interest, as mudrock moisture content will never exceed that value.

Linear shrinkage and shrinkage limit was determined for intact specimens prepared from samples S14 and S15. Both samples, located within several metres of each other, were from horizon 28a (Trueman 1930), - Summerhouse (SS 99580 66424) yellow brown in colour, sample S15 was more cohesive and apparently acid weathered (table 5.6 and section 5.2.6).

In these tests particular care was taken to ensure that specimens dried out slowly; a process which took several days.

Brickettes were prepared for both tests by trimming with a knife. In the linear shrinkage test, location points were marked to facilitate accurate vernier gauge measurement.

The T.R.R.L. (1952) designed apparatus was used to determine shrinkage limits. Sample details and results are presented in fig. 6.8. It is difficult to make comparisons between the two specimens used in linear determinations because of the variation in moisture content. However, the proportional shrinkage perpendicular to laminae and relative to parallel shrinkage is much greater in specimen S15. Shrinkage limits were satisfactorily determined (fig. 6.8), but below the limit fissuring parallel to laminations, preventing the normal straight line plot. Undoubtedly mercury entered these fissures negating results.

It is perhaps surprising that linear shrinkage test specimens did not fissure, and that shrinkage limit ones did. Magnitude of perpendicular shrinkage does suggest the development of high internal stresses, but these are enhanced when coupled with uplift forces during immersion in mercury.

6.8 Mudrocks & Limestones - temperature and environmental controlled Movements

Response (change in unit length and water content) of representative mudrocks and limestones to different climatic and environmental conditions were determined on removal from the particular laboratory controlled environment.

Demec buttons for use with a 100mm gauge were bonded to specimen surfaces, two sets to each NX sized core, and one set to each hand trimmed mudrock specimen. Demec buttons were positioned on mudrocks to facilitate measurement parallel to the bedding. Specimens, carbonate contents in brackets, were from mudrock samples ; (description table 5.6) S11 (25%), S17 (37%), and S24 (50%) and limestones from (description table 8.4) L6a (61%) and L7a (80%)(note : suffix refers to core orientation - table 8.8).

In fig. 6.10 change in length has been plotted against environmental temperature, and water contents noted. Values joined by 'paths' are broken or solid depending on environment, and arrows denote test path. Lower case key letters are used to reference various environments scheduled in table 6.10. Water contents are expressed as a percentage of the dry weight measured immediately on removal from stage (d). Stages (n & p) involved immersion in water, prior to subsequent weighings surfaces were dried. Final water contents are moisture contents determined in accordance with current practice (Test 1A BS 1377).

Specimens S11 and S17 contracted during the initial heating stages (i.e. a to d) while the others all expanded. Coefficient of expansion/contraction for initial stages, (calculated from the best fit straight line to the four points a-d) are plotted against carbonate content in fig. 6.11. The graph (fig. 6.11) shows that at carbonate contents above 55% the clay phase is fully restrained.

Stage (a) water content is the laboratory air dry value. To obtain a bond between demec buttons and weaker mudrocks initial moisture content reduction was necessary.

Assuming as an end point the T.R.R.L. shrinkage limit, and by linear extrapolation the contraction of specimen S11 is 0.56%. It is difficult to define the shrinkage mechanism below the T.R.R.L. limit. Relatively small, the order of magnitude appears insignificant compared to shrinkage in mudrocks and clays where the moisture contents are above the shrinkage limit. However, in these intercalated limestones and shales such movements can instigate instability (section 10.2 & 3).

After oven drying at 80°C fragments from sample S11 exfoliated when immersed in water (plate 6.18). Fabric examination of sample S11 (plate 6.5) indicated a crenulated structure. A possible mechanism for buckling of clay platelets, is post-dehydration response to crystallite positive end charges and negative surface charges. Jackson (op. cit.) notes that dehydration weight loss of illites occurring between 25°C and 350°C is approximately 1.6%.

Thermal gravimetry weight loss following apparent initial moisture loss is negligible (fig. 6.3a and section 6.3.9). Consequently almost all dehydration must occur at temperatures below 100°C. Crystallite buckling would facilitate mechanical separation in water and could be the shortening mechanism.

Figure 6.10 shows similar subsequent cooling and heating 'paths' for all samples. Final stages of the mudrock tests indicate, sample S11

quickly breaking down when immersed in water, and sample S17 breaking down after immersion for an hour. Sample S24 although showing a small expansion on immersion was able to sustain subsequent freezing.

6.9 Compression strength testing (Sample S17)

6.9.1 Strength criteria

Testing was carried out on specimens from sample S17 only. Weakly cemented, and with a marked fissility parallel to the bedding, recovery of suitably long cores was not possible. In calibrating the N.C.B. cone indenter, Szlavín (1974) used Hobbs (1964) formula to standardise compression results :

$$f_c = \frac{fx}{0.304\frac{D}{H} + 0.848} \quad (6.4)$$

where f_c = Standard uniaxial compression strength Hobbs (op. cit.)
suggested a standard H/D ratio of 2. (Core diameter = 25.4mm)

fx = Actual compressive strength.

D = Diameter.

H = Sample height.

The N.C.B. cone indenter was generally used to estimate mudrock unconfined compression strength (section 5.4.7). Therefore, in direct uniaxial compression tests Hobbs (op. cit.) correction was used for consistency. No adjustment was made to triaxial compression test results. Mogi (1966a) has shown that the effect of H/D ratio on strength rapidly diminishes with increased confining pressure.

Haas (1983) notes problems in manufacturing weak mudrock cores to high standards. He suggests end capping, which is forbidden by the

I.S.R.M. (International Society for Rock Mechanics - 1978 and 1979). Air flush facilitated coring; however accurate parting off proved impossible, and it was necessary to hand lap ends. The high manufacturing standards specified by I.S.R.M. (op. cit.) were not achieved, (for discussion see section 8.5.3) but this does not appear detrimental to results, (fig. 6.12). Specimens such as these, with low elastic moduli are readily able to deform, and thus compensate for manufacturing imperfections of the magnitude recorded in table 6.11.

To standardise moisture content, specimens other than those strain gauged, were stored for 72 hours in a concrete curing room (relative humidity 100%). Details of compression testing machine and methodology are described in section (8.5.4). Specimen data is recorded in table 6.11.

Throughout much of the brittle range, the linear shear strength envelope fig. 6.12 is a good fit to plotted triaxial compression test data. Uniaxial tensile strength perpendicular to the laminae, if not zero, is negligible and therefore at low values of normal stress the shear strength envelope can be assumed circumferential to the uniaxial compression Mohrs circle. Mogi (1966b) notes that the transition between brittle and ductile behaviour is defined by :

$$f_1 = 3.4 f_3 \quad (6.5)$$

where f_1 = Maximum principal stress.

f_3 = Minimum principal stress.

The specimen confined at 35 MPa exhibited ductile behaviour at failure (plate 6.19). In plate 6.19 and 6.20 specimens tested in triaxial and uniaxial compression have been reconstructed to show failure modes. Directly measured uniaxial compressive strength is within the 90% confidence limits of the mean N.C.B. index value (fig. 5.8).

Sensitivity to moisture content variation is emphasised by the plotted Mohrs circle for uniaxial compressive strength of the strain gauged sample (fig. 6.13). A reduced moisture content from 3.29% to 2.23% contributed to a 50% strength increase.

6.9.2 Deformation Characteristics

Electrical resistance strain gauges located at core mid-heights were used to facilitate this investigation. Details of measuring equipment and methodology are given in section 8.5.7. Two laminated mudrock specimens from sample S17 were tested :

- i) Cored perpendicular to the bedding and laminae.
- ii) Cored parallel to the bedding and laminae.

One pair of strain gauges set diametrically opposite were used to measure strains in the directions indicated in fig. 6.14 and 15. In fig. 6.13 the stress strain curves are plotted for i) above. Strain gauge bonding failure occurred at just over 40% of the ultimate load. E (tangent elastic modulus) value at 40% f_c , reported in fig. 6.13, is much lower than the values determined for the sample cored parallel to the bedding (fig. 6.14 & 6.15). Gradient of the stress/strain curve is initially less as might be expected. However, the magnitude of change in slope does not suggest significant pressure relief instigated fissuring. Thermal gravimetric weight loss attributed to illite and pyrite is comparatively high (table 5.7) suggesting a relatively high clay content. Plate 6.4 shows the crenulated fabric of high clay content sample S11. The low E value can largely be attributed to fabric, and the small value of ν (poissons ratio i.e.: 0.084) is conducive with crenulations having resulted from dehydration (section 6-8). In table 6.11 a slightly mottled yellow ochre colour is noted in the upper part of the sample suggesting some acid weathering. Clay mineral double layer swelling (section 6.6) together with replacement of interlayer potassium by hydronium ions will increase compressibility, and particularly so if clay mineral (001) planes are orientated parallel to laminae.

Fig. 6.14 and 6.15 show the stress/strain curves for the shale specimen loaded parallel to laminae. At right angles to the laminae restraint is poor, and during loading shortening, both by buckling and axial compression, will occur. Consequently there is an anisotropy of deformation characteristics. Recoverable deformation measured from an unloading hysteresis is similar regardless of anisotropy, and equal to full recovery of compression test instigated axial and circumferential deformation measured parallel to laminae. Just prior to sample failure, and as a result of local failure remote from strain gauge sites, with consequent stress relief, a large reduction in measurement strains are recorded (fig. 6.14 and 6.15).

6.10 Summary

Varied strengths and durabilities are exhibited by the Lower Lias mudrocks of South Wales. Three samples, listed below, were selected for detailed mineralogical analysis because they exhibited the extremes of properties.

Sample S11:- an incompetent shale from Horizon 28a. Where exposed in the sea cliff, regardless of elevation, this horizon forms a marked line of weakness.

Sample S21:- a completely weathered mudrock (WV) from Horizon 38a. Fissile, of high carbonate content and brownish yellow in colour.

The brownish yellow colour is caused by pyrite oxidation, and resulting acid weathering has degraded the mudrock. Although a contemporary mechanism, it is conjectured that there have been periods in fairly recent geological history which would have been more favourable to such weathering (section 2.1).

Sample S24:- a highly competent, strongly cemented mudrock from Horizon 43a.

The results of analyses have been compiled in table 6.2 to provide a quantitative estimate of the significant mineralogical phases.

Staining techniques used to identify carbonate types are described in section 6.4. Carbonates are generally high in calcium, but the presence of both magnesium and iron was detected. Results from staining frequently suggested that carbonates had higher magnesium contents than Mg^{2+} values, determined from wet chemical analysis indicated. More reliance is put on the wet chemical analysis; however, secondary carbonates are invariably high in magnesium and are frequently dolomitic.

Mudrock fabrics are described in section 6.5. Patchy spar inhibited the examination of fabric, but it was possible to infer the following arrangement of matrix material.

Plate 6.5 - a crenulated fabric in sample S11.

Plate 6.8 - degraded crystallinity and interweaving clay bunches between apertures - Sample S21.

Plate 6.15 - although masked, a planar laminated structure is inferred. Crystallinity appears greater than in S11 or S21.

Consolidation tests (section 6.6), cation exchange capabilities (table 6.3 and section 6.3.8), clay mineral solubility (table 6.5) and fabric investigations (section 6.5), all suggest degradation and structural changes to the clay phase of sample S21. Although having a lower clay content than sample S11, activity is higher. Primary consolidation ratios at low overburden pressures (100kN/m² per. se.) appear linearly proportional to activity (fig. 6.7a). Swelling ratios are apparently proportional to phyllosilicate content - which seems to confirm the observation of Osion and Mesri (1970) that severely compressed illitic double layers are reticent to swell, and serve as a partial explanation as to why the activity of sample S11, with its high clay content, is low. Clay phase thermal gravimetric

dehydroxylation losses, particularly those of sample S21 were greater than suggested by Jackson (1969). It is postulated that removal of potassium and replacement by hydronium ions (suggested by Grim 1968) would enhance thermal gravimetric dehydroxylation as well as compressibility. Degradation of clay minerals is attributed to acid attack, the result of pyrite oxidation. Perhaps fortunately, it appears that only sulphide phases in mudrocks of low clay/high carbonate contents are of low stability (section 5.5.1) and consequently are more likely to be subject to acid weathering.

Fig. 6.8 and 9 detail the T.R.R.L. shrinkage limits of various intact and remoulded specimens. Below the shrinkage limit, intact specimens fissured and a volume increase was recorded. Specimens from samples S14 and S15 were used to determine linear shrinkage and did not fracture on drying. Linear shrinkage recorded at right angles to fissility was much greater in the acid weathered specimen (sample S15 - fig. 6.9).

Small, but not insignificant shrinkage in poorly cemented mudrocks at moisture contents below the shrinkage limit, was recorded in laboratory controlled environment tests (fig. 6.10). Contraction is attributed to low temperature dehydration (section 6.8). Coefficients of expansion/contraction associated with the initial heating phase are plotted against carbonate content (fig. 6.11). The graph serves to emphasise the effectiveness of the cementitious phase in restraining physico-chemical response of clay minerals. When the carbonate content rises above 55% in unweathered specimens, the clay phase appears totally restrained.

The shear strength envelope, plotted, for sample S17, from uniaxial and triaxial compression tests results, shows that shear strength, over much of the brittle range, is defined by a linear envelope (fig. 6.12). A Mohr's circle for a uniaxial test specimen with a slightly lower moisture content is also plotted, and shows almost a 50% increase in strength.

Load induced deformation characteristics in specimens, from sample S17, cored parallel and perpendicular to bedding is largely fabric controlled. Deformation anisotropy is detailed in fig. 6.12, '13, 14, 15 and 16 - section 6.9.2.

Mineralogical analyses and tests to determine physical and physico-chemical mudrock behaviour have been described in this chapter. Investigations were largely confined to three mudrocks exhibiting extremes of physical behaviour, and these to some extent make index test and thermal gravimetry results on intermediate samples more meaningful.

It was, perhaps, rather fortuitous that a completely weathered mudrock, sample S21, with small clay/high carbonate content was chosen. The choice served to show rather well the degradation effect of pyrite oxidation, not only in breaking down what was probably a strongly cemented mudrock, but also in impairing the engineering properties of the clay phase.

CHAPTER 7

LEACHING

7.1 Introduction

According to Peltier (1950, see fig. 3.1), contemporary weathering might be described as

".....moderate chemical with frost action".

In Chapters 5 and 6, properties, behaviour and mineralogy of the mudrocks were described. In this chapter, weatherability under the leaching action of locally derived rainwater is examined.

Precipitated calcareous tufa, located at seepage zones on many of the more stable sections of these rapidly alternating limestone/mudrock cliffs, provides evidence of contemporary carbonate leaching.

Thicker and less competent bucklandi zone mudrocks, with lower vertical discontinuity frequencies than the intercalated limestones inhibit vadose water seepage, and perched water tables develop. Frequently even major and master vertical discontinuities bisecting these barrier mudrocks are closed, but where they are sufficiently open they act as collector drains conveying water to a lower level, or permitting egress from the rock mass. Such springs are frequently associated with caves quarried along major discontinuities, examples of which are common between Dimhole (SS 952 676) and Tresilian (SS 946 677).

Seepage in low permeability mudrocks is along a system of low angled and horizontal discontinuities. Plate 7-1 (near infrared) shows a seepage line at horizon 28a (Trueman 1930) - Summerhouse (section 4.3.10 - SS 992 665).

In poorly lithified mudrocks with low carbonate contents it has been

demonstrated (Chapter 6) that the clay phase influences mudrock behaviour. Leaching of the cementitious phase reduces the restraint which it affords, and enhances the influence of the clay phase.

Yellowish brown staining adjacent to discontinuities is attributed to pyrite oxidation. The resulting drop of solution pH is contemporaneously restored to that with the dominant carbonate phase by carbonate leaching. Iron is precipitated from basic solutions, and consequently hydrated oxides/hydroxides form at, or in close proximity to, the site of weathering. Sulphates, on the other hand, are usually transported from the site of oxidation as ions in solution. Under earlier, but more aggressive climatic regimes chemical weathering would have been far more active (section 2.2.2). However, amongst the flora, Clematis Vitalba (Old Man's Beard), a calcicole, and Gorse U Europaeus, a calcifuge, were found, the latter suggesting that pyrite oxidation is a contemporary weathering mechanism of some significance.

Pyrite is a mineral stable at low pressures and temperature and in water (Curtis 1976). Curtis (op.cit.) supported by the argument that spontaneous combustion can occur in unconsolidated pyritic rich shale tips, where aerobic conditions exist, determined that pyrites (a highly reduced phase) had a free energy change of $-17.68 \text{ K cal g atom}^{-1}$, i.e. the same order as hydrocarbon combustion. Yet Attewell and Farmer (1976) note that there is little evidence in the work of Attewell and Taylor (1971) to suggest that any non-detrital minerals play a dominant role in the breakdown process of coal measure rocks (which to some extent is confirmed by the work of Jones - pers. com. 1984). Martna (1970) described problems of constructing underground openings in metamorphic rocks containing pyrrhotite - highly unstable in the presence of oxygen, the reactant products of oxidation (i.e. Gypsum) caused rapid expansion in weak fissured rock. Other similar cases have been reported and several of these are reviewed by Taylor and Cripps (1984). Ground water analyses by Vear and Curtis (1981), and laboratory investigation by Steward and Cripps (1983) suggest that pyrite weathering is the major instigator of instability at Mam Tor, Yorkshire.

Vadose and perched ground water seepage, along the area of interest, fluctuates rapidly in response to rainfall. Undoubtedly the majority of rock face seepage is permeating rainwater of local origin, and consequently will be rich in dissolved oxygen. In the presence of oxygen, pyrites may be unstable.

Literature suggests that the significance of pyrite oxidation as a major weathering agent in carbonaceous mudrocks is, at best, unpredictable.

Decomposition characteristics of various allotropic forms of iron sulphides were discussed with respect to weatherability in section 5.5.1. Thermal gravimetry implied that decomposition of poorly crystalline forms occurred at lower activation energy levels. A sudden weight loss characteristic of strong exothermic reactions typified poorly crystalline iron sulphides. With more crystalline types, magnitude of sudden weight losses were much less and gradual weight loss with increasing temperature typified decomposition.

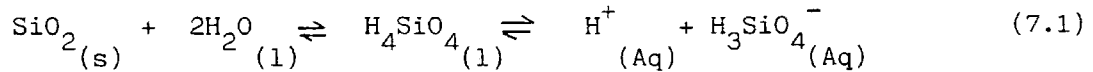
Evidence suggests (section 5.3.3.5 and 6) that crystallinity of pyrites is greater in the less well lithified and relatively incompetent shales, and is therefore, less likely to oxidise and enhance the leaching potential of seeping water.

The 1949 Coastal Protection Act makes provision for grant aid, only where marine erosion is the major instigator of instability. Geomorphological, geotechnical and mineralogical evidence (Chapters 4,5 and 6) has been presented which shows that, both above and below the level of marine attack, mudrock 28a is a major line of weakness. Therefore, the role played by chemical weathering in the degradation of these less competent shales is of considerable financial, as well as engineering, significance. Experiments to assess the likely contribution of leaching to instability were conducted and are reported in this chapter. A specimen of incompetent shale 28a (sample S11) is contrasted with that from highly competent mudrock 43a (sample S24). Both samples were leached with rain water (section 3-2) collected at Nash.

7.2 Chemical Weathering Reaction

7.2.1 Hydrolysis

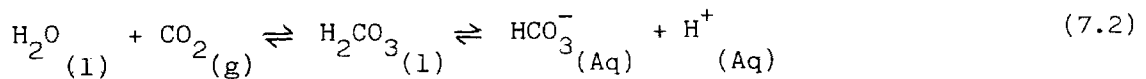
Hydrolysis is the reaction of a compound with water to form a weak acid or base. Silicates react with water to form weak silicic acid which dissociates above pH 9 i.e. :-



Below pH 10 dissolved silica is not likely to exceed $10 \mu\text{g ml}^{-1}$; however, colloidal silica may occur in suspension and it is also possible that amorphous silica may be precipitated at the site of weathering (Brownlow 1979).

7.2.2 Solution Weathering of Carbonates

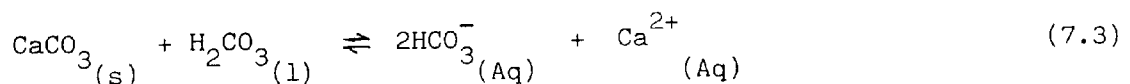
Leaching water takes on carbon dioxide to form a weak carbonic acid



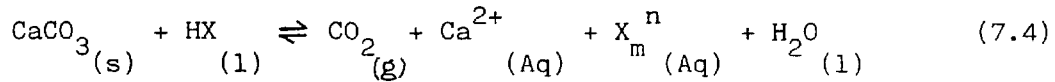
with approximately 50% dissociation at pH 6.5 and 90% at pH 7 (Brownlow 1979). Garrels and Christ (1966) show that the increased solubility of carbonate rocks as a result of dissolved carbon dioxide in rainwater (molarity of approx. $10^{-4.8}$) is only in the order of 10%.

However, they conjecture that the effect of hydrolysis and CO_2 in the soil atmosphere contributes significantly to increasing carbonate rock solubility.

Calcite solution can be represented by the equation :



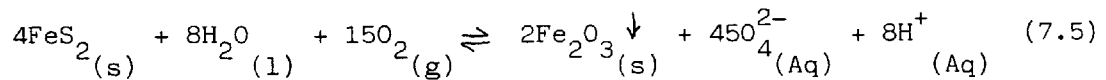
Strong acids also facilitate carbonate solution, i.e. :



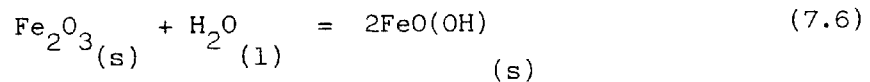
Where x is the anion of a strong acid.

7.2.3 Iron Sulphide Oxidation

The decomposition of pyrite in an oxygenated environment is usually represented by the equation 7.5 (Brownlow op.cit.), showing haematite as the precipitated ferric salt :



However, the initial precipitate, a hydrous oxide of indeterminate water content, is unstable in respect of both haematite (Fe_2O_3) and goethite (FeO(OH)), the relationship between these can be expressed as:



Limonite, a common weathering product of pyrites is described by Whitten and Brooks (1972) as comprising various amorphous and cryptocrystalline constituents of hydrous iron oxides and hydroxides.

Vear and Curtis (1981), and Hawkins and Pinches (1984) both note that ferrous oxidation is enhanced in an acid environment by acidophilic bacteria, i.e. Thiobacillus ferro oxidans and Thiobacillus thio oxidans. The nitrate ion with an oxidation number of +5 is a strong oxidising agent, and its presence in aqueous solution may well further facilitate pyrite decomposition.

7.2.4 Ion Exchange

The dominant clay mineral is illite (Chapter 6). Adsorbed ions at particle edges are readily exchanged. However, replacement of interlayer structural potassium is likely to be slow (Grim 1968), although Gillot (1968) indicates that fixity becomes less effective in an acid environment.

If interlayer potassium has been leached or exchanged to form degraded illites the process is readily reversed, i.e. depleted interlayer potassium is replenished if and when a source becomes available.

7.3 Previous Work

Sensitivity of clay is dependant on cation species and concentration in the adsorbed layer. Sherrard, Ryker and Decker (1972), suggest that clay made up from natural moisture content with distilled water to the liquid limit, could be left for several hours under vacuum filtration, and the extract analysed for Ca^{2+} , Mg^{2+} , Na^+ and K^+ . The percentage Na^+ to total dissolved salts (T.D.S.) and the sodium absorption rate (S.A.R.) calculated from equation 7.7 is suggested as a criterion for assessing sensitivity.

$$\text{S.A.R.} = \frac{\text{Na}^+}{\sqrt{\left(\frac{\text{Ca}^2 + \text{Mg}^2}{2}\right)}} \quad (7.7)$$

Laboratory leaching experiments are often carried out using leaching fluids more acid or alkaline than naturally occurring waters. Consequently, cementitious phases and free salts are leached, and the ionic concentration of adsorbed and interstitial water rapidly reduced; effects on geotechnical properties are then ascertained.

Moore, Brown and Rashid (1977) investigated the effect of leaching on the engineering properties of a marine sediment, using 0.5N solution of Sodium hydroxide and a 25% solution of acetic acid. Apparatus permitted leaching and subsequent testing of standard triaxial, and 70mm diameter oedometer samples without disturbance at any stage of the tests. It was concluded that a 60% loss in shear strength resulting from Sodium hydroxide leaching was largely the result of a breakdown in organic compounds bonding aggregations of clay particles. The recorded reduction in organic content, maximum initial content 1.53%, varied between 50% and 60%.

Steward and Cripps (1983) introduced solutions of sulphuric acid, and sodium and potassium nitrates into specimens of Edale Shale during shear strength testing in a modified Bromhead ring shear box. The 0.14% solution of sulphuric acid used, represented ground water concentration of sulphate ions. A 1.0 metre head was found adequate to maintain flow of the leaching fluid through the specimen.

When the leaching fluid was changed from distilled water to 0.14% sulphuric acid, residual shear strength values showed a 2° to 5° increase from 22°. A 0.1 M sodium nitrate solution resulted in a decrease to 20° and predictably a 1 M potassium nitrate an increase to 23°.

7.4 Experimental Details and Procedures

7.4.1 Introduction

The weathered product of laboratory strong acid or base leaching experiments may well be different from that found on the site which the experiment is intended to model; e.g. Jackson (1969) notes that solutions of both high and low pH can modify clay minerals. A major problem of leaching experiments using naturally occurring leaching water solutions is the time scale necessary to see a discernable physical change. Sulphide oxidation is accompanied by increased

ground water acidity and therefore leaching potential. Stability of the iron sulphide phase in the vadose or perched ground water is a prime factor in the assessment of leaching as a major instigator of instability. Details of experiments, using locally collected rain water and at vertical stress levels similar to those generated by the present overburden, and conducted using a 5 tonne capacity soil testing rig with modified triaxial cell, are described in this section. Arrangement of apparatus is shown in plate 7.2, and schematically in fig. 7.1.

7.4.2 Specimens

Specimens were cored perpendicular to the bedding from larger pieces of mudrock collected from the cliffs. The specimens L1 and L2 from samples S24 and S11 respectively (Horizon 43a and 28a) were cored perpendicular to the bedding. Platen specimen interface was sealed using rapid hardening araldite, leaching water gained egress from an axially drilled hole in the core along a transverse joint formed by fracturing the specimen in the point load apparatus. Chisel points were used to induce the fracture which in both cases occurred at lower values of applied stress than could be estimated from the apparatus load dial. Specimen S24 fractured along a plane parallel to a pronounced tectonic cleavage, rather than along a laminae influenced path as specimen S11. Specimen dimensions and details are given in table 7.1, and plate 7.3 shows BX size air dried cores (sample S24 and S11) prepared for duplicate leaching experiments but not used. Shrinkage fractures parallel to the mechanical induced fracture are apparent in sample S11; these are inclined to the laminae and have a sub-stepped profile indicating laminae influence (plate 7.3). With drying, sulphates crystallized on the surface of sample S11 and are readily discernable in plate 7.3.

7.4.3 Leaching Water - Introduction and Collection Systems

Pressurized leaching water was introduced into BX sized cored mudrock specimens from a perspex cylinder reservoir (fig. 7.1).

Contamination from the Bishop pot constant pressure apparatus, used to pressurize the system was prevented by a cling film separating membrane in the perspex cylinder. Membrane permeability was checked by placing cling film containing a 0.5M NaCl solution in a beaker of deionised water. After a ten day period the concentration of Na⁺ in the deionised water was 4 µg ml⁻¹.

Side drains, made from Whatmans No.1 filter papers were used to convey the leachate from the specimen to a radially drilled perspex disc which collected the leachate and introduced it to a nylon tube draining into the collection vessel. In experiment 1 (the well lithified specimen), a problem in controlling seepage rate was anticipated, and a continuous filter paper used as a drain rather than the slotted variety suggested by Bishop and Henkel (1957). In experiment 2 (the poorly lithified specimen), it was anticipated that filter clogging might become a problem, and consequently the filter drain was slotted.

To minimize contamination, leaching water/leachate contact with metallic parts of the apparatus was avoided. A nylon tube was passed through the waterway in the triaxial cell base, and a perspex pedestal manufactured. Metallic threaded connectors, joining nylon tubing to perspex platens compressed the flanged ends of tubes against perspex members, avoiding any water/metal contact. All plugs and valves in the perspex cylinder were nylon or polypropylene. A cling film wrapped filter drain avoided leachate contamination from the rubber membrane. The cork stopper to the leachate collection vessel was also cling film wrapped, avoiding any contamination from the stopper, and also giving a better seal between the collection vessel and stopper, minimizing :-

1. Diffusion of argon gas.
2. Contamination from the atmosphere.

The leachate collection vessel immersed in a water bath to minimize temperature fluctuation, was argon filled, in an attempt to prevent any reduced species from oxidizing during the period of collection.

Seepage rate Q according to Darcy's law is given by

$$Q = Aki \quad (7.8)$$

where i is the hydraulic gradient
 k is the coefficient of permeability
 A is the cross sectional area through which seepage occurs.

During specimen leaching head loss occurred across the plane of seepage, i.e. the discontinuity, and it can be shown that :-

$$kS = \frac{Q \ln r_o}{2 \pi R (H - H_f)} \quad (7.9)$$

where S is a variable dependant on discontinuity frequency

r_o is the radius of axial hole

R is the specimen radius

H_f is the head loss through filter drain

H is the hydrostatic head

Q is the measured discharge into the leachate collection vessel

Seepage rate control was exercised by varying both confining and leaching water pressure. During the course of the experiment seepage rates decreased. To enable the varying apparent coefficient of permeability k to be plotted against time, tests were conducted to determine the loss in head through the filter drain.

In fig. 7.2, a schematic diagram of the arrangement is indicated, a perspex cylinder with a hole along the cylinder axis and radial drainage holes at approximately mid-height was used as a blank (or specimen substitute). Water was introduced as in the leaching specimen (fig. 7.1). Drainage path lengths (x in fig. 7.2) were made equal to the specimen average, and filter drain arrangements were kept identical. Friction losses are velocity dependant, seepage rate is low and controlled by the permeability of the compressed filter drain, consequently hydrostatic head at (3) is approximately equal to that at (1) (fig. 7.2).

Graphs (fig. 7.2) show discharge against hydrostatic pressure at various confining pressures for the two blanks. Cell pressure and discharge are both known, consequently hydrostatic head at (3) could be determined, and from equation (7.8) the value of kS .

It is recognised that filter drain clogging could well contribute to decreasing permeability, and therefore the coefficient of permeability is referred to as 'apparent'. Following leaching experiment 1, the discharge characteristics of the filter drain, removed intact, were re-assessed, similar results to those initially determined were obtained, suggesting that drain efficiency was not impaired. Plate 7.4 shows this filter drain, and a narrow band of sediment 'washed' from the joint is apparent along the joint trace. The alignment of the perspex blank, representing the average joint position, and joint trace do not completely coincide, and consequently the check is not entirely conclusive.

The discontinuity system within low permeability mudrocks can be considered semi-closed, as seepage rates vary so does the ability to transport particulate matter. Therefore detritus removed from the joint surface by the action of water may remain in the system for a considerable period, reducing permeability. Such a model for mudrock seepage would be complex, and cannot be accurately represented by an open system in which the detritus is readily removed, or by a closed one which completely retains it. It is arguable that the developed system; i.e. with a fast filter drain, allowing the passage of particles finer than 11micronis a reasonable approximation of the actual system.

7.4.4 Monitoring for change in specimen circumference

An ocular measuring device sensitive to + 0.1mm was secured to the triaxial testing rig, and was so positioned to detect any movement of a belt placed around the specimen. The arrangement is shown in plate 7.5. Calibration graphs, and method of calibrating for measurement through perspex cylinder and cell water are presented in fig. 7.3.

7.4.5 Apparatus Stress/deformation characteristics

A steel bar 40mm in diameter was used to investigate stress/deformation characteristics of the modified triaxial testing rig which incorporated perspex platens, drainage disc and pedestal.

The graphs presented in fig. 7.4 show :

a) time dependent stress relaxation - leaching experiment graphs of deviator stress against time (figs. 7.6 and 7.7) have been adjusted accordingly.

b) elastic deformation for a loading phase up to 1350 kN/m^2 . During the final stage of leaching experiment 2, the specimen was loaded to failure, and a stress/strain curve, corrected using the data presented in fig. 7.4, plotted.

7.4.6 Temperature effects

During hot weather the measured temperature around the apparatus frequently rose to over 35°C . With rising temperature, an increase in deviator stress was noted. Several short term periods (i.e. several days) of continuous temperature and stress monitoring gave similar temperature/time and stress/time traces. Stress was measured and recorded using a L.D.T. (linear displacement transducer), measuring proving ring deflection, connected to a chart recorder. At the sensitivity necessary to detect temperature influenced stress change considerable drift occurred, consequently there is little value in reproducing graphs. However, it became apparent that during the hottest summer weather, diurnal deviator stress variation in the order of 3% could be expected i.e. $\pm 15 \text{ kN/m}^2$. Graphs of maximum and minimum temperatures, as well as temperature at the time of reading, have been recorded for comparison with deviator stress and permeability/time graphs (figs. 7.6 and 7.7).

7.4.7 Contamination

Solute concentrations, as might be expected in any such experiment where natural waters are used as leaching fluids, were low. Consequently, contamination levels were critical and the level had to be less than experimental sensitivity in order that trends could be observed with any degree of confidence.

Various cleaning methods are reviewed by Laxen and Harrison (1981). The methods adopted for this work were those used by Morris (pers. comm. 1982), based on considerable experience gained at Imperial College and the University of Lancaster.

- a) Rinse in tap water.
- b) 1 hour soak in a 10% solution of Decon 90, a strong surfactant.
- c) Rinse in deionised water.
- d) 1 hour soak in 10% Nitric acid.
- e) Rinse twice in deionised water.

These cleaning procedures were used for all glassware and parts of apparatus in contact with leachate and leaching fluid; with the exception of filter drains and papers where procedures c) and d) only were used, and cling film which it was found impracticable to clean before use.

Using the perspex cylinders described in section 7.4.3, experiment blanks 1LB1 (leaching experiment 1 - Blank 1) and 2LB1, were run to determine contamination levels, results are presented in table 7.2. Both blanks were run before commencement of respective experiments. Deionised water was substituted for leaching water and 40ml allowed to drain daily from the system over a period of 5 days. Blank determination 1LB2 (table 7.2) was made immediately following

completion of experiment 1, and without separating membrane replacement or dismantling perspex cylinder. The system on the leaching water side of the separating membrane was cleaned using procedures d) and e) only (previously listed in this section). The cylinder was filled with deionised water, pressurised to 300 kN/m² and allowed to stand overnight before 200ml was drawn off from the perspex cylinder and analysed (table 7.2).

7.4.8 Analytical water chemistry procedures

Methods described were adopted both for the analyses of leachate and the various water sampled in the field area (table 3.2). The titration method adopted for determining the higher chloride concentration of field area sampled waters is also described (section 7.4.8.8). Problems experienced in determining sulphate content using the barium chloranilate method described by Vogel (1978) is alluded to in section 7.4.8.6.

7.4.8.1 Specific Conductance

Defined as the current, measured in siemens / cm , in a solution (at a constant 25°), when a potential difference of 1 volt is applied to two electrodes 1cm² in area and 1cm apart.

In natural waters of relatively low ionic content it can be used as an estimate of the total anions or cations in solution. Mackereth, Heron and Talling (1978) suggest the approximate relationship :

$$\text{ionic content in meql}^{-1} \approx \frac{\text{specific conductance}}{100} \quad (7.10)$$

Specific conductance is traditionally noted by k, in this text K is used to avoid any confusion with the coefficient of permeability.

A Radiometer conductivity meter with a pp1042 conductance cell was

used; prior to each use the conductivity cell was standardised in a 0.01 M solution of KCl with specific conductance of $1410 \mu\text{Scm}^{-1}$ at 25°C . To enable the specific conductance to be determined at temperatures other than 25°C , the formula suggested by Mackereth, Heron and Talling (op. cit.) was used; i.e. :

$$K_{25} = \text{antilog} \left[\log K_t + \log 1.023(25 - t) \right] \quad (7.11)$$

where t is the temperature of the water at the time of reading.

7.4.8.2 pH

Laboratory determinations were carried out using a digital pH meter with a single glass calomel combination electrode.

The meter was calibrated using B.D.H. standard buffers of pH 4 and 9. Readings were made to an accuracy of ± 0.1 .

In contact with air, CO_2 in solution is unstable, consequently pH was determined with the minimum of atmospheric exposure, and the pH of various sampled ground waters determined at sampling site using close range papers.

7.4.8.3 Eh

Defined by Garrels and Christ (1965) as the equilibrium potential of an oxidation reduction reaction, relative to the potential of a standard hydrogen electrode.

Developed potential is related to the activities of the oxidised and reduced species by the Nernst equation :

$$E_h = E^\ominus + \frac{RT}{nF} \left(\ln \frac{[\text{ox}]}{[\text{red}]} \right) \quad (7.12)$$

where E^{\ominus} = the standard reduction potential.
 R = the gas constant
 T = absolute temperature
 n = no. of electrons involved
 F = Faraday constant.

Potential difference between a calomel reference electrode, supplying a known e.m.f., and an inert platinum electrode immersed in solution was measured.

The half cell potential (Eh) is given by :

$$E_h = \text{emf}_{\text{measured}} + \text{emf}_{\text{calomel}} \quad (7.13)$$

The e.m.f. of the used saturated calomel electrode was given as 0.2415 volts at 25°C. The following expression was used to adjust for solution temperature.

$$\text{emf}_{\text{calomel}} = 0.2415 - 7.6 \times 10^{-4} (25 - t) \quad (7.14)$$

Prior to use, the electrodes and measuring system were checked in the manner suggested by Zobel (1946), using a solution of 0.003M Potassium ferricyanide and 0.1M Potassium ferricyanide; quoted Eh at a temperature of 25°C is 0.430 volts.

Experimental readings were characterised by drift and instability, duplicate results using a second platinum electrode did little to enhance confidence. Immersed at the same time, the two platinum electrodes were alternately connected into the measuring system.

Drift is indicative of a poorly poised system and readings gave positive Eh values showing an oxidising potential. Therefore, it can

be assumed that ions in aqueous solution were oxidised. Increase in stability and decrease in drift would indicate the presence of reduced ions in solution. The importance of the iron sulphide phase has been discussed. Eh measurement and the degree of stability provided an important indicator for the presence of reduced ions in solution. Exposed to the atmosphere, reduced species in aqueous solution are unstable, and particularly so in dilute solutions. Ideally, procedures to eliminate such exposure are desirable, but for these determinations it was only practical to minimize it. i.e. :

- 1) Carrying out Eh determination first.
- 2) Minimizing exposure of leachate to the atmosphere.

7.4.8.4 Alkalinity

Mackereth, Heron and Talling (op. cit.) define alkalinity as the concentration of anions of weak acids (largely bicarbonate). However, they note that in very alkaline waters the concentration of OH^- and CO_3^{2-} can be considerable, and that in acid water the sum of the alkaline components will be negative.

0.01M hydrochloric acid was standardised with a 0.01M sodium carbonate solution. 5ml of the leachate was pipetted into a flask, and one drop of B.D.H. 4.5 indicator added, this was titrated against the 0.01M hydrochloric acid which was discharged from a 10ml micro burette. The stoichiometric point is indicated by a change in colour from blue, through grey to pink and the alkalinity is calculated and expressed in terms of meq l^{-1} (milli equivalents/litre).

7.4.8.5 Anions of Strong Acid

Largely sulphates, chlorides and nitrates. Procedure used is that detailed by Mackereth, Heron and Talling (op. cit.). Leachate was passed through an ion exchange column. Amberlite I.R.120 analytical grade resin (B.D.H. chemicals) was used to exchange aqueous cations for Hydrogen. Concentration of free strong acids was then found by

titrating an aliquot against 0.01M sodium hydroxide using B.D.H. 4.5 indicator. Stoichiometric point was indicated by a colour change from pink, through grey, to blue. The sodium hydroxide is unstable; therefore immediately prior to each use it was standardised against the 0.01M hydrochloric acid used in alkalinity determinations.

7.4.8.6 Sulphates

A 5ml aliquot taken from the leachate passed through an Amberlite I.R.120 ion exchange column, was used to determine sulphate content, using the method described by Fritz (1955). 20mls of Iso-propyl alcohol was added to the aliquot, and one drop of thorin indicator (a 0.2% w/v solution in water), followed by titration against 0.005M barium perchlorate. The titrant was made up by dissolving 2g of barium perchlorate tri-hydrate in 200ml of water, adding 800ml. of Iso-propyl alcohol and adjusting the pH to 3.5 using perchloric acid.

The Stoichiometric end point is indicated by a change to pink. Titrant was standardised against a solution containing $55 \mu\text{gml}^{-1} \text{SO}_4^{-2}$ made up from potassium sulphate and passed through the ion exchange column. Fritz (op. cit.) notes that concentrations as low as $10 \mu\text{g ml}^{-1}$ can be determined to an accuracy of $\pm 1 \mu\text{gml}^{-1}$.

Vogel (1978) describes a method for determining sulphate content spectrophotometrically using barium chloranilate. Chloranilic acid liberated from barium chloranilate under a controlled pH is measured colourimetrically using a spectrophotometer at a wavelength of 530nm. Verification of this method proved unsatisfactory; however, it must be noted that anal R (analytical reagent) barium chloranilate was not readily available, and the method was attempted using G.P.R. (general purpose reagent).

7.4.8.7 Chlorides

Two methods were used :

- i) Potentiometric method where concentration was less than $50 \mu\text{gml}^{-1}$

ii) Mohrs titration for higher concentrations.

i) Potentiometric method

The silver chloride electrode was prepared by electrolysing a silver wire (anode) in 1M hydrochloric acid for 5 - 10 minutes.

A beaker of deionised water, acidified with 1ml of nitric acid to give a total volume of 300ml, was connected by an ammonium nitrate salt bridge to a beaker containing 0.1M silver nitrate solution. A silver chloride electrode in the acidified water, and a silver electrode in the silver chloride solution were connected to a voltmeter. A magnetic stirrer and follower were used to ensure mixing. Voltage reading is first allowed to stabilize then small increments of standardised 0.5M sodium chloride solution were added from a 10ml micro burette, and recorded after allowing the voltage to stabilize. Antilog e.m.f. was plotted against chloride concentration. The silver chloride electrode and salt bridge were washed with deionised water, and a 50ml beaker with 20ml of acidified deionised water substituted. Initial voltage was noted and several additions of the sample were made by pipette, eg. 1ml, 2ml and 5ml. Chloride content was then determined by interpolation from the graph and an appropriate adjustment made for sample dilution.

ii) Mohrs titration

The titrand was brought to between pH 6 and 7 and titrated against a 0.02M silver nitrate solution, using a saturated potassium chromate solution as indicator. The procedure is described by Head (1980).

7.4.8.8 Silicates

Soluble reactive silicon reported as silicates occurs in solution as silicic acid and is the result of hydrolysis.

In an acid solution, silicic acid reacts with molybdate to form yellow molybdosilicic acids, these are reduced to intensely coloured silicomolybdenum blues, and measured colourimetrically by spectrophotometer at a wave length of 810 nm.

7.4.8.9 Ferrous Iron

Ferrous iron is usually only found in natural waters depleted in oxygen. Monitoring for ferrous iron and Eh was carried out because of the reducing potential of the mudrock iron sulphide phase. Ferrous iron reacts in mildly acid solution with the chromogenic reagent 2,2 bipyridyl forming the pink $(\text{Fe}(\text{bipyridyl})_3)^{2+}$ complex, the absorbance is determined spectrophotometrically at a wavelength of 520nm. The method is described by Mackereth, Heron and Talling (op. cit.). All deionised water used in this experiment was deoxygenated by boiling for several minutes, and allowing nitrogen to bubble through during cooling.

7.4.8.10 Cation analyses by flame photometer and atomic absorption

20ml of 1M hydrochloric acid were added to digested samples (section 7.4.9) 24 hours before analysis.

A Corning 400 flame photometer was used for Ca^{2+} , Na^+ and K^+ determinations, a Varian techtron 1100, and subsequently a Varian 1275 A.A.S. (atomic absorption spectrophotometer) for Mg^{2+} , Al^{3+} , Fe^{total} , Mn^{total} and Cu^{total} . Standards sensitive to sample concentration were made up in 1M HCl as follows :

1) A combined K^+ and Na^+ standard : Duplicate stock solutions were made from potassium and sodium chloride to give accurate concentrations of $1,000/300 \mu\text{gml}^{-1} \text{Na}^+/\text{K}^+$. Dilution to give a range of standards, within the instrument range $0-100 \mu\text{gml}^{-1} \text{Na}^+$, and $0-30 \mu\text{gml}^{-1} \text{K}^+$ were prepared for instrument calibration. Accuracy of initial weighings were verified by comparing standards prepared from the duplicate stock solutions.

2) Combined Ca^{2+} and Mg^{2+} standards were prepared from B.D.H. spectrosol stock solutions, concentrations in the range 0/0 to 20/100 μgml^{-1} $\text{Mg}^{2+}/\text{Ca}^{2+}$. To suppress interference an addition of lanthanum chloride was made to give a final concentration of 10,000 μgml^{-1} La^{3+} in both standards and samples.

3) Combined Fe^{total} , Mn^{total} and Cu^{total} : standards were prepared from B.D.H. spectrosol standard stock solution in the proportions 1:1:1. Standards were made giving concentrations from 0-10 μgml^{-1} but with four in the range 0-2 μgml^{-1} .

4) Al^{3+} was prepared from spectrosol standard stock solutions - To suppress ionisation, potassium chloride was added to standards and sample to give a final concentration of 2,000 μgml^{-1} . Although the Varian handbook (1979) indicates no wave length where the instrument is sensitive to low Al^{3+} concentrations, a stable calibration was obtained at a wavelength specified as suitable for a higher concentration range, and this was found more accurate than spiking samples and standards with aluminium nitrate stock solution to increase the concentration by 40 μgml^{-1} .

Detailed operational and analytical procedures are described in the Corning 400 flame photometer (Anon-1976) and Varian atomic absorption manuals (Anon - 1979).

7.4.9 General procedure for Chemical analysis of leachate and other waters

All reagents used in the water analysis with the exception of the nitric acid for cleaning, were Anal R. grade, and glassware, without exception was pyrex.

Leachate for analysis was transported to the chemistry laboratory in its collection vessel. Prior to this it was necessary to remove the stopper housing the leachate outlet lead, the sample was then immediately sealed by covering with cling film.

Analyses were usually carried out on two consecutive evenings, and always completed within 30 hours, the less stable quantities being determined during the first session. To minimize atmospheric content and retain some of the inert gas over the leachate, required aliquots were gently poured from the collection vessels. On completion of pouring, both aliquot and sample were immediately covered with cling film.

Session 1 : Prior to analyses a 10% nitric acid, 10% Decon 90 and deionised water baths were set up; deoxygenated water was prepared for ferrous iron analysis by boiling water and then passing nitrogen through it as it cooled, apparatus prepared, and instruments calibrated for Eh, pH and conductivity measurements.

Approximately 20ml aliquots were used for Eh estimations and a further 15ml for conductivity and pH measurement. Once the deoxygenated water had cooled, and the spectrophotometer had sufficiently warmed up, ferrous iron was determined. Alkalinity, the final analysis of session 1, required two 15ml aliquots. Most titrations were carried out in a 25ml flask using a 10ml. micro burette, - mixing was facilitated by magnetic stirrer and follower.

Session 2 : samples, other than leachate which had passed through a filter drain, were filtered.

5ml of nitric acid was added to 20ml of sample in a narrow necked, conical flask, - if there was sufficient sample volume a duplicate was prepared, together with a blank (20ml of deionised water and 5ml of nitric acid in a similar flask). The samples were gently evaporated to dryness at a temperature not exceeding 80°C. The digested samples were allowed to cool, covered with cling film and stored for cation analyses at a later date.

Standards and samples for silicate determination were made up to volume in 25ml. volumetrics, and consequently sample volumes of 12.5ml. were used instead of the 25ml indicated by Mackereth, Heron and Talling (op. cit.).

Using the potentiometric method, chloride determination was made with only 5ml of sample. 50ml. of sample was necessary for ion exchange prior to sulphate and anion of strong acid determinations - occasionally this necessitated dilution, but never by more than a factor of 2.

During the course of analysis, rinsing water was frequently changed. Decon 90 and the nitric acid bath were used, at the most, for two sets of analyses.

7.5 Rainwater Collection, Analyses and Storage

Rainwater - samples RW3, 4, 5 and 7 were used as experimental leaching water. Collected at Nash (SS 917 682), analyses, collection method and prevailing climatic conditions are detailed in table 3.1. Wind roses for the relevant days (00 hours to 23.00 hours) are recorded in fig. 3.3.

An early attempt to collect rainwater was made with polythene bottles and funnels. These were partly buried, and left for a period of several weeks, at a location providing some protection from the wind.

Volume of water collected was small, and contaminated by vegetation and sediment. Analysis of one such sample, RW1, is included in table 3.3. A high concentration of chlorides and sodium indicates contamination from the sea.

Subsequent collections were made with a polythene sheet. Cleaning procedures before each use included washing with tap water, the 5% nitric acid, followed by rinsing with deionised water: a check on the pH of rinse water ensured that acidity was neutralised.

Sample RW6 was collected during storm conditions, high ionic concentration (table 3.3) is the result of ground splash and sea spray mixing with rainwater.

Although it could be argued that enhanced sodium and chloride

concentration is more representative of locally derived vadose waters, sample RW6 was not used as leaching water. To achieve a fair comparison between the leaching of the two specimens, a reasonably consistent leaching water quality was used throughout.

At pH 6, 70% of the carbonate content, in aqueous solution, is dissolved carbon dioxide and the remainder bicarbonate ions (Brownlow 1979). Therefore it is surprising that at the higher pH values alkalinity was below detection level. In an attempt to enhance detection, titrands were increased to 10ml, making the minimum level of detection approximately equal to 0.03 meql^{-1} . An exception is RW6, which appears to largely represent the hydrolysed silicate ion (table 3.3). The rain analysed was acidic, acidity is apparently greater in rain immediately following a prolonged dry period.

Prior to use in the leaching experiment, rainwater was filtered and stored in a pre-cleaned polypropylene container at 4°C . To ensure the quality of the leaching water, conductivity was monitored.

7.6 Monitoring and Specimen response

During the experiments, fine eroded material, and in specimen L2 (sample S11) softening adjacent to the discontinuity, effected permeability reduction, permitting and necessitating adjustment of hydrostatic leaching pressure, specimen confining pressure and deviator stress. Experimental effective stress paths are plotted in fig. 7.5, and total stresses f_1 and f_3 and hydrostatic leaching pressure u are tabulated for each experimental time stage. In this figure continuous lines represent stress relaxation, and broken lines manual stress adjustment.

Continuous monitoring included :

- 1) The apparent coefficient of permeability expressed as a function of discontinuity spacing. i.e. kS (section 7.4.3).

- 2) Deviator stress variation.
- 3) Change in specimen circumference.
- 4) Maximum and minimum temperatures.
- 5) Temperature at the time of measuring 1. to 4. above.

In figs. 7.6 and 7.7 the above, with the exception of specimen circumference which showed no significant measurement change (at \pm 0.1mm sensitivity), are plotted against time.

Variation in coefficient of permeability function k_S (section 7.4.3) was much greater in experiment 1 than experiment 2. This is attributed to the nature of the material. In specimen L1 (sample S24) high carbonate content (table 5.7) meant that the clay phase had little influence on mudrock behaviour (sections 6.6, 6.7 and 6.8). Although only occurring to a small extent, spalling of the fractured surface during fracture propagation formed low impedance seepage paths. Fine material eroded from the leached surfaces, and failing to find egress, progressively blocked these seepage paths reducing permeability: validity as a rock mass permeability model has been discussed in section 7.4.3. Carbonate content of specimen L2, a fissile shale, (sample S11) is much lower (table 5.7), and unlike specimen L1 the clay phase influences behaviour (section 6.6, 6.7 and 6.8). Seepage path closure during initial loading is suggested by the initially low k_S value. Filter drain arrangement (section 7.4.3) more readily allowed eroded particle egress than the arrangement used in experiment 1. However, reduction in permeability is attributed to seepage path clogging as well as cohesive bonding developing between softening fracture surfaces. In calculating permeability coefficients no account is taken of the f_1 and f_3 stress values, and in these experiments it would seem likely that a reduction in these stresses would result in seepage path flushing, with a consequent increase in permeability. Because of rock characteristics, normal stress reductions were only possible in experiment 2 (fig. 7.5).

Although following such stress reductions, initial increases in seepage can be inferred from fig. 7.7, the last three recorded kS values show a dramatic drop from approximately 3 to 1 cm²/sec - suggesting the development of cohesive bonds between fracture surfaces.

Deviator stress records (figs. 7.6 and 7.7) have been corrected for apparatus stress relaxation using values presented in fig. 7.4.

Low magnitude short term deviator stress variation, and to a lesser extent permeability variation, was shown to be temperature dependent, both by plotted records (fig. 7.6 and 7.7) and short term continuous monitoring (section 7.4.6). Stress relaxation in experiment 1 appeared to level off after 2,500 hours with a deviator stress relaxation of 5.9% (fig. 7.6). In experiment 2 the stress/time graph levelled off at 12% relaxation after 1,000 hours (fig. 7.7).

Given the high clay content of specimen L2 (sample S11 - table 6.2) it is perhaps surprising that no change in specimen circumference is recorded. However, diagenetic changes have resulted in clay mineral dehydration and structural changes, and consequently clay mineral activity is small (section 6.6).

Quantities of leachate and times between leachate analyses are recorded in figs. 7.6 and 7.7. Chemical analyses, using the methods described in section 7.4.8 are recorded in :

figs. 7.8 and 7.9 - leaching experiment 1.

figs. 7.10 and 7.11 - leaching experiment 2.

In figs. 7.8a and 7.10a, total cations show good comparison with total anions, the latter determined from the addition of alkalinity and anions of strong acid. Alkalinity, anions of strong acid and the measured milli equivalent sum of chlorides and sulphates are also plotted. The positive differences between anions of strong acid and $\text{Cl}^- + \text{SO}_4^{2-}$ are possibly indicative of nitrates.

pH, Eh and conductivity are plotted in figs. 7.8 and 7.10 b) c) and d). pH fluctuated between 7.4 and 8.0, recorded values were slightly higher in leaching experiment 2 where the concentration of strong acids was lower. Little significance is attached to the highly unstable Eh values except that they indicate a poorly poised oxidised system with no reduced ions (section 7.4.8.3).

Conductivity provides an estimate of the ionic concentration (7.4.8.1). In experiment 2 (fig. 7.11), after initially high quantities of sulphates were flushed out, conductivity reduced to a lower level than that recorded for specimen L1. It is conjectured that the sulphate concentrations largely control the total ion concentration in so much that an equilibrium exists between the carbonate and sulphate phase. Sulphate, an anion of strong acid, enhances carbonate leaching potential. Various anion/cation concentrations for the two leaching experiments are plotted in figs. 7.9 and 7.11.

Chemical analyses (table 6.2) suggested that iron sulphide concentrations were greater in sample S11 (specimen L2) than sample S24 (specimen L1) but that the stability of pyrite in sample S24 was much lower, and consequently the weatherability higher. Highly weathered sample S21 (Chapters 5 and 6) gave every indication of having been weathered from a highly indurated mudrock. In section 5.3.3.6 various degrees of stability were demonstrated for different pyrite polymorphs. More highly reactive pyrite was commonly shown to be present in the strong highly indurated mudrock (table 5.7). It was conjectured that weatherability was largely a function of pyrite stability (sections 5.2.6 & 5.5.1). This supposition gains credibility from comparison of leachate sulphate concentrations - the order of concentration in specimen L1 leachate is generally ten times that of specimen L2 leachate.

In section 7.1 it was suggested that iron was precipitated close to the site of oxidation and it appears that, because of the absence of ferric iron staining, the initially high sulphate concentration in leachate sample 2L1, (leached from specimen L2 - horizon 28a) was the result of precipitated salts. Ferric iron staining would also be

expected if these sulphates were the result of the action of oxidation by acidophilic bacteria (section 7.2.3).

In Chapter 6, evidence suggested that in sample S24 carbonates were relatively high in magnesium content. In analysed leachates the ratio of Ca^{2+} to Mg^{2+} is much higher in samples leached from specimens L1 than those from L2 (figs. 7.9 to 7.11).

Concentrations of sodium and chlorides generally decreased through both experiments, suggesting that their presence was the result of sea water penetration, and higher silicate and potassium contents in specimen L2 leachate reflects the mudrock mineralogy (table 6.2).

The higher ionic concentration in vadose/perched ground water (table 3.2) is largely from sea water contamination. By assuming that all chlorides are the result of sea water contamination, it follows from sea water analyses (table 3.2) that the proportional Ca^{2+} reduction, due to sea water contamination, is relatively small. Larger Ca^{2+} concentrations and greater alkalinity suggest that more CaCO_3 is leached during seepage through the cliffs than that measured in the laboratory leaching experiments.

During the final stage of leaching experiment 2, specimen L2 was loaded to failure (fig. 7.5). The stress/strain curve, corrected for apparatus deformation (using fig. 7.4), is reproduced in fig. 7.12. Plate 7.6, showing specimen L2 following loading to failure, confirms the brittle type failure recorded in fig. 7.12. Leaching was continued during loading to failure, and subsequently, with cell pressure increased to 300 kN/m^2 for a period of 24 hours. Analyses of leachate sample 2L11 is recorded in table 7.2.

Although to some extent loading specimen L2 to failure throws some doubt on a comparison of leached surface morphology and texture, such a comparison was possible because failure mode was brittle and subsequently the leached discontinuity readily identified.

Leached surfaces of both specimens were friable. Silty in texture, the quantity of friable material appeared greater in sample L2 where it was also slightly cohesive.

Plates 7.7 and 7.8 show leached surfaces of specimens L1 and L2 respectively. On completion of the leaching experiments, a small tensile force had to be applied, in both cases, to separate specimen halves. Specimen L1 separated readily at the induced discontinuity, but specimen L2 did not; approximately 75% of the surface indicated in plate 7.8 (i.e. the higher area) is that of the leached plane. Laminae boundaries on the leached surface (plate 7.8) stand out in relatively high relief indicating lifting by the separating force and suggesting that a bonding with the adjacent leached surface had been effected. In contrast to this, the leached surface of specimen L1 appears indurated (plate 7.7), although just above the axial hole where a small unleached area is exposed (surface removed for thermal gravimetry analyses), a marked tonal variation between leached and unleached surfaces is apparent.

Results of thermal gravimetry for material sampled at, or close to, the leached surfaces are reproduced in table 7.3. Comparison with table 5.7 indicates an increase in unstable iron sulphides in specimen L1. Recorded carbonate decomposition is similar in quantity to that noted in table 5.7. However, perhaps rather surprisingly, duplicate carbonate content for specimen L2 (table 7.3) is consistently slightly higher, suggesting that the poorly cemented, non cementitious phase was more rapidly eroded than carbonates leached.

The high sulphate content recorded for specimen L2 (table 7.3) demonstrates that leaching only had a very local effect. No ferric iron products (e.g. goethite, limonite or haematite) were indicated by DTG traces, again suggesting that the gypsum was a precipitate.

Elemental qualitative analysis traces for pre- and post-leached specimens, determined by the S.E.M. (scanning electron microscope)

micro analyser, are reproduced in fig. 7.13. Effects of leaching can only be conjectured by comparing the relative heights of peaks in the same trace, e.g. K^+ and Ca^{2+} . The implication of the traces reproduced for specimen L1 (fig. 7.13) is that solution weathering is selective.

Comparison of uniaxial compressive strength/moisture content graphs for unleached mudrocks and samples taken from close proximity to leached surfaces of specimens, is produced in fig. 7.14. Some leaching induced weakening is indicated for both mudrocks, but the curve for leached specimen L1 appears somewhat erratic, again suggesting selective weathering.

Specimen L1 was leached for a period of approximately 3,500 hours, and specimen L2 2,500 hours, and although sulphides were oxidised and iron sulphide stability decreased, there was no evidence of oxidised ferrous iron, i.e. no discolouration or diagnostic DTG peak. Nevertheless, the experiments served to demonstrate the relative importance of pyrite stability in relation to weatherability, and that thermal gravimetry can be used to identify the presence of reactive sulphides. Perhaps rather fortunately, low stability pyrite appears to be more common in the unweathered competent, highly calcareous mudrocks, although in many of the more highly weathered mudrocks, unstable pyrite is apparent, suggesting weatherability increases as weathering advances.

Reference to grant aid for protection works under the 1949 Coastal Protection Act, eligible only in cases where marine erosion could be shown to be the instigator of instability, was made in section 7.1.

In Chapter 4, horizon 28a was defined as a prominent line of weakness and instigator of instability. In Chapter 5 its relative incompetence was demonstrated by a comparison of engineering index properties, and in Chapter 6 it was shown to be comparatively more argillaceous and less indurated. However, in Chapter 7 chemical weathering has been shown to be of less significance than in the more indurated rock. Therefore, chemical weathering cannot be construed as being significant in the development of this prominent line of weakness.

7.7 Summary

Laboratory leaching experiments carried out in a modified triaxial cell and using natural waters have been described. Both highly competent and incompetent mudrocks were leached and physical and chemical monitoring was compared.

To effect dramatic changes in specimen properties, leaching with more aggressive solutions than water would have been necessary. These low contamination, natural leaching water experiments confirmed the supposition of section 5.5.1 that pyrite in the more highly calcareous mudrocks is less stable than that in the less competent mudrocks, and that this low stability pyrite is more readily oxidised. As well as modifying clay mineralogy (Chapter 6), oxidation enhances leaching potential. The ionic concentration of leachate of the highly competent mudrock was greater than that from the incompetent mudrock. Sulphide instability was predicted prior to leaching by thermal gravimetry, and subsequently thermal gravimetry of samples from the leached surface indicated a decrease in pyrite stability in the indurated mudrock.

Finally it was concluded that chemical weathering was an insignificant contributor to the inherent weakness exhibited by horizon 28a.

CHAPTER 8

LIMESTONES

8.1 Introduction

Instability is largely the result of mudrock erosion; and the consequent increase in disturbing forces. Instability occurs when disturbing forces exceed the maximum resisting force which can be developed along the path of minimum resistance. The major contributor to these resistance forces are strengths developed by interlocking limestones and by the shear resistance developed along limestone discontinuities. Although general stress levels relevant to the problem of instability are much lower than the micro and meso fractured rock strengths determined in this chapter, the treatise is highly relevant because locally, (i.e. in interlocking limestones and discontinuity protruberances) rock stresses do rise to the higher ultimate stress levels.

Representative specimens for analysis and testing were taken from several horizons and were selected on a morphological basis (table 8.1).

In this chapter, variation in limestone fabric and material properties, other than discontinuity shear strength (Chapter 9) are described. Meso and micro description, together with index properties and major phase mineralogy (Thermal gravimetry) are presented.

The limestones are characterised by a well developed system of micro fractures (section 2.5). Both micro and meso scale fractures are frequently carbonate filled which to some extent facilitated coring of the fractured rock. A programme of testing to ascertain the strength of sampled fractured rocks and investigate any strength anisotropy is described. The empirical criterion of Hoek and Brown (1980) proved to provide a realistic representation of rock strength; and their criterion has been adopted. Several uniaxial compressive strength

specimens were strain gauged, and stress/strain curves are presented and elastic constants compared.

Sample preparation for strength testing proved problematic and the I.S.R.M. - International Society for Rock Mechanics (1978 and 1979) quoted tolerances frequently not achieved. Consequently preparation procedures and discussion relating to tolerances are also included.

8.2 Sample Description

8.2.1 Introduction

Three schemes are commonly used by geologists to describe carbonate type rocks.

1. Grain size - Working Party Report 1977.
2. Texture - a classification after Dunham (1962).
3. Compositional - a classification after Folk (1959).

Folk's (1959) and Dunham's (1962) classifications are summarized in table 8.2 and 8.3 respectively.

Fookes and Higginbottom (1975) recognised the need to formulate and standardise descriptions for engineering purposes, particularly the description of young carbonate deposits of tropical and sub-tropical shelf areas. However, their classification was designed for use where at best laboratory and back up facilities are meagre.

Wobber (1963) has described the South Wales Lower Lias lithology and petrology in some detail. An extended form of Wobber's (op. cit.) (Table 8.1) morphological classification provided the basis of sampling and investigation described in this chapter. In assessing differences in engineering properties and behaviour, micro and meso scale descriptions are considered of paramount importance.

Burnett and Epps (1979) reviewed carbonate classification, and in deriving a system aimed at being both simplistic and geologically accurate, proposed descriptive elements similar to those suggested by the Engineering Group of the Geological Society Working Party (1977).

- i) Colour
- ii) Grain Size
- iii) Discontinuities
- iv) Weathering
- v) Cementation
- vi) Texture and particle shape
- vii) Strength
- viii) Lithological characteristics
- ix) Rock Type.

These descriptive elements are seen as significant and provide the basis for the adopted scheme (table 8.4), which is subsequently discussed in context with the Lower Lias Limestones of South Wales; however, strength assessment is omitted as it is considered quantitatively in section 8.5.

Sample descriptions were facilitated by examination of stained thin sections (section 6.4) under petrological microscope in plane polarized light. Several of the micrographs and sample photographs referenced in table 8.4 (i.e. 8.1 to 8.16) are overlaid and annotated to facilitate identification of relevant features.

8.2.2 Colour and Meso Scale Lithological Characteristics

The scheme recommended by the Working Party (1977) and reproduced in table 5-2 is adopted for both limestones and mudrocks.

Unweathered, colours vary from black to light grey depending on the organic carbon/carbonate content. Rock adjacent to discontinuities is often discoloured by limonite, the weathering product of pyrite

oxidation, which imparts a brownish yellow colour.

The origin of the rhythmic limestone mudrock sequence has interested many geologists and has been the subject of considerable debate. e.g. Hallam (1957, 1960 and 1964) and Wobber (1963). Hallam (1964) and Wobber (1963) both agree that evidence for both primary sedimentation and secondary carbonate migration exists.

Wobber, to avoid the contention and complexity of a generic or fossil based classification, proposed a morphological system recognising four types:

- 1) Isolated elliptical nodules.
- 2) Nodular limestones including units where elliptical nodules are joined by intervening concave-convex limestone bodies.
- 3) Semi-nodular limestone, having hummocky top and bottom surfaces.
- 4) Planar limestones.

Sampling for testing and analyses was made on such a morphological basis.

It soon became apparent that the above classification required extending (table 8.1) and that factors other than surface morphology were important; i.e.:

a) Meso examination indicated that concretionary type structures were not always apparent from surface morphology. e.g. samples L4, L8 and L10 (plates 8.5, 8.10 and 8.13) all suggest such a structure. Three distinguishing features were frequently observed :-

- 1) Central seeds were usually very dark in colour, i.e. darker than usual for rocks of similar thickness and surface morphology and not appearing to exhibit such an internal structure.
- 2) Cleavage, and/or distinguishable narrow iron oxide horizons parallel to the central ellipsoid or 'seed'.

3) A fractured profile across the central 'seed' was frequently different from the adjacent material.

b) Colour: An examination of thicker competent flaggy limestone within the bucklandi zone suggests that flagginess might increase with thickness and that the typical unweathered grey colour become lighter in tone. However, flaggy limestones often less than 50mm in thickness are to be found in the mudrock dominant angulata strata, these are very dark in colour and have a high organic carbon content (table 8.6(1)).

Sample Colour and meso scale lithological characteristics are described in column 5 of table 8.4. Colour, and colour variation are noted, as is the morphological classification from table 8.1, thickness and internal structure. Any necessary clarification is given by an included diagram.

8.2.3 Grain Size, Composition and Texture

The Working Party Report (1977) proposed a carbonate rock type classification based on grain size. i.e. :-

Calcirudite - most grains coarser than 2mm.

Calcarenite - most grains between 2mm and 60 μ m.

Calcisiltite - most grains between 60 μ m and 2 μ m.

Calcilutite - most grains finer than 2 μ m.

This is particularly useful in the description of clastic limestones.

Fookes and Higginbottom (op. cit.) note that Calcisiltite and Calcilutite are not necessarily synonymous with the terms silt and clay, 'lime mud' being entirely different to clay minerals. In the terms of this work, the classification has been used to describe grain size of lime muds i.e. intra and litho, but not bio-clastic material. Although stained with potassium ferricyanide and Alazarin Red S solution, when viewed through a petrological microscope in plane polarised light, the fine grained material which generally dominates the thin sections has a brownish hue which is typical of Calcilutite.

In many of the micrographs, subordinate sub angular to rounded particles discernable under the microscope but generally smaller than 20 μm are apparent (Calcisiltite). e.g. plate 8.3. Composition has been classified using the system proposed by Folk (1959 and 1962); a summary of which is reproduced in table 8.2. Limestones are largely micritic, allochems include;

1) Pelloids (faecal matter) and other organic rich material such as grasses and wood fragments.

2) Bioclasts, or fossil debris. Few identifiable fossils are to be found, although debris is common and varied in size. Not all original fossil structures have been altered by neomorphism. e.g. the relatively large bioclast (plate 8.14) still exhibits much of its original structure.

3) Occasional voids are found (e.g. plate 8.1). The carbonate cutan enveloping both authogenic particles and allochems suggests secondary cementation.

Sparite frequently occurs, both as a neomorphic replacement in fossil debris and infilling joints. Poorly developed spar of varied size and crystallinity is also commonly seen in cavities. This is described as patchy spar (e.g. plate 8.4). Contention in respect of a possible neomorphic origin is discussed in section 6.4. Patchy spar truncating discontinuities (plate 8.1) suggest that it post dates the cementation phase associated with sparite discontinuity infilling. Dolomitised carbonate forming patchy spar (sample L4 - plate 8.7) appears to coalesce in a zone of relatively high density, bioclastic debris. Tucker (op. cit.) notes that pelloid definition is often lost by advanced diagenesis, which tends to produce a clotted type structure. The clots may exceed 30 μm in diameter, and are known as structure grumeleuse.

Plate 8.11 indicates partial dolomitisation of organic material, and

it appears that many of the rounded dolomite inclusions present in most micrographs may be organic in origin.

Dunham (1962) classified limestones on the basis of depositional texture (table 8.3). All limestones examined were mud supported, and the majority of these were mudstones.

In column 6 of table 8.4, limestones are classified in accordance with the three schemes described, other applicable features are noted - e.g. plate 8.9 suggests bioturbation (limestone sample L6).

8.2.4 Carbonate Type

The staining procedures of Dickson (1965) were used to identify carbonate types (table 6.8).

Thin sections took on a purple/mauve hue indicating that micrite was generally ferroan calcite.

Although many bioclasts are calcitic, a number have been dolomitised (indicated by the absence of stain and a turquoise hue - ferroan dolomite - plate 8.6). Patchy spar and organic material, e.g. pelloids, are often dolomitised (e.g. plate 8.11) and Micro and Meso scale discontinuities are frequently filled with a sparry ferroan dolomite (e.g. plates 8.1 and 8.2).

8.2.5 Meso and Micro Tectonic Structure

Although many of the fabric factors already discussed can have a significant influence on rock strength, i.e. acting as stress concentrators within a stressed rock fabric, tectonic structure is arguably the most important descriptive element. Fractures, dependant on their orientation in a stress field, can facilitate cracking or stop cracking. Meso and micro fractures apparent in both bulk samples and thin sections are described in column 8 of table 8.4.

8.2.6 Weathered State

The scheme suggested by the Working Party Report (op. cit.) - table 5.4, has been adopted. Weathering was generally observed to have penetrated some distance from discontinuities, weakening the rock fabric. Penetration depth is noted in column 5 and weathered state in column 9. In a modified weathering classification for carbonate rock, Burnett and Epps (1979) imply less disintegration and decomposition than the adopted scheme, and this could have resulted in many of the samples classified as WIII instead of WII.

8.3 Index Properties

A fine cotton halter was secured to fragments taken from bulk samples, these were immersed for one hour in deionised water. After surface drying specimens were weighed for absorption coefficient assessment (Section 5.4.4). Following this, fragments were again submerged in water and volumes determined. The samples were subsequently left for ten days in an atmosphere of 60% to 70% relative humidity, after which they were reweighed prior to oven drying at 105°C and determination of dry weight.

Calculated absorption coefficients, dry densities and equilibrium moisture contents (section 5.5.5) are reported in table 8.5.

Comparison of results for fragments from weathered and non-weathered zones (table 8.5) shows reductions in dry density, and higher absorption index and equilibrium moisture contents for weathered material which is indicative of strength loss.

8.4 Thermal Gravimetry

TG (Thermal Gravimetry) procedures together with DTG (Differential Thermal Gravimetry) curve characterisation have been described in section 5.3 and fig. 5.3. Typical TG and DTG curves are reproduced

in fig. 8.0. Results presented in table 8.6 suggest that carbonate contents vary between 52% and 90%. However, both carbonate and organic carbon content values appear unreliable.

Carbonate contents determined from triplicate wet analyses using Schrotters' apparatus (Jeffrey 1975) are compared with T G values in table 8.7. Although not as sophisticated as Collins' apparatus (Head 1982) which permits pressure and temperature standardisation, the apparatus has an advantage in that it can be gently heated to effect dolomite decomposition. Tabulated mudrock values (table 8.7) indicate reasonable agreement in view of sample size variation (i.e. 200-500mg Schrotters method and 20mg for TG). However, deviation in limestone values is considerable, and this is attributed to :-

- 1) Rock fabric variation.
- 2) Sample size and inaccuracies inherent in Schrotter method determinations.

Consequently, limestone carbonate contents can only be considered a guide, and are not sufficiently accurate for use as a parameter in limestone characterisation.

The measured organic content for sample L9, an angulata limestone, is suspiciously low, whilst that for sample L14, a more calcareous limestone, high. Variation is attributed to :

- 1) Fabric variation (section 8.2.3).
- 2) Method sensitivity inadequate for the measurement of low organic carbon content.

Thin flaggy limestones (less than 100mm thick) are a relatively common occurrence in the angulata zone, from rock colour they can be deduced as being generally more carbonaceous than those of the bucklandi zone. Results from the thin flaggy bed analysis (table

8.6(1)) indicate both high carbonate and organic carbon content; the latter may be deduced as an important factor in the formation of such thin flaggy beds. However, table 8.6 generally suggests that as the carbonate content increases above say 55% CaCO_3 (CO_2 loss 22%), the amount of unstable pyrite decreases. The thin flaggy angulata limestone is an exception (table 8.6(1)) but in this case organic carbon content appears to be exceptionally high. Sedimentary conditions conducive to non-carbonate conversion would have been similarly conducive to the formation of highly stable pyrite. Therefore relatively high organic carbon and carbonate contents are something of an enigma, and sedimentary/post-sedimentary environment leading to such a balance is likely to be conducive to low stability pyrite formation.

Consequently, in conjunction with results presented in section 5.3, it can be concluded that the least stable pyrite is to be found in mudrocks/limestones where carbonate contents are in the region of 55%.

8.5 Strength and deformation

8.5.1 Introduction

186 AX sized cores, for uniaxial and triaxial compression tests, and 99 largely NX sized discs for Brazilian indirect tensile tests, were cored from eleven of the samples scheduled in table 8.4. 13 of the specimens tested in uniaxial compression were strain gauged and deformation characteristics measured. In table 8.8 the testing schedule, coring direction in relation to field orientation is specified as are tests and the sizes and numbers of specimens cored in each direction.

Specimen preparation, testing and analyses of the various rock types are described in the subsequent sub-sections. A comparison of strength and deformation characteristics (figs. 8.1 and 8.2) suggests that strength variation is largely a function of existing fracture frequency and orientation.

8.5.2 Specimen Size and Length to Diameter Ratio

The nominal diameters of core specimens referred to in this work are :-

- NX - 54mm diameter
- BX - 41mm diameter
- AX - 28mm diameter.

8.5.2.1 Uniaxial and Triaxial Test Specimens

The size of rock samples obtained and fracture density precluded the use of NX core sized specimens. Although some preliminary testing was carried out with BX core specimens, AX sizes were finally chosen for two main reasons :-

1) Comparability of results with mudrock uniaxial compressive strengths. These values were determined by the NCB cone indenter (section 5.4.7) and although an indirect method, instrument calibration, by Szlavín (1974), was against values determined from AX sized cores with L/D rates of 2, or adjusted to 2 by the formula of Hobbs (1964) (i.e. formula 6.2).

2) To obtain the maximum benefit from three directional core compression tests, it was decided that maximum number of specimens cored from a single block would provide the most realistic comparison.

L/D (length/diameter) ratio means and standard deviations are reported for each specimens set in fig. 8.1 (1-11). Even with AX sized core specimens L/D ratios of 2 were frequently not achieved, and uniaxial compressive strengths were adjusted accordingly to L/D ratio 2 strengths by the formula of Hobbs (op. cit.). Although the I.S.R.M. (1979a) recommend triaxial specimen L/D ratios of 2.5 to 3, with increasing confining pressure the effect of L/D on triaxial strength (Mogi 1966a) diminishes rapidly and adjustment is made for aspect ratio only where confining pressure is 20 MPa or below.

I.S.R.M. (1978b) recommended the testing of NX sized specimens with L/D ratios of 2.5 to 3 for uniaxial compression strength. Miller (1965) used NX sized cores to correlate L type Schmidt hammer values with uniaxial compressive strengths. The Schmidt hammer was used in the field to assess uniaxial compressive strength (sections 4.2.7 & 9.2.4.1). The comparison of laboratory test results and field results necessitate adjustment for size. Literature related to Uniaxial Compressive strengths and size effects is briefly reviewed by Hoek and Brown (1980) who suggested the empirical relationship adopted in this research.

$$f_c = f_{c50} (50/d)^{0.18} \quad (8.1)$$

where f_c is the unconfined compressive strength of 50mm diameter
D

f_{c50} is the unconfined compressive strength of 50mm diameter
of NX sized specimens.

8.5.2.2 Brazilian test Specimens

The I.S.R.M. (1978b) recommended NX size specimens with a thickness approximately equal to the radius. In some cases fracture density and sample block size precluded NX sized coring, and BX sized specimens (denoted on table 8.8 were tested).

Mean specimen L/D ratios, together with standard deviations are presented in Table 8.9.

8.5.3 Specimen Manufacture

8.5.3.1 Uniaxial and triaxial test specimens

Specimen manufacture is an important factor in obtaining high quality test results. Manufacturing techniques are discussed by Hawkes and Mellor (1970), Hoek and Brown (1980) and Atkinson and Casspi (1983).

A Qualters and Smith radial arm drill was used to core specimens from large block samples. Water flush was generally used, but with mudrock coring (specimen S17 - section 6.9) and some of the limestones where fracture density was high and where the material proffered variable resistance to coring, air flush was found necessary.

A review of literature suggested tolerances is given in table 8.10. Although coring and specimen manufacture was carried out by an experienced technician, AX sized compression test specimens could not be readily manufactured to the I.S.R.M. (op. cit.) specified standards. Two parameters were measured to monitor specimen quality.

1) End parallelism : A dial gauge on a magnetic stand was set on an engineers flat plate and used to measure the variation in specimen height as it was moved across the flat plate.

2) Length straightness : A dial gauge was used to measure the maximum deviation from true radii as the specimen was rotated in a Vee block, and cylinder straightness when the specimen was moved along its length. The maximum deviation from three rotational and length passes were recorded.

Flatness was not a problem, specimens were highly polished by the manufacturing processes. I.S.R.M. (op. cit.) quoted length straightness standards although readily achieved (fig. 8.1 (1-11)) were not sufficiently accurate to produce square and parallel ended

specimens when parted off and ground in the lathe. Even when a four jaw chuck was tried instead of the self centering three jaw variety, little improvement in quality was noted. However, it is the writers opinion that the quality of the compression test results were not impaired by this apparent inadequacy. However, preliminary tests on a far less stiff testing machine did imply rather the opposite, suggesting that testing rig strain energy is highly significant in exploiting imperfections.

Brazilian test specimens were readily manufactured to the specified tolerances (table 8.10). Specimen manufacture quality is summarised in fig. 8.1 (1-11) and table 8.9, where means and standard deviations for end parallelism and specimen straightness are recorded.

The polishing action of coring, cutting and grinding has been noted, and in plate 8.17 an electron micrograph shows the edge of a fractured, highly calcareous mudrock core (S24). The polished core surface, and an adjacent honeycombed zone, suggest pressure solution effects.

8.5.3.2 Brazilian test specimens

The I.S.R.M. (1978b) specified manufacturing tolerances were readily achieved.

8.5.4 Test Procedures

8.5.4.1 General

During specimen manufacture, moisture contents are significantly altered from field values. Generally, more weathered specimens have a greater hygroscopy, and strength has been observed to decrease with increasing moisture content (e.g. Colback and Wild 1965). To maximise these effects, specimens were stored in a concrete curing room (relative humidity 100%, temperature 20°C) for 10 days prior to testing.

Strength testing was carried out using an ELE rock testing machine, essentially a very stiff machine - it had recently been calibrated and rated grade A. Prior to testing, accuracy was ratified by a further check with a 100 kN capacity proving ring.

8.5.4.2 Uniaxial and Triaxial Compression Tests.

Specimens were located in the testing machine between hardened steel platens, these incorporated spherical seatings lightly smeared with mineral oil to correct for poor parallelism of specimen ends. Under a small axial force, specimen alignment was checked and adjusted. Load increase was applied at a steady rate by manual control. The rate, depending on confining pressure, ranged between 10 kN/minute and 50 kN/minute, but was sufficiently slow to induce failure between 5 and 15 minutes. Confining pressure in the triaxial tests was applied by means of a 'Hoek cell' (Hoek and Franklin - 1968) and pressure was controlled and maintained by an ELE constant pressure system.

To facilitate post test specimen reconstruction, a 38mm soil triaxial rubber membrane was placed loosely over AX sized uniaxial compression specimens. Failed specimens, both triaxial and uniaxial, were sufficiently reconstructed to show failure planes, these were recorded by sketch and photograph.

Typical specimen record sheet and post failure photographs are produced in table 8.11a and plates 8.18 and 19 respectively.

8.5.4.3 Brazilian Tests

As suggested by Hawkes and Mellor (1971) and recommended by the I.S.R.M. (1978b), a loading jig was manufactured for Brazilian testing NX sized disc specimens. Tests were carried out in accordance with the I.S.R.M. (op. cit.) suggested method.

Although when compared with NX sized specimen test results those for BX sized specimens (tables 8.8 and 9) appear satisfactory, they were not confidently determined. No testing jig was used, and specimens were tested between ELE machine platens. Because specimen failure load was often at the lower limit of testing machine sensitivity, a different, much 'softer' machine was tried. Results indicated a discrepancy between the two sets of measured values, the magnitude of the soft machine results being considerably greater than those determined using the stiffer one; for consistency the ELE machine was used.

Elastic analyses indicate that for results to be valid a single vertical crack should propagate from the centre (Vutukuri Lama and Saluja 1974). Mellor and Hawkes (1971) note that Hudson (1969) recorded little variation in strength resulting from off centre propagation. They also indicated that many additional cracks that might develop could be secondary in nature and that these were the result of imperfect testing techniques.

In practice it proved easy to distinguish between invalid and valid tests by :

- 1) An inappropriate primary crack.
- 2) Presence of flaws from which crack propagated, or influenced propagation e.g. bioclast or discontinuity.
- 3) Poorly developed hackle markings (section 8.5.5)
- 4) Deviation from fairly consistent tensile strength measurements.

Typical result sheets and post test photographs are reproduced in table 8.11b and plates 8.20 and 21.

8.5.5 Fracture

Griffith's (1921 and 1924) failure criterion is generally accepted as

being the most applicable failure theory for brittle material. He showed by an energy balance that cracks propagated from tips of flaws where tensile stresses were high. Although Griffiths criterion was, as indeed were subsequent derivatives (e.g. McClintock and Walsh (1962)), less than adequate as panacea for rock failure, he recognised the importance of flaws and inclusions as stress concentrations, a factor not recognised by earlier classical criteria e.g. Navier-Coulomb and Poncelet criteria.

In table 8.12, failure modes recognised during the course of testing have been tabulated. Modes 2 and 6 are more common in uniaxial test specimens, and modes 1, 4 and 5 in triaxial test specimens; Mode 5 was observed in the triaxial test (confirming pressure 35 MPa) carried out on Mudrock S17 (section 6.9). Influence of mode type 3 and 7 (table 8.12) was most pronounced in the uniaxial test, but both commonly occurred in triaxial tests.

Patterns which are sometimes observed on fracture surfaces are often well developed on those of the fine grained Lias Limestone, and consequently the material is highly conducive to the study of rock fracture.

Two fracture surface types were commonly observed :

- 1) Hackle marked - with hackles radiating from the point of propagation, and the most well developed hackles forming chevron type structures. Plate 8.20 indicates typical, but particularly well developed chevron structures on Brazilian specimen L6B, and this associates these markings with Griffith and/or Poncelet type fractures (i.e. crack extension and crack initiation respectively). Hackle marks and chevrons were commonly observed on minor and major fracture planes in both uniaxial and triaxial compressive tests. In the former, they often tended to be more well developed, e.g. plate 22 shows well developed chevrons on a fracture plane of a specimen tested in uniaxial compression. At the fracture source, friable light grey surface material was frequently observed and it appeared as though a highly localized violent cataclasis had caused this discernable tonal and texture variation (plate 8.22).

2) Shear failures which are more accurately defined by McClintock and Walsh (1962) or Navier-Coulomb criteria than Griffiths were more commonly observed in specimens tested in triaxial compression. Textural and tonal variation of failure surface is readily distinguished in plate 8.19. Both striae parallel with, and ridges orthogonal to, the direction of shearing were observed on friable surfaces; although the latter may well be associated with existing joint sets.

Specimens tested in uniaxial compression rarely exhibited only mode 2 (table 8.12) type failure, typically only the upper cone was well developed; e.g. specimen L2a3 (plate 8.18). In plate 8.19 (specimen L13a2 - confining pressure 20 MPa) a frequently observed perimeter zone differentiated by both surface features and tone is clearly defined. The shape of this boundary zone is such that it can be construed that the fracture mode is related to mode 2 (table 8.12). General observations suggest that the extent of this perimeter zone is a function of confining pressure. However, although fracture surfaces within this zone are not friable, they frequently exhibit mode 5 type fracture patterns.

8.5.6 Failure Criterion.

Given the variety of failure modes and the complexity of several occurring simultaneously, it is not surprising that Hoek and Brown (1980) note :

....."Many of the available failure theories offer an excellent explanation for some aspects of rock behaviour but fail to explain others or cannot be extended beyond a limited stress range."

In most rock slope stability problems, zero or very low confining pressures are applicable. However, uniaxial compressive strength is highly variable and is dependant on distribution and frequency of fabric flaws, i.e. Inclusions and fractures. Although rock genesis

implies preferred sedimentary orientation and tectonic structure, at both meso and micro scale, rock fabric remains highly variable. (Micrographs - plates 8.1 to 8.16, compressive specimen strength records, figs. 8.1 (1-11) and sample records - table 8-4). A programme of uniaxial testing would only further substantiate this, providing little or no quantifiable information on the influence of fabric and tectonic structure.

Based on the work of Griffith (1921 and 1924), McClintock and Walsh (1962) and their own practical experience, Hoek and Brown (op. cit.) suggested the empirical criterion :

$$f_1 = f_3 + \sqrt{\frac{mf_c}{f_3} + \frac{sf_c^2}{f_3}} \quad (8.2)$$

where f_1 is the major principal stress at failure

f_3 is the minor principal stress at failure

f_c is the uniaxial compressive strength of the intact rock material.

m and s are constants which depend upon the properties of the rock and upon the extent to which it has been previously fractured, i.e. prior to being subject to stresses f_1 and f_3 (s for intact rock = 1).

In chapter 6 and appendix 5 of their book 'Underground excavations in rock', Hoek and Brown (op. cit.) set out a rationale and equations for the analyses of both intact and fractured rock.

Their criterion quantifies to what extent previous fracturing processes influence the uniaxial compressive strength by the factor s ; i.e. under uniaxial compression equation 8.2 reduces to :

$$f_1 = (sf_c^2)^{\frac{1}{2}} \quad (8.3)$$

In Hoek and Browns (op. cit.) suggested method of analysis, regression correlation coefficients are also determined. Although to some extent this is affected by specimen quality and testing technique, it is more specifically a measure of rock fabric variation.

Consequently, although only rock strengths at zero confining pressures are considered relevant, in the writers opinion Hoek and Browns criterion offered the most relevant method of rock strength characterisation.

A prerequisite of analyses for fractured rock was determination of uniaxial compressive strength. Hoek and Brown (op. cit.) suggest the point load test. However, any such test is open to doubt, as measured strengths would still reflect the meso and micro fabric. In this work Hoek and Brown's (op. cit.) criterion method for determining uniaxial compressive strength of unfractured rock was adopted, and highest recorded uni-directional sample data used to assess the intact strength which was, on the basis of qualitative fabric assessment, (section 8.2) considered to be constant irrespective of direction. Highest values were invariably measured from specimens where no, or few, meso scale flaws were apparent.

Accepted tensile strength results were averaged (data presented in table 8.9) and used in strength characterisation, along with each measured compressive test data pair. Results are presented in fig. 8.1 (1-11), a maximum of 3 different direction result sets are presented for each sample; and notes relevant to their interpretation are present on sheet 1 of the figure.

With the exception of sample L2a where recorded uniaxial compressive strength was much lower, the uniaxial compressive strength varied between 207 MPa and 261 MPa (mean 234 MPa standard deviation 14 MPa).

These results are perhaps surprisingly consistent, and the deviation is only of the order that might be expected to result because of minor fabric flaws.

Highest uniaxial mudrock compressive strengths were typically 60 MPa (fig. 5.8). Strengths determined for sample L2a appear to be intermediate between those for sample L2a and the more competent limestones. These results compared with observations and other data recorded in this chapter, chapters 5 and 6 suggest strength is a function of induration, but that at a carbonate content of approximately 50% strength and induration increase rapidly, and that the range of carbonate content over which the transition from a relatively weak rock to a strong component rock occurs is no more than 10%.

\bar{m} values ranged between 5.29 and 11.68 parameter mean and standard deviations were 8.76 and 1.46 respectively.

Comparison of \bar{s} values indicate considerable variation, and for sample L12 recorded values were the lowest at 0.09 and 0.11 (direction II and III). The 0.5. value recorded along direction I was determined from highly variable results (regression correlation coefficient 0.69) and the regression correlation coefficient suggests a similar fabric.

In section 2.5 the work of Roberts (1974) is reviewed, he describes a micro fractured fabric which he considered unique in rocks not heavily folded and faulted and conjectures that within the Lower Lias of South Glamorgan it predates other tectonic fractured systems. Generally \bar{s} values of tested specimens reflect this micro fracturing.

Where specimens have been sampled from a site in close proximity to a fault (i.e. L12 and L14), the \bar{s} value determined is indicative of further additional micro fracturing and a consequential strength reduction. Micro fractures associated with major discontinuities are commonly observed and it seems reasonable to conjecture that the \bar{s} value of adjacent material is likely to fall to a value close to 0.1.

Although from the plotted directional envelopes (fig. 8.1) it was not possible to infer macro scale anisotropy, the influence of discontinuities recorded both as pre-test observations and in table 8.4 are clearly apparent.

8.5.7 Deformation of specimens tested in Uniaxial compression

Deformation of brittle rock material tested in uniaxial compression varies from that of an idealised elastic material. Mechanisms of variation are complex and include processes of crack closure, development of frictional resistance and sliding between closed crack surfaces, crack formation and crack growth. In the pseudo-elastic range (up to yield point) Bieniawski (1966) identified the fracture processes as one of stable propagation, but past the yield point he considered the process to be characterised by unstable fracture propagation.

Transition from yield to rupture in the specimens tested, with the exception of specimens from sample L2, was too rapid for effective measurement. During unstable fracturing, deformations are frequently relatively large and not conducive to measurement with electrical resistance strain gauges. Consequently, meaningful deformation measurements are confined to the pseudo-elastic zone.

In order to carry out tests in the ELE compression testing machine, a compression load cell, working range 0-250 kN was manufactured. To facilitate vertical and lateral strain measurement, pairs of wire electrical resistance type strain gauges were mounted on rock specimens diametrically opposite at mid height. Dummy gauges were also specimen mounted and used to complete the bridge circuit. A B&K system (Brüel and Kjaer system - strain indicator 1526, multipoint selector and control 1544, and alphanumeric thermal printer 2312) was used to measure and record strain and applied load.

Channels were scanned every 10 seconds, reading duration per channel was 0.5 seconds. Graphs plotted from the recorder output are produced in fig. 8.2 (1 to 4).

Prior to testing, specimens were not allowed to equilibrate in a moisture saturated atmosphere for fear of adverse effects to strain gauge bonding. Consequently, measured strengths were not included in strength analyses (fig. 8.1 (1-11)) but Mohr's circles, indicated by a broken line, are plotted in the relevant diagrams of those figures.

Specimen data records similar to those produced in fig. 8.1 (1-11) are reproduced in table 8.13.

Bieniawski (1966) noted that a more correct elastic modulus for unfractured rock material could be determined from the unloading part of a hysteresis. In table 8.13 tangent elastic constants (i.e. elastic moduli and Poisson's ratios) for the following parts of stress/strain curves are recorded.

- 1) Initial Loading - where crack closure is likely to have a maximum influence.
- 2) Unloading - elastic constants of uncracked material
- 3) At approximately 50% of specimen strength - where stable crack propagation is likely to dominate.
- 4) Close to specimen failure - During, or close to the onset of unstable crack propagation.

Recorded values for the limestone nodule (L2a3) are lower than for the other specimens and a plastic zone indicating more ductile behaviour is relatively well defined.

Results obtained, although often showing little variation for the four phases, generally confirmed the preceding characterisation. Recorded values of Elastic modulus and Poisson's ratio at 50% specimen strength (during stable crack propagation) were typically 55 to 60 x 10³ MPa and 0.26 respectively.

8.6 Summary

Limestones sampled on a morphological basis (table 3.1) have been described (section 8.2) and tested to determine index properties, mechanical strength and deformation characteristics. With the exception of a limestone nodule (sample L2), strength and deformation characteristics are similar. Variations in strength are largely the result of existing fracture frequency, continuity and orientation.

The use of Hoek and Brown (1980) criterion has facilitated the evaluation of tectonic fracture influence on rock strength. Mean value of intact uniaxial compressive strength for limestone was found to be 233 MPa, and \underline{s} values were shown to vary between 0.99 and 0.09. Rock strength is represented in fig. 8.1 (1-11).

Although variation in stress/strain graph slope was relatively small, deformation under uniaxial compression was found to be generally consistent with Bieniawski (1966) hypothesis of :-

- 1) Crack closure during initial loading.
- 2) Unloading part of the hysteresis being representative of uncracked rock material elasticity.
- 3) Stable crack propagation following initial crack closure, and continuing up to yield point.
- 4) Unstable fracture propagation following yield and prior to rupture.

Behaviour during unstable fracture propagation could not be ascertained by the method adopted which was unsuitable for measuring rapid and large deformations.

Index properties determined included dry density equilibrium moisture content and absorption coefficient, and results are presented in table 8.5.

Thermal gravimetry weight losses are recorded in table 8.6. A number of carbonate and organic carbon content values appeared inconsistent with anticipated results. These are discussed in section 8.4, and attributed to sample size and fabric variation.

Generally accepted tolerances for NX sized compressive strength testing could not be achieved in the manufacture of AX sized specimens. Results indicated that, providing testing was carried out in a stiff testing machine, the tolerances achieved were adequate for this particular specimen size and rock type.

Coring effects on perimeter rock fabric are also discussed; although the effect on strength was not determined it seems unlikely that a narrow zone of 100 μm would have any significant adverse effect.

The nature of the Lower Lias is such that differences between shear fractures and tensile fractures could both be readily distinguished, and fracture modes are discussed in section 8.5.5.

From the strength analyses based on results from small cores of known orientation, it was not possible to detect the influence of the tectonic induced anisotropy. Carbonate filled micro joints form part of a tectonic structure and these are reflected in the \underline{s} values determined from Hoek and Browns (1980) analyses. Close to master and major discontinuities associated micro fracture effect further \underline{s} value reduction in the adjacent rock material.

Tectonic induced anisotropy could not be detected from tests on the small diameter (AX sized) specimens. Nevertheless, strength and deformation data, presented together with fabric studies and other relevant results, provide a comprehensive representation of mechanical behaviour and performance.

CHAPTER 9
ROCK MASS SHEAR STRENGTH

9.1 Introduction

Stability of fractured rock masses is dependant on the resistance to disturbing forces developed along fractures or discontinuities.

The assessment of discontinuity shear strength is complicated by varying degrees of roughness, weathering intensity and micro/meso scale fracturing of adjacent rock, and laboratory test/field scale effects.

Within the Lower Lias the problem is further complicated by the rapidly alternating limestone/mudrock composite.

Stability analysis can also be highly complex and even the most complicated numerical models prove to be only a poor facsimile. Accurate shear strength assessment and, more realistically, the confidence limits with which it can be applied, is essential. Blind acceptance of shear strength parameters without appreciation of their limitations and the variation which might be expected, can invalidate even the most sophisticated of analysis.

Limestone discontinuity shear strength is considered of prime importance and to an extent this is reflected by the related chapter content. However, the contribution of mudrocks together with shear strength of filled discontinuities is also considered.

9.2 Limestone discontinuity shear strength

9.2.1 Literature review

Resistance of two planar contacting surfaces to sliding is governed by Amontons laws.

$$F_T = \mu F_N \quad (9.1)$$

Where F_T is the friction force required to resist sliding.

F_N is the force normal to the surface of sliding.

μ is the coefficient of friction dependant on the nature and condition of the surface of sliding.

In geotechnical engineering shear strength is traditionally defined by the well known Coulomb equation.

$$\tau = C + f_n \tan \phi \quad (9.2)$$

where τ = shear strength
C = cohesion
 f_n = normal stress
 ϕ = internal angle of friction

In soils and superficial deposits this failure criterion has proved adequate. However, as a failure criterion for rock discontinuity shear strength, with the complication of roughness, adjacent micro/meso scale fracturing and weathering, Coulomb's equation has proved inadequate (Goldstein, Goosev, Pyrogovsky, Tulinov and Turovskaya 1966 and Patton 1966).

Surface texture studies of smooth metal surfaces have indicated two scales of surface roughness i.e.

- 1) Small amplitude, high frequency projections - termed roughness, and
- 2) Larger amplitude, long wavelength undulations - termed waviness (British Standards Institution 1982).

Although the coarseness of rock discontinuity surface texture is many orders of magnitude greater than that of machined metal surfaces, there are similarities i.e. both waviness and roughness can be readily recognised. Patton (op. cit.) showed that rock shear strength was dependant on the degree of waviness only, which he termed 1st order projections, and roughness or 2nd order projections proved to be relatively insignificant. On this basis he proposed a modification to

the internal angle of friction to give the rock discontinuity shear strength formula.

$$\tau = f_n \tan (\phi + i) \quad (9.3)$$

where i is the angle formed between the peaks of 1st order projections and the mean plane of shearing, in the direction of shearing.

Barton (1973) defines three components of shearing applicable to rough rock discontinuities i.e.:

- 1) Friction resistance of the rock material
- 2) Dilation
- 3) Shearing through protruberances or asperities.

He indicated that the degree of dilation and shearing are intrinsically related by the strength of the rock material.

Ladanyi and Archambault (1970 and 1980) also recognised these mechanisms, and proposed the following equation:-

$$\tau = \frac{f_n (1 - a_s)(\psi + \tan \phi) + a_s SR}{1 - (1 - a_s) \psi \tan \phi} \quad (9.4)$$

where : f_n = normal stress.

τ = Peak shear strength.

a_s = Shear area ratio - the proportion of discontinuity surface where the projections have been sheared.

SR = Shear strength intact rock.

ψ = Dilation rate at peak shear strength.

The authors suggested that shear strength of intact rock could best be represented by the criterion proposed by Fairhurst (1964). Rock slope failure is most frequently initiated along master or major discontinuities. Observations and strength testing of Lias material (chapter 8) indicated that rock adjacent to such major discontinuities has a greater propensity for both micro and meso scale fractures (table 8.4 (3) and fig. 8.1). Consequently the empirical relationship (eqn. 8.2) suggested by Hoek and Brown (1980) would appear to be more applicable.

To facilitate assessment of a_s and dilation rate at peak shear strength Ladanyi and Archambault (op. cit.) proposed the empirical relationships.

$$\gamma = (1 - f_n/f_T)^k \tan i_0 \quad (9.5)$$

$$a_s = 1 - (1 - f_n/f_T)^L \quad (9.6)$$

where : i_0 is the roughness angle.

$k = 4$ and $L = 1.5$ for rough surfaces.

f_T is the transition pressure at which friction strength exceeds the shear strength of intact rock and is frequently assumed to be the uniaxial compressive strength.

In their later work Ladanyi and Archambault (1980) introduced into equations (9.4,5 and 6) a term expressing progressive failure of interlocking protruberences. In this modification transition pressure, which is usually assumed to be the uniaxial compressive strength is multiplied by a factor η which is an expression for interlock i.e.

$$\eta = (1 - \Delta x/L_1) \quad (9.7)$$

where Δx = shear displacement.

L_1 = projected length of ascending part of protruberences.

Barton (1971 and 1973) proposed equation 9.8 after direct shear tests on model tension joints.

$$\gamma/f_n = \tan (JRC \log_{10} JCS/f_n + \phi_b) \quad (9.8)$$

where JRC = The joint roughness coefficient a number between 1 and 20 depending on surface texture.

JCS = the joint compressive strength.

f_n = the normal strength.

ϕ_b = the basic friction angle of rock material.

Barton and Choubey (1977) suggest rationale and discuss the application of equation 9.8 in practice. They suggest that JRC determined by back analysis from the results of simple tilt tests; i.e. by measuring the angle of tilt necessary to induce sliding of field sampled mated discontinuity surfaces, provides a reasonable estimate of JRC.

In determining basic angle of friction values, Barton and Choubey (op. cit.) again advocate the use of a tilt test, but indicate that weathering and wetting of the discontinuity surface will reduce this value. Suggesting that tested surfaces are sawn, they indicate that an approximation (equation 9.9) could be used to estimate the residual (basic) angle of friction of the weathered material, i.e. :

$$\phi_r = (\phi_b - 20^\circ) + 20 (r/R) \quad (9.9)$$

where ϕ_r = the basic angle of friction of the weathered or altered surface

ϕ_b = the basic angle of friction of the unweathered surface.

r = the Schmidt hammer rebound number for weathered wet surfaces.

R = the Schmidt hammer rebound number for dry unweathered sawn surfaces.

The authors also suggest that JCS is determined in the field on wet weathered discontinuities using an L type Schmidt Hammer and the correlation for uniaxial compressive strength suggested by Miller (1965). Barton and Choubey (op. cit.) noting that Schmidt hammer tests are subject to variability recommended that the highest five of ten measured values at different locations within a metre square are averaged.

In a more recent paper Bandis, Lumsden and Barton (1981) reported significant reduction in measured shear strength of various sized, but similarly rough, replica joints. Their work indicated that both JRC and JCS reduce with increasing joint size. Barton and Choubey (op. cit.) indicated that adjustment to Schmidt hammer determined uniaxial

compressive strengths were necessary and suggested that for dense, hard rock this reduction factor should be 2.5, while for porous, weathered rock a reduction factor of 10 was more applicable. Bandis, Lumsden and Barton (op. cit.), while still advocating the use of small scale tilt tests to determine shear strength, recognise the need for a correction to the determined JRC value. They suggest that the asperity inclination of sample and prototype joints be measured at frequent intervals along the length, i.e. $0.02 \times \text{length}$ and the ratio of average asperity inclination ($\bar{\alpha}_0$) be used to adjust JRC, i.e.

$$\text{JRC (field)} = \text{JRC}_{\text{lab}} (\bar{\alpha}^{\circ} \text{ field} / \bar{\alpha}^{\circ} \text{ lab}) \quad (9.10)$$

Research leading to the recognition of joint morphology as controlling a significant, yet very difficult to define, set of parameters pertinent to discontinuity shear strength, has been reviewed. Rationale has been developed principally by Ladanyi and Archambault (1970) and Barton (1971 and 1973). Subsequent papers while indicating shortcomings in these rationales, serve to emphasise the complexity of rock discontinuity shear strength.

Compared to hard rock, the shear strength of soils can be readily determined. Soil responds to newly imposed stress fields, and the effects of earlier imposed stress regimes are only a relatively short term consideration. On the other hand, history of the rock mass, and in particular that of the rock adjacent to the discontinuity, has highly significant influence on rock shear strength. Weathered and alteration state, surface texture and micro and meso scale jointing add considerable complications in their own right and these are likely to be accentuated by the variability of their extent and distribution.

The most appropriate conclusion to this review would be a reiteration of Hoek and Brays (1977) timely caution:

'.... poor quality shear tests are worse than no shear tests at all since the results of such tests can be extremely misleading and give rise to serious error.....'

9.2.2 Rationale

Shear tests were carried out on previously diametrically fractured specimens generally NX sized and cored from the rock samples used in

the strength testing programme (chapter 8). Sample references, number of specimens tested and directional data are recorded in table 8-8. Although core size is perhaps rather small for discontinuity shear tests, NX sized cores are marginally larger than the size suggested by Hoek and Bray (1977) as a practical minimum.

Literature, e.g. Hoek and Bray (1977), Patton (1966) Ladanyi and Archambault (1970 and 1980), Barton and co-authors (op. cit.), Ross, Brown and Walton etc. all emphasise the importance of roughness in the assessment of discontinuity shear strength.

It had been initially intended to adopt the criterion and procedures developed by Barton and co-authors, but although appealing in their simplicity, several dilemmas (subsequently listed) prevented the author from initial implicit acceptance of their rationale. The modification and extension of the shear strength testing programme that resulted, and which is summarised in fig. 9.1 led to the rejection of Bartons (1973) criterion for this work. Surprisingly, a simple plot of discontinuity shear strength against normal-stress, uncorrected for roughness and shear plane slope, provided the best representation (section 9.2.5.3). The dilemmas referred to previously, which resulted in the author opting initially for shear box tests instead of tilt tests as suggested by Barton and Choubey (1976) were :

- 1) Lumsden, Bandis and Barton (1981) both indicated considerable scale effects for both JRC and JCS.
- 2) Much of Barton and his co-authors work is based on shear testing replica discontinuity surfaces (i.e. made from a cast). This ignores the effect of associated micro and meso scale fractures in the adjacent rock material.
- 3) Although normal stresses generated in rock slope are generally orders of magnitude lower than the uniaxial compressive strength, they are much higher than those which exist in the tilt test suggested by Barton and Choubey (1976). When normal stresses similar to those generated in rock slopes can be readily reproduced

in a Hoek type shear box, it would seem sensible to use such apparatus and test at representative normal stress levels.

In deciding to use the Hoek shear box (described by Ross-Brown and Walton 1976) it appeared that given the curvilinear shape of discontinuity shear strength/normal stress envelope, a better prediction of JRC would be obtained from shear tests at higher levels of normal stress.

Barton and Choubey (op. cit.) suggested that JRC could be best estimated from field collected specimens containing single representative discontinuities, or from replica casts of discontinuity surfaces. In the harsh coastal environment there were relatively few discontinuities which had not been subject to some erosion or wear, rendering them unrepresentative of those in the rock mass; sampling or field push-pull testing would also have been a highly hazardous process. This reinforced the decision to carry out laboratory shear tests in a Hoek type shear box. Joints tested were indirect tensile fractures formed in the point load apparatus (Broch and Franklin 1972) with wedged shaped platens. Field investigation (chapter 4 and 11) indicated that the factor controlling the stability of many sites was the limiting shear strength along conjugate shear discontinuities; the result of high north south and low east west compressive forces. Hackle markings and chevrons are a common feature of their surfaces (section 2.5) and it is considered that their mode of fracture is similar to that observed in Brazilian tests (section 8.5.5).

Data recorded from shear box tests included joint morphology, profiles, post test wear, shear strength, normal stress, dilation and horizontal travel. Shear strength results suggested that JRC was stress dependant, and to investigate this further, computer programs prepared by McBride (1983) were used to digitize surface roughness, plot bearing ratio and top point count curves (British Standards Institution 1982). These representations commonly used in machined metal surface texture assessments were considered by Pitt (1983) to provide a highly realistic assessment of surface roughness and resistance to sliding. Typical roughness profiles for the range of JRC values presented by Barton and Choubey (1976) were analysed and

used as standards for assessing shear box measured JRC values. Correlation between digitized profile assessments of JRC and shear box determined values were poor, it was consequently assumed that JRC was stress dependant.

Basic angle of friction tests were carried out in the Hoek shear box on cut shot blast surfaces, and both values for wet and dry test were determined. Barton and Choubey (op. cit.) suggest the use of formula 9.9 for adjusting basic angles of friction to residual angles, i.e. those of weathered surface. The modifier is based on Schmidt hammer rebound numbers. The Schmidt hammer was found to be insensitive to closed micro and meso scale joints and to slightly weathered surfaces.

In comparing rock compressive strength (fig. 8.1) against shear strength, it was evident that fractured state affected shear strength to some extent, but it was also clear that the value of Hoek and Browns (1981) parameter \underline{s} as determined for the normal stress direction could not be singularly used to define this weakening effect.

Although in the field discontinuity shear strength is always varied, nature always dictates that failure surfaces are minimum energy paths.

To some extent this simplifies shear strength assessment as minimum energy paths, which are dependant on both disturbing and resisting forces, tend to coincide with surfaces where shear strength approaches minimum values. Consequently lower percentile/discontinuity shear strength/normal stress curves determined from analysed data have been used in stability analyses. (Chapter 11)

The paper by Bandis, Lumsden and Barton (1981) is primarily concerned with scale effects, they effectively demonstrate a reduction in JRC with joint length. The roughness of joints measured in the field was found to be generally greater than the relatively small specimens tested in the laboratory, and it is conjectured in section 9.2.4.2 that this variation in roughness may compensate for scale effect.

9.2.3 Surface Texture

Mean asperity angle was suggested by Patton (1966) to be a surface

texture measurement particularly relevant to discontinuity shear strength. Widely accepted, (Hoek and Bray 1977) direct surface measurement of asperity angle has been adopted by several workers e.g. Frecker and Rengers (1971) and Bandis, Lumsden and Barton (1981); the latter using it to assess the influence of scale on JRC. Other workers, notably Weisbach (1978), Wu and Ali (1978), Tse and Cruden (1979) and Krahn and Morgenstern (1979) have used various stochastic functions including root mean square, centre line average, probability density function, auto-correlation function and spectral density function to assess discontinuity roughness.

Two simple roughness parameters often used in surface texture measurements of machined surfaces and providing a good assessment of resistance to lateral movement are the bearing ratio, and high spot count (peak frequency)(Pitt 1983). These parameters are defined by British Standards Institute (1982) and in fig. 9.2.

Bearing ratio is the ratio of a length of bearing surface at any specified depth in the profile to the evaluation length E (fig. 9.2) and is given as a percentage of the expression.

High spot count (peak frequency) is the number of profile peaks projecting above the mean line or a parallel pre-set line to the mean, and is expressed as a ratio of the evaluation length (fig. 9.2b).

The bearing ratio and peak frequency curves (fig. 9.2) show how these parameters vary with level, and these, as previously stated were evaluated and plotted from digitised data using a computer program written by McBride (1983). Discontinuity profiles were recorded by means of a carpenters profile gauge, the digitised profile was plotted and checked against the drawn profile before proceeding with bearing ratio and peak frequency evaluation and plots.

Barton and Choubey (1976) produced typical discontinuity profiles for the range of joint roughness coefficients, adopted as standards, these are reproduced in fig. 9.3. Peak frequency and bearing ratio curves for these typical profiles are reproduced in fig. 9.4. Although not

without anomalies, a general trend of increasing peak frequency and peak height with increasing roughness can be observed from these standard plots. After assessing the potential of several measurements from these curves for joint roughness evaluation it was decided to opt for :

- 1) height between 75% and 25% bearing ratio (h)
- 2) Average peak frequency for 75% to 25% bearing ratio.

Within a certain low range of values the greater the value of this simple geometric parameter h the greater the resistance to shearing, but as h increases, the angle between asperity surface and mean shear surface also increases and a transition from profiles inclined to dilate, to those where asperity fracturing is the dominant process takes place. A general trend, within the apparent limits of discontinuity geometry, for JRC to increase with roughness, was observed and average peak frequency between 25% and 75% bearing ratios selected as the second parameter.

As can be inferred from the previous discussion and the bearing ratio/peak frequency curves (fig. 9.4), some anomalies exist and three empirical corrections or modifiers were found necessary (listed below). It must be emphasised that these are tentative, but never the less were found to provide a working solution in developing the classification used for assessing JRC (fig. 9.5) of analysed profiles.

- 1) Where h is abnormally high asperity/mean plane of shearing angles are large. Considering asperities of equilateral triangle shape (ratio of h to total height of bearing ratio curve = 0.47) for pure shear induced dilation i.e. with no asperity fracturing during shearing, dilation angle has to equal 60° . With increasing asperity/mean plane of shearing angle a transition from dilation to asperity fracturing is likely to occur and dominate shearing processes. Fig. 9.4 indicates that roughness of typical profile JRC 10-12 is greater than suggested by the JRC coefficients. However, a study of the curve geometry indicates that the ratio of h to total height is 0.62, suggesting asperity shearing is an important mechanism and that the transition from dilation necessitates a correction. Where the ratio of h to total height of

bearing ratio curve is greater than 0.5 the following tentative empirical correction was used and found satisfactory.

$$\begin{aligned} \text{if } h/H > 0.5 \text{ then } h/H - 0.5 = x \\ h \text{ (revised)} = h - 0.468e^{0.431x} \end{aligned} \quad (9.11)$$

where h = Height between 75% and 25% bearing ratios.

H = total height of bearing ratio curve.

2) A second correction to h was made for the eccentricity of the 50% bearing ratio when compared with the mid-height of 25% to 75% bearing ratios.

$$\begin{aligned} 0.5 - a/h = x \text{ if } x > 0.1 \\ h \text{ (revised)} = h - 0.0037e^{16x} \end{aligned} \quad (9.12)$$

where a = the minimum of the two measurements between :

- i) 50% and 75% bearing ratios
- ii) 50% and 25% bearing ratios.

If measurement (i) is minimum the correction is negative, and if measurement (ii) is minimum the correction is positive.

3) When profiles were flat, peak frequencies tended to be high, but these 2nd order asperities are not critical to shear strength (Patton 1966). The broken lines in fig. 9.5 compensate for any misleadingly high peak frequency measurements.

In fig. 9.5 values of h and peak frequency from fig. 9.4 for typical JRC profiles of fig. 9.3 have been corrected as necessary in accordance with the previously described scheme and plotted. Using these values as a guide the adopted, but tentative classification for JRC evaluation has been superimposed.

9.2.4 Field Assessment

9.2.4.1 Schmidt Hammer tests

Barton and Choubey (1977) suggest that joint compressive strength (JCS) and correction of the fresh rock basic angle of friction to represent that of the weathered material can be best ascertained by Schmidt hammer testing (section 9.2.1).

Schmidt hammer rebound values were determined for both fresh and weathered material at 60 different locations, following the method recommended by Barton and Choubey (op. cit.). A typical record sheet is reproduced in fig. 9.6. Values of uniaxial compressive strength determined from the relationship suggested by Miller (1965) for the unweathered material were typically in the range 160 to 210 MPa. Millers' (op. cit.) relationship was based on the uniaxial compressive strength of NX sized cores. The average intact uniaxial compressive strength of AX sized cores tested in this work was 233 MPa (section 8.5). Adjustment to the NX sized equivalent strength using Hoek and Browns (1981) formula (equation 8.1 give an average f_c value of 207 MPa.

Values of the parameter \underline{s} which indicates the fractured state of the rock specimen (fig. 8.1) range from 0.092 to 0.995. Schmidt hammer determined values of uniaxial compressive strength appear to be representative of intact strength rather than fractured strength. The extent of micro and meso fracturing adjacent to the discontinuity, and its effect on rock strength is obviously highly pertinent to the discontinuities performance in shear, and the adoption of Schmidt hammer values as an estimate of rock strength in any shear strength assessment is likely to result in an overestimation of shear strength.

Although Schmidt hammer results for weathered surfaces (fig. 9.6) show a reduction in strength, the writer is not at all confident of their validity. Results measured from weathered discontinuity

surfaces were highly variable. At one end of the scale, where meso and micro joints had opened to some degree, recorded rebound numbers were low, giving f_c values less than 10 MPa, while at the other end recorded values, although for discoloured and apparently weathered rock, suggested no weathering induced reduction in strength. Schmidt hammer tests on weathered surfaces were confined to those sites showing some reduction in rebound value. The frequency of such sites along apparently weathered surfaces were less than 10%.

Although rebound values suggest that much of the rock adjacent to discontinuities and typically classified as weathering zone, WII had not resulted in strength loss, strength test results (fig. 8.1) and index properties (table 8.5) provide evidence to the contrary.

9.2.4.2 Discontinuity Profiles

Field examination of discontinuity surfaces indicated varying textures from planar to extremely rough and undulating. As a generalisation, planar discontinuities are frequently associated with zones of more intense shearing e.g. Col-Huw (plate 9.1 SS 957 674). However, even within these zones discontinuity profiles are subject to considerable local variations, and this can often be attributed to the variation of limestone fabric induced by concretionary type formation (section 8.2.2).

152 discontinuity profiles were measured in the field by means of a 150mm carpenters profile gauge and examples of these, showing the range of roughness are reproduced in fig. 9.7. Joint roughness coefficients (JRC) were estimated by the method outlined in section 9.2.3. JRC is given for the total length and in several cases for 50mm sample lengths (i.e. a & b - fig. 9.7).

Bandis, Lumsden and Barton (1981) indicated that JRC as determined from laboratory shear tests on different size joint replicas of similar roughness decreased with increasing size. They attributed this to two factors:

1) Decreasing uniaxial compressive strength with increasing specimen size.

2) Decreasing roughness with increasing specimen size.

However, JRC as assessed by computer analysis (section 9.2.3) gave largest coefficient for the greatest profile lengths analysed (fig. 9.7), suggesting a larger scale roughness or waviness.

This larger scale roughness or waviness was recognised by Fookes and Denness (1969) in their paper on fissure patterns in Cretaceous sediments of South East England, where they suggested terminology to describe trace patterns of closed discontinuities or fissures. It is conjectured that along discontinuities which exhibit waviness, the relative model to prototype roughness enhancement and mechanical strength reduction is to some extent compensatory.

9.2.5 Laboratory based investigation

9.2.5.1 Ancillary Procedures

The Hoek shear box described by Ross, Brown and Walton (1975) was used for discontinuity shear strength tests. To economically facilitate a large number of shear box tests, high strength concrete reinforced with polypropylene fibre was used in the manufacture of locating blocks. These were cast in the triangular shaped perspex moulds supplied with the apparatus. After being allowed to cure for seven days the blocks were cored centrally, and to a sufficiently large size to permit location of NX size specimens.

Following fracturing in the point load apparatus the specimen halves were wired together and cast into the locating blocks with Kaffir D plaster. Shear tests were performed after allowing at least twelve hours for the plaster to harden. Following the tests, cores and plaster casts were removed with the aid of a hydraulic ram

arrangement. Horizontal travel and dilation were both measured by means of linear displacement transducers (LDT's) connected via a bridge circuit to a chart recorder. A mounting for the LDT measuring dilation was fixed between the bearing housing and the top of the normal pressure ram, and displacement of the ram relative to its sleeve was recorded by attaching a reference plate to the sleeve by means of a jubilee clip. Peak shear strength was easily recognised by the sudden change of gradients on both vertical and horizontal displacement curves (e.g. fig. 9.8).

Cutting and coring processes polished specimens, and as suggested by Barton and Choubey (1977), specimens used in basic friction angle tests were shot blasted prior to testing, and between each loading stage. The jig made to standardise shot blasting intensity and confine the shot is illustrated in plate 8.2. The sample set in its locating block was maintained in a position 250mm from the nozzle exit. Iron shot, 0.5mm to 0.8mm in diameter was discharged from the gun at a pressure of 550 kN/m². Time to obtain a satisfactory surface was found to vary between 30 seconds and 2 minutes.

9.2.5.2 Basic Angle of Friction tests

Shot blasted specimens were used in a series of tests to determine the basic angle of friction (ϕ_b) (table 8.8). One specimen from each sample was cut diametrically and the cut, shot blasted, planar surface tested at various stress levels in the Hoek shear box.

Tests for both dry and wet surfaces were performed. Prior to carrying out the wet tests specimens were soaked for 24 hours, and on placing a specimen limb into the lower part of the shear box, a film of water was added to its surface before positioning the upper part of the specimen. A typical shear strength/normal stress graph is reproduced in fig. 9.9. The small recorded intercept was common on all graphs and is the result of interlock caused by small scale roughness, the effect of shot blasting.

ϕ_b values for both dry and wet surfaces are recorded in table 9.1. For NX sized specimens the value of ϕ_b is typically 39° while for wet ones it averages at 35.75°. These values are within the range for limestone, recorded by Barton (1976), who has tabulated ϕ_b values determined by several authors.

Tabulated results for BX sized specimens (table 9.1) are perhaps surprising. The results for samples J8E, J11E and J14E all indicate reduced values for ϕ_b , this is the reverse to the scale effect which is normally the case in strength tests.

9.2.5.3 Laboratory Shear testing of rough joints

In section 9.2.2 the reason for testing laboratory induced fractures was explained, and it was postulated that the fracture mode was similar to that of many of the major discontinuities within the area of interest.

Specimens tested were laboratory air dried. Prior to testing, three profiles along, and three transverse to the direction of shearing were recorded, together with surface morphology. In fig. 9.10 analysed profiles (mainly along the centre line and in the direction of shearing) together with pre-test surface morphology and test induced wear are recorded.

To facilitate the plotting of surface morphology and wear, fractured surfaces were photographed both before and after tests, and the surface detail traced, after correction for orientation using the method described in section 4.2.2, from the image of projected 35mm transparencies.

Data measured in discontinuity shear tests is recorded in table 9.1(1). The instantaneous angle of dilation (column 11) was determined from the arctan of a small increment of dilation/-horizontal movement ratio measured just prior to shear strength reaching peak strength value. The recorded shear plane mean slope

(i) was calculated as part of the computer analysis (section 9.2.3) from the digitised centre line profile. Barton (1973) in ascertaining the importance of the instantaneous angle of dilation (d_n°) implies the following relationship :

$$d_n^\circ \propto \tan^{-1} \gamma/f_n - \phi_b - i \quad (9.13)$$

No such meaningful relationship could be implied from the recorded data (table 9.1, columns 11 and 14) and consequently JRC determined from Bartons empirical criterion (equation 9.8), based on this relationship, appeared to be invalid and stress dependant. JRC values determined from profile analysis of the centre line profiles (section 9.2.3) and other profiles reproduced in fig. 8.10, showed no correlation with those experimentally determined.

Where JRC has been determined from two parallel profiles across a single specimen by analyses, both values are indicated in column 16 of table 9.1. Parallel traces were only analysed in cases where roughness varied appreciably over the specimen surface, and as might be expected, this is reflected by the recorded values.

Basic angles of friction (section 9.2.5.2), intact rock strength, moduli of elasticity and poissons ratios (section 8.5.7), suggest similar mechanical properties for the intact fresh rock material.

From collective analysis of all 48 data sets, several relationships defining shear strength were investigated, and equations for best fit curves, together with their respective coefficients of determination are listed below :

$$(\arctan \gamma/f_n - i) = 24.435 (f_n/f_c)^{-0.151} \quad (9.14)$$

$$r^2 = 0.73$$

$$\gamma/f_{cs} = 0.249 (f_n/f_{cs})^{0.621} \quad (9.15)$$

$$r^2 = 0.938$$

$$\gamma / I_s = 0.992 (f_n / I_s)^{0.598} \quad r^2 = 0.944 \quad (9.16)$$

$$\gamma = 1.638 f_n^{0.607} \quad r^2 = 0.944 \quad (9.17)$$

where i is the mean slope of the plane shearing
 f_{cs} is the fractured uniaxial compressive strength
 I_s is the strength index (wedge platens) as defined by Broch and Franklin (1972)
 r^2 is the coefficient of determination.

Equation 9.17, derived from a simple plot of shear strength against normal stress gave the best curve. Normal stress levels were often common for several tests, and a plot showing mean, 1st and 9th decile values for the several normal stress levels is presented in fig. 9.11. Regression analysis of shear strength mean values showed an enhancement of curve fit. The coefficient of determination of 0.987 provides a highly convincing argument for shear testing rough joints at representative stress levels and a simple shear strength/normal stress representation of results.

9.2.6 Suggested Shear Strength Criterion

Bartons' (1971) empirical rationale which makes separate assessment of shearing components and their modifiers, has been demonstrated as an inadequate criterion for this particular investigation. This is attributed to :

- 1) The insensitivity of the Schmidt hammer to measure fractured uniaxial compressive strength, where the rock fabric is micro fractured and these fractures are closed or carbonate filled.
- 2) The low degree of confidence with which the Schmidt hammer could be used to assess strength variation of the weathered rock.
- 3) Bartons (1971) criterion, which is based on roughness consideration only, i.e. established from testing of joint surface replicas, and therefore it ignores the complexity of the rock fabric flaws adjacent to the discontinuity.

Regardless of shear plane slope, roughness and degree of weathering, a simple plot of shear strength against normal stress determined from shear box testing of rough discontinuities provided the best fit curve.

This is attributed to the influence of micro fractures within the adjacent fabric.

Minimum energy paths and their relationship to paths of minimum shear strength have been discussed in section 9.2.2. It is conjectured that the 99% confidence level indicated in fig. 9.11, while providing a more realistic assessment of the critical shear strength value, could also provide the basis of a lower bound solution.

9.3 Shear Strength of filled Discontinuities

Although very few discontinuities are filled to an extent where interlock is completely lost, weathered mudrock material migrates into discontinuities and effects opening (section 10-2). This phenomenon is more pronounced in strata outcropping near the top of the cliff. Occasionally faults are also filled with a mixture of brecciated limestone and gouge material; the latter appears to be a weathered silty clay derived from the mudrocks.

Barton (1974) notes that as the width of the filled discontinuity increases, shear strength decreases and that at the width where interlock of the two rock limbs is lost, shear strength approaches the value of the infilling material.

Mudrock sample S21, completely weathered material described and classified in Chapter 5 and one of the mudrocks analysed and investigated in Chapter 6, is typical of the residual soil material migrating into joints. Such migrating or gravitating soil can be considered normally consolidated and well drained. Consequently, drained shear box tests were carried out on remoulded specimens (of sample S21) to determine relevant lower bound shear strength values for filled discontinuities.

Tests were carried out using a 60mm square shear box. Dried, powdered material was mixed with deionised water to give a moisture content approximately equal to the liquid limit. After curing for a 24 hour period, the material was added to the shear box and allowed to consolidate in several stages, the final pressure increment giving the value of normal stress at which shearing was carried out. E_{100} (time to 100% consolidation) was estimated from the $\sqrt{\text{time/consolidation}}$ curve, and the approximations (equations 9.18 and 9.19) which were derived by Gibson and Henkel (1954) were used to estimate t_f (time to failure) and c_v (coefficient of consolidation).

$$c_v = 0.103 H^2 / t_{100} \quad (9.18)$$

$$t_f = 12.7 t_{100} \quad (9.19)$$

where H is sample thickness - length of drainage path.

Machine shearing speed was based on the calculated time to failure and an estimated displacement to failure. Vertical and horizontal displacements were recorded by linear displacement transducers (LDT's), and chart recorder output has been reduced and is reproduced in fig. 9.12, together with relevant test data (table 9.2). Three shear tests were carried out at different normal stress levels, they gave a value of ϕ_d (drained internal angle of shearing resistance) equal to 31° . The Mohr Coulomb envelope, together with plots of both final moisture content and dilation angle against shear strength are presented in fig. 9.13.

9.4 Mudrocks

Only in the lower horizons of the angulata zone, where limestones are relatively thin, nodular and discontinuous, is the shear strength of mudrock of any great significance to rock mass stability; e.g. Williams (1980) describes rotational slips in weathered shales in the vicinity of Trwyn-y-Witch (SS 890 725). In fig's 6.14 and 15, and

table 8.13, modulus of elasticity values are reported for both a typical mudrock and limestones. Throughout much of the bucklandi and angulata zone, limestones are sufficiently continuous and frequently distributed to provide a 'framework' capable of sustaining normal stresses. Variation in modulus of elasticity (figs. 6.14 and 15, and table 8.13) show that forces generated normal to near vertical discontinuities (chapter 11) will stress the limestones rather than the mudrocks. The low normal stresses in mudrocks will be reduced even further by the dilation process involved in shearing movement along rough rock discontinuities. Consequently, along minimum energy paths where some fracturing of mudrocks is likely to have occurred, mudrock contribution to rock mass shear strength is negligible, and, in any lower bound stability solution, ignored.

A discontinuity in the limestone does not necessarily imply a discontinuity in the mudrocks, as the more ductile mudrocks are capable of sustaining greater distortion without fracturing during tectonic stressing (chapter 2). Although mudrock strengths vary considerably, and in fresh or unweathered material largely with the amount of cementitious material (section 5.5.2); at the limestone/mudrock transitional carbonate content, the rock is still very much weaker than a typical limestone (e.g. specimen L2. fig. 8.2).

Intact shear strengths along a predetermined plane perpendicular to laminae could be considered as contributing to an upper bound value of rock mass shear strength. Coring parallel to the laminae proved a difficult process, and only AX sized cores could be produced. Three cores from sample S17 and one core from sample S24 (description table 5.6) were tested using the Hoek shear box, and shear strength/normal stress plots and relevant data are reproduced in fig. 9.14.

In fig.11. dilation is shown to result in shearing along low angled discontinuities or laminae within the mudrocks. Although beyond the scope of this thesis, any sophisticated numerical analytical technique would need to assign a shear strength value to these potential slip planes.

NX sized cores (sample S17) and BX sized cores (sample S24) were tested and the shear strength envelopes and relevant data recorded in fig. 9.15. Failure of all specimens sheared in a direction parallel to the laminae were along low angled planar discontinuities rather than inter-laminae planes. A correction for the inclination of failure plane has been made by assuming a zero origin for each result set.

Index test and descriptions (chapter 5) indicate sample S24 to be a high strength mudrock, and sample S17 a middle range member, and plotted test results (figs. 9.14 and 15) reflect this.

9.5 Summary

On the basis of a literature search briefly reviewed in section 9.2.1, it was decided with a few variations outlined in section 9.2.2 to adopt the criterion and methodology of Barton and his various co-authors.

The investigation of fissure or closed discontinuity shear strength was complicated by a test proven inadequacy of Barton's (1971 and 1973) empirical criterion. This was attributed largely to the system of carbonate filled micro and meso scaled fractures, adjacent to the discontinuity. This phenomenon appears to be ignored by Barton (op. cit.) whose criterion is based on surface texture, frictional characteristics and strength, and modified for weathering effects. Schmidt hammer testing advocated by Barton and Choubey (1977) as a satisfactory method for strength measurement also proved inadequate for assessing the fractured strengths relevant to this material.

The investigation, which included laboratory shear tests, basic angle of friction tests, and field assessments of strength and joint roughness was further extended to include surface texture measurement and profile analysis. Parameters adopted in analysis were bearing ratio and top peak count, both are commonly used in surface texture analysis of machined metal.

The most satisfactory criterion apparent was that derived from simple shear strength/normal stress plots (fig. 9.11).

Rock mass failure surfaces follows minimum energy paths, which although defined by two variables, i.e. disturbing and resisting forces, are usually along surfaces where shear strength is close to the minimum. Consequently it is postulated that the 99% confidence level plotted on fig. 9.11 could be reasonably adopted in lower bound assessment of the limestone discontinuity shear strength.

Barton (1974) suggested that shear strength of filled discontinuities where interlock of the hard rock surfaces is effectively lost, reduces to that of the infilling material. Although there are relatively few discontinuities where interlock has been completely lost, residual soil material derived from the mudrocks does migrate into the discontinuities and is particularly active in reducing rock mass shear strength close to the cliff top. Drained values of shear strength of residual soil material were considered pertinent, and shear box tests on remoulded samples of completely weathered material from sample S21 gave a ϕ_d (drained angle of internal shearing resistance) of 31° .

Modulus of elasticity is greatest for the limestones and consequently it is in the limestones that generated stress levels normal to discontinuity surfaces are greatest. Therefore, in a lower bound assessment of stability, a reasonable assumption would be to ignore the contribution of mudrock shear strength. Because mudrocks are more ductile than limestones, vertical fractures are less frequent, and intact shear strength values along planes perpendicular to laminae have some relevance to upper bound stability assessment. Shear strength results on specimens from two samples are presented in fig. 9.14.

In section 9.4 it is conjectured that shearing in mudrocks parallel to laminae may be induced by dilation. Shear strength results from test data on specimens from the same two samples as used in the tests previously mentioned are reproduced in fig. 9.15.

CHAPTER 10

FIELD MONITORING AND THE EFFECT OF CONTEMPORARY SUBAERIAL WEATHERING PROCESSES ON CLIFF STABILITY

10.1 Introduction

Erosion and weathering by subaerial processes, when compared with the obvious effects of exposure to full force of the sea in a high energy marine environment, appear insignificant. A change in erosion time scale such as might be afforded by protection works may well prove that subaerial processes are highly active.

In a report to the Nature Conservancy Council on Coastal Protection at the Isle of Thanet, Grimes (1984) noted that since the completion of a sea defence west of Friends Gap, Margate in 1982, considerable quantities of colluvium had fallen from the protected chalk cliff at the rear of a wide berm slab abutting the cliff. Such falls were clearly instigated by subaerial processes and presented some risk to large numbers of people to whom the wide berm slab was a promenade.

Consequently, in the design of any protection works, full consideration must be given to all weathering mechanisms in context of facilities and benefits the works are anticipated to provide.

In this chapter the role and significance of mechanisms, other than marine erosion, active in both the degradation and instability of the Glamorgan Lower Lias Cliffs are considered.

10.2 Subaerial Weathering

The weathered slate, i.e. the degree of alteration under the influence of contemporary and previous hydrospheric and atmospheric environmental regimes, has been described for both mudrocks and limestone fabrics in sections 5.2.6 and 8.2.6 respectively. Weathering processes are summarised in table 5.5; in this section

active contemporary processes are considered primarily in the context of rock mass and rock fabric weatherability, i.e. short term susceptibility to weathering.

10.2.1 Chemical

Both carbonate leaching and the oxidation of finely disseminated pyrite are currently active processes and contribute to the weakening of both rock fabric and mass.

In section 2.2 it was conjectured that previous environments may well have been more conducive to chemical weathering processes than that of the present day. Both cliff face tufa deposits and chemical analyses of ground water (section 3.3) indicate carbonate dissolution.

At Nash Lighthouse (SS 918 680, section 4.4, Map 4.8(4)) the cliffs were protected and underpinned in 1860. During the intervening 125 years dissolution of limestone adjacent to several discontinuities appears sufficient to permit top soil to gravitate and expose lengths of widened discontinuities in the cliff top Lighthouse site. This does not invalidate the protection and stabilization which is still serviceable after some 125 years; during which time maintenance has been relatively small. However, it does serve to demonstrate that processes not sufficiently active to be readily apparent in the time scale imposed by marine erosion do take place, and may warrant consideration in a long term stabilization proposal.

Measured groundwater sulphate contents (table 3.1) are greater than those which would be expected if their source was only contaminating sea water. Vadose water is primarily charged by locally derived rain water, and in Chapter 7, oxidation of the mudrock pyrite phase reduced by the action of permeating water of such origin was demonstrated. In sections 5.3 and 8.4 finely disseminated pyrite present in both limestone and mudrocks was shown to exhibit varying degrees of stability. Although not without a few anomalies, a

significant conclusion drawn from investigations described in Chapters 5, 6, 7 and 8 was that in fresh (unweathered) mudrocks and limestones, the least stable pyrite was present where carbonate contents were close to 50%.

The anion product of sulphide oxidation, sulphate, enhances the leaching potential of vadose water, and carbonates are slowly leached from rock material adjacent to water carrying discontinuities, actively reducing discontinuity shear strength. Water is frequently conveyed along the more vertically persistent major and master discontinuities which permit perched ground water egress through impermeable mudrocks. These discontinuities are generally planes of minimum shear strength, consequently leaching can be construed as a significant process impairing rock fabric strength to the greatest extent along critical shear planes.

In Chapter 7 it was demonstrated that pyrite oxidation was less in a fresh unweathered specimen of weak incompetent mudrock (28a) than in fresh unweathered competent mudrock. However, it was construed in both Chapters 6 and 7 that the degradation of such unweathered mudrocks was long term. In section 6.6 it was shown that acid weathering resulting from pyrite oxidation had degraded and caused rehydration of phyllosilicates, and that pyrites still present in a completely weathered sample (i.e. WV) were highly unstable.

It would seem that the high weatherability of mudrocks already altered by pyrites oxidation, i.e. mainly those in the upper cliff, may be a significant contributor to instability, particularly to the frequent small magnitude falls from the upper cliff.

10.2.2 Pressure Release

Nichols (1980) has noted numerous reports of rebound deformations in intercalated limestone shale sequences. Rebound is the movement resulting from pressure release. During diagenesis extremely high vertical and lateral pressures are generated by large thicknesses of accumulating sediment.

Post depositional history is conjectured in table 2.1. Marine conditions prevailed until late Jurassic times. Donovan, Lloyd and Stride (1971) established the existence of a complete Jurassic succession in the Bristol Channel with a total thickness of approximately 1600m. Subsequently, events are rather more uncertain.

However, if Jurassic strata along the area of interest reached the thickness present in the Bristol Channel, then the rocks exposed would have been subjected to an overburden of some 32 MPa from Jurassic strata alone.

During compaction of sediments pore volume is reduced. This is achieved by :

i) More efficient particle packing and the dispelling of excess water.

ii) Elastic compression, flexing and/or deformation of particles.

iii) Grain crushing.

Marine clays have a flocculated structure. Stacks of very small platelet-like particles or domains readily slide and flex. In coarse-grained sediments grain crushing increases inter-particle contact, modifying the stress distribution until it is less than the particle yield strength. Grain deformation, a function of stress and elastic modulus, will occur in all particles. These strains become locked in during lithification. Subsequent erosion is effective in removing overburden. Reduced gravity pressures are no longer in equilibrium with internal stresses. Well lithified rocks such as limestones are more able to sustain these internal rock fabric stresses. Where there is a reduction in the level of external pressures, and as a consequence the fabric stress exceeds the tensile strength, fracturing will occur.

"..Such extensional fractures are usually sub-parallel to local topography and increase in density towards the surface, and are only local in extent...." (Nichols, op. cit.)

Internal rock fabric and rock mass stress are modified by subsequent events. Recession of the Jurassic sea was followed by a period of erosion and possibly a marine transgression in mid-Cretaceous times (contentious - George 1974). Crustal instability throughout much of the Tertiary period generated north-south compression waves, and these flexed, faulted and fractured strata. Many fractures in the limestone exhibit features of extensional type brittle fracturing (section 8.5.5). Deformation characteristics and elastic constants for a mudrock and range of limestones are reported in sections 6.9.2 and 8.5.7. Under uniaxial load applied parallel to laminae, axial deformation at failure for both tested limestone and moderately competent mudrock is in the same range. However, vertical fractures often tend to be more frequent in limestones than in mudrocks, and primarily this is attributed to :

- 1) Elastic modulus of the mudrock, a shale measured in a uniaxial compression test and in a direction perpendicular to laminae indicate that under a direction of load parallel to laminae, the laminae would be poorly restrained and thereby fail by buckling at relatively low deformation. Subjected to confining pressure, laminae would be restrained and axial deformation to failure enhanced.
- 2) Shearing within mudrocks along planes making low angles with laminae.

Laterally induced tectonic strains in limestones and mudrocks must be compatible and therefore tectonic forces would have stressed the limestone to a greater level than the mudrocks. Conjugate extensional mode type fractures (permitting north-south shortening) are frequently observed in the limestone (section 2.5). Small movements (e.g. less than 5mm) would have been adequate to increase the strain in the intercalated mudrocks, thereby distributing stress in the rock mass.

Variability in rock mass geometry will tend to modify a displacement response which can be directly correlated with recession. Therefore, parts of the rock mass may well be able to sustain greater lateral pressure than others, and these act as internal buttresses until such time as erosive processes impair their effectiveness. The internal restraint system is thus slowly but continuously modified, and store strained energy is released via. the unrestrained cliff face.

The rock mass adjacent to the cliff is ineffectively restrained against lateral movement. Lateral expansion in incompetent shales would provide traction to the overlying rock mass, opening discontinuities with a resulting loss in shear strength and interlock. However, observations made both from laboratory tests and in the field suggest that such differential lateral pressure release is very small.

Long term leaching test stress paths for incompetent shale 28a and highly competent mudrock 43a are plotted in fig. 7.5. No significant change in circumference is recorded for either specimen (fig. 7.7). Rock face monitoring (section 10.3) indicated no significant movement which could be attributed to rebound.

The lower angulata zone is characterised by thick mudrock and highly discontinuous limestone. Consequently, relatively large strains would have been induced by the Alpine Orogenic forces. Where angulata mudrocks are exposed basally, movements are sufficient to effectively reduce interlock in the overlying limestone dominant strata, to the extent that toppling is a rarity and that intact blocks of bucklandi limestone translate vertically (e.g. plate 4.1 and 4.20). Such geomorphologic features as shallow hollows formed where topsoil has migrated into opening discontinuities and developing tension cracks, are also indicative of reducing interlock and in these relatively unweathered mudrocks this to a large extent is attributed to rebound.

It is unlikely that tectonism modified the limestone fabric stresses. However, fracturing the more competent rocks and increasing strain energy levels within the mudrocks would have significantly altered the state of stress in the rock mass.

Extensional movements in poorly lithified clay rocks is not simply dependant on the release of stored strain energy as the diagenetic bonds break down. The physico-chemical behaviour of the clay phase can significantly contribute to the amount of rebound.

Diagenetic alteration of clay results in :

- i) The formation of illite and chlorite.
- ii) The development of stronger secondary bonds.
- iii) Reduction of moisture content to typically 3-4%.
- iv) Dehydration.
- v) Restraint of clay phase by partial cementation.

Clay absorbs water, and as the moisture content increases, swelling occurs accompanied by a loss in strength. The phenomenon which is time dependant can be referred to as strain softening. Details of active physico-chemical processes in the swelling of clays are described by Osion and Mesri (1970). Chemical weathering processes contribute to the process; most notably the oxidation of pyrite, the acid product of which degrades and enhances rehydration of the clay phase (section 10.2.1).

Pressure release is likely to be a maximum in the north-south direction; i.e. the direction of the major principal stress. Away from the cliff, stresses modified by subsequent history but primarily residual of those induced by the Alpine Orogeny are locked into the rock mass. As lateral restraint is impaired by cliff recession, recovery of the elastic shortening effected in limestones is likely to be spontaneous with the removal of restraint. Residual strains in poorly lithified mudrocks, both of sedimentary and tectonic origin, will respond more slowly to changes in boundary conditions.

The cliff/platform intersection acts as a restraint against any seaward extensional movement in the cliff face. The localised angular shaped notch acts as a stress concentrator, and as such erosion is facilitated.

10.2.3 Climatic Effects

The extremes of climate are not only effective in degrading and disintegrating the rock fabric and thereby reducing resisting forces along critical planes within the rock mass, they can also trigger failures in cliff sections where equilibrium has been impaired to a value just above limiting in more convivial conditions.

Rock strength in both mudrock and limestone reduces with increasing moisture content. Fig. 5.8 shows the influence of moisture on mudrock uniaxial strengths. Weathered limestones are porous and moisture contents rise appreciably higher than in unweathered limestones. Limestones are most weathered adjacent to discontinuities; not only is discontinuity shear strength impaired, but the leaching of cementitious material and the oxidation of pyrite is facilitated (section 10.3.1) effecting further weakening.

Freezing water expands by approximately 9% of its volume and is capable of exerting pressures of up to 14 MPa. Consequently, water freezing in weaker mudrocks and weathered porous limestone can effect disintegration.

Moisture contents of mudrocks, even within a range of values below the TRRL shrinkage limit, exhibit shrinkage on drying and swelling on wetting (section 6.8). Limestones typically have a coefficient of expansion of 4×10^{-6} mm/mm per °C. During a wet cold period discontinuities open and fine grained colluvium migrating into these inhibits closure and facilitates further opening. Ice formation in discontinuities or in infilling fine grained colluvium is another mechanism whereby discontinuities are opened.

It is possible to postulate the mechanisms which make extreme climatic conditions likely to effect a significant reduction in orthogonal discontinuity shear strength, and thereby enhance the probability of falls.

The high incidence of summer falls are considered in conjunction with the temperature induced rock face movements (section 10.3.3).

During winter, higher rainfall increases the volume of water permeating through the rock mass. The less competent shales are not jointed to the same extent as the more competent rock, and impede seepage; consequently there is an increase in moisture content accompanied by swelling. As a result limestone discontinuities open, and this opening is enhanced by falling temperatures which cause limestones to contract. Ice may also form in discontinuities wedging them open further. Master discontinuities (i.e. including those likely to form critical shear surfaces) frequently contain fine colluvium or gouge, adjacent shales are often highly weathered and associated seepage is relatively high. Consequently such discontinuities are particularly vulnerable to the formation of ice. If ice causes shear surfaces to dilate, movement along the shear plane results and if dilatancy is great enough, failure occurs.

Samples of completely weathered mudrock S21 and S22 from the same horizon and close in location showed marked difference in linear shrinkage ratios, 5.67% and 10.27% respectively (table 5.9). During prolonged dry summer periods polygonal shrinkage cracks developed in the cliff top soil; during drought conditions cracks as wide as 10mm have been noted. These cracks are partly filled with migrating soil and on swelling displacement towards the unrestrained cliff edge takes place, loosening soil, limestones and mudrocks of the upper weathered zone. Shear strength effectively reduced by loosening and increased moisture content, impairs stability of upper cliff edge material, and the cyclic process is responsible for recession of the upper cliff edge.

The weatherability of the upper zone rock is highest and it is these rocks which are most susceptible to the weathering agencies described in this section, and which are largely responsible for degradation of the upper cliff zone and instigation of frequent but small magnitude failures.

10.2.4 Salt Crystallization

In the high energy marine environment the whole cliff is often sprayed by fine droplets of sea water airborne by strong winds. On drying, salt crystallizes in surface cracks and voids, facilitating opening and disintegration of more weathered upper cliff face rocks.

Inter-laminae sulphate crystals observed in mudrocks (plate 6.1) are attributed largely to salt crystallization from the evaporation of soil water during dry weather, and as such act as a mechanism of disintegration by prising adjacent laminae apart.

Tufa precipitating on the cliff face, far from impairing stability, appears to enhance it by providing a protective rendering and to some degree cementing discontinuities close to the cliff face.

10.2.5 Biological Disintegration

There is little evidence of root growth having a significant adverse effect. Brassica Oleracea (wild cabbage) grows on cliff face ledges particularly towards the top of the cliff, and to some extent root wedging contributes to small falls.

Hippophae Rhamnoides (a buckthorn) grows at some cliff top locations; little evidence of instability at these locations suggests that the root system may contribute to stability of the upper zone.

Varieties of mosses, grasses and lichen grow on some of the tufa deposits, and these appear to have no adverse effect on stability.

There is no evidence of animal burrowing in the upper cliff.

10.3 Rock Face Monitoring

10.3.1 Introduction

Site monitoring to record opening and closing of vertical discontinuities in limestone and movement in mudrocks perpendicular to bedding both indicated a small extensional trend. Consecutive readings, typically at monthly intervals, often showed variation many times greater than that which could be expected from the trend line. Monitoring was carried out at the following sites :-

- 1) Dimhole (SS 95220 67615) - The site of a recent fall.
- 2) Col-Huw (SS 95450 67530)
- 3) Summerhouse (SS 99170 66520) The site of a recent fall.
- 4) Summerhouse (SS 99615 66435) The end of cliff.

Results for all sites showed similar trends and deviations, and consequently only the Dimhole results are reported (section 10.3.2).

The large variation in consecutive readings was attributed primarily to climatic conditions prevailing at the time of reading, and an investigation at Dimhole to establish the effect of temperature was carried out to confirm this and is described in section 10.3.2.

10.3.2 Long Term Monitoring at Dimhole (SS 95220 67615)

Demec monitoring was installed in February 1980, approximately four weeks after a fall. The topographical and geomorphological setting is shown in plate 10.1. The site forms part of the east rising limb from the dry valley known as Dimhole. Two master discontinuities (plate 10.2) strike approximately at right angles to the cliff (fig. 4.8.8), both contain highly fractured limestone, breccia and gouge. The lower parts of these discontinuities have been exploited by wave

attack and small caves have formed. To the east of the fall, the cliff steps seaward along a series of approximately North-South striking discontinuities.

To monitor horizontal differential movements between adjacent limestone blocks, and vertical movements in a mudrock, metallic buttons with a central seating were located at prepared positions on limestone surfaces. Locations are shown in plate 10.2 and in fig. 10.1.

Measurement between Demec points was periodically made (approximately monthly intervals) using a mechanical extensometer. Locating points of the extensometer fit into Demec button seatings and measurement to a manufacturers claimed accuracy of $\pm 3 \times 10^{-6}$ mm/mm is recorded on a dial gauge. Graphs of movement against time are recorded in fig. 10.2.

The following procedural problems were encountered :

1. Although fall debris facilitated Demec point positioning and early monitoring, during the course of monitoring debris was reduced and transported by the sea, and it became increasingly difficult to make measurements.
2. On several occasions rebonding of Demec points proved necessary. These are denoted on fig. 10.2 by broken horizontal lines transposing previous readings to the date of rebonding.

Given the accuracy of this type of monitoring, deviation from the general extensional/expansion trend is not adequately explained by procedural problems.

Monitoring for temperature effects (section 10.3.3) goes a long way to explaining the considerable deviations.

Except for block A (fig. 10.1), results (fig. 10.2) show a general

extensional trend. The poor restraint and lack of basal support to block A is apparent in plate 4.2, and it might be expected that rotation would have been evident. Opening is effected by mechanical weathering agents. However, the small degree of opening is attributed to the relatively small movement in the moderately strongly cemented adjacent mudrocks, and relatively poor restraint facilitating opening and closing.

The monitored mudrock (44a), a competent, well lithified, calcareous shale, slightly weathered (WII), showed a small expansive trend (fig. 4.2). When monitoring was terminated, small patches of sulphates had crystallized on the shale surface and penetrated inter-laminae a small distance, rendering parts of the surface slightly friable.

10.3.3 Influence of Temperature on Rock Face Movements

Rock face monitoring, air temperature and rock face temperature were checked hourly between 07.00 hours and 19.00 hours on 25th August 1981. Results are recorded in fig. 4.3. With increasing temperature a decrease in discontinuity width was recorded.

Joint closure is frequently inhibited by fine migrant colluvium filling open discontinuities. Above Demec point sets 7, 8 and 9 (fig. 10.1) a source of such fine colluvium material exists (plate 10.2) and would appear to be one explanation for the lower recorded closure. A second explanation is that Demec points 7, 8 and 9 were afforded slightly more protection from early morning sun, and this is certainly reflected in the earliest readings.

Movement of adjacent blocks is dependant on the degree of restraint afforded by the rock mass, and which is principally provided by two mechanisms.

- 1) Block end restraint - dependant on effective end contact of adjacent blocks.

- 2) Frictional - the frictional forces mobilized laterally along horizontal discontinuities, limestone/mudrock interfaces, or in mudrocks near their boundary laminae.

During a hot dry spell and when rock face temperature is at a maximum, data presented in sections 6.7 and 6.8 in respect of mudrocks suggest that stress induced axial shortening may well occur in the limestone. If the degrees of restraint are high, but making some allowance for slip and discontinuity width reduction, shortening may well be of the order of 10 to 20×10^{-5} mm/mm at the cliff surface which is the equivalent of a stress of some 5 to 10 MPa.

Thermal gradients are likely to be steep and reach an equilibrium only a short distance from the cliff face. However, close to the cliff face the effect on stress levels may be considerable, particularly on a critical shear plane where shear strength may be partly mobilized. Previous in plane displacement due to shear strength mobilization may concentrate stresses at protuberances and any dilation induced would increase block end restraint, enhancing thermally induced stresses. Local failures so induced on critical shear planes will obviously impair stability, and cause failures where the critical section is close to limiting equilibrium.

The condition is exacerbated by drying shrinkage within the mudrocks. At master discontinuities mudrocks are fractured and the lack of restraint facilitates opening when the rock face is cold and within the rock mass beyond the limit of diurnal temperature effects. Major discontinuities are opened to some extent by traction developed between shrinking mudrock and adjacent limestone. Reduction in normal stress facilitate dilations and small scale movement along the shear plane.

Investigation into temperature effects described in this section was instigated by the results of long term monitoring. However, the investigation described in section 6.8 and its consideration in context of cliff instability was motivated by field observations made

in the hot dry summer of 1983, when a high incidence of falls was noted. In a report to the Welsh Office, Grimes and Williams (1983) note :

"....Assessment of newly fallen debris indicated that the majority of these summer falls were less than 500 tonnes, but, there was one notable exception. Some 20,000 tonnes of rock toppled at a site between St. Donats and Nash (SS 92700 67000). The writer first noted this fall on the afternoon of July 2nd. It was apparent from the debris and vegetation scattered over the platform, and below the recent high tide mark, that the fall had occurred very recently....."

In section 11.2.2.3 it is demonstrated that small scale movement along the torsional shear plane of the Nash - St. Donats fall would have raised the ultimate shear stress value from the region of 0.3 MPa to 1.78 MPa. Consequently in this particular fall a small residual movement along the shear planes would have instigated instability.

10.4 Tension Crack Monitoring (SS 92990 67648)

The unstable block is located immediately to the east of a large toppling failure and is indicated on the geomorphological map 4.8(5). The fall, including the site of the unstable block is geomorphologically mapped in fig. 4.10. Discontinuity traces apparent in the platform are plotted in fig. 4.11. Plate 4.14 shows the cliff including the unstable block, and plate 4.15 the remains of well ordered toppled debris from the fall immediately west of the unstable block.

Monitoring was commenced soon after tension cracks had opened. Wooden pegs, some 300 to 400mm long, with nails hammered in to the ends to facilitate accurate measurement, were driven into the ground for their full length at the locations shown on fig. 10.4. Monthly monitoring for lateral movement and change in level was carried out. On each occasion levels were referenced to an Ordnance Bench Mark on a boundary wall (SS 92709 67110) some distance away from the unstable block.

No large vertical or horizontal movements were recorded (fig. 10.5), although there does appear to be a seasonal influence causing the small scale oscillatory movements indicated in the lateral movement against time graph (fig. 10.5). The formation of Polygonal shrinkage cracks, with crack width often as wide as 10mm, were noted in cliff top soil during prolonged hot dry periods. Much of the apparent seasonal oscillatory movement can be attributed to this swelling and shrinkage.

Annual geomorphologic surveys are presented in Fig. 10.6. In the initial survey (March 27, 1981) the major line of weakness was characterised by deep angular depressions. An open fissure (Chainage, 7.0-8.8, Fig. 10.4) was deep enough to insert 2.0m ranging rod to full height. Subsequent surveys (Fig. 10.) indicated little sign of further movement, migrant soil is filling depressions and fissures, and vegetation is re-establishing.

Photographs showing change in morphology are scheduled in Table 10.1.

Tension crack development is rare where the cliff comprises only limestone dominant strata, and in fact this is the only observed cracking during the period of this study.

It is conjectured that the block would fail by toppling; the major restraint is torsional along the discontinuity striking almost orthogonally to the cliff line. The included angle between the westerly striking cliff and the master discontinuity trace at the eastern end of the fall is 85° (fig. 4.10). Any rotational movement would increase the normal stress on the torsional shear surface thereby enhancing shear resistance.

Failures occur when peak discontinuity shear strength is exceeded. This shear strength is generally mobilised at very small displacements, and consequently, there is usually little movement prior to failure.

Upper cliff line recession is indicated in the inset of fig. 10.6. Highly frequent small magnitude falls (i.e. less than 1 tonne) are instigated by subaerial processes (section 10.2).

10.5 Summary

Although when compared with marine erosion subaerial erosion often appears irrelevant, within the design life of any cliff protection or stabilization scheme it may well prove significant and should be considered.

In this chapter the significance of subaerial processes are considered :

- 1) in context of rock mass degradation and
- 2) as instigators of instability.

Carbonate leaching facilitated by the acid product of pyrite oxidation is most active in degrading the rock fabric adjacent to continuous vertical master discontinuities which are often planes of least shear strength (section 10.2.1).

The effects of pressure release are discussed in section 10.2.2. Where the lower angulata mudrock dominant lithology is exposed basally in the cliff, failure mode suggests that the interlock is less than where limestone dominant lithology persists for the full cliff height; reduction in interlock is largely attributed to pressure release.

Climatic effects are discussed in section 10.2.3.

Temperature induced movements proved to be the most significant rock face measurements recorded over an almost two year period at Dimhole (section 10.3). Limestones expand in hot weather, mudrocks shrink and swell with variation in moisture content even when the range is

below the TRRL shrinkage limit (sections 6.7 and 6.8). Temperature and moisture induced movements, as well as loosening the rock mass, trigger falls at both the extremes of hot and cold weather.

Field evidence suggests that failures are sudden where limestone dominant lithology exists throughout the full height of the cliff. Monitoring of the only tension crack found in such lithology is recorded in section 10.4. Little further movement was recorded over the two year period and was attributed to an increase in the normal stress component of the shear strength equation induced by wedging action of the toppling block against the torsional shear surface which made an included angle of 85° with the cliff line at the rear of the fall.

Weatherability of both rock fabric and mass is greatest towards the more highly weathered cliff top and it is here that subaerial processes are most active, typically causing high frequency, low magnitude falls (section 10.2.3).

Subaerial processes are actively degrading the rock fabric and mass, thereby reducing resisting forces; while marine erosion is primarily most active in increasing disturbing forces. Both are effective in exploiting the least resistant strata and lines of greatest structural weakness.

CHAPTER 11

LIMITING EQUILIBRIUM, STABILITY ANALYSES, CLIFF PROTECTION AND STABILIZATION

11.1 Introduction

The analysis of a number of cliff falls that occurred during the course of the investigation are briefly presented in this chapter. A short discussion is also given of possible low cost stabilization and protection methods.

11.2 Assessment of Large Scale Instability

In view of the nature of the cliff falls that have occurred the writer has concentrated primarily on toppling failures within the limestone dominant lithology.

There is, however, evidence of other failure modes particularly where the mudrock dominant strata are exposed in the lower cliff. These comprise largely translatory slides and falls with some rotational slides. The analysis of these modes of failure are well documented elsewhere (e.g. Hoek and Bray 1977) and therefore are only briefly discussed in sub-section 11.2.1.

Analyses of the type of secondary toppling observed within limestone dominant lithology and involving the assessment of torsional restraint proffered by the adjacent stable rock mass is, to the writers knowledge, not documented (e.g. de Freitas and Watters(1973), Goodman and Bray (1976) and Hoek and Bray (1977) and is consequently considered in more detail.

11.2.1 Failure where Mudrock dominant lithology is exposed in the lower part of the cliff.

Lower angulata zone strata are mudrock dominant, and limestones are

frequently nodular and highly discontinuous. In section 4.3 translatory falls and slides are noted where such lithology is basally exposed.

Pressure release within the mudrock dominant strata reduces interlock in the overlying limestone dominant strata (section 10.2.2) to such an extent that the cliff is effectively a series of discrete columns.

Under the vertical load generated by these columns, shearing occurs in the mudrock dominant sub-strata and takes place along minimum energy paths. Most of these paths appear to be influenced, if not entirely controlled, by discontinuities within the mudrocks, and are usually linear or near linear planes (fig. 11.1a).

Rotational failure is described in such lithology at Trwyn-y-witch (SS 888 726) by Williams (1980). However, he does not describe or attempt to classify the slip surface trace. The influence of both lithology and discontinuities is likely to effect a deviation from the idealized typical circular trace or logarithmic spiral of purely cohesive and granular materials.

From field measurement of discontinuity directional trends, frequency and persistence, and assessment of shear strength of mudrocks, an estimate of potential instability can be made using limiting equilibrium techniques. Depending on the significance of rock mass geometry, parameters to define either intact or discontinuity shear strength, or indeed both, need to be determined.

Shear failure of the type described and shown in fig. 11.1a are not entirely confined to lower angulata mudrock dominant strata, they have also been observed between bucklandi zone horizons 21 and 28 in the vicinity of Summerhouse (SS 990 665 - section 4.3.10). In this area fig. 4.5 indicates an increase in mudrock/(mudrock + limestone) ratios. Limestones are generally more discontinuous, and mudrocks in the zones of shearing are all to some extent weakened by weathering and typically classified as slightly weathered (WII).

11.2.2 Toppling failure within limestone dominant lithology

11.2.2.1 Methodology and assumptions

Toppling failures are described and discussed in section 4.4. Marine erosion undermines the rock mass. When limiting equilibrium between resisting and disturbing forces is reached, and if a suitable fulcrum is established, which may necessitate translation (figs. 4.15 and 4.16), toppling occurs.

The three dimensional sketch (fig. 4.14) indicates how torsional restraint of an undermined part of cliff likely to topple, is provided by the adjacent relatively stable section. Any attempt to analyse the instability must include this torsional restraint and therefore analysis must take into account the complete volume of the fall and not just an idealized cross section.

The level of normal stress generated on the plane of torsional restraint cannot be directly determined. Dilation, a mechanism of shearing and a function of the discontinuity roughness, acts as a normal stress generator, as do several of the various contemporary geomorphological processes described in Chapter 10. Consequently, analysis of several falls which occurred during the course of this work, and which were documented pre and post event, cannot be confidently used to establish a rationale for assessing potential instability. Nevertheless, analyses (using limiting equilibrium techniques) of sites a, b & c listed subsequently, provides an estimate of ultimate torsional shear strength mobilised along the orthogonal/near orthogonal failure surface.

a) Toppling fall, Nash - St. Donats (SS 927 677 - fig. 4.8(5);
Analysis section 4.2.2.2 - fig. 11.2).

b) Toppling fall, Tresilian (SS 94560 67740 - fig. 4.8(7);
Analysis section 4.2.2.3 - fig. 11.3).

c) Unstable section of cliff, Nash - St. Donats (SS 92990 67648 - fig. 4.8(6); Analysis section 4.2.2.4 - fig. 11.4).

Calculations are summarised in figs. 11.2, 3 and 4, and discussed in sections 11.2.2.2, 3, 4 and 5. Analytical procedures and assumptions made were as follows :-

1) Cliff top areas lost in falls were determined from aerial photographs using the measurement technique described in section 4.2.2 and the cliff top area of the small, but potentially unstable site (SS 94560 67740) was measured in the field.

2) Field assessment photography and photogrammetry (section 4.2.2) facilitated the determination of typical cliff profiles and area proportionality factors. Area proportionality factors relate the average cross section area of cliff in the horizontal plane and for part of the vertical height to the cliff top area (e.g. fig. 11.2).

3) Area factors (a) were considered to be synonymous with average width factors, and assuming the average density of 25 kN/m^3 the resultant disturbing force and the position of its line of action was determined.

4) Assessment of the fulcrum point is subjective and a possible major source of error. Notes applicable to establishment of the estimated positions are made in each of the relevant figures (i.e. figs. 11.2, 3 and 4).

5) The horizontal distance between the resultant disturbing force and the fulcrum is the eccentricity; and it is used in the calculation of the overturning moment.

6) The interested reader is referred to Timoshenko (1956) for a detailed treatise on torsion and membrane analogy. A relevant summary, largely applicable to the determination of ultimate torsional shear stresses, is included in the following text.

i) The deflected shape of a uniformly loaded, homogeneous flexible membrane is analogous to the stress distribution across a twisted member (fig. 11.5a).

ii) The tangent to a contour line at any point of the deflected membrane gives the direction of shearing stress at the corresponding point in the cross section of the twisted member (fig. 11.5b).

iii) The membrane slope at any point is equal to the magnitude of the torsional shear stress (v_t) at the corresponding point on the cross section of the twisted member (fig. 11.5c).

iv) Twice the volume induced by membrane deflection; i.e. that between the surface of the deflected membrane and the plane of its outline is equal to the torque in the twisted member (fig. 11.5d).

v) At the ultimate value of torsional shear stress the membrane shape is defined by that of a sand heap at its natural angle of repose, and poured onto a flat plate of the same shape as that of the cross section of interest (fig. 11.5e).

In assessments of limiting equilibrium it is the ultimate value of torsional shear stress which is of interest and therefore the sand heap analogy which is applicable. As an example the ultimate value of torsional shear stress is derived for a rectangle (refer fig. 11.5f).

$$\text{Sand heap volume} = \frac{h_{\min} H}{2} (h_{\max} - \frac{h_{\min}}{3})$$

$$v_{t_{\text{ult}}} = \text{slope } \theta = \frac{2H}{h_{\min}}, \text{ and } T = \text{twice the sand heap volume}$$

$$v_{t_{\text{ult}}} = \frac{2T}{h_{\text{mm}}^2 (h_{\max} - \frac{h_{\min}}{3})} \quad (11.1)$$

where T = torque and $v_{t_{\text{ult}}}$ = ultimate torsional shear stress.

Ultimate torsional shear strength values are presented for each instability analysed.

Adopting the simplified rationale suggested in section 9.2.6, the normal stress on the torsional shear surface could be estimated from the equation given for the 99% confidence level (fig. 9.11).

In such an analysis, because both the elastic constants and the magnitude of inherent discontinuity shearing induced dilation are greater for limestone than for mudrock, it would appear a reasonable assumption that the limestone transmits all but a negligible amount of the load normal to the orthogonal discontinuity. Normal stress levels generated may also to some extent vary vertically throughout the strata, this variation is unlikely to be directly proportional to depth of overburden, but probably represents the influence of post-depositional history, pressure release and other degradation processes.

Although the interlock between limestone surfaces primarily mobilizes shear strength, the mudrocks act compositely with the limestone to form an integral member, torsional shear stresses are thus distributed throughout the integral member and not just discrete limestones. However, the torsional shear stress values presented are likely to be modified to some extent because of the anisotropic and heterogeneous nature of the composite or integral member.

11.2.2.2 Stability Analysis; Fall between Nash - St. Donats (SS 927 677)

This large fall occurred in the summer of 1983 and is described in section 4.3.5. The significance of its occurrence during hot weather is discussed in section 10.3.3. Calculations to determine the ultimate torsional shear stress along boundary discontinuities are summarised in fig. 11.2. Diagrams in fig. 11.2 indicate 7 principal torsional shear surfaces; along the back face of the fall several other small surfaces were also observed, but as the maximum width of any of these did not exceed 0.5m they were ignored.

Analysis (fig. 11.2) indicates that if the torsional shear surfaces acted integrally then at ultimate conditions the level of torsional shear stress would be much lower than if they acted discretely. It seems likely that a transition from one condition to the other could have been effected by both temperature and shrinkage induced movements. Therefore it can be concluded that the ultimate value of torsional discontinuity shear stress rose from a value of 0.27 MPa some way towards 1.78 MPa and failed. The ultimate value depends on the level of normal stress. However, because a small amount of rotational movement must have taken place for fractures such as indicated in fig. 11.2A to occur it is conjectured that the value of 0.27 MPa is close to the ultimate value.

Because of dilation, small movement along the shear plane would enhance normal stress level, but the obtuse angle formed by the torsional shear plane and back face of the fall would have a reducing effect as the magnitude of rotation movement increased.

11.2.2.3 Stability Analysis; Fall at Tresilian (SS 94560 67740)

This large fall of approximately 18,000 tonnes occurred during cold weather in the winter of 1979/1980 and is described in section 4.3.7.

A summary of calculations to determine the ultimate torsional shear stress along the torsional failure surface is presented in fig. 11.3.

Analysis suggests that, under ambient conditions, the ultimate torsional shear stress would have been low. However, the high degree of fracturing apparent on the torsional shear surface indicates otherwise. Snow fell in early January 1980 and temperatures (fig. 3.2) dropped to -8°C . Ice forming in only the upper metre of the opening, rear of fall, master discontinuities would have raised the torsional shear stress from 0.056 MPa to 0.208 MPa. Cold weather appears to have continued for the first two weeks in January and it is quite likely that in this case the estimate of ice generated overturning force is low; nevertheless the importance of extreme conditions as an instigator of instability is again demonstrated.

11.2.2.4 Stability Analysis; Unstable block, Nash - St. Donats (SS 92990 67648)

This is the site of tension crack monitoring described in section 10.4. A large scale geomorphological survey of the unstable block and adjacent fall is detailed in fig. 4.10. A summary of analysis to determine the value of torsional shear stress along the near orthogonal surface, and assuming that the value is approaching the ultimate value, is presented in fig. 11.4.

This analysis suggests a rather higher value of torsional shear stress than might be expected from the values presented in the previous two sections. However, the substantial movement occurring circa March 1981 suggests that a limiting shear strength under typical normal stress conditions had already been reached, and that the value was of the same order as that previously demonstrated. In this case the included angle formed by the master discontinuity constituting the torsional shear surface and the tension crack is less than 90°; restraint is also further enhanced by a seaward step of the cliff plan profile at the torsional shear surface. The unstable block appears to have effectively wedged against the master discontinuity after movement, thus enhancing normal stress levels and torsional shear strength.

11.2.3 Discussion

From the analyses of toppling falls presented in the preceding sections, it would appear that ultimate torsional shear stress developed along orthogonal/near orthogonal shear planes is of the order 0.2 to 0.3 MPa. The analyses of the two large falls (sections 11.2.2.2 and 3) both serve to emphasise the importance of extreme weather conditions as instigators of instability.

Cliff top tension crack development is rather unusual in cliffs consisting solely of limestone dominant lithology; the tension crack

monitored (SS 92990 67648) being the only one observed during the course of the fieldwork. Falls are usually sudden with only very little movement proving necessary to mobilize and exceed peak shearing strength along the majority of limestone fractures (section 9.2). Although analyses such as that carried out in section 11.2.2 could be readily performed to assess the likelihood of instability, the recognition of potential fall boundaries, and particularly the rear one, may prove problematic. Fig. 11.2A shows a small shear failure in the lower cliff. This type of failure has been noted at other sites, particularly between Nash and St. Donats, and also appears as though in some cases it may be a good indicator of impending toppling.

Opening discontinuities, vertical surface displacement and features in the cliff top soil indicative of soil gravitation, have been observed with sufficient frequency for the writer to postulate mechanisms presented in section 11.2.1, where mudrock dominant strata are exposed in the lower part of the higher cliffs (i.e. 30m - 50m). However, the writer must warn that he considers the evidence compiled insufficient to confidently assert that these features are apparent in all cases of impending instability. From slake durability tests (section 5.4.6) the erodibility of angulata mudrock appears low, and erosion is facilitated by contemporary weathering mechanisms (section 10.2) and by differential environmental response of the intercalated discontinuous nodular limestones. Consequently the rock mass close to the cliff edge needs to be treated with some considerable caution.

11.3 Cliff Protection and Stabilization

11.3.1 Strategy

The only cliff top structures of any importance along the coast are the Lighthouses at Nash (SS 920 680). With land use primarily agricultural, and therefore of relatively low monetary value, the primary need is for protection of the many people who use this area - which is designated a recreational facility by virtue of it being

part of the Heritage Coast. It would seem that any strategy should be twofold, incorporating :

1) Planned and regular reconnaissance to identify and monitor potential instability.

2. A cost effective work programme to stabilize and protect the cliffs, thereby minimising the risk of both low and high magnitude falls.

In realistic budget terms, any protection works where the benefit is solely for recreation must be low cost (Walters 1981). A second requirement which would be sought by any Heritage Coast Management Committee is that any revetment, stabilization or protective structure must harmonize with the environment (Howden 1980).

In both Chapter 10 and section 11.2 it has been demonstrated that both prolonged hot and cold weather can instigate falls. Providing a works programme could be commenced immediately after, it would seem that early spring is the ideal time to carry out regular reconnaissance. During the winter, usage of the facility is nominal and consequently the risk, from falls, to life and limb is minimal. Falls instigated by natural processes during cold winter periods are therefore to some extent desirable; the modified cliff profile is likely to be more stable than the original, and works that would have been otherwise necessary, avoided.

In any work of this kind, budget restrictions are likely to apply. The engineer must make an assessment of cost effectiveness which in real terms means the removal of the largest amount of risk for the smallest amount of money. In evaluating this he must be aware of the distribution of users and the extent of usage.

Optimum budget expenditure may not be readily apparent. During the period of this project, the writer became aware that increasing numbers of people were visiting less readily accessible sections of

coast, and seemingly invariably basing themselves at the foot of the cliffs, often apparently oblivious to precariously balanced weathered rock partly dislodged from the upper cliff. A programme to 'scarp' (i.e. remove loose material from) the upper cliff of such obscure areas may alleviate more risk than stabilization works to part of a cliff on a large usage beach, and particularly if that section of cliff is in a position where it can be readily isolated.

In the subsequent text, various low cost expedients are considered in context of the stabilization problems presented.

11.3.2 Protection and Underpinning

Emphatic
Grandiose schemes such as breakwaters and revetments designed to prevent waves impinging the lower part of the cliff are clearly both high cost structures and likely to run into opposition in respect of the planning ethos.

In Chapters 5 and 6, considerable variation in the competence of fresh unweathered rock classified as mudrock has been demonstrated. In Chapter 4 and again in Chapters 5 and 6, horizon 28a in particular is shown to be a marked line of weakness. In fig. 5.7, the range in slake durability of sampled mudrocks is presented. After three slaking periods in sea water, total time duration 50 minutes, less than 5% by weight of fresh unweathered mudrock 28a remained. Subjected to the same slaking regime, sample S7, also a weak mudrock exhibited the next lowest slake durability of the fresh unweathered samples (sample description : table 5.6) with a value of 57%.

Where exposed to marine erosion, cliff stability could be enhanced by providing localised protection to horizon 28a. Assuming the horizon is notched, it may well prove desirable to increase the underpinning provided by wedged cobbles; reduction of rock mass shear strength by subaerial weathering processes (described in section 10.2) is likely to result in a gradual increase in the underpinned vertical load. A readily available source of well shaped, ideally sized masonry is

provided by cliff fall material. Such a localised masonry protection to the notch has remained intact at the Nash Lighthouse site for many years (section 10.2). Serviceability is undoubtedly enhanced by compression induced in the masonry by increasing vertical load; i.e. as previously described. Additional underpinning may well be best achieved by grouting small sections of notch with a high viscosity grout. Although in the execution of such works it is unlikely that ground water seepage will be impeded, the nature of the weak mudrock 28a is such that it is desirable to facilitate any such seepage.

This method of stabilization and protection is clearly best suited to the limestone dominant strata of the bucklandi and upper angulata zone. Although described in context of the least competent lithology, horizon 28a, it could be obviously used for other lithologically weak horizons (section 4.4.1), or where marine erosion has been facilitated by low angled discontinuities within the mudrocks (section 4.4.2).

Although in section 4.4.2 it is suggested that caves quarried along near vertical/vertical discontinuities are indicative of a relatively high degree of cliff stability, it is foreseeable that in some instances it may be desirable to take action to prevent further marine erosion. This could be readily achieved by the construction of suitably designed masonry.

excellent substrate
Masonry also provides an excellent medium for protective infilling of small cavities.

11.3.3 Blasting

Williams (1980)(reviewed in section 1.4) describes how blasting at Col-Huw (SS 958 673) failed to provide a long term solution and effected the opening of very narrow spaced discontinuities at the poorly restrained west end of the cliff, which in the long term is likely to exacerbate stability problems. This does not invalidate blasting as a stabilizing technique, but it does sound a note of

caution. Careful consideration of blasting proposals in light of discontinuity geometry, lithology and variations in weathered state are essential. The engineer is reminded that the limestones (section 8.2.5) contain a well defined system of micro joints.

The blasting at Col-Huw in 1969 was carried out using bulk blasting techniques. Presplitting would appear to be a better technique, offering a high degree of control. Simultaneously fired holes emit shock waves which, when they meet within the 'shockwave web', place the web in tension facilitating rock mass shearing.

In the complex and highly variable Lower Liassic rock mass, low energy blasting (i.e. using a small amount of explosive) and closely spaced holes are likely to afford the best cliff profiling results. However it must be emphasised that careful planning of any blasting scheme is essential, not only in light of the forgone discussion, but in order to achieve the desired finished profile.

Instability where mudrock dominant strata are exposed in the lower part of the cliff has been described in section 11.2.1. Although perhaps translatory falls and slides do not present quite the same risk as toppling where debris is often spread across a much larger area of platform, risk is increased by the invariably greater height of the cliff. Blasting techniques could be readily used to remove the upper limestone dominant strata; a bench formed at the junction between these two major lithological divisions would retain any debris falling from the highly weathered upper horizon (fig. 11.1b).

11.3.4 Stability of the upper highly weathered cliff

The weathered nature and high weatherability of the upper cliff means that subaerial weathering processes are highly active in the degradation of this zone, and consequently, small magnitude falls are highly frequent (section 10.2).

Given the comments made in section 11.3.1 in respect of many users

disregard for personal safety, an annual programme of reconnaissance and 'scarping' (removal of loose material from cliff face) is, in the writers opinion, desirable. Although, where access would permit, much of the potentially hazardous, tenuously supported material would be within the reach of an extended arm, wheel based excavator (such as a JCB 3CX), the operator would be unsighted and therefore the operation too risky.

In some areas it may be possible for skilled climbers to abseil from the cliff and remove isolated loose blocks. Although a possible expedient, it has obvious dangers and would only be economically expedient for a localized area.

Competent intact limestone strata such as horizons 49, 55, 58, 60 and 61 are often close to the top of a cliff. Blasting to profile the upper weathered cliff, terminating at a suitably competent, intact upper cliff limestone with a bench, may well prove an effective expedient for several years.

In section 10.2.5 mention was made of possible upper cliff stabilization by the root system of Hippophae Rhamnoides (a buckthorn). Growth of this plant is often prolific and therefore difficult to control, and although its root system generally appeared to enhance stability, it is foreseeable that under some local conditions the reverse may be true. However, the use of a suitable geofabric on a profiled upper cliff slope and the adjacent cliff top would have all the advantages of a stabilizing root system, and none of the disadvantages, although there would be an initial cost implication.

11.4 Summary

In section 11.2, assessment of large scale instability has been examined. The writer considers the stability of cliffs where mudrock dominant lithology is exposed in the lower cliff in section 11.2.1, but because analyses of translatory slides and falls are well documented in literature, it is only briefly described.

Torsional restraint proffered by the adjacent stable rock mass is significant in the toppling failures occurring within limestone dominant lithology. Examples of instability are analysed in sections 11.2.2.2, 3 and 4, and the value of ultimate torsional shear stress developed along the shear plane assessed, and typically found to be in the region 0.2 MPa - 0.3 MPa.

Analyses presented in figs. 11.2. and 3 serve to emphasise the highly significant role played by extreme climatic conditions as instigators of instability.

A section on cliff protection and stabilization (section 11.3) relevant to these Lower Lias cliffs is included. It is intended that this should provide both interested authorities and practising engineers with some guidance in exercising their responsibility to maintain this section of coastline. Various methods of low cost protection and stabilization are also considered, - the most viable and cost effective of these are, in the writers opinion :

- 1) Masonry infill and dispersed grout support as necessary to lines of lithological and structural weakness.
- 2) Presplit blasting to enhance the stability of the higher cliff where mudrock dominant strata is exposed in the lower cliff (fig. 11.1b).
- 3) Presplit blasting to remove unstable sections of cliff which cannot be readily supported as in (1) above.
- 4) Presplit blasting to enhance stability of the upper cliff.

CHAPTER 12

CONCLUSIONS

12.1 Scenario

Although primarily addressing the subject of cliff instability the writer has resisted the temptation to undertake any stability analyses more sophisticated than approximations employing limiting equilibrium techniques. More sophisticated numerical modelling would be limited by :

- 1) Inaccuracies and uncertainties in representing physical boundaries and rock mass geometry.
- 2) The accuracy with which the various parameters, and in particular discontinuity shear strength, can be assessed.

A first impression of the regular and somewhat monotonous banding of the rapidly alternating limestone/mudrock Lower Lias lithology might be that there is very little variation in the mineralogy and engineering properties of the various mudrock and limestone units. In fact there is appreciable variation. With this complication and the added complexities of well defined systems of macro, meso and micro scale discontinuities, varied weathered states and the harsh coastal environment, the writers endeavour has been principally towards :

- 1) Defining the problem of instability relevant to the field area.
- 2) Identifying modes and mechanisms of instability.
- 3) Establishing the mechanical properties and physical/physico-chemical response of both hard and soft rocks, together with the effects of the imposed environment.

4) Identifying potential instability and providing guidance to the Engineer/Engineering Geologist who is having to implement a low cost stabilization/protection scheme.

12.2 Final Summary

The thesis records an investigation into the engineering geology and instability of some 16km of rapidly alternating limestone and mudrock sea cliffs, of Lower Lias age. The cliffs are located on the north Bristol Channel Coast of Glamorgan. This coastal section has recently been designated a Heritage Coast, the inherently unstable cliff and increased recreational usage has generated concern for public safety and provided the impetus for this research.

In the introductory chapters, available literature addressing the geomorphology and geology are reviewed. In Chapter 2 sections on depositional and post depositional history and tectonic structure are included; the former providing a valuable insight to the sequence of events which modified and altered the rock mass and its state of stress to that currently existing, and the latter an insight to the rock mass geometry. The most significant contributions on the stratigraphy of the area are those of Trueman (1920, 1922a and 1930).

Trueman (1930), in mapping Nash Point, noted the lateral consistency of strata, and it is the numbering system he introduced which has been used to reference the bucklandi strata in this work.

The morphogenic environment is considered in Chapter 3, climatic data for the period 1980-1983 inclusive is presented together with additional wind data for the period 1977 to 1980. Chemical analyses of sampled stream water and ground water showed that the carbonate phase controlled equilibrium, and rainwater analyses showed that most rainfall was slightly acid, with acidity increasing following dry weather. Although the marine environment has been described largely from a review of literature, tidal hydrographs prepared from field measurements are presented. These, together with topographical data presented in Chapter 4, facilitate assessment of exposure to marine attack.

During a severe storm on the 13/14th December 1981 a surge of 1.5m was recorded. Although the storm was severe enough to cause structural damage to property and uproot trees, little effect on the cliff line was observed.

In Chapter 4 the geomorphology of the coastal area with particular emphasis on features relevant to cliff instability is presented in ten 1:2500 scale geomorphological maps and complimentary text. Both toppling and translatory mode rock falls are identified as are the mechanisms of failure, i.e. discontinuity shearing, shear fracturing and dilation.

Where exposed, horizon 28a was seen to be a particularly incompetent mudrock forming a marked line of weakness even where elevated above the level of marine attack. Apart from exploiting the least competent lithologies, marine attack was observed to exploit sub-horizontal discontinuities within the mudrocks and sub-vertical major and master discontinuities, the latter resulting in cave formation at locations where only the more competent mudrocks were exposed to marine erosion.

Twenty surveyed profiles across the wave cut platform and thirty-three stereonets recording discontinuity directional data along the field area are presented. Six plotted stratigraphical sections show that the mudrock/(mudrock + limestone) ratio decreases from the west towards Tresilian (SS 946 677) and then increases towards the east (i.e. towards Summerhouse SS 993 654).

Survey methods used in field work are also described. One of these which did much to facilitate the work, a photogrammetric technique employing a 35mm camera was evaluated prior to use and found accurate to $\pm 3\%$. Various film types were used for field photography. In this work no advantage was gained by using infrared or ektachrome near-infrared, the best results invariably being achieved with Kodachrome 64 ASA film.

In Chapter 5 a programme of work to evaluate the engineering properties and investigate physical/physico-chemical behaviour of some 27 mudrocks is recorded. Thermal gravimetry was used to quantify the major mineralogical phases. The following engineering index tests were carried out; dry density, atterberg limits, linear shrinkage, absorption tests, equilibrium moisture content, slake durability test and NCB indenter tests. The latter was used to assess uniaxial compressive strength variation with moisture content.

Recorded average uniaxial compressive strengths ranged between less than 5 MPa and 64 MPa. Equilibrium moisture content, effectively a measure of the hygroscopic properties of the mudrock, appeared to be a good measure of the weathered state where effected by pyrite decomposition.

Comparing fresh unweathered mudrocks, slake durability index values for horizon 28a (maximum 12%) were typically at least 50% higher. Based on the work recorded in this chapter, a classification to facilitate assessment of mudrock performance in a marine environment is presented.

Thermal gravimetry showed that iron sulphides present in mudrocks varied in stability, this was largely attributed to the environmental conditions which existed at the time of formation. It was noted and subsequently demonstrated in Chapter 7 that the weatherability of mudrock was much greater in mudrocks where low stability iron sulphides were identified.

More detailed analyses of fabric, texture, mineralogy and physical/physico-chemical behaviours of mudrocks is recorded in Chapter 6. Three mudrocks were selected for these investigations and included highly competent (43a) and incompetent (28a) unweathered mudrocks, in addition to a highly weathered mudrock (38a). The clay content of horizon 28a proved to be highest, with an illite content of 27.7% and a smectite content of 11.7%, the latter present only as

a component of a smectite/illite interstratified mixture. Although the illite/smectite content of the highly weathered sample was only 8.4/4.4% the activity was found to be much greater. This was attributed largely to a rehydration of the clay mineral phase and appeared to be instigated by acid weathering, the result of pyrite oxidation.

Shrinkage movement at moisture contents lower than the T.R.R.L. shrinkage limit were demonstrated in all but the most competent mudrocks. Such shrinkage is indicative that clay is not fully restrained by the cementitious phase. It would appear that full restraint of the clay phase is achieved when the carbonate content rises to 55%. Results for uniaxial and triaxial compression tests on a slightly weathered fissile mudrock are reported. Loading was applied perpendicular to laminae, the resulting shear strength envelope was linear and a ϕ value of 30° and shear strength axis intercept value of 9 MPa recorded. The results of tests carried out on the same mudrock to determine deformation anisotropy under uniaxial compression are also reported. Loaded parallel to laminae the circumferential strain anisotropy ratio ranged between 7 and 38, while the axial strain anisotropy ratio ranged between 2.4 and 7.5.

Mudrocks are more ductile than the limestone and reduced vertical fracture density in mudrocks can act as an impermeable boundary to vadose water, the water, either finding egress via the cliff face or one of the major/master discontinuities passing through the mudrock, seeps along a system of horizontal/sub-horizontal discontinuities within the mudrock. A laboratory experiment to compare the leaching of a competent and incompetent mudrock under conditions simulating those in the field, is described in Chapter 7. Specimens from samples S11 and S24, the incompetent mudrock (28a) and competent mudrock (43a) were both leached. The less stable pyrite in the more competent mudrock oxidised more readily and leaching of that specimen was much greater than the less competent mudrock. This conclusion is an important one, the 1949 Coastal Protection Act makes provision for grant aid only in cases where the sea is the instigator of

instability. Field evidence indicates horizon 28a to be a line of weakness regardless of elevation in the cliff. The findings of this experiment demonstrate that chemical decomposition is of less significance than in more durable mudrock and that, therefore, weakness is inherent in its mineralogical composition only.

A programme of work to investigate the fabric mineralogical composition strength and deformation characteristics of the limestones is described in Chapter 8. Limestones were sampled on a morphological basis. Meso and Micro examination showed that :

1) Many of the sampled limestones exhibited concretionary type structure.

2) The limestone was mainly comprised of micrite, although neomorphism had taken place at sites of bioclast and that micro and meso scale joints were most frequently infilled with ferroan dolomite.

3) That the limestone contained well defined meso and micro discontinuity trends.

An extensive programme of triaxial and uniaxial compression and Brazilian testing is reported. AX sized specimens were cored along a maximum of 3 known directions from eleven samples and Hoek & Brown's (1980) empirical criterion was used to characterise rock strength.

No macro scale strength anistropy could be inferred from the results which reflected the orientation of meso and micro discontinuities within the specimens. Excluding sample L2, a low carbonate content limestone nodule, the average intact uniaxial compressive strength was 234 MPa. Meso scale discontinuities and other flaws are recorded for each specimen as are failure modes. Triaxial specimens typically exhibited shear type failure while uniaxial specimens showed a mixed failure mode.

Well developed chevron patterns on fracture surfaces of Brazilian specimens indicated that chevrons were a feature of tensile mode type fracturing. Similar structures were frequently noted on north/south striking discontinuity surfaces in the field implying a similar mode of fracture.

A number of specimens were strain gauged and tested in uniaxial compression. Stress/deformation plots were generally found to be consistent with the stages recognised by Bieniawski (1966).

- 1) Crack closure during initial loading.
- 2) Unloading part of a hysteresis being representative of uncracked rock material elasticity.
- 3) Stable crack propagation - continuing to yield point.
- 4) Unstable fracture propagation following yield and prior to rupture.

Elastic moduli for the intact limestone with the exception of sample L2, a calcareous nodule, ranged between 56 and 68 MPa, while Poisson's ratio for all specimens ranged between 0.21 and 0.28.

In Chapter 9 an investigation into discontinuity shear strength is described. Cores (NX sized) were fractured using wedge type platens in the point load test apparatus. The resulting rough joints, fractured in the same mode as many of the major discontinuities within the field area, were shear tested at a variety of different stress levels. Unsuccessful attempts were made to fit Bartons (1973) equation to the results. Surface profiles were also digitised and the surface roughness classified by comparing roughness parameters with those derived from the standard profiles proposed by Barton & Choubey (1977).

A plot of normal stress against shear strength produced a curvilinear relationship. A regression analyses of all values gave the equation

$$\tau = 1.638 f_n^{0.607} \quad (r^2 = 0.944) \quad (12.1)$$

where τ = shear strength
 f_n = normal stress

The results suggest that roughness and inclination of shear plane made little difference to shear strength once a certain threshold roughness had been exceeded. Although unexpected and to some extent attributed to the influence of well defined meso and micro discontinuity trends, the results do cast some doubt on the validity of the criterion proposed by Barton (op. cit.)

Open discontinuities particularly in the upper cliff are frequently infilled with residual soil material. Barton (1974) notes that as these discontinuities become more open, their shear strength reduces to that of the infilling material. Drained shear box tests on sampled typical material gave a ϕ'_d value of 31°. Results of direct shear strength tests on laminated mudrocks carried out both perpendicular and parallel to the laminae are also reported.

Shear strength within the fractured rock mass is largely contributed to by the rough limestone discontinuities. In a lower bound approximation of strength the contribution of the mudrocks could be ignored. Rock mass failure surfaces follow minimum energy paths, which although defined by two variables, i.e. disturbing and resisting forces, are usually along surfaces where shear strength is close to the minimum. Consequently it is postulated that the 99% lower confidence level for limestone discontinuity shear strength (given below) could be reasonably adopted in lower bound assessment of discontinuity shear strength.

$$\tau = 0.686 f_n^{0.704} \quad (12.2)$$

In Chapter 10 the significance of subaerial processes are discussed. Carbonate leaching facilitated by the acid product of pyrite oxidation is active in degrading the rock fabric adjacent to discontinuities resulting in reduced discontinuity shear strength. Pressure release is most significant in higher cliffs where angulata mudrock dominant lithology is exposed basally.

Climatic effects are discussed, monitoring laboratory tests and field observations demonstrated that rock falls are most likely to occur during prolonged hot or cold spells.

Weatherability of the more highly weathered upper cliff rock fabric and mass is generally greatest, and this results in high frequency, low magnitude falls.

Monitoring of the only open tension crack found where limestone dominant lithology exists throughout the full height of the cliff is also recorded in this chapter. No significant movement was recorded in the two year monitoring period. This was attributed to the attitude of the torsional shear surface and consequent wedging action.

It was concluded that subaerial processes are actively degrading the rock fabric and mass, thereby reducing resisting forces, while marine erosion is primarily most active in increasing disturbing forces. Both are effective in exploiting the least resistant strata and lines of greatest structural weakness.

In Chapter 11 the writer, using limiting equilibrium techniques, analyses examples of toppling mode instability. The significance of torsional restraint proffered by the adjacent stable rock mass is demonstrated by these analyses, which showed that the ultimate torsional shear stress developed was in the region of 0.2 MPa to 0.3 MPa. In two of the three analysed examples, toppling had actually occurred, one during the extreme cold weather the other during a prolonged hot spell. The analyses served to emphasise the significance of extreme weather conditions as instigators of instability.

The extensive contemporary wave cut platform bears witness to the effectiveness of wave energy along this section of coast. In such a high energy marine environment it would be presumptuous to assume that cliff recession could be cost effectively permanently halted. Nevertheless the effectiveness of low cost stabilization and protection works is demonstrated by those constructed some 100 years ago under Nash Lighthouse. In the second part of Chapter 11 low cost stabilization and protection expedients are considered. As well as emphasising the need for regular inspection and work programmes, the writer indicated that he considered the most viable and cost effective solutions to be :

- 1) Masonry infill and dispersed grout support as necessary to lines of lithological and structural weakness.
- 2) Presplit blasting to enhance the stability of the higher cliff where mudrock dominant strata is exposed in the lower cliff.
- 3) Presplit blasting to remove unstable sections of cliff which cannot be readily supported as in (1) above.
- 4) Presplit blasting to enhance stability of the upper cliff.

12.3 Future Work

Recorded data appertaining to the mineralogy, strength, mechanical properties and physical/physico-chemical behaviour of both Lower Lias mudrock and limestone is seen as a valuable source in its own right, and should prove useful in any correlation of the mineralogical properties and performance of mudrock and limestone. The empirical fractured rock strength criterion of Hoek and Brown (1980) proved to be a good representation of Lower Lias limestone strength. The results recorded in this thesis should provide a valuable data set to anyone wishing to assess rock strength data and the range of applicability of Hoek & Brown's (op. cit.) criterion.

The rather unexpected discontinuity shear strength results indicate a real need for further investigation and indeed suggest that a different approach to that of Barton & Choubey (1977) is required. The writer is of the opinion that his work demonstrates that discontinuity shear strength testing should be performed

- 1) Using natural rock material specimens.
- 2) At a range of stress levels representative of those in the field.

Limiting equilibrium analyses (Chapter 11) demonstrates the significance of torsional restraint proffered to the toppling block by the adjacent rock mass. Problems in undertaking more sophisticated analysis are indicated in the opening section of this chapter. Nevertheless such analysis, which would need to employ a three dimensional model, could prove most useful in the assessment of instability and provide valuable information about the shear strength mobilized along torsional shear planes.

Any management strategy for maintaining the stability of the cliffs would benefit from a 'risk map' which would highlight areas of potential instability.

The monitoring of any cliff stabilizing/protection works would prove valuable in optimising appropriate solutions.

To the writers knowledge very little work has been done to quantitatively assess shear pressures which might be generated in marine notches by wave slamming forces. An investigation to assess the likely magnitude of such pressures is prerequisite to any numerical analyses of sea cliff stability, which aims to take into account all pertinent variables.

REFERENCES

- Ager, D.V. (1974) The Jurassic period in Wales In: The upper Palaeozoic and post Palaeozoic rocks of Wales. (Ed. Owen, T.R.) University of Wales Press, Cardiff. pp. 323-340.
- Anders, F.J. & Leatherman, S.P. (1982) Mapping techniques and historical shoreline analysis Nauset Spit Massachusetts. In Geotechnology in Massachusetts (Ed. Farquhar, O.C. pp. 501-509)
- Anon (1973) Shore protection manual - Glossary of terms. Vol.III, U.S.Army Coastal Engineering Research Centre.
- Anon (1977) N.C.B. Cone indentor. N.C.B. M.R.D.E. handbook No.5.
- Anon (1976) Corning 400 Flame Photometer handbook.
- Anon (1979) Analytical methods for flame spectroscopy. Varian, Springfield, Australia. Revised edition pub. 85 - 100009-00
- Arkell, W.J. (1933) Jurassic systems in Great Britain. Oxford Univ. Press, London. p.125.
- Atkinson T.A., Cassap, V.B. (1983) The Preparation of Laboratory cored specimens from friable rock. The Mining Engineer, April pp. 541-547.
- Attewell, P.B. & Taylor, R.K. (1971) Investigations, tests and experiments on the mechanical strength and breakdown characteristics of certain overconsolidated clay shales. Interim and final reports on DA-ERO-591-70-G0002, Euro. Research Office, U.S.Army.
- Attewell, P.B. & Farmer, I.W. (1976) Principles of engineering geology. Chapman and Hall, London.
- Bagnold R.A. (1939) Interim report on wave-pressure research. J. Inst. C.E. Vol.12, No.7, pp. 202-226.
- Bandis, S., Lumsden, A.C. & Barton, N.R. (1981) Experimental studies of scale effects on the shear behaviour of rock joints. R. Mech., Min. Sci. & Geomech. Abstr. Vol. 18, pp. 1-21.
- Barton, N. (1974) A review of the shear strength of filled discontinuities in rock. Norwegian Geotech. Inst. pub. No. 105, 38p.
- Barton, N.R. (1971) A relationship between joint roughness and joint shear strength, Proc. Int. Symp. on Rock Fracture, I.S.R.M., Nancy. Paper 1-8.
- Barton, N.R. (1973) Review of a new shear strength criterion for rock joints, Engineering Geology, Vol.7 pp. 287-332.

- Barton, N.R. (1976) The shear strength of rock and rock joints, Int. J. Rock Mech., Min. Sci. & Geomech. Abst., Vol. 13, pp.255-279.
- Barton, N. & Choubey, V. (1977) The shear strength of rock joints in Theory & Practice. Rock Mechanics. Vol. 10, pp. 1-54.
- Bieniawski, Z.T. (1966) Mechanism of rock fracture in compression. CSIR report MEG 459, Pretoria, South Africa.
- Bowen, D.Q. (1970) South-east & Central South Wales. In: The Glaciations of Wales & adjoining regions. (Ed. Lewis, C.A.) Longmans, London. pp. 197-227.
- Bowen, D.Q. (1974) The quaternary of Wales In: The upper palaeozoic and post Palaeozoic rocks of Wales. (Ed. Owen, T.R.) University of Wales press, Cardiff pp. 373-426.
- Brindley, G.W. (1980) Quantitative X-Ray Mineral analysis of clays. In: Crystal structures of clay minerals and their x-ray identification. (Ed. Brindley, G.W. & Brown, G.) Mineralogical Society, London.
- British Standards Institution. (1975) Methods of testing for soils for Civil Engineering purposes. B.S.1377. London.
- British Standard Institution. (1982) Introduction to surface texture. BSI Education section, P.D. 706, London.
- Broch, E. & Franklin, A. (1972) The point-load strength test, Int. J. Rock Mech. Min. Sci. Vol.9 pp. 669-697.
- Bromhead, E.N. (1978) Large landslides in London Clay at Herne Bay, Kent. Q.J. Eng. Geol. Vol. 11, No. 4, pp. 291-304.
- Bromhead, E.N. (1979) Factors affecting the transition between the various types of mass movement in coastal cliffs consisting largely of overconsolidated clay with special reference to Southern England. Q.J. Eng. Geol. Vol. 12, No. 4, pp. 291-300.
- Brownlow, A.H. (1979) Geochemistry Prentice Hall Inc., Englewood Cliffs, New Jersey.
- Bullock, P. & Loveland, P.J. (1974) Mineralogical analyses. In: Soil survey laboratory methods. (Ed. Avery, B.W. & Bascomb, C.L.) Soil Technical Monograph No. 6, pp. 57-69.
- Burnett, A.D. and Epps, R.J. (1979) The engineering geological description of carbonate suite rocks and soils. Ground Engineering No. 2 pp. 41-48.
- Caldwell, N.E. (1983) The morphological sedimentary and hydraulic properties of two coarse clastic (pebble) beaches along the Heritage Coast of Glamorgan, Wales. PhD. Thesis, C.N.A.A., Polytechnic of Wales, 2 Vols.

- Carr, A.P. & Graft, J. (1982) The tidal immersion factor and shore platform development : discussion. *Trans. Inst. Br. Geogr.* N.S. 7 pp. 240-245.
- Church P. (1983) Digestion of River Taff sediments for elemental analysis of heavy metals. *Pers. Comm. Dept. of Science, Polytechnic of Wales.*
- Clayton, C.R.I., Simons, N.E. and Matthews, M.C. (1982) *Site Investigation, a handbook for Engineers.* Granada, London.
- Colback, P.S.B. & Wild, B.L. (1965) The influence of moisture content on the compressive strength of rocks. *Proc. of the symp. Rock Mech., Toronto.* pp. 65-83.
- Collins, B.J., Madge, B. & Evans, G.J. (1985) Development and application of the 'photo-radiation method of terrestrial photogrammetry.' *Proc. of Vith Int. Cong. of the Int. Soc. for Min. Surveying, Harrogate.*
- Collins, K. & McGowan, A. (1974) The form and function of microfabric features in a variety of natural soils. *Geotechnique.* Vol. 24, No. 2, pp. 223-254.
- Cope, J.C.W. (1971) Mesozoic rocks of the Southern part of the Vale of Glamorgan. In: *Geological Excursions in South Wales* (Ed. Basset, D.A. & Basset, M.G.) *Geologist Assoc., South Wales Group* pp.114-123.
- Culver, S.J. (1976) A study of post glacial foraminifera of Swansea Bay, South Wales. *Ph.D. thesis, Univ. of Wales.*
- Crampton, C.B. (1966) Certain effects of glacial events in the Vale of Glamorgan, South Wales. *J. Glaciol.* Vol.6, pp. 261-267.
- Curtis, C.D. (1976) Stability of minerals in surface weathering reactions : a general thermochemical approach. *Earth Surface processess* Vol.1, pp. 63-70.
- Davis, W. (1977) Crenulated Cleavage. (EU 13) In: *Atlas of rock cleavage.* (Ed. Bayly, B.M., Borradaile, G.J. & McApowell, C.) *University of Tasmania.*
- de Freitas, M.H. (1981) Introduction: Conf. on Mudrocks of the U.K. *Q.J. Eng. Geol.* Vol. 14, No. 4, pp.241-242.
- de Freitas, M.H. and Watters, R.J. (1973) Some field examples of toppling failure. *Geotechnique* 23, No.4. pp. 495-514.
- de La Beche, H.T. (1846) On the formation of the rocks of South Wales and South Western England. *Mem. Geo. Survey, I.* 269p.
- Dean, R.G. & Harlem, D.R.F. (1966) Interaction of structures and waves in Estuary & Coastline Hydrodynamics, (Ed. Ippen, A.T.) *McGraw Hill, New York,* pp.341-401.

- Dearman, W.R. (1974a) The characterisation of rock for civil engineering practice in Britain. Centenaire de la societe Geologique de Belgique, Colloque Geologie de L'ingenieur, Liege, pp.1-75.
- Dearman, W.R. (1974b) Weathering classification in the characterisation of rock for engineering purposes in British Practice. Engineering Geology Vol. 9, pp.33-42.
- Dearman, W.R. (1984) State of weathering : The search for a rational approach. 20th Reg. Conf. of Geol. Soc. Eng. Group. University of Surrey. pp. 132-142.
- Denness, B. (1972) A revised method of contouring stereograms using variable curvilinear cells. Geol. Mag. Vol. 109, pp. 157-163.
- Denny (1951) Further experiments on wave pressures, J. Inst. C.E. Vol.35, No.4, pp.330-345.
- Dickson, J.A.D. (1965) A modified staining technique for carbonates in thin section. Nature. No. 4971, Feb. 6th, p.687.
- Donovan, D.T., Lloyd, A.J. & Stride, A.H. (1971) Geology of the Bristol Channel. Proc. Geol. Soc. 1664 pp.294-295.
- Driscoll, E.M. (1958) The denudation Chronology of the Vale of Glamorgan. Trans. Inst. of Brit. Geog. Vol. 25, pp.45-57.
- Drury, G.H. (1976) The face of the Earth. 4th Ed. Penguin, England.
- Dunham, R.J. (1962) Classification of Carbonate rocks according to depositional texture. In: Classification of Carbonate rocks. (Ed. Ham, W.E.) Am. Ass. Pet. Geol., Mem.1, pp. 108-121.
- Fairhurst, C. (1964) On the validity of Brazilian test from brittle materials, Int. J. Rock Mech. Min. Sci., Vol.1, pp. 535-546.
- Fecker, E. & Rengers, N. (1971) Measurement of large scale roughness of rock planes by means of profilograph & geological compass, Proc. Symp. on rock fracture, I.S.R.M., Nancy, paper 1-18.
- Ferentinos, G. (1978) Ph.D. Thesis, University of Wales. Hydrodynamic and sedimentation process in Swansea Bay and along the central northern Bristol Channel coastline.
- Folk, R.L. (1959) Practical petrographic classification of limestones. Bull. of the Am. Assoc. of Pet. Geol., Vol. 43. No.1 pp. 1-38.
- Folk, R.L. (1962) Spectral subdivision of limestone types. In: classification of carbonate rocks. (Ed. Ham, W.E.,) Am. Assoc. Pet. Geol., Mem. 1. pp. 62-85.

- Folk, R.L. (1974) Petrology of Sedimentary rocks. Hemphill Pub. Co. Austin, Texas 78703
- Fookes, P.G., Dearman, W.R. & Franklin, J.A. (1971) Some engineering aspects of rock weathering with field examples from Dartmoor and elsewhere. pp.139-185.
- Fookes, P.G. & Denness, B. (1969) Observational studies on fissure patterns in cretaceous sediments of South-East England. Geotechnique Vol.12 No.4, pp. 453-477.
- Fookes, P.G. and Higginbottom, I.E. (1975) The classification and description of near shore carbonate sediment for engineering purposes. Geotechnique Vol.25 No.2 pp. 406-411.
- Franklin, J.A. & Chandra, R. (1971) The slate-durability test. Int. J. Rock Mech. Min. Sci. Vol. 9, pp.325-341.
- Friedman, G.M. (1970) Staining. In: Procedures in Sedimentary Petrology. (Ed. Carver, R.E.) John Wiley, New York. pp.511-530.
- Fritz, J.S. & Yamamura, S.S. (1955) Rapid microtitration of sulphate. Analytical Chemistry Vol.29, No.9.
- Gamble, J.C. (1971) Durability - plasticity classification of shales and other argillaceous rocks. PhD. Thesis. University of Illinois.
- Garrels, R.M. & Christ, C.L. (1965) Solutions, Minerals & Equilibria, Harper & Row Inc., New York.
- Geological Soc. Eng. Group Working Party Report. (1972) Engineering Geology Mapping. Q.J. Eng. Geol. Vol.5, pp.295-382.
- Geological Soc. Eng. Group Working Party Report. (1977) The description of rock masses for engineering purposes. Eng. Geology. Q.J. Eng. Geology, Vol.10, pp.355-388.
- George, T.N. (1974) The Cenozoic evolution of Wales In: The upper Palaeozoic and post Palaeozoic rocks of Wales. (Ed. Owen, T.R.) University of Wales Press, Cardiff. pp. 323-340.
- Gibson, R.E. & Henkel, D.J. (1954) Influence of duration of tests at constant rate of strain on measured drained strength Geotechnique Vol.4 pp. 6-15.
- Gillott, J.E. (1968) Clay in Engineering Geology. Elsevier pub. Co. Amsterdam.
- Goldstein, M., Goosev, B., Pyrogovsky, N. Tulinov. K. & Turovskaya, A. (1966) Investigation of mechanical properties of cracked rock, Proc. of the 1st Int. Congr., I.S.R.M., Lisbon paper 3-49.
- Goodman, R.E. and Bray, J.W. (1976) Toppling of rock slopes; ACSE conference on Rock Engineering for Foundations and Slopes. Boulder Colorado University. Vol.2 pp. 201-234.

- Goodwin, H. & Willis, E.H. (1964) Cambridge University natural radiocarbon measurements III. Radio carbon. Vol.3, p.60.
- Goskar, K.L. & Trueman, A.E. (1934) The coastal plateaux of South Wales. Geological Magazine. Vol. 71, pp. 468-477.
- Griffin, G.M. (1971) Interpretation of X-Ray diffraction data. In: Procedures in Sedimentary Petrology. (Ed. Carver, R.E.) John Wiley, New York. pp. 541-570.
- Griffith, A.A. (1921) The phenomena of rupture and flow in solids. Phil. Transc., Royal Soc. London. Series A Vol. 221, pp.163-198
- Griffith, A.A. (1924) Theory of rupture. Proc. Int. Congress. Appl. Mech., Delft, pp. 55-63.
- Griffiths, J.C. (1940) the glacial deposits west of the Taff PhD thesis Univ. of London.
- Grim, R.E., Bray, R.H. and Bradley, W.F. (1937) The mica in argillaceous sediments. A.M.Mineralogist. Vol. 22, pp.813-829.
- Grim, R.E. (1968) Clay Minerology. 2nd Ed., McGraw-Hill, New York.
- Grimes, J.N. (1980) The appraisal of a photogrammetrical technique using 35mm photography, its accuracy and application to a cliff stability investigation. Internal report. Polytechnic of Wales. 16p.
- Grimes, J.N. (1984) Proposed Coastal Protection Foreness Point - Friends Gap, Margate. Unpublished preliminary report to the Nature Conservancy Council. 13p.
- Grimes, J.N. & Williams, A.T. (1984) Cliff instability in rapidly alternating limestones and shales of the Glamorgan Sea Cliffs. Interim report No. 4. 45p.
- Haas, C.J. (1983) Proposed new standard test method for dimensional and shape tolerances of rock core specimens. Geotechnical testing JL. GTJODJ, Vol. 6, No. 4, pp.226-229.
- Hallam, A. (1957) Primary origin of the limestone shale rhythm in the British Lower Lias. Geol. Mag., Vol. 94, pp. 175-176.
- Hallam, A. (1960) A sedimentary and faunal study of the Blue Lias of Dorset & Glamorgan. Phil. Transc. R. Soc. Series B. Vol.243, No.698 pp. 1-44.
- Hallam, A. (1964) Origin of the limestone-shale rhythm in the Blue Lias of England: A composite theory. Jl. of Geology. Vol.72, pp. 157-169.

- Hamrol, A. (1961) A quantitative classification of the weathering and weatherability of rocks. Proc. 5th Int. Conf. Soil Mechanics & Fdn. Eng. Vol. 2, paper 7-3, pp.772-774.
- Hawkes, I. & Mellor, M. (1970) Uniaxial testing in rock mechanics laboratories. Eng. Geol., Vol. 4, pp. 177-285.
- Hawkins, A.B. & Pinches, G. (1984) Timing and correct chemical testing of soils/weak rocks 20th Regional Conf. Eng. Grp. of the Geol. Soc. Uni. of Surrey. pp.265-273.
- Head, K.H. (1980) Manual of soil laboratory testing. Vol.1 Pentech Press, Plymouth. 339p.
- Head, K.H. (1982) Manual of soil laboratory testing. Vol.2, Pentech press, Plymouth. 743p.
- Heathershaw, A.D., Carr, A.P. & King, H.L. (1980) Swansea Bay (sker) Project Topic report No.5, Wave data : Observed and computed wave climates. Inst. Oceanographic Sci. Report 99/80, 72p, Upbl. ms.
- Hobbs, D.W. (1964) The dependance of rock compressive strength on cylinder length, and three simple methods for assessing rock compressive strength. Colliery Eng. pp.287-292.
- Hoek, E. & Bray, J.W. (1977) Rock Slope Engineering, revised 2nd Ed., The Inst. of Min. & Met., London.
- Hoek, E. & Brown, E.T. (1980) Underground excavations in rock. Inst. Min. & Met., 525p.
- Hoek, E. & Franklin, J.A. (1968) A simple triaxial cell for field and laboratory testing of rock. Trans. Inst. Min. Metall., London. Section A Vol. 77. pp. 22-26.
- Holmes, A. (1965) Principles of physical geology. 835 p.
- Howden, J. (1980) Environmentally acceptable engineering work along the Glamorgan Heritage Coast. Pers. Comm. The G.H.C. Management Committee, Cardiff.
- Hudson, J.A. (1969) Tensile strength and the ring test. Int. J.R. Mech. Min. Sci., Vol. 6 pp. 91-97.
- Hutchinson, J.N. (1965b) The stability of cliffs composed of soft rocks with particular reference to the coast of S.E. England. Ph. Thesis, Univ. of Cambridge.
- Hutchinson, J.N. (1965b) A reconnaissance of coastal landslides in the Isle of Wight Building Res. Sta. Note EN 11/65.
- Hutchinson, J.N. (1965c) A survey of coastal landslides of Kent Building Res. Sta. Note EN 35/65.

- Hutchinson, J.N. (1970) Field and laboratory studies of a fall in upper Chalk cliffs at Joss Bay, Isle of Thanet. Proc. Roscoe Mem. Symp. Cambridge, pp.692-705.
- Hydraulics Research Station (1979) The Severn Estuary wave climate study. Report No. EX.887.
- Hydraulics Research Station (1980a) The Severn Estuary wave climate study. Report No. EX.914.
- Hydraulics Research Station (1980b) The Severn Estuary wave climate study. Report No. EX.933.
- Hydraulics Research Station (1981) The Severn Estuary wave climate study. Report No. EX.944.
- Ingram, R.L. (1953) Fissility of Mudrocks. Bulletin of the Geol. Soc. of America. Vol. 64, pp. 869-878.
- International Society for Rock Mechanics. (1978a) Suggested methods for determining the strength of rock materials in triaxial compression. Int. Jl. of R. M. & Min. Sc. Vol. 15, pp. 49-51.
- International Society for Rock Mechanics (1978b) Suggested methods for determining tensile strength of rock materials. Int. J. of R.M. & Min. Sci., Vol. 15 pp. 101-103.
- International Society for Rock Mechanics. (1979a) Suggested methods for determining the uniaxial compressive strength and deformability of rock materials. Int. J. of R. Mech., Min. Sci. & Geomech. Abst. Vol. 16, pp. 137-140.
- International Society for Rock Mechanics (1979b) Suggested methods for determining water content, Porosity, Density, Absorption and related properties and swelling and slake durability index properties. Commission on standardisation of Laboratory & field tests. Int. J. Rock Mech. & Min. Sc. & Geomech. Abstr. Vol. 16, pp. 141-156.
- Jackson, M.L. (1969) Soil Chemical Analysis - Advanced Course. 2nd. Ed., Published by Author, Madison, Wisconsin, 53705 U.S.A.
- Jeffery, P.G. (1975) Chemical methods of rock analysis. 2nd Ed. Int. Series of monographs in analytical Chemistry, Pergamon Press, Oxford. p. 176.
- Jones, G. (1984) Weatherability of carboniferous Mudrocks in the South Wales coalfield. Pers. comm. Dept. of Civil Engineering, Polytechnic of Wales.
- Keatch, D.R.A. (1965) Geomorphology of the coast Cardiff to Porthcawl with special reference to the transportation of beach material. Ph.D. Thesis, University of Wales.

- Kemp, P.H. (1958) The effect of groynes on beach formation and erosion. Unpubl. Ph.D. Thesis, Univ. London, 2 Vols.
- Kemp, P.H. (1960) The relationship between wave action and beach profile characteristics. Proc. 7th Conf. Coast. Eng'g's. pp.262-272.
- Kemp, P.H. (1963) A field study of wave action on natural beaches. Proc. 10th Conf. Int. Assoc. Hydraul. Res., pp.131-138.
- King, C.A.M. (1972) Beaches and Coasts. Arnold, London 2nd ed. 570p.
- Krahn, J. & Morgenstern, N.R. (1979) The ultimate frictional resistance of rock discontinuities, Int. J. Rock Mech. Min. Sci. & Geomech. Abstr., Vol.16 pp. 127-133.
- Krumbein, W.C. & Sloss, L.L. (1958) Stratigraphy and sedimentation Freeman & Co., San Francisco.
- Kubler, B. (1966) La Cristallinité de l'illite et les zones tout à fait supérieures du méta-morphisme. In: Colloque sur les Etages tectoniques, Univ. Neuchâtel Baconnière. Neuchâtel. pp.105-122.
- Laxen, D.P.H. & Harrison, R. (1981) Cleaning methods for polythene containers prior to the determination of trace metals in freshwater samples. Analytical Chemistry Vol. 53, pp.345-350.
- Ladanyi, B. & Archambault, G. (1970) Simulation of shear behaviour of a jointed rock mass, Rock Mechanics : theory & practice, (Somerton, W.H., Ed.) pp. 105-125.
- Ladanyi, B. & Archambault, G. (1980) Direct and indirect determination of shear strength of rock mass. preprint 80-25, Am. Inst. Min. Eng.
- Mackereth, F.J.H., Heron, J., Talling, J.F. (1978) Water Analysis : some revised methods for Limnologist. Freshwater Bio. Assoc. Scientific. Pub. No. 36.
- Martna, J. (1970) Engineering problems in rock containing pyrrhotite, 'Large Permanent Underground Openings' Proc. Int. symp., Oslo, 1969. (Eds. Brekke, T.L. & Jorstad, F.A.) pp.87-92.
- Matheson, J.L. (1939) An aerial survey of the estuary of the River Dee employing a simple method of rectifying oblique photographs. Jl. Inst. C. Eng. Vol. 10 paper 5157 pp. 47-54.
- McBride, J. (1980) DEC 20 computer Plotting routines for equal area stereonet. Pers. Comm. Computer Centre, Polytechnic of Wales.
- McBride, J. (1983) Suite of DEC 20 computer programs for digitising profiles evaluating plotting bearing ratio and peak frequency. Pers. Comm. Computer Centre. Polytechnic of Wales.

- McClintock, F.A. & Walsh, J.B. (1962) Friction on Griffith cracks under pressure, Proc. 4th National Congress of Appl. Mech. pp. 1015-1021.
- Mellor, M. & Hawkes, I. (1971) Measurement of tensile strength by diametral compression of discs and annuli. Eng. Geol., Vol. 5 pp. 173-225.
- Miller, R.P. (1965) Engineering classification and index properties for intact rock, Ph.D. thesis, Univ. Ill., pp. 1-332.
- Minkin, R.R. (1963) Winds, waves & maritime structures. 2nd Ed. Griffin, London. 294p.
- Mitchell, J.K. (1976) Fundamentals of Soil Behaviour. John Wiley & Sons, Inc., New York.
- Mogi, K. (1966a) Some precise measurements of fracture strength of rocks under uniform compressive stress. Felsmechanik und Ingenieur-geologic. Vol. 4, pp.41-55.
- Mogi, K. (1966b) Pressure dependance of rock strength and transition from brittle fracture to ductile flow. Bull. Earthquake Res. Inst., Japan. Vol.44, pp.215-232.
- Moore, J.G., Brown, J.D. & Rashid, M.A. (1977) The effect of leaching on engineering behaviour of a marine sediment. Geotechnique 27, No. 4, pp.517-531.
- Morris, E.B. (1982) Cleaning procedures in analytical Chemistry - Pers. comm. Dept. of Science, Polytechnic of Wales.
- Muir-Wood, A.M. (1969) Coastal Hydraulics, MacMillan London.
- Nichols, T.C. (1980) Rebound. Its nature and effect on engineering works, J. of Eng. G., Vol.13, No.3.
- North, F.J. (1929) The evolution of the Bristol Channel - with special reference to the coast of South Wales. National Museum of Wales, Cardiff, 103p.
- Oslon, R. and Mesri, G. (1970) Mechanisms controlling compressibility of clays. Proc. A.S.C.E. Vol. 96, SM6. pp.1863-1878.
- Patton, F.D. (1966) Multiple modes of shear failure in rock & related materials, Ph.D. thesis, Univ. of Ill. pp. 282.
- Paul, B. & Gangal, M. (1966) Initial & subsequent fracture curves for biaxial compression of brittle materials. Proc. 8th Symp. Rock Mech., Minneapolis, Minn., pp. 113-141.

- Peltier, L. (1950) The geographic cycle in periglacial regions as it is related to climatic geomorphology. *Ann. Assoc. Am. Geol.* Vol.40, pp.214-236.
- Perkins, J.W., Gayer, R.A., Baker, J.W. & Williams, G.D. (1979) *The Glamorgan heritage Coast a guide to its Geology.* 2nd Ed., The Glamorgan Heritage Coast Jt. Management & Advisory Committee, Cardiff. 36p.
- Pitt, G. (1983) Bearing ratio and High Spot count on evaluating surface texture. *Pers. Comm. Dept. of Mech. Eng. Polytechnic of Wales.*
- Quigley, R.M. (1962) The engineering properties of illite related fabric and pore water composition. *Nat. Resources Council Canada. Proc. 10th Canadian S.M. Conf.* pp.21-42.
- Read, H.H. (1947) *Rutley's Mineralogy.* Thomas Murby & Co. London.
- Rees, T.D. & Hilton, J. (1978) A rapid method for determination of heavy metals in sewage sludges. *Laboratory Practice.* pp.291-293.
- Richardson, W.A. (1923) The shales with beef. *Q.J. Geol. Soc. London.* Vol.79, pp.88-89.
- Roberts, J.C. (1974) Jointing and Minor tectonics of the Vale of Glamorgan between Ogmere by Sea & Lavernock Pt. *South Wales. Geol. Jl.* Vol.9, pt.2 pp. 97-113.
- Ross-Brown, D.M. (1975) A portable shear box for testing rock joints. *Rock Mechanics.* Vol.7, pp.129-153.
- Ross-Brown, D.M. & Walton, G. (1975) A portable shear box for testing rock joints. *Rock Mechanics* Vol.7 No.3 pp. 129-153.
- Sanders, M.K. & Fookes, P.G. (1970) A review of the relationship of rock weathering and its significance to foundation engineering. *Eng. Geol.* No. 4, pp.289-325.
- Shaw, H.F. (1981) Mineralogy and petrology of the argillaceous sedimentary rocks of the U.K. *Mudrocks of the U.K. Q.J. Eng. Geol.* Vol. 14, No. 4, pp.277-290.
- Sherrard, J.L., Ryker, N.L. and Decker, R.S. (1972) Piping in earth dams of dispersive clays *Proc. A.S.C.E. speciality conf. the performance of earth and earth supported structures.* Vol.1, pp. 602-611.
- Skempton, A.W. (1953) The colloidal activity of clays. *Proc. 3rd Inter. Cof. Soil Mech. Fdn. Eng. (Switzerland)* Vol.1, pp. 57.
- Steward, H.E. & Cripps, J.C. (1983) Some engineering implications of chemical weathering of pyritic shales. *Q.J. of Eng. Geol.* Vol.16, No.4, pp. 281-290.

- Stow, A.V. (1981) Fine-grained sediments terminology in Mudrocks of the U. K.. Q.J. Eng. Geol. Vol. 14, No. 4. pp. 243-244.
- Strahan, A. & Cantrill, T.C. (1904) The geology of the South Wales Coalfield part VI. the country around Bridgend Memoir of the Geol. Survey, 120p.
- Szlavin, J. (1974) Relationships between some physical properties of rock determined by laboratory tests. Int. J. of R.M. & Min. Sci. & Geomech. Abst. Vol. III, pp. 57-66.
- T.R.R.L. (1952) Soil Mechanics for Road Engineers. H.M.S.O. London. (Chapter 3).
- Tawney, E.B. (1866) On the western limit of the Rhaetic beds in South Wales and on the position of the "Sutton Stone", with a note on the corals by P.M.Duncan. Quarterly Jl. Geol. Soc. Vol. XXII, p.69.
- Taylor, R.K. & Cripp, J.C. (1984) Mineralogical controls on volume change. In: Ground movements and their effects on structures (Ed. Attewell, P.B. & Taylor, R.K.) Surrey University press, (Blackie group) pp. 268-303.
- Taylor, R.K. & Spears, D.A. Laboratory investigation of mudrocks. Mudrocks of the U.K. Q.J. Eng. Geol. Vol. 14, No. 4. pp.291-310.
- Timoshenko, S. (1956) Strength of Materials. Part I (advanced). 3rd. Ed. Van Nostrand Reinhold Co., New York. 571p.
- Todor, D.N. (1976) Thermal Analysis of Minerals. Abacus press.
- Trenhaile, A.S. (1969) A geomorphological investigation of shore platforms and high water rock ledges in the Vale of Glamorgan. PhD. Thesis, Univ. of Wales.
- Trenhaile, A.S. (1971) The shore platforms of the Vale of Glamorgan, Wales. pp.127-144.
- Trueman, A.E. (1920) The Liassic rocks of the Cardiff district. Proc. Geol. Assoc. Vol. XXXI, pt.2, pp.93-107.
- Trueman, A.E. (1922a) The Liassic rocks of Glamorgan Proc. Geol. Assoc., Vol. XXXIII, pt.4 pp.245-284.
- Trueman, A.E. (1922b) The use of gryphaea in the correlation of the Lower Lias. Geol. Mag., Vol.59 pp.256-268.
- Trueman, A.E. (1930) The Lower Lias (Bucklandi zone) of Nash Point. Proc. Geol. Assoc. Vol. XLI, pp.148-159.
- Tse, R. & Cruden, D.M. (1979) Estimating joint roughness coefficients. Int. J. Rock Mech. Min. Sci. & Geomech. Abstr. Vol.16 pp.303-307.

- Tucker, M.E. (1981) Sedimentary Petrology an Introduction. Blackwell Scientific Pub. London.
- Uvarov, E.B., Chapman, D.R. & Isaacs, A. (1971) The Penguin dictionary of science 4th Ed., Penguin.
- Vear, A. & Curtis, C. (1981) A quantitative evaluation of pyrite weathering. Earth surface processes and land forms. Vol.6, pp.191-198.
- Vennings, D. (1980) Records appertaining to underpinning at Nash Point Lighthouse. Pers. Comm. Trinity House, London.
- Vogel, A. (1945) A textbook of qualitative inorganic analysis. 3rd Ed., Longman, London.
- Vogel, A. (1978) A textbook of quantitative inorganic analysis. 4th Ed., (revised by Bassett, J. Denney, R.C., Jeffrey, G.H. & Mendham, J.) Longman, London.
- Vutukuri, V.S., Lama, R.D. & Saliya, S.S. (1971) Testing Techniques and results, Handbook on Mechanical properties of rocks, Vol.1 Trans. Tech. Ohio, U.S.A.
- Walters, A. (1981) Limitations to scale of engineering works associated with cliff stabilization along the Glamorgan Heritage Coast. Pers. Comm. Environment Protection Division. Welsh Office, Cardiff.
- Weaver, C.E. (1960) Possible uses of clay minerals in the search for oil. Bull. Am. Assoc. Petrol. Geologists Vol. 44 pp.1505-1518.
- Weinert, H.H. (1965) Climate factors affecting the weathering of igneous rock. Agr. Meter. Vol.2, pp.27-42.
- Weisbach, G. (1978) A new method for determination of surface roughness of rock joints in the Laboratory, Int. J. Rock Mech. Min. Sci. & Geomech. Abstr. Vol. 15 pp.131-133.
- Whitten, D.G. & Brooks, J.R. (1972) Dictionary of Geology. Penguin.
- Williams, A., Caldwell, N. & Davies, P. (1981) Glamorgan Heritage Coast land form guide. The Glamorgan Heritage Coast jt. Management & Advisory Committee Cardiff. 61p.
- Williams, A.T. & Davies, P. (1980) Man as a geological agent : the sea cliffs of Llantwit Major, Wales, U.K. Zeit. fur Geomorph. pp.129-141.
- Williams, G.D. (1980) Slope stability problems in the Carboniferous & Liassic Limestones. In: Cliff and slope stability in South Wales. (Ed. Perkins, J.W.) Dept. of Extra-Mural Studies, U.C. Cardiff, pp.135-155.
- Wobber, F.J. (1963) The Stratigraphy and Palaeontology of the Liassic rocks of Glamorgan. Ph.D. Thesis. Univ. of Wales. 249p.

Wobber, F.J. (1965) Sedimentology of the Lias (Lower Jurassic) of South Wales. J. of Sed. Pet. Vol. 35, No. 3, pp.683-703.

Wobber, F.J. (1967) Post depositional structures in the Lias, South Wales. J. of Sed. Pet. Vol.37, No.1, pp. 166-174.

Wobber, F.J. (1968) Microsedimentary analysis of the Lias in South Wales. Sed. Geol., Vol.2, pp.13-49.

Wooldrige, S.W. and Linton, D.L. (1938) some episodes in the structural evolution of S.E.England Proc. Geol. Assoc. Vol.49, p.264.

Wu, H.T. & Ali, E.M. (1978) Statistical representation of joint roughness, Int. J. Rock Mech. Min. Sci., & Geomech. Abstr. Vol.15 pp. 259-262.

Zobell, C.E. (1946) Studies on redox potentials of marine sediments : Bull. Am. Assoc. Petrol Geol. Vol.30, pp.447-513.